A Monte Carlo Study of Carbon Monoxide Layers Adsorbed on Ionic Crystals: Structures and Phase Transitions

Ngoc-Thanh Vu

A Thesis

in

The Department

of

Chemistry and Biochemistry

Presented in Partial Fulfilment of the Requirements
for the Degree of Doctor of Philosophy at
Concordia University
Montreal, Quebec, Canada

May 2002

ABSTRACT

A Monte Carlo Study of Carbon Monoxide Layers Adsorbed on Ionic Crystals: Structures and Phase Transitions

Ngoc-Thanh Vu, Ph.D.
Concordia University, 2002

The adsorption of CO on NaCl(100) at monolayer, submonolayer and multilayer coverages, and on LiF(100) at monolayer coverage were studied. The Metropolis Monte Carlo method was used to study the structures of the overlayers and to characterize the phase transitions. The simulations were performed in the temperature range from 1K to 75K.

At low temperature and monolayer coverage, both of these systems form ordered phases that become disordered as the temperature is increased. For the CO/NaCl system the estimated transition temperature is between 32K and 35K whereas for CO/LiF a temperature between 40K to 45K is estimated. Below the transition temperatures, both systems have an ordered p(2x1) type structure due to correlated azimuthal orientations. The ordered phases have two molecules per unit cell connected by a glide plane. In the CO/NaCl case the projections of the molecular axes upon the surface are antiparallel. We find that in monolayer of CO/NaCl the molecules are tilted by about 27Å whereas larger tilt angle ($\theta \sim$ 44Å) is observed in a monolayer CO/LiF. At high temperatures, both systems undergo a phase transition to an azimuthally disordered p(1x1) phase, *i.e.* one

with no preferred orientation in the surface plane. Yet on average, the molecular axes remain tilted with the surface normal. Evidence for a continuous order-disorder phase transition is found in the form of a characteristic divergence of the heat capacity and susceptibility within the estimated transition temperature range.

Coverages of less than a monolayer of the CO/NaCl system have also been studied. The CO molecules are found to aggregate and form islands with an ordered structure in the middle of the islands. Apparently, these islands also undergo an order-disorder transition but at lower temperatures. At high temperatures, gas-solid coexistence in two dimensions is also observed.

Simulations of adsorption of multilayer systems are found to destabilize the p(2x1) phase of the bottom layer in favour of a p(1x1) structure with the upper layers adopting the correct orientational ordering of the bulk solid α-CO. Nonetheless, the molecules fail to form a correct head-to-tail ordering as in the bulk structure. Preliminary results show that the ability to adopt the correct bulk structure depends upon the number of the layers present in the system. The more layers the system has the better chance the system has to adopt the correct head-to-tail ordering.

To mother, Andrew and Daniel.

ACKNOWLEDGEMENTS

I would like to express my sincere thanks to Prof. David B. Jack for the opportunity to study under his guidance. I am greatly indebted for his support, suggestions, encouragement as well as the freedom he has provided throughout the research.

Special thanks are also due to Prof. Marcus F. Lawrence and Prof. George Denes for being members of my committee. I am greatly thankful for their time and encouragement during the committee meetings.

I would also like to thank the many graduate students who help me along the way, particularly Abdulwahub Sallabi for all useful discussions and Amine Benrehbouh for helping me with computer technical problems. I have also greatly appreciated their friendship and I truly enjoyed their humour.

The assistance provided by Carole J. Coutts with all my paper works has been invaluable and I am grateful for that.

Finally, Duc, my parents, my relatives, my best friends and my in-laws have supported and encouraged my education all along. My sincere gratitude is extended to them.

TABLE OF CONTENTS

List of Figures

List of Tables

List of Important Abbreviations and Symbols

Fe(110)	Iron. '110' refers to the plane of cleavage of the iron.
NaCl(100)	Sodium chloride. '100' refers to the plane of cleavage of the sodium chloride.
MgO(100)	Magnesium oxide. '100' refers to the plane of cleavage of the magnesium oxide.
CO	Carbon monoxide.
FTIR	Fourier transform infrared.
HAS	Helium atom scattering.
θ	Polar angle is the angle between the molecular axis and the surface normal.
φ	Azimuthal angle is the angle between the projection of the molecular axis and the x-axis of the surface plane.
p(2x1)	Epitaxial structure of the adsorbed layer: primitive two by one structure.
p(1x1)	Epitaxial structure of the adsorbed layer: primitive one by one structure.
L-J	Lennard-Jones.
LiF(100)	Lithium fluoride.
CO/NaCl(100)	Carbon monoxide adsorbed on sodium chloride surface.
MM	Molecular mechanics.

QM	Quantum mechanics.
PES	Potential energy surface.
SM	Statistical mechanics.
N	Number of particles.
T	Temperature in Kelvin.
P	Pressure.
$\vec{r}$	Position vector.
$\vec{\Omega}$	Orientation vector.
NVT	number of particles, volume and temperature.
$E(\vec{r},\vec{\Omega})$	Potential energy of the system.
δE	Energy difference.
B	Boltzmann factor.
ξ	Random number.
MC	Monte Carlo.
C_v	Heat capacity at constant volume.
k_B	Boltzmann constant.
M	Total number of cycles.
Ψ	Total molecular order parameter.
Φ_x, Φ_y	Transformed orientations on the x and y directions, respectively.
L	The size of the surface lattice.

nx, ny	The position of the adsorbed molecule on x and y directions on the surface lattice, respectively.
χ	Susceptibility.
V	Potentail energy of the whole system.
v	Potential energy of the individual molecule.
V_{ele}	Electrostatic energy.
V_{dis}	Dispersion energy.
V_{rep}	Repulsion energy.
q	Charge.
μ	Dipole moment.
Θ	Quadrupole moment.
Ω	Octupole moment.
SCF	Self-consistent field calculation.
C_6, C_8, C_{10}	Dispersion parameters.
A_{ij}, β_{if}	Born-Mayer parameters.
a_o	Lattice constant of the surface.
V_{coul}	Coulombic energy.
$\Phi(\bar{r})$	Electrostatic potential generated by the ion from the surface.
α	Polarizability.
$\alpha_\perp$, $\alpha_{//}$	Polarizabilities in the perpendicular and parallel directions with respect to the molecular axis, respectively.

$V_{d\text{-}r}$	Dispersion-repulsion (van der Waals) energy.
$f_{2n}(r)$	Damping function.
$W_G(z_\alpha)$	Fourier coefficient.
q_{st}	Isosteric heat of adsorption.
H	Enthalpy.
ω_α	Frequency of the α^{th} degree of freedom.
E_0	Potential energy minimum of the physisorbed energy well.
n	Number of degrees of freedom of the molecule.
$\hbar$	Dirac constant.
$\Delta\varphi$	Intermolecular angle.

CHAPTER 1: INTRODUCTION

When a solid is exposed to a foreign gas or vapour, some of the molecules disappear from the gas phase. The foreign gas molecules either enter the solid bulk or remain attached at the surface, *i.e.* they reside at the interface between the two different bulk phases, (usually a solid and a gas). The former process is termed *absorption* and the latter *adsorption*. Sometimes, both processes occur simultaneously and the whole process is called *sorption*.

The discovery of the process of adsorption dates back almost two hundred years ago. In the nineteenth century, Michael Faraday (1834) performed some of the earliest work on gas adsorption and heterogeneous catalysis.[1] Since then, technological developments have improved the experimental techniques in the area of this research, not only to gain a better understanding on how the process works, but also for insights into its application to both experiments (from light bulbs, catalysis, to the nanofabrication of microelectronics) and theory. Intensive investigations of the structures of layers adsorbed to well-defined surfaces have been performed for many decades. The experimental methods and the results are well documented in the literature, especially of those small and simple molecules such as H/Fe(110),[2] CO_2/NaCl(100),[3,4,5] CO/MgO(100),[6,7] H_2O/NaCl(100),[8,9,10] N_2/NaCl(001)[11] naming just a few. On the other hand, an understanding at the molecular level of the interaction of the surface bound molecules to their substrates cannot be completed using just the traditional experimental techniques or theoretical calculations. In order to complete the study,

'computational chemistry' has been employed as a complementary to the two traditional approaches. The central importance of this approach is developing model systems using a computer. Computer simulations yield information that help understanding the factors giving rise to a particular structure or favouring one over the others. In order to do so, it is reasonable to start by studying those systems whose bonding arrangements are simple such as the adsorption of small molecules on alkali halide crystals. In those systems, the bonding of the molecule to the substrate is largely controlled by electrostatics[12] and is governed by physisorption. Among them, the adsorption of CO gas on NaCl(100) has been considered as a model system[13] for this kind of study because of the simplicity of its bonding.

In the next two sections an overview of physical adsorption and some literature citations on experimental and theoretical works related to the study of physical adsorption of CO gas layers on NaCl(100) surfaces will be discussed.

1.1 Theory of Adsorption

A plane that separates two adjacent bulk phases is known as an interface or surface if one of the phases is a gas or a vapour. The properties of the molecules at surfaces are found to be different than those in the bulk phases.

Therefore, the study of surfaces has been attractive to scientists of all backgrounds (especially in physics and chemistry) for many years. It continues to grow and be an important and interesting subject. In addition to that, the improvements of the experimental techniques have tremendously increased scientists' abilities to study surface structures and phenomena. It has evolved into a separate sub-discipline of chemistry and physics.

One of the most fundamental subjects in the field is *adsorption*. Adsorption is a process in which a thin film is formed at an atomically flat solid surface (the so-called *adsorbent*) when it is exposed to a foreign gas at a pressure P, and a temperature T. When the system gas/solid is at equilibrium, the gas is always found to accumulate at the surface of the adsorbent, creating a surface excess of molecules or a so-called *thin film*. Adsorption, therefore, does not involve bulk penetration of the gas into the structure of the solid or liquid as in comparison with *absorption*. Since the process of adsorption of a gas on a solid surface is a spontaneous process, the change of Gibbs free energy of the system during adsorption is always negative. There is also a decrease in entropy (*i.e.* negative ΔS) because a free gas molecule always loses some freedom of motion when attached to a surface.[14] This is seen in the following thermodynamic relationship,

$$\Delta G = \Delta H - T\Delta S \qquad (1.1)$$

where ΔG is the change in Gibbs free energy of the adsorbed gas with respect to the gas phase ($\Delta G = G_{ads} - G_{gas}$). A spontaneous process (*i.e.* negative ΔG) with a

negative ΔS must have a negative enthalpy of adsorption ($\Delta H < 0$). Thus, heat is always liberated on adsorption.[1]

The adsorbed molecules are held to the surface by intermolecular forces between the gas molecules and the surface atoms. The formation of a thin film creates a new class of condensed matter (i.e. a two-dimensional phase) that is of interest in both theoretical and experimental fields. The process is of theoretical interest because of the information it provides on the nature of gas-surface interactions, on the structure of the adsorbed layers (*e.g.* any epitaxial relationship with the substrate) as well as the existence of two-dimensional (2D) phase transitions (the transition of the adsorbed layer's structure to a different one when the temperature or the pressure is changed). It is also of practical interest because of its various applications in industry such as water purification, ozone layer protection (by trapping chlorofluorocarbon molecules), coating industry, heterogeneous catalysis, enhanced oil recovery, detergency, odour removal and chromatographic separation, naming just a few. Hence, understanding the process of adsorption is very important; indeed, numerous studies have been done for decades in an effort to have a good understanding of the subject.

Two main types of adsorption can be clearly distinguished by just comparing the magnitude of the enthalpy change. In the first type, chemical

negative ΔS must have a negative enthalpy of adsorption ($\Delta H < 0$). Thus, heat is always liberated on adsorption.[1]

The adsorbed molecules are held to the surface by intermolecular forces between the gas molecules and the surface atoms. The formation of a thin film creates a new class of condensed matter (i.e. a two-dimensional phase) that is of interest in both theoretical and experimental fields. The process is of theoretical interest because of the information it provides on the nature of gas-surface interactions, on the structure of the adsorbed layers (*e.g.* any epitaxial relationship with the substrate) as well as the existence of two-dimensional (2D) phase transitions (the transition of the adsorbed layer's structure to a different one when the temperature or the pressure is changed). It is also of practical interest because of its various applications in industry such as water purification, ozone layer protection (by trapping chlorofluorocarbon molecules), coating industry, heterogeneous catalysis, enhanced oil recovery, detergency, odour removal and chromatographic separation, naming just a few. Hence, understanding the process of adsorption is very important; indeed, numerous studies have been done for decades in an effort to have a good understanding of the subject.

Two main types of adsorption can be clearly distinguished by just comparing the magnitude of the enthalpy change. In the first type, chemical

adsorption or *chemisorption*, the adsorbed molecules are held to the surface by covalent forces. The process involves the transfer of electrons between the gas (or the *adsorbate*) and the solid (*i.e.* the *adsorbent*), forming a new chemical compound between the adsorbate and the outermost layer (or *surface*) of the adsorbent atoms. The newly formed compound is different than both the bulk and the gas phase. The heat evolved in this type of adsorption is usually comparable to that evolved in chemical bonding, namely 24 to 120 kcal/mol. It was suggested by H. S. Taylor[1] that chemisorption is frequently associated with large activation energies and may therefore be a relatively slow process. It was found by Irving Langmuir[1] that the surface becomes saturated after it is covered with a single layer of adsorbed gas; and thus, terminating the chemisorption process.

In the second type of adsorption, physical adsorption, the forces involved are of a physical nature and are relatively weak since they are caused by intermolecular interactions. Physical adsorption, sometimes called *physisorption*, refers to the weak binding forces between atoms or molecules and surfaces. Since these forces do not involve the transfer of electrons, no chemical bonds are formed between them. The heat evolved in the process of physisorption is usually one order of magnitude smaller than that of chemisorption (less than 5 kcal/mol). Physisorption usually occurs at a faster rate because it is not associated with an activation energy.

Even though the distinction between physical and chemical adsorption can usually be determined by direct comparison between the heats of adsorption (which is usually measured by a direct calorimetric method), the distinction is not always clear-cut. In this case, other considerations that are listed below can be used to do the task.[14]

- Physical adsorption can take place with any gas/solid system, provided the conditions of temperature and pressure are suitable. By contrast, chemisorption can only occur if the gas is capable of forming a chemical bond with the surface atoms.
- Physisorption is a reversible process and a physically adsorbed layer may be removed by reducing the pressure, at the temperature at which adsorption occurs. The removal of a chemisorbed layer, however, often requires much more drastic measures. Sometimes a mixture of gas is produced (*e.g.* oxygen on charcoal, desorbs as a mixture of carbon monoxide and carbon dioxide instead of just oxygen gas).[14]
- Multilayer adsorption can take place in physical adsorption whereas chemisorption is usually considered completed once a monomolecular layer (or *monolayer*) is built up.

Although both processes have equal importance in studying surface phenomena, physisorption is simpler in terms of interactions and adlayer

structure. As was previously mentioned, thin films resulting from physical adsorption at solid surfaces represents a two-dimensional (2D) phase of matter with different properties (*i.e.* epitaxial growth, 2D phase transition, *etc.*) compared to its bulk (3D phase). Among the newly formed structures, those which are commensurate with the substrate, *i.e.* ones in which the over layer has its positional order (periodicity) determined by the substrate, makes the study of these films interesting. In addition, because of various combinations between the adsorbates and the solid surfaces, numerous new structures can be found in a 2D phase. Prediction of those new structures is a challenging task for theory. Fortunately, most of the time theorists are only interested in the most stable structure. Nonetheless, the determination of the most stable structure can be very time consuming and tedious. In order to determine the most stable structure one has to successfully replicate the relevant forces of the system and carefully analyze the energetic states of all possible structures. The one with the lowest calculated energy will presumably be the most stable structure of all. Despite all that, physical adsorption is still an ideal subject for basic research in understanding the fundamental interactions between the molecules. Hence, it has been attractive to scientists for several decades.

In order to have a better understanding of such a complicated subject, a reasonable starting point would be the examination of a simple system such as small molecules adsorbed on ionic surfaces. The system that has been considered

as a model for doing such a task is the adsorption of CO on an isolated and stable solid surface of NaCl(100). The CO/NaCl(100) system is ideal because the CO molecule is small and has a stable bond while the sodium chloride solid has a well-understood surface. In addition, with a small dissociation energy of D_o= 18 kJ mol^{-1} compared to the huge crystal energy of NaCl (760 kJ mol^{-1}) the monolayer of CO on NaCl(100) would not likely alter the ionic arrangement at the surface.[13] Hence it is considered as being " ... a model system for the study of physisorption. *I.e.* one presumes that the bonding is dominated by classical electrostatic forces and the properties of adsorbed species remain close to their gas phase value."[15] A review of the literature related to the CO/NaCl(100) model system will be given in the following section.

1.2 The Literature Background

1.2.1 The Experimental Papers

The pioneering work of Gevirzman and coworkers on the subject were conducted more than four decades ago. In their paper "Infra-red Spectra and Spectral Shifts of CO Adsorbed on Evaporated Alkali-Halides",[12] they described the infrared spectra of CO gas adsorbed on NaCl, NaBr and NaI crystalline films at -196°C (77.15K) as single and sharp peaks. The bands were found to shift

towards higher frequency (blue shift) with respect to the value of the gas phase. The values range from 14cm^{-1} for low coverage to 10cm^{-1} for high coverage. They also observed a small weak shoulder, which is red shifted to the main peak, that they assigned to molecules adsorbed on some energetically different sites, *e.g.* defect sites.

Since then, with the improvements of the experimental methods, studies on adsorption have grown. In the 1980's Ewing *et al.* reported a series of experiments of CO gas adsorbed on the (100) plane of NaCl solid surface using Fourier Transform Infrared Spectroscopy (FTIR). They explored various topics such as spectroscopic measurements (*e.g.* vibrational dephasing and band shapes,[16] structure examinations, studied submonolayers and isotopic mixtures[17]), and also examined the dynamical aspects of energy relaxation (energy flow from excited molecules on salt surfaces[18]). From the spectroscopic measurement,[18] at 22K the adsorption band in E_p polarization (electric field parallel to the plane of incidence) was centered at 2155.01 cm^{-1}, resulting in a blue shift (a shift towards higher frequency) with respect to the gas phase[19] (which has a value of 2143.00 cm^{-1}) and a small shoulder at 2154.8cm^{-1}, whose origin they could not determine with certainty. No absorption was detected with E_s polarization (electric field perpendicular to the plane of incidence). They proposed that at T= 22K the CO molecules were adsorbed at the sodium sites with the carbon ends down and are aligned perpendicular to the surface. In

another study, using thermodynamic measurements, Ewing and co-workers reported the experimental heat of adsorption of CO on a well-defined NaCl single crystal.[20] At half coverage, $\Delta H_{(l)} = 14 \pm 1$ kJ/mol (3.34 ± 0.23 kcal/mol). In a different study they commented that all adsorbed layers beyond the first one would have the same structure as those from solid α-CO.[18]

At the beginning of the 1990's, Heidberg and coworkers also investigated the adsorption of carbon monoxide on a cleaved sodium chloride single crystal surface. They also used Polarized Fourier transform infrared (Polarized FTIR) methods to examine the structure and phase transition of the monolayer CO.[21] Spectra at monolayer coverage were collected at 40, 24 and 6K. They confirm the results from Ewing's group[18] by stating that only E_p radiation was absorbed for a monolayer, but at T= 40K and not at T= 22K as Ewing *et al.* have claimed; a discrepancy of $\Delta T = 18$K. They also found there was no absorption by E_s polarized light at this temperature. Hence, they concluded that at T= 40K, a CO layer has a *p*(1x1) structure with one molecule per surface unit cell, oriented perpendicularly at the sodium site. However, this structure was only present at temperatures above 35K. Below this temperature, *e.g.* at 30K, a second peak was detected in the p-polarized spectrum and an even stronger one in with s-polarization. The new p-polarized peak was redshifted from the first one by about 6 cm^{-1}. The peak was found to shift to higher frequency and the integrated absorption increased at 6K. The second p-polarized peak could not be due to

adsorption at defect sites as had been proposed by Ewing *et al.*[18] It was argued that this was explainable by correlation field splitting due to the presence of at least two molecules per adsorbate lattice unit cell, resulting in a *p*(2x1) structure where "...The molecules are translationally inequivalent but adsorbed on identical adsorption sites connected by a glide plane".[21] The molecules are tilted away from the surface normal. In order to determine $\Delta\varphi$ (which is the intermolecular angle between the projections of the molecular axes of translationally inequivalent molecules onto the surface), positions at x, and y for the structure at 6K, they simulated the infrared spectra of the monolayer using equations of classical electrodynamics. They found that x and y positions had very little effect on the results of the calculations. Hence, results of calculations for different tilt angle, θ, and the intermolecular angle $\Delta\varphi=180°$ (which was fixed in order to interpret the p(2x1) structure at low temperature) were presented.[21] The best agreement with the experimental spectra was obtained when the tilt angle, θ, was 65° with respect to the surface or θ of 25° with respect to the surface normal at 6K. At T= 40K, the tilt angle was found to be 90° with respect to the surface (θ~0° with respect to the surface normal). There thus existed a transformation of the monolayer structure from a high-temperature *p*(1x1) phase above 35K to a low-temperature *p*(2x1) phase below 35K. Hence, a reversible phase transition was concluded to exist in the system of CO/NaCl(100). The isosteric heat of adsorption was found to be q_{st} = 16.3 ± 1.6 kJ/mol (3.89 ± 0.38 kcal/mol) for a coverage of 75% saturation coverage at the temperatures T= 73,

84, and 95K, in an earlier study.[22] They also conducted an experiment in growing the CO multilayers on the monolayer CO/NaCl(100) using High Resolution Fourier-Transform Infrared methods.[23] A change in the spectral features of the monolayer had been reported upon additional adsorption of CO multilayers on top of it. The disappearance of the doublet and the appearance of the single absorption of the first layer was explained either by a structural change (from a (2x1) to a (1x1) structure), by changed dipole-dipole coupling, or by a combination of both. No clear answers could be given without doing additional experiments.

Concurrently, another group of scientists used the Helium Atom Scattering (HAS) method to confirm the monolayer phase transition of CO/NaCl(100).[24] Toennies *et al.* reported the observation of an ordered monolayer of CO on NaCl(100) plane which was commensurate with the substrate in the entire range of temperatures (T= 26, 45, and 53K) of the HAS experiments. At T=45K, a (1x1) structure was formed. At T ≤ 30K the adsorbate lattice formed a (2x1) structure with two molecules per unit cell, related by a glide plane, which was in accordance with the observation that the molecules are tilted in an antiparallel way, *i.e.* $\Delta\varphi = 180°$.

In conclusion, different groups of scientists reported similar results for the adsorption of CO molecules on NaCl(100) surface using different methods. In

brief, a low-temperature structure (p(2x1)) of the monolayer was transformed to a high-temperature one (p(1x1)). The transition temperature was inferred to be $30K \leq T \leq 35K$. However, no information was available on the position of the CO molecules with respect to the substrate. Moreover, assumptions and estimates had to be made to deduce the tilt and intermolecular angles of the adsorbates.

Although experimental techniques for studying surface structures and related phenomena have been numerous and more sophisticated in the last thirty years, such experiments cannot always reveal the details of the binding forces involved in the system. Moreover, some of the details of the structures, such as the binding site, and the molecular orientation, cannot always be clearly assigned using just the experimental results. Here theoretical studies are of fundamental importants in trying to understand those questions thoroughly. A summary of some theoretical papers will be presented in the next section.

1.2.2 The Theoretical Reviews

At the same time as the improvements of the experimental methods, the invention of the computer was found to have a big impact on doing extensive calculations such as interaction potentials analysis. Over the years, with the remarkable developments in the computer science world, more powerful computers have been created, thus making the calculation of some sophisticated

and detailed potential functions feasible. Moreover, in the course of the past two to three decades, the cost of computing has decreased substantially, thus encouraging scientists in general, and chemists in particular, to expand their research interests to a quite novel branch in the field: computational chemistry.[25] With the aid of the computer, one can not only calculate potential energy surface but also simulate interactions between the molecules on an atomic scale.

In particular, studies of the model system CO gas adsorbed on NaCl(100) have greatly increased since one of the initial potential calculations from Gevirzman's paper were published in the late 1960s.[12] In the paper, the interaction potential was written as a sum of pair-interactions that represent the van der Waals, repulsion, induction and electrostatic energies between a CO molecule and the NaCl substrate. The potential was calculated for different adsorption sites and orientations of the CO molecules on the NaCl surface. In all cases considered, a minimum in the potential curve was obtained. The calculated adsorption potential for the CO molecule with a minimum energy closest to the experimental data is the one where the CO molecule is situated on a Na^+ ion in a perpendicular fashion. The adsorption potential minimum, Φ_{min}, was found to be 4.159 kcal/mol. The heat of adsorption in this case was calculated using, $-\Delta H = -(\Phi_{min} + \varepsilon_0) + RT$ where ε_0 is the zero point energy (per mole) of the whole molecule. $-\Delta H$ was calculated to be 4.2 kcal/mol, in agreement with experiment

value (q_{st} at zero coverage was equal ~ 4.5 kcal/mol) from the calculation of the isosteric heat of adsorption from the adsorption isotherms.

In subsequent years, Picaud and co-workers used energy minimization to optimize the structure of a CO adlayer on NaCl(100) at zero temperature (T= 0K).[26] They calculated the most stable geometries of the adsorbed molecules using a semi-empirical interaction potential that contains contributions from lateral interactions between the adsorbed molecules as well as adsorbate-substrate interactions. The total energy was the sum of the electrostatic interactions (which were calculated using a distributed multipole analysis (DMA)) and dispersion-repulsion interactions, which were represented by either the Lennard-Jones (L-J) or Buckingham form. Different results were reported depending on the two different forms used for the dispersion-repulsion interactions. For single molecule adsorption, the Buckingham potential showed that the most stable adsorption site was above the sodium ion with the CO in a perpendicular orientation. In contrast, when the L-J potential was used the molecule shifted along a Na^+ row by about 0.3 a_o = 1.2 Å where a_o is the distance between the adsorption sites. The molecular axis was found to incline by about 30° with respect to the normal. The difference in energy between the two models was 42 meV (0.968kcal/mol), where the energy of the former was -192 meV (or -4.43 kcal/mol) and the later was -150 meV (or -3.46 kcal/mol). For a (1x1) monolayer (where all molecules have the same orientation) the results were

similar to that of the isolated molecule. Specifically, the molecules still stood upright above the Na^+ sites with the corresponding energy of -205 meV (-4.73 kcal/mol) when the exp-6 form was used. In the calculation when the L-J form was employed, the molecules are found to shift yet further from the sodium site by $0.37a_o$ = 1.46Å. The inclination of the molecular axis with respect to the normal was found to increase to $\theta \sim 42°$; and the intermolecular angle, $\Delta\varphi$, was 0°. The influence of the lateral interactions was to increase the energy minimum to -170 meV (-3.92 kcal/mol). As for the (2x1) CO monolayer, the exp-6 potential did not yield a stable (2x1) structure; instead it reverted to the (1x1) structure result. Although better results were found when the L-J form was used, the two molecular sites within the (2x1) unit cell were not translationally equivalent (*i.e.* the molecules did not lie on symmetrical sites) and thus were not consistent with experiment. The tilt angle was calculated to be $\theta \sim 45°$, a value that is much greater than the tilt angle of $\theta \sim 25°$, extracted from Heidberg's experiment.[21] The value of the azimuthal angles were $\varphi_1 = 90°$ and $\varphi_2 = 270°$, resulting in a difference, $|\Delta\varphi|$, of 180°, and thus described a configuration with molecular axes tilted antiparallel as assumed by Heidberg *et al.* using their FTIR result.[21] In both calculations, with different forms of dispersion-repulsion interactions, they found that the potential surface was very flat at the minimum region. There was only a very small difference in energy (~ 1 meV, or 0.023kcal/mol) between the high-temperature p(1x1), and the low-temperature p(2x1) structures of the CO monolayer. As a result, they concluded that both structures were considered as

the most stable commensurate geometries in the region of the minimum. Hence, it was argued, they were energetically equivalent structures; and there was a possibility for a phase transition to occur between them as experimentally reported.[21,24] There were differences between the molecular orientation and position of a single molecule adsorbed on the surface plane when two different analytical forms for the dispersion-repulsion interactions were used as previously described. In both cases, especially the (2x1) structure, they were not able to successfully describe the position and orientation of the CO monolayer in comparison to the estimations of the experiments.

The results of a perturbation study done by Stone and co-workers (1995) revealed similar results.[19] In this study, they used similar methods to express the total interaction potential but with the interaction parameters derived from *ab initio* intermolecular perturbation theory. They reported that an isolated molecule was found to bind perpendicular to the surface at a Na^+ ion with the C atom pointing downwards. However, there existed several possible structures for the monolayer adsorption: three (1x1) and two (2x1) structures that all had very similar energies. Among the three (1x1) structures, two had molecules tilted at about 28°. The third one is perpendicular to the sodium site. Again the energy differences between the structures reported were too small to be able to pick out the most stable structure for the CO monolayer. Of the (2x1) structures, one structure has a tilt of 28° and $\varphi \sim 37.7°$ and the other with a tilt of 26.4° and $\varphi \sim$

90°. However, the calculations were not able to determine their relative energies with confidence because the difference in their energies was small. They also concluded that the energy gap between the configurational energies of one of the p(1x1) and one of the p(2x1) structures, respectively, that had closest match to the experimental results, was about 0.3 $kJmol^{-1}$ (which is about 35K in term of temperature unit), presumably the p(2x1) structure was observed at the lower temperatures. They argued that this could be interpreted as an indication that the phase transition between the two structures was possible and that the transition temperature should be 35K as experimentally cited.

In 1996, a study by Hoang *et al*, using the above model in a molecular dynamics simulation, also suggested that the phase transition was possible.[37] They simulated the CO adlayer at five temperatures 15, 25, 35, 45 and 55K. They found that at low temperature, T= 25K, the molecules formed a (2x1) structure with a tilt angle of 39° from the surface normal. The (2x1) unit cell did contain a glide plane but the molecular axes of the molecules were found to be perpendicular to each other rather than being antiparallel as interpreted in the infrared experiments. The transition temperature was suggested to be around 50K, a much higher temperature compared to the one deduced from the experiment.

As previously mentioned, some of the fundamental questions about the binding process between CO and NaCl(100) have been left unanswered in the experimental studies. Also, discrepancies between different theories and experiments remain. In an attempt to clarify these points and resolve the discrepancies, we decided to investigate this model using different potentials and a different method of simulation: the Metropolis Monte Carlo method. These results match the experimental observations and were initially published in Refs. [27,28]. These results form a part of this thesis.

1.3 Our Project and its Objectives.

Inspired by the experimental results, and noting the diversity and lack of concensus in the theoretical investigations, as well as the need to understand the basic interactions between the adsorbates and the solid surfaces at a molecular level, we decided to look at the subject at a slightly different angle: investigating the structure and phase transition of the physical adsorption of CO adlayers on NaCl(100) by means of Monte Carlo computer simulations.

Although numerous theoretical studies had been done to examine the adsorption of CO gas on NaCl(100), none of the studies were performed using the Monte Carlo simulation method. Most of the investigations used either *ab initio* or semi-empirical methods to calculate the potential energy surface and

examine the structure of the system and did not include finite temperatures. Therefore, we chose to investigate the above system using Monte Carlo simulation where finite temperatures can be incorporated through the Boltzmann distribution in the course of a simulation.

The driving force to do the project in the beginning was to study the structure of the adsorbed CO molecules on NaCl(100) surfaces. From the structure of the adsorbed film, we then investigated the phase transition of the CO monolayer that has been experimentally reported. Also a detailed analysis of the binding force was carried out by examining the break down of the contributions from the total intermolecular interactions.

To the best of our knowledge, in all the previous attempts of modeling the CO/NaCl system, no one has been able to describe properly all the experimental results. We, however, are the first to be able to report correct structures of the CO adlayer that match the description proposed from the experimental results. From the results of our study, we also confirm the phase transition between the high-temperature and the low-temperature phases of the monolayer. The predicted transition temperature is also matched to that obtained from the experiments ($T \approx 35K$). We report structures of the submonolayer system and those obtained from the multilayer system as well. In addition, we can predict the structure of the physically adsorbed CO on LiF(100) surfaces.[30] From our detail analysis of

the total interaction energy, one can have a better understanding of the nature of the forces behind the adsorption process of the above system.

Although the CO/NaCl system does not directly contribute to any industrial applications just yet, the basic interactions of the system can be understood by our studies and these understandings can be used in creating model potentials to describe the basic interactions between the molecules in a system. This method can then be applied to investigate larger molecules such as biological ones. This can certainly be expanded to study more complicated systems such as the reactions of molecules at surfaces. One can use our study to help examine the structures of adsorbed films. An example where these methods could be applied would be to study the structure of $NaNO_3$ and H_2O adsorbed on NaCl surfaces using a Monte Carlo simulation in order to help understand the heterogeneous reaction between NO_2 gas and NaCl in the marine troposphere. This process is of interest because of the production of volatile chlorine-containing gas, which might contribute to the depletion of the stratospheric ozone layer.[31] The experiments can confirm the reactions but the structure of the adsorbed species cannot be determined.[32] One can use a Monte Carlo simulation to predict the structure, and from this the mechanism can be understood; hence helping in investigating means to allow a determination of the seriousness of the problem and prevent other processes which are caused by human activities that give rise to the same undesired results.

The structure of the rest of the thesis is composed as follows: a brief description of the simulation method is given in chapter II. In chapter III the potential function will be discussed. The results of the adsorption of the CO adlayer on NaCl will be given and discussed in the following chapters IV, V, and VI. Lastly, the study of the adsorbed CO monolayer on LiF(100) will be presented in chapter VII. A conclusion will be given in chapter VIII.

CHAPTER 2: THE METROPOLIS MONTE CARLO METHOD

2.1 Computer Simulation and the Metropolis Monte Carlo Method

Chemistry is a science that primarily deals with the construction, transformation and properties of molecules; in computational chemistry (a significant branch of theoretical chemistry), one combines mathematical methods with fundamental laws of physics to study processes of chemical relevance using the powerful ability to do calculations of a computer.

One of the subfields in computational chemistry is molecular/simulation modeling. Most molecular/simulation modeling studies involve three phases: choosing a model to represent all the interactions between molecules in the system, then a method to calculate the energy of the system as a function of molecular positions, and finally the results are analyzed and the required properties are calculated.[33] The applications of molecular/simulation modeling range widely from single molecule calculations, to calculations of assemblies of molecules to reactions amongst molecules.[25] The decision to choose a model and a method depends on the objective of the study.

To achieve our primary goal in this study, which was to investigate structures of CO gases adsorbed onto the insulator surface of NaCl (100) at finite temperatures using computer simulation, we chose the Metropolis Monte Carlo

method. In this method the molecules are moved without the influence of any forces (non-physical move). A Monte Carlo simulation creates configurations of a system by making random moves to the positions and orientations of the molecules (sometimes this method is also termed *random sampling*). Since the moves are non-physical, there is no energy barrier for the molecule to cross; thus it can enhance the ability to explore phase space significantly in appropriate cases. In order for the Monte Carlo simulation to generate new configurations with an appropriate statistical weighting, a special set of criteria is used to decide the acceptance of each new configuration.[25,33] These criteria ensure that the probability of obtaining a given configuration is equal to its Boltzmann factor, $exp\{-U(\mathbf{r}_i)/k_BT\}$, where $U(\mathbf{r}_i)$ is the potential energy function of the system. Application of these criteria over enough configurations in the whole trajectory yields properly Boltzmann-weighted averages for thermodynamic properties calculations. In addition, finite temperatures are incorporated into the simulation through the use of the Boltzmann factor. In short, this technique considers small replications of the macroscopic system with manageable numbers of atoms or molecules for calculations. The results are representative configurations of these small replications. These configurations are then used to accurately calculate values of structural and thermodynamic properties with a reasonable amount of computer time and cost.

Another important factor for a successful simulation is the ability to choose the right model in order to define a good potential energy function to represent the interaction for the whole system. In order to simulate the adsorption of large number of CO molecules on the NaCl(100) surface, we used a Molecular Mechanics (MM) model as opposed to a Quantum Mechanics (QM) model. In a QM model a set of nuclei and electrons are given, and the Potential Energy Surface (PES) for variations in the nuclei positions can be constructed by explicitly solving the Schrödinger's equation for the motion of the electrons. An accurate determination of the electronic wave function is very demanding and constructing a complete PES for molecules containing more than three to four atoms is almost impossible in terms of computer time and cost. On the other hand, the molecules in a MM model are represented as a collection of atoms held together by bonds and may be regarded as a set of vibrating spheres. The interaction energy is usually written as a sum of the bonding (energies from the changes in bond length and bond angles) and non-bonding terms (energies arise from van der Waals and electrostatic interactions) between the atoms. Also, the parameters used in the function are fit to experimental results to further refine the chosen potential. A detailed analysis of the potential function used will be given in chapter three.

The last step of a molecular simulation comprises the calculations of the desired *macroscopic* terms like pressure, internal energy etc. from detailed information of the molecules at the *microscopic* level (atomic positions, orientations and velocities *etc*).[34] The conversions are made possible by the use of *statistical mechanics* (SM). For a simple one-component system (*i.e.* one type of molecule), its thermodynamic state is usually defined by a small set of parameters such as the number of particles N, the temperature T, and the pressure P. The positions and momenta of the individual molecules can be thought of as coordinates in a multidimensional space, *i.e.* its *phase space*. Let Γ denote a particular point in phase space; then the instantaneous value of some property **A** (for example the potential energy function) may be expressed as a function of $\mathbf{A}(\Gamma)$. The function will change in time and the experimentally observable 'macroscopic' property $\mathbf{A}_{obs}$ is obtained by taking the time average of $\mathbf{A}(\Gamma)$ over a long time interval: *viz.*

$$A_{obs} = \langle \mathbf{A}(\Gamma) \rangle_{time} = \lim_{t_{obs} \to \infty} \frac{1}{t_{obs}} \int_0^{t_{obs}} A(\Gamma(t))dt \qquad (2.1)$$

The above integration cannot be done in infinite time, but it might be satisfied by taking an average over a long finite observation time, t_{obs}. In a simulation, t_{obs} can be expressed as τ_{obs}, which is purely a number obtained by counting the observations made through out the whole trajectory. Therefore, Eq. 2.1 can be rewritten as follows,

$$A_{obs} = \langle \mathbf{A}(\Gamma) \rangle_{time} = \frac{1}{\tau_{obs}} \sum_{\tau=1}^{\tau_{obs}} A(\Gamma(\tau)) \qquad (2.2)$$

In the above equation, $\tau_{obs} = \frac{t_{obs}}{\delta t}$. In short, τ is an index running over the successive cycles in Monte Carlo simulation. Because of the complexity of the time evolution of $\mathbf{A}(\Gamma(\tau))$ for large numbers of molecules, one can instead do an *ensemble average (Gibbs average)* by sampling a set of uncorrelated configurations of the system. The average value includes the result for every molecule in the simulation. This corresponds to the concept of an ensemble of molecules and is therefore called an ensemble average[35] and this is the central idea in Monte Carlo simulations

An ensemble is a collection of points Γ in phase space that are distributed according to a probability density $\rho(\Gamma)$. Each point in phase space represents the dynamical state of a typical system at any particular instant of time. Each system is found to evolve in time independently of other systems. With time, the phase space density, $\rho(\Gamma(t))$, will change. If $\rho_{ens}(\Gamma)$ represents an equilibrium ensemble, each system will cover all regions in phase space, and the system is termed *ergodic*. Consequently, one can successfully replace the time average in Eq. (2.2) by an ensemble average taken over all the points in a set of states in phase space.

However in order for this ensemble average to work some conditions have to be satisfied:[34]

- the probability density, $\rho_{ens}(\Gamma)$, for the ensemble should not change as the system evolves,
- as the simulation proceeds, any starting condition distribution $\rho(\Gamma)$ should evolve to the same $\rho_{ens}(\Gamma)$, and
- we should be able to assume that the system is ergodic in principle, even though we can not hope to prove that it truly happens in practice.

If the above conditions are satisfied, from an initial state and in the long term, one should be able to generate a succession of state points in accordance with the probability density $\rho_{ens}(\Gamma)$. Hence, the ensemble average in this case is considered to be equal to a kind of conventional 'time average':

$$A_{obs} = \langle \mathbf{A} \rangle_{ens} = \langle A | \rho_{ens} \rangle = \sum_{\Gamma} A(\Gamma) \rho_{ens}(\Gamma) \approx \frac{1}{\tau_{obs}} \sum_{\tau=1}^{\tau_{obs}} A(\Gamma_{(\tau)}) \rho(\Gamma_{(\tau)}) \quad (2.3)$$

In a sensible simulation, τ_{obs} would be a large finite number to ensure ergodicity for the system. There are four common statistical ensembles used in computer simulations and they are:

- The microcanonical with fixed number of particle *N*, volume *V*, and energy *E*, or constant-NVE ensemble.

- The canonical with fixed number of particle N, volume V, and temperature T, or constant-NVT ensemble.

- The grand canonical with fixed chemical potential μ, volume V, and temperature T, or constant-μVT ensemble.

- The isothermal-isobaric with fixed number of particle N, pressure P, and temperature T, or constant-NPT ensemble.

The choice of the ensemble again depends on the question that one wishes to resolve. For example the microcanonical ensemble can be used to simulate a close system because of fixed energy and number of particle. The canonical is suitable for simulating adsorption process while the grand canonical can be used to study desorption process because it can handle a change in number of particles.

2.2 The Simulation Set-Up

To understand the simulation set up, consider a system of N molecules where their positions are placed in a Cartesian coordinate system, as illustrated in Fig. 2.1. The origin of the (100) surface is located on a Cl^- ion in the plane of the surface. The top view of the NaCl(100) surface showing the x and y axes running along the [1,-1,0] and [1,1,0] crystallographic directions, respectively, while the z

axis is perpendicular to the surface pointing out of the page. The (+) symbol represents the Na^+ ion while the (-) symbol represents the Cl^- ion. The molecules are also placed in spherical polar coordinate system to discuss the orientation of the molecules with respect to the surface as may also be seen in Fig. 2.1. A molecule in this system is represented by $\vec{r}_i$, the position vector of the molecule from the origin to the carbon atom, and by the orientation vector $\vec{\Omega}_i$ of the molecule "i". The orientation $\vec{\Omega}_i$ can be specified by the angles the molecular axis makes with the z-axis, θ (polar angle), and with the x-axis in the xy-plane, φ (azimuthal angle).

To simulate an overlayer of CO molecules, a canonical ensemble of N molecules, with constant NVT, was placed in the NaCl surface potential. The steps in a Monte Carlo simulation are as follows:[35]

a. Choose an initial set of atom positions with the coordinates according to the above definitions.

b. Compute the initial potential energy for the system $E(\vec{r},\vec{\Omega})$. The calculated potential for each molecule is the summation of all the $E(\vec{r},\vec{\Omega})$ between the molecule of interest and the other sites surrounding it. It is stored as the old energy, $E'_{old}(\vec{r},\vec{\Omega})$:

$E(\vec{r},\vec{\Omega})$ between the molecule of interest and the other sites surrounding it. It is stored as the old energy, $E^{i}_{old}(\vec{r},\vec{\Omega})$:

$$E^{i}_{old}(r,\Omega) = \sum_{j=1}^{N} E(r_{ij},\Omega_{ij}) \qquad j \neq i \tag{2.4}$$

where $\vec{r}_{ij} = \vec{r}_i - \vec{r}_j$, $\vec{\Omega}_{ij} = \vec{\Omega}_i - \vec{\Omega}_j$ and the indexes i, j denotes molecule *i* and *j*, respectively.

c. Randomly choose a trial move for the system by moving one molecule at a time. At the beginning of the simulation a single molecule is chosen at random and moved by randomly translating it along the three directions x, y, and z (positional change) or rotating it around its molecular axis (orientational change) to generate a new configuration. The move is carried out by multiplying the amplitudes (maximum allowed displacement of the molecule, *i.e.* the size of the move) of translation or rotation by a randomly generated number to create a change in position. The amplitudes are adjustable parameters that are used to control the acceptance ratio and to govern the convergence and efficiency of the simulation. These parameters should neither be too small nor too large because in both cases the phase space of the system is explored slowly. If these parameters are too small (hence, the size of the move is also too small) then a large fraction of moves are needed for the atom locations to

change. On the contrary, if amplitudes are too large (so does the size of the move) then nearly all trial moves are rejected. The satisfactory ratio of acceptance to failure (i.e. the hit:miss ratio) in a MC simulation should be 1:1 and so the acceptance rate should be 50%. This ratio is maintained near this value throughout the simulation by regularly adjusting the amplitudes at small intervals, *i.e.* at every 10 cycles.

d. Compute the potential energy of the system in the new configuration, $E^{i}_{new}(\vec{r},\vec{\Omega})$; and calculate the energy difference, δE^{i}, where $\delta E^{i} = E^{i}_{new}(\vec{r},\vec{\Omega}) - E^{i}_{old}(\vec{r},\vec{\Omega})$.

e. Decide whether to accept the new configuration. There is an acceptance criteria based on the old and new energies, which will ensure that the results reproduce a Boltzmann distribution, p. There are two cases to consider for the acceptance of the move:

- $\delta E \leq 0$ then the move is always accepted
- $\delta E > 0$ then its Boltzmann factor $p = exp(-\delta E/k_B T)$ is calculated.

This factor is then again compared to a random number, ξ, generated between 0 and 1, if

- $p \geq \xi$ (*e.g.* point ξ_1 in Fig. 2.2) the new configuration is accepted

otherwise,

- $p < \xi$ (*e.g.* point ξ_2 in Fig. 2.2) the move is rejected.

If the move is rejected, the molecule resumes its previous position. The acceptance criteria can be viewed from Fig. 2.2. This procedure can be summarized by noticing that we accept all moves with $\delta E_{ij} \leq 0$; on the other hand, moves with $\delta E_{ij} > 0$ are accepted only if they have properly weighted Boltzmann probability, *p*.

f. The above process is repeated until all the molecules in the system have attempted a move; thus ending one 'cycle'. Next another molecule is chosen at random to start the new cycle; and the process continues until the system has equilibrated. In common practice, the molecules can be moved sequentially (i.e. in order of molecule index) instead of in a random fashion in order to save some computer time in generating random numbers.

g. Continue to iterate steps c through f and collect data to compute the desired property. The expectation value of any property is its average value (sum divided by the number of iterations summed). This is correct as long as the acceptance criteria in step "e" ensured that the probability of a configuration being accepted is equal to the probability of it being included in a Boltzmann distribution.

In order to run an efficient MC simulation, care must be taken in setting up the boundary conditions and interaction cut-off. One of the advantages of a computer simulation is the ability to calculate 'macroscopic' properties from results of a relatively small number of particles by implementing periodic boundary conditions. This condition is especially useful in forming an infinite system from a small finite number of particles because they eliminate boundary effects so that the system has only bulk like behaviour.[34] For molecules at a surface in Fig. 2.3, the two-dimensional square of particles is replicated in all directions to give a periodic array. Eight neighbours surround each square box; and by simply adding or subtracting integral multiples of the box size one can compute the coordinates of each particle in the image square box. During the simulation, should one of the particles in the central box cross the boundary, one of its periodic images will move in through the opposite face.[34] The size of the central box depends on the range of the intramolecular force, which in turn determines the maximum interaction distance (i.e. cut off distance) between two molecules. The solid surface is set up as an infinite array of Na^+ and Cl^- ions by the use of periodic boundary condition. Since our investigations are of the adsorption of small molecules onto isolated surfaces, it is inappropriate to put a boundary condition in the direction perpendicular to the surface. Instead a wall (at a distance of 18.0Å from the surface) is applied to this direction to prevent the molecules from evaporating. The size of the central square box was originally set up as 39.88Å (10 surface square lattices). The box size was later increased up to

79.76Å (20 surface square lattices) in some studies to minimize the finite size effects and minimize the fluctuations of the statistical results in quantitative studies of the phase transition.

In order to determine the cut-off distance, one considers the contributions to the potential calculation of molecule *i* from other molecules *j*; presumably the potential is pair-wise additive. Then, one must include interactions between molecule *i* and every other molecule *j* in the simulation box. For a system of N molecules there will be (N-1) terms. In principle one must also include the contributions from the periodic images of the other molecules *j* lying in the neighbour boxes; and this is an infinite numbers. However in practice, it is impossible to perform such a task for simulation of a large number of molecules (let's say for 1000 molecules). Moreover, it is inappropriate to calculate negligible energy between molecules that are very far apart, i.e. those whose distances are greater than the effective range of the potential. To cut down on the amount of unnecessary computing, one can restrict the number of interactions to those molecules *j* that are close enough to be influenced by molecule *i*. That is to apply a spherical cut-off radius r_c around molecule 1, which is represented by the dash circle in Fig. 2.3. In other words one just needs to calculate all the interaction potentials for $r_{ij} \leq r_c$ where r_{ij} is the distance between molecules *i* and *j*. This application significantly reduces the simulation time. For a system that also has a

periodic boundary condition the cut-off radius should not be so large (if the distance is more than half the box) that the particle can see and interact with its own image nor interact with more than one image of other molecules. Hence, the cut off radius must be less than half the length of the box. For the lateral interactions of the adsorbed molecules in our studies, the cut-off distance was defined to be 16.5Å in all monolayer and submonolayer coverage studies; and it was increased to 18.5Å in multilayer system in order to have better interactions between molecules in different layers.

In simulations of molecules adsorbed onto surfaces, a molecule's neighbours (*i.e.* those molecules that are within the cut-off radius, r_c) do not change significantly over a short number of MC iterations. Thus a list of each molecule's neighbours can be initially computed and updated at regular time intervals throughout the simulation. Between updates, the neighbours' identities are kept constant and they are used directly in calculating the system's energy without recalculating the distances between the adjacent molecules. The construction of the neighbour list can save a substantial amount of computer time used in the calculation of the pair distances for each molecule. However in our studies, we did not have to update our lists because the lateral movements in our system are so small that the molecules remain in the same local area during the simulation. Initially we constructed the lists using the surface ionic

coordinates. These are fixed throughout the simulations but we still calculate the pair distances for each move in order to calculate the new energy of the system. In other investigations whenever the lists could be changed, they were updated at a frequency of 5 cycles.

The length of the simulations after being properly equilibrated varied from $7x10^5$ cycles up to $2.5x10^6$ cycles depending on how close the system was to the transition temperature. Large fluctuation in this transition region requires an increase of the length of the simulation in order to yield reliable sample averages. Studies of the structure and thermal stability are done in the temperature range from 1K to 75K for most of the simulations in the monolayer system.

To begin a simulation, we chose an energy model to describe the interactions within the system. Next we established the initial configuration for the system. Then once an algorithm to generate the phase space "trajectory" was specified, the simulation was performed. First, an equilibration phase was carried out. During this phase, energy was monitored until stability was reached within the system. This was determined by examining the energy fluctuations within the system. If the energy fluctuated around a constant average value then the system was in equilibrium. After the system was equilibrated, the production

phase commenced. In this phase observable properties of the system were calculated by simply averaging over a finite number of configurations. The last stage of the investigation was analyzing the statistical data obtained during the production phase.

2.2 Data Analysis

Once the equilibration phase finishes the production phase begins. At the end of this phase, if the system is allowed to have large enough numbers of iterations, correct sampling of all possible configurations, *viz.* its phase space, is obtained. During the simulation, some properties are computed and stored for later analysis.

To study the structural properties of the adsorbed molecules we use the actual coordinates of the atoms to represent the positions of the CO molecules at the surface, and the angular distributions (θ and φ) to provide a complete description for the molecular orientations. The tilt angle, θ, and the azimuthal angle, φ, are defined as shown in Fig. 2.1. A study of the progression of the angular distributions can be used to qualitatively monitor the existence of the

two-dimensional phase transition of the monolayer as well as to estimate the transition temperature. However, a determination of an exact temperature as well as the nature of the transition is not possible. In order to do that, we need to calculate the statistical average quantity of the internal energy, the order parameter and their associated fluctuations. Plots of these quantities as a function of the temperature give the information needed on the phase transition of the monolayer system. By definition, a phase transition occurs when there is a singularity in the energy or one of its derivatives (*viz.* fluctuations). If there exists a finite discontinuity in one or more of the first derivatives of the appropriate thermodynamic potential the transition is classified as a first-order phase transition, for example the process of melting and vaporization. On the other hand, if the first derivatives are continuous but second derivatives are discontinuous or infinite, the transition will be described as higher order or continuous. This type of transition corresponds to a convergent heat capacity.[36] Examples from the higher order phase transition include order-disorder transition in alloys, and the onset of ferromagnetism. Since the shape of the heat capacity in this case looks like the Greek letter λ, this type of phase transition is also termed a λ-transition. Analogous behaviour to the potential energy is seen in the study of the order parameter and its first derivative (*i.e.* susceptibility). Therefore, these quantities are also included in our quantitative analysis in order to determine the nature of the phase transition.

The total energy of the system E_j is computed at each cycle "j" and stored for later analysis. At the same time, one should also compute E_j^2 for later calculation of the energy fluctuations. At the end of the simulation, the total energy of the system is calculated as follows:

$$\langle E_j \rangle = \frac{1}{M} \sum_{j=1}^{M} E_j \tag{2.5}$$

where M is the total number of cycles throughout the production step. The associated heat capacity, C_v, which is the fluctuation of the binding energy, is defined to be

$$C_V = \frac{1}{M} \sum_{j=1}^{M} \frac{\left(\langle E_j^2 \rangle - \langle E_j \rangle^2 \right)}{N k_B T^2} \tag{2.6}$$

where N is the total number of molecules, k_B is the Boltzmann constant and T is the simulation temperature.

Another quantity of interest in monitoring the phase transition is the orientational order parameter, Ψ. This quantity is defined as the sum of the transformed molecular orientations. In the ordered state the molecules are found to form a p(2x1) structure where molecules in the same rows are aligned with each other whereas they are oriented in the opposite direction with those in the

neighbouring rows. In order to define an order parameter that has a value of 1 in the ordered state, we temporarily flip the molecules in every second row so that the molecules of the whole layer line up in the same direction. It should be noted that this operation is done at the end of each cycle and does not interfere with the real orientation of the molecules. A value of 1 indicates that the molecules are perfectly ordered and an orientational disorder is indicated by a value of 0. The order parameter, ψ, is the average of the transformed molecular orientations, Φ_{xj} and Φ_{yj}, in the x and y directions at cycle "j", respectively, as defined below

$$\Psi_j = \frac{1}{M}\sum_{j=1}^{M}\sqrt{\Phi_{xj}^2 + \Phi_{yj}^2} \tag{2.7}$$

For a given cycle "j" the transformed orientations are summed over all molecules, N, *viz.*

$$\Phi_x = \frac{1}{N}\sum_{i=1}^{N}(-1)^{nyi}\cos(\varphi_i) \tag{2.8}$$

and

$$\Phi_y = \frac{1}{N}\sum_{i=1}^{N}(-1)^{nxi}\sin(\varphi_i) \tag{2.9}$$

where the index j has been suppressed, $\cos(\varphi_i)$ and $\sin(\varphi_i)$ are respectively the orientations in the x and y directions of molecule "i", , and nxi,nyi = 1,2,3,...,L represent the x and y positions of the cation adsorption site of molecule "i" on the surface lattice. Note that $L^2 = N$. The susceptibility, χ, which is defined as the fluctuation of the order parameter, is also calculated using the following expression

$$\chi = \frac{1}{M}\sum_{j=1}^{M}\frac{\left(\left\langle \Psi_i^2 \right\rangle - \left\langle \Psi_i \right\rangle^2\right)}{T^2} \qquad (2.10)$$

again M is the total number of cycles and T is the simulation temperature.

During the simulation, the energy and order parameter are computed at the end of each cycle and are then averaged while their associated fluctuations are calculated once at the end of the simulation using the required averaged quantities. Those values are then plotted against the simulated temperature for the quantitative analysis of the two-dimensional phase transition in the monolayer regime.

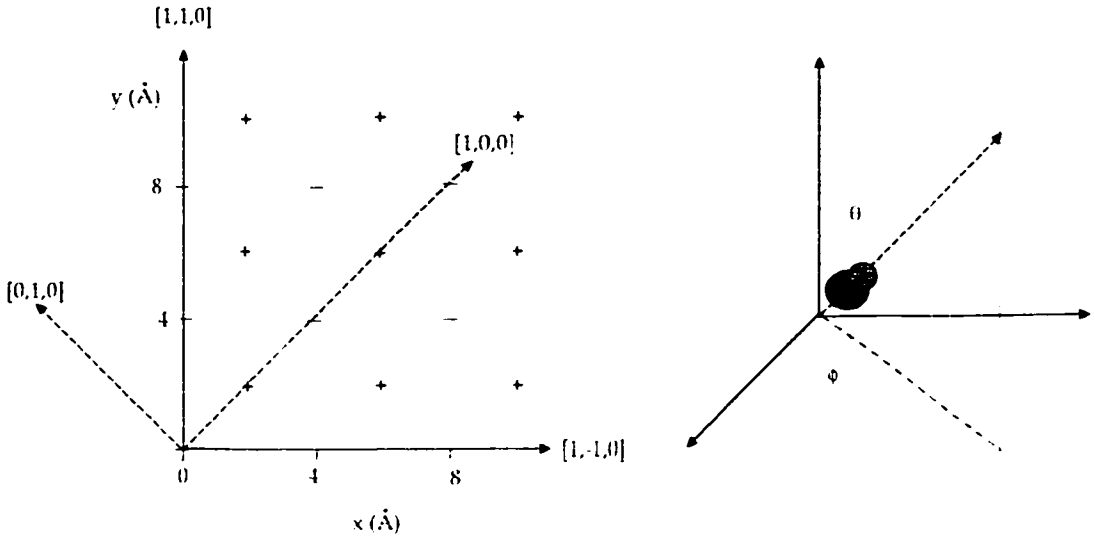

Figure 2.1. The Cartesian and the Polar coordinates of the molecule

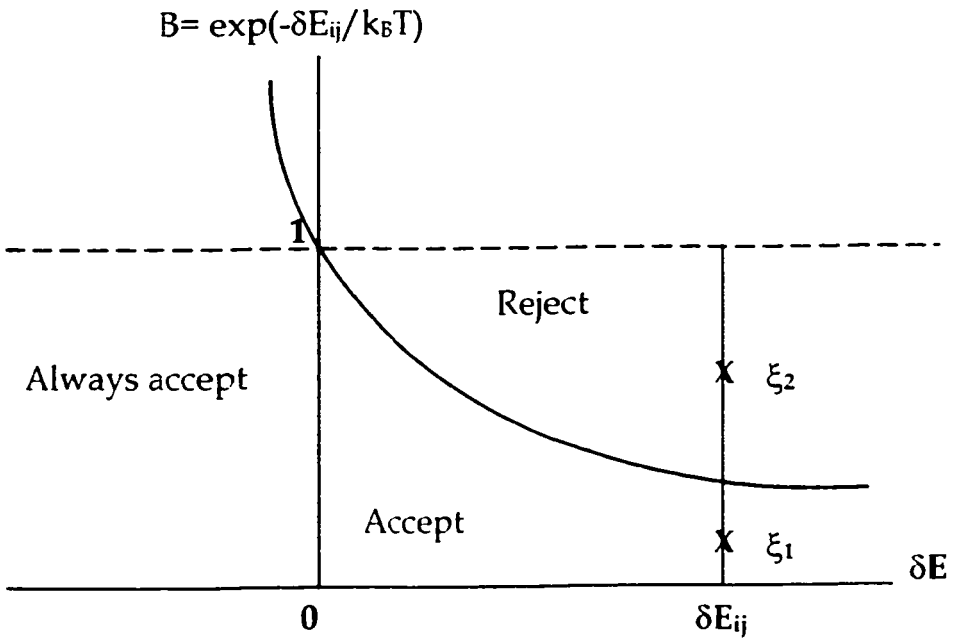

Figure 2.2. Illustration of the acceptance criteria in the Monte Carlo Simulation. Taken from Ref. [21]

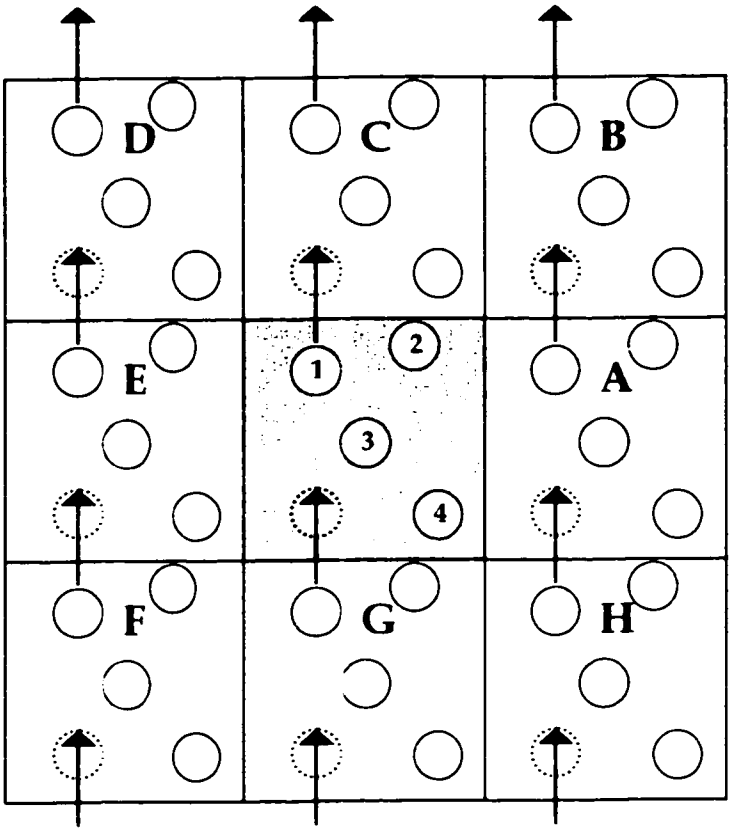

Figure 2.3. The boundary effect in two-dimensional box. The darker shade square is the central box. The white squares are the replicated boxes of the central one (i.e. the neighbour boxes). The dotted circles are the periodic images of the circle number 1. The arrows represent the moves. Taken from Ref. [21].

CHAPTER 3: INTERACTION POTENTIALS

The effectiveness of computer simulations to solve chemical problems depends on choosing a good potential energy function that can best describe the interactions between the molecules present in a given system. Typically such a potential is a set of mathematical equations that is used to calculate the physical interactions between collections of molecules. In the case of molecules at a solid surface the potential can be conveniently regarded as being comprised of two additive parts: the molecule-molecule and molecule-surface interactions. These in turn are constructed from the interactions between the various atomic sites (i.e. atom-atom and atom-ion interactions), assuming the two-body additive approximation. Each contribution is comprised of a long-range electrostatic part V_{ele}, which can be handled via the classical multipole expansion of the coulombic interactions between all particles in a system; a dispersion part V_{dis}, which arises at closer separations for all molecules when the motions of their electrons are correlated; and a short-range repulsion part V_{rep} due to core interactions when overlap of the molecular orbitals can no longer be ignored. Finally, the total interaction is treated as the sum of the above pairwise contributions between all molecules in the system. Our chosen potential has been adapted from the study of HBr on LiF(001) by Polanyi and coworkers.[37,38] A detailed analysis of these contributions to the total potential energy function will be discussed in the next two sections along with a brief overview of how the system's parameters are derived.

3.1. The Molecule-Molecule (CO-CO) Potential Function

As was briefly mentioned earlier, the calculated details for the intermolecular interactions that characterize the CO-CO potential have contributions from classical electrostatic interactions, which are calculated by using distributed multipoles (point charges and point dipoles), and from core repulsion-dispersion interactions, which are described by an undamped form of the Tang-Toennies potential, at the atomic sites. Since CO is a diatomic molecule we have two atomic sites for each molecule and four atom-atom pair interactions for each pair of molecules. These atom-atom pairwise interactions are then summed up to yield the total CO-CO potential in the system.

In our model, the CO molecule is constructed as spherical carbon and oxygen atoms connected by a fixed bond. The gas phase bond length[39] used is 1.128 Å. The molecule was made rigid because at the cold temperature region (T= 1 - 80K) of our simulations the ground state of the CO triple bond is too stiff to have significant vibrations.

The CO molecule has a permanent dipole by virtue of the difference in the electronegativities between the atoms, which results in an unequal distribution of charge within it. With a higher electronegativity, the oxygen atom attracts the electron cloud toward its nucleus more than carbon does, creating a polar bond

with a small negative charge positioned at the oxygen end and a small positive charge at the carbon end. This polar bond gives the CO molecule a small permanent dipole and a large permanent quadrupole moment that contribute to the electrostatic potential energy. These charge distributions can be represented using a distributed multipole expansion. In this method, the CO molecule is divided into two regions, each located at the atomic nucleus and having its own multipole moments: point charge and point dipole as shown in Fig. 3.1; hence the name 'two point charges two point dipoles'. With this distributed multipole set up, we can reproduce the CO electrostatic multipole moments up to the octupole level.

Another possible long-range contribution comes from the induction energy, which is attractive. When a molecule is placed in an external electric field a distortion of the electron cloud in the molecule occurs. This results in an induced dipole, which then interacts with the inducing electric field to produce an attractive force. However, the induction energy was found to be small compared to that of the electrostatic interaction from the distributed multipole expansion (it is found to be about 1% in value). To simplify the calculations, the electric field generated by the surrounded adsorbed molecules is incorporated into the electric field generated by the surface and it will be discussed later. Thus the calculated induction energy is a sum of both the induction energy between the lateral adsorbed molecules as well as from the surface.

3.1.1. The Electrostatic Potential

For a pair of atoms, *i* of molecule A and *j* of molecule B, separated by a distance $r_{ij} = |\vec{r}_{ij}| = \vec{r}_i - \vec{r}_j$, the electrostatic potential, $V_{ele}(\vec{r}_{ij})$, is expressed as a sum of the various electrostatic contributions between charge-charge, charge-dipole and dipole-dipole in terms of atomic separation, $\vec{r}_{ij}$, and molecular orientations, $\vec{\Omega}_A$ and $\vec{\Omega}_B$:[40]

$$v_{ele}^{ij}(\vec{r}_{ij}) = \frac{1}{4\pi\varepsilon_0}\sum_{i\in A}^{2}\sum_{j\in B}^{2}\left\{\frac{q_i q_j}{r_{ij}} + \frac{(q_i\mu_j + q_j\mu_i)}{r_{ij}^2}\cos\theta_{ij} + \frac{\mu_i\mu_j}{r_{ij}^3}\left(\frac{\cos^2\theta - 1}{2}\right)\right\} \qquad (3.1)$$

where $q_{i,j}$, $\mu_{i,j}$ are the magnitudes of the point charges and point dipoles located at the atomic sites of the molecules, and θ_{ij} is the angle between the orientation vectors of molecules A and B. The values of the point charges and dipoles can be determined using the definitions of the molecular multipole moments, namely dipole, quadrupole and octupole moments of the CO molecule.

According to the "2-point charge, 2-point dipole" model (Fig. 3.2) we set up the following equations to solve for the point charges and point dipoles based on the definitions of the molecular multipole moments for linear molecules:

$$\begin{aligned}\mu &= \mu_C + \mu_O + r_C q - r_O q \\ &= \mu_C + \mu_O - r_{CO} q\end{aligned} \qquad (3.2a)$$

$$\begin{aligned}\Theta &= 2r_C\mu_C + 2r_O\mu_O + (r_C^2 - r_O^2)q \\ &= 2r_C\mu_C + 2r_O\mu_O - r_{CO}q(r_C + r_O)\end{aligned} \qquad (3.2b)$$

$$\Omega = 3(r_C^2\mu_C + r_O^2\mu_O) + (r_C^3 - r_O^3)q$$
$$= 3(r_C^2\mu_C + r_O^2\mu_O) - r_{CO}q(r_C^2 + r_C r_O + r_O^2) \quad (3.2c)$$

where $r_{CO} = r_O - r_C = 1.128$ Å, $r_C = -\frac{4}{7}r_{CO}$, and $r_O = \frac{3}{7}r_{CO}$ (r_C and r_O are with respect to the center of mass of r_{CO}. Solving for q, μ_c and μ_o:

$$\mu_C = \frac{1}{r_{CO}^2}\left[\Omega - 2(\frac{r_{CO}}{7})\Theta - 15(\frac{r_{CO}}{7})^2\mu\right] \quad (3.3a)$$

$$\mu_O = \frac{1}{r_{CO}^2}\left[\Omega + 5(\frac{r_{CO}}{7})\Theta - 8(\frac{r_{CO}}{7})^2\mu\right] \quad (3.3b)$$

$$q = \frac{1}{r_{CO}^2}\left[2\Omega + 3(\frac{r_{CO}}{7})\Theta - 72(\frac{r_{CO}}{7})^2\mu\right] \quad (3.3c)$$

Substituting the experimental values of dipole moment μ,[41] the average quadrupole moment Θ (from *ab initio*),[42,43] and the SCF calculated octupole moment Ω[44,45] listed in Table 3.1 into equations 3.3 (a, b, c) gives the values of the atomic point charges and point dipoles used in equation 3.1, and are listed in Table 3.2 as well as shown in Fig. 3.2.

Table 3.1. Experimental electrostatic multipole moments of CO molecule.

Dipole (μ) - (D)	0.11
Quadrupole (Θ) - (D.Å)	-2.02
Octupole (Ω) - (D.Å^2)	2.77

Table 3.2: Electrostatic parameters for CO-CO interaction potential. The dipoles are oriented along the molecular axis with the carbon to oxygen direction.

	Point charge (q_i) (esu)	*Point dipole* (μ_i) (D)
Carbon (i=1)	3.03628	2.65499
Oxygen (i=2)	-3.03628	0.87993

3.1.2. The Dispersion-Repulsion Potential

The electrostatic potential function alone cannot account for interactions at shorter distances, i.e. when the distance between the molecules is smaller than their dimensions. At close separation, the dispersion-repulsion energy will make a significant contribution to the interaction between molecules. The dispersion energy varies with the separation: at infinite distance the energy is zero, and as the separation gets smaller the energy decreases and passes through a minimum (the molecules are attracted to each other); then it rapidly rises as the separation gets very small (the molecules repel at short separations).

The nature of the dispersion forces between a pair of atoms or molecules is that of the interaction between instantaneously induced multipole moments brought about by the correlation of electron clouds.[40] The electrons in the atom are constantly moving around the nucleus, giving rise to instantaneous multipole

moments, which in turn induce instantaneous moments in neighbouring atoms. At large separations (usually farther apart than the equilibrium separation), those multipole moments in phase with those of the first atom, result in an attractive force known as dispersion. The dispersion energy, $v_{dis}(\vec{r}_{ij})$, can be expressed as follows:

$$v_{dis}(\vec{r}_{ij}) = \sum_{i=1}^{2}\sum_{j=1}^{2} -\frac{C^{ij}_6}{r_{ij}^{6}} - \frac{C^{ij}_8}{r_{ij}^{8}} - .... \qquad (3.4)$$

where $r_{ij} = |\vec{r}_{ij}|$ is the atomic distance and the C^{ij}_6, C^{ij}_8 are the attractive constants at various atomic sites: C-C, C-O, O-C and O-O. The first term in the summation represents the instantaneous dipole-dipole interaction, and the second one is the expression for the instantaneous dipole-quadrupole interaction. The dispersion energy is seen to be attractive and to fall off as r^{-6} for the first term, and as r^{-8} for the second contribution. At large distances only the first term makes a considerable contribution to the energy. However, at short distances the contributions from the higher order term should not be neglected.

The value of C_6^{CO} for a CO molecule (C_6^{CO} = 88.400 a.u. = 34.900 Å^6.kcal.mol^{-1})[46] is documented from the critical study of Mulder *et al.* The value for higher order dispersion term can be calculated from the ratio $R^{CO\text{-}CO} = \frac{C_8^{CO}}{C_6^{CO}} = 30.400$ a.u. = 2.8980 Å^2,[46] which is obtained from a generalized *ab*

initio Kirkwood (SCF) calculation. As such, these molecular values are not suitable in our energy potential function, which has interactions at the atomic sites. To obtain the atomic values for the first parameter from the dispersion series, namely C_6 of the like-atom (i.e. interaction between C-C and O-O) we used the computer program WMIN[47] to optimize the binding energy, assuming the following relation,[48]

$$C_6^{CO-CO} = C_6^{C-C} + C_6^{O-O} + 2C_6^{C-O} \tag{3.5}$$

by varying C_6^{C-C} and C_6^{C-O} subject to equation 3.5 with the constraint that the molecular value of C_6^{CO} is kept constant. The atomic parameters are allowed to vary while the cohesive energy of the crystal is minimized in the program. In order to do this calculation, we input the crystal structure (such as position, orientation, lattice constant) of the solid α-CO along with the atomic electrostatic parameters and the molecular value for the C_6^{CO}. The atomic dispersion parameters, c_6^C and c_6^O, obtained from WMIN are given in Table 3.3 where $C_6^{C-C} = (c_6^C)^2$. In order to calculate the unlike-atom dispersion parameters, C_6^{C-O}, between the C-O interaction, we used the combining rule, $C_6^{C-O} = (c_6^C c_6^O)^{1/2}$.

The higher atomic coefficients, c_8^C and c_8^O, are obtained using the above molecular ratio[46] R^{CO-CO} assuming that the atomic ratios are equal to the molecular one, hence,

$$R^{CO\text{-}CO} \approx \frac{C_8^{C\text{-}C}}{C_6^{C\text{-}C}} \approx \frac{C_8^{O\text{-}O}}{C_6^{O\text{-}O}} \tag{3.6}$$

In terms of the atomic dispersion parameter, c_8^C, we have the following relation,

$$\frac{C_8^{C\text{-}C}}{C_6^{C\text{-}C}} = \frac{\left(c_8^C\right)^2}{\left(c_6^C\right)^2} \approx R^{CO\text{-}CO} \tag{3.7}$$

Hence,

$$c_8^C \approx c_5^C \sqrt{R^{CO\text{-}CO}} \tag{3.8}$$

The c_8^O parameter is similarly calculated and the values for the atomic dispersion parameters are listed in Table 3.3.

Table 3.3 Dispersion coefficients and repulsion parameters for CO-CO interaction potential calculated from WMIN program.[47]

	Carbon	*Oxygen*
ar (Å)	1.7618	1.6562
br (Å)	0.1357	0.1711
c_6 *(Å^6·kcal.mol^{-1})*	17.9900	16.9100
c_8 *(Å^8·kcal.mol^{-1})*	52.1340	49.0100

At still shorter separations, the overlap of the electron cloud is significant, and the repulsive potential between of two molecules, $v_{rep}(\vec{r}_{ij})$, is expressed as follows:

$$v_{rep}(\vec{r}_{ij}) = \sum_{i=1}^{2}\sum_{j=1}^{2} A_{ij} \exp(-\beta_{ij} r_{ij}) \tag{3.9}$$

where $r_{ij} = |\vec{r}_{ij}|$ is the distance between the atoms, the Born-Mayer parameters A_{ij} and β_{ij} are the strength and the decay constants which represents the range of the repulsive potential at various atomic sites, respectively. The Born-Mayer parameters can be expressed in terms of the atomic radii, *br*, and range of the repulsion interaction, *ar*, at the atomic sites:

$$A_{ij} = (br_i + br_j)\exp\left\{\frac{ar_i + ar_j}{br_i + br_j}\right\} \tag{3.10}$$

$$\beta_{ij} = \frac{1}{br_i + br_j} \tag{3.11}$$

The atomic parameters, *br*, and *ar*, were also obtained from the WMIN program. Again, the program minimizes the energy by varying the *br* and *ar* parameters. A list of these values can be found in Table 3.3

The potential $v(\vec{R}_{AB}, \vec{\Omega}_A, \vec{\Omega}_B)$ for a pair of molecule A, and B at the atomic sites *i* (belongs to A), and *j* (belongs to B) whose centers of mass are separated by a distance $R_{AB} = |\vec{R}_{AB}|$ (usually taken as the distance between the centers of mass

of the atoms) is a sum of all the atom-atom pairwise contributions from electrostatic, dispersion and repulsion potential functions,

$$v(\vec{R}_{AB},\vec{\Omega}_A,\vec{\Omega}_B)=\sum_{i=1}^{2}\sum_{j=1} v_{ele}(\vec{r}_{ij})+v_{dis}(\vec{r}_{ij})+v_{rep}(\vec{r}_{ij}) \qquad (3.12)$$

where $\vec{\Omega}_A$ and $\vec{\Omega}_B$ (specified by the molecular axis for a diatomic molecule) describe the orientations of molecule A and B. The total molecule-molecule potential, $V(\vec{R}_{AB},\vec{\Omega}_A,\vec{\Omega}_B)$, of the system is the sum of all the molecule-molecule pair potentials:

$$V(\vec{R}_{AB},\vec{\Omega}_A,\vec{\Omega}_B)=\sum_{A}^{N}\sum_{B>A}^{N} v(\vec{R}_{AB},\vec{\Omega}_A,\vec{\Omega}_B) \qquad (3.13)$$

where N is the total number of the molecules in the system.

3.2. The Molecule-Surface (CO-NaCl) Potential Function

Owing to the small experimental frequency shift upon adsorption (at 22K the adsorption band of CO admolecules[18] is at 2155.01 cm^{-1}, blue shifted from the gas phase[39]) with a value of 2143 cm^{-1}, as well as the small observable adsorption energy[20,22] (-14.0 ± 1 kJ/mol (3.35 ± 0.2 kcal/mol) to 16.3 ± 1.6 kJ/mol (3.89 ± 0.4 kcal/mol), we can rule out the possibility of chemical bonding between adsorbed CO molecules and the NaCl surface. Thus the physisorption potential may be treated as a pair-wise additive sum, assuming the two-body approximation, between the constituent atoms and ions of the CO molecules and ionic substrate.

The NaCl surface was constructed as an array of closed-shell ions, with periodicity in the x, y directions and the z-axis taken to be perpendicular to the surface. According to a perturbation theory[19] study by Stone *et al.*, there is only a slight expansion of the ions in the outer layer compared to the interlayer spacing within the bulk (2.895Å from the SCF study and 2.814 Å at the experimental value) was observed. Hence, the structure of the NaCl(100) clean surface could be considered ideal and we are justified in assuming that there is no relaxation at the surface (i.e. it has the same lattice constant as in the bulk structure) and the surface ions are constructed with the same positions as those from the perfect bulk lattice so that the surface has the same periodicity in the x, y plane and interlayer spacing in the z direction as in the bulk solid phase. To make the calculations simpler, thermal motions of the ions were ignored in our calculation because of the cold temperature region of the simulations (T= 1 - 80K).

Figure 3.3 shows a schematic diagram of the (100) plane of NaCl bulk lattice as well as our simulated NaCl surface. In our calculations, the x-y plane of the simulated surface was rotated 45° relative to the x′-y′ plane of the bulk lattice, with a simulated lattice constant of $a_o = \frac{a}{\sqrt{2}} = 3.988$ Å (where a is the bulk solid lattice constant and equal to 5.64 Å). Such a rotation aligns the $\hat{x}$ and $\hat{y}$ axes along the edges of the surface unit cell which are both simplified and rotated from the bulk unit cell.

For a molecule that was placed above a surface as seen in the following Fig. 3.4, its three-dimensional vector $\vec{r}$ can be broken up into a two-dimensional component parallel to the surface, denote by $\vec{R}$, and a z component normal to the surface layer; hence, we expressed its coordinate $\vec{r} = (\vec{R}, z)$ with $\vec{R} = \frac{x}{a_0} a_1 + \frac{y}{a_0} a_2$, where a_1 and a_2 are one-dimensional direct lattice vectors of the surface unit cell, and a_0 is the unit cell length which is equal to 3.998Å for NaCl(100). The origin was positioned on top a Cl^- ion. The z axis is perpendicular to the surface, and the x and y axes run along the <1,-1,0> and the <1,1,0> directions, respectively. In a similar approach to the calculation of the molecule-molecule potential energy function, we computed the potential energy between CO molecules and NaCl surface ions as a sum of pair-wise atom-ion interactions (i.e. $C\text{-}Na^+$, $C\text{-}Cl^-$, $O\text{-}Na^+$, $O\text{-}Cl^-$ interactions). Each contribution included a long-range electrostatic potential energy and a short-range 'core' dispersion-repulsion interaction, which is expressed as a Fourier sum.

3.2.1. The Surface Electrostatic Potential

The electrostatic potential energy between the i^{th} atom of the adsorbed molecule, and the i'^{th} ion of the surface lattice contains contributions from the direct Coulomb electrostatic and induction energies. The Coulomb potential, v_{coul} describes the interactions between the distributed atomic charge q_i and

dipole $\vec{\mu}_i$ at the atomic sites of the adsorbed CO molecule *i* and the electrostatic potential $\Phi(r_i)$ and electric field $\vec{E}(r_i)$, respectively, of the NaCl (100) substrate as follows.

$$v_{coul} = \sum_{i=1}^{2} \Phi(\vec{r}_i)q_i + \vec{E}(\vec{r}_i)\cdot\vec{\mu}(\vec{r}_i) \tag{3.14}$$

The electrostatic potential generated by the ions from the substrate lattice is expressed as follows:[37,49]

$$\Phi(\vec{r}) = -\frac{4e}{a_o}\left[\frac{\exp\left(\frac{2\pi z}{a_o}\right)}{1+\exp(\sqrt{2}\pi)}\right]\times\left[\cos\left(\frac{2\pi x}{a_o}\right)+\cos\left(\frac{2\pi y}{a_o}\right)\right] \tag{3.15}$$

where a_o is the lattice constant and e is the charge on a single proton. The electric field is then given by,

$$\vec{E}(\vec{r}) = -\vec{\nabla}\Phi(\vec{r}) \tag{3.16}$$

3.2.2. The Induction Energy

When a CO molecule is placed in a static electric field, E, an electric dipole is induced in it through a distortion of its charge distribution by the external field.[40] The induced electric dipole is proportional to the field and is parallel to it. It has the following expression:

$$\vec{\mu}_{ind} = \tilde{\alpha}\vec{E} \tag{3.17}$$

where the $\tilde{\alpha}$ is the diagonal matrix of the polarizability of the molecule. In our model, anisotropic atomic polarizabilities are used and placed at the nucleus of the carbon and oxygen atoms because their strengths are found to be different in the parallel and in the perpendicular directions. The energy of the induced dipole $\vec{\mu}_{ind}$ in an electric field E is

$$v_{ind} = -\sum_{i=1}^{2} \int_{0}^{\vec{E}} \vec{\mu}_{ind}(\vec{r}_i) \cdot d\vec{E} = -\frac{1}{2}\sum_{i=1}^{2} \alpha^{i}{}_{\perp} E^2(r_i) - \frac{1}{2}\sum_{i=1}^{2} \alpha^{i}{}_{//} E^2(r_i) \qquad (3.18)$$

where $\alpha_{\perp}$ and $\alpha_{//}$ are the polarizabilities in the perpendicular and parallel directions, respectively.

3.2.3. The Surface Dispersion-Repulsion Potential

Assuming the two-body approximation, the dispersion-repulsion interaction energy $v^{i'}_{d-r}$ of a single atom *i* of the admolecule can be thought of as the sum of pairwise interactions $v^{i}_{d-r}(\vec{r}_{ii'})$ where $\vec{r} = (\vec{R}, z_a)$ as previously described and the superscript *i'* refers to the i'th ion of the surface; i.e.,

$$V_{d-r}(\vec{r}_i) = \sum_{i'} v^{i'}_{d-r} \qquad (3.19)$$

The individual $v^{i'}_{d-r}$ are then approximated by expression of the damped Tang-Toennies potential[37,50]

$$v^{i'}_{d-r}(r) = A\exp(-\beta r) - \sum_{3}^{\infty} f_{2n}(r)\frac{C_n}{r^{2n}} \qquad (3.20)$$

where $r = |\vec{r}_{ii'}|$ is the distance between the admolecule i and the i'^{th} ion, and $\vec{r}_{ii'} = \vec{r}_i - \vec{r}_{i'}$. The first term represents the repulsion and the second term represents the dispersion series with damping functions $f_{2n}(r)$ defined by,

$$f_{2n}(r) = 1 - \sum_{k=0}^{2n} \frac{(\beta r)^k}{k!} \exp(-\beta r) \tag{3.21}$$

The damping function, $f_{2n}(r)$, acts to dampen the dispersion series at small internuclear dispersion in the vicinity of the potential well.[50] In other words, it serves to cut off the dispersion series at short distances and avoid the asymptotic divergence in the dispersion series.

However, to run a more efficient Monte Carlo simulation, we replaced the direct sum in the following Eq. (3.22) by a two-dimensional Fourier series for the core potential $V_{d\text{-}r}$[37] because of the periodicity of the NaCl lattice structure. The contribution to the dispersion-repulsion $V_{d\text{-}r}(r_\alpha)$ due to a gas atom (C or O) placed at r interacting with the ions (Na^+ or Cl^-) in a layer of the (100) surface with layer index α (where α denotes a plane) was written as:

$$V_{d\text{-}r}(r_z) = V_{d\text{-}r}(\vec{R}, z_\alpha) = \sum_G W_G(z_\alpha) \exp(i\vec{G}\cdot\vec{R}) \tag{3.22}$$

where the Fourier coefficients $W_G(z_\alpha)$ are given by

$$W_G(z_\alpha) = \frac{1}{a_0^2} \int_{a_0} v^{t'}_{dr}(R, z_\alpha) \exp(-i\vec{G}\cdot\vec{R}) dR \tag{3.23}$$

and a_0^2 is the area of the unit cell as previously defined in Fig. 3.4. The set of G's in the summations are the reciprocal lattice vectors of the substrate lattice. The reciprocal lattice vectors[51] b_1 and b_2 are defined such that $a_1 \cdot b_1 = a_2 \cdot b_2 = 1$ and $a_1 \cdot b_2 = a_2 \cdot b_1 = 0$

$$G = G(m,n) = 2\pi(mb_1 + nb_2) \ , \qquad m,n \text{ integers} \tag{3.24}$$

The G(0,0) in the Fourier series gives the laterally averaged energy as a function of z over the unit cell at constant height z_α above the nuclear plane. It depends only on z_α and it is expressed as $V_{00}(z_\alpha) = W_0(z_\alpha)$. The remaining nonzero G components represent the periodic corrugation, which varies with lateral position over the surface unit cell. Since the corrugation contributions from lower layers ($\alpha \neq 0$) are negligible, only the corrugation resulting from the 'core' dispersion-repulsion potential of the uppermost layer ($\alpha=0$) of the NaCl solid surface is included in the calculations. Consequently, the total interaction (equation 3.22) for a given gas-atom with lattice-ion may be rewritten as follows:

$$V_{d-r} = \left[V_{00}(z_\alpha) + \sum_{G \neq 0} W_G(z_\alpha) \exp(i\vec{G} \cdot \vec{R}) \right]_{\alpha=0} + \sum_{\alpha \neq 0} V_{00}(z_\alpha) \tag{3.25}$$

where the explicit expression for the individual potential has the damping Tang-Toennies form, Eq. (3.20), as previously mentioned. The terms in the square brackets give the laterally averaged and corrugation contributions, respectively, from the top layer ($\alpha=0$) and the last term includes only the sum over the laterally averaged of other lower layers ($\alpha \neq 0$).

The parameters used in Eq. (3.25) are also located at the atomic sites and are constructed in a similar manner as the lateral interaction parameters, namely, from the molecular or 'dislike-atom' values with the application of suitable combining rules. The values for the strength, $A_{i'}$, and the dipole polarizability,[52] $\alpha_{i'}$, for the ions 'in-crystal' can be found in the literature from the work of Fowler *et. al.* as listed in Table 3.4. The 'like-atom' parameters for the atoms are calculated using the values of the radius, *ar*, and softness parameters, *br*, of the C and O atoms obtained from WMIN program. The 'like-atom' parameters, A_{ii} and β_{ii}, are calculated using the equations 3.10 and 3.11 with i=j, respectively. Their values are listed in Table 3.3. The strength of the potential, $A_{ii'}$, between two dislike atoms are derived using the combining rules from Gilbert[53] and Smith,[54]

$$A_{ii'} = \frac{1}{\beta_{ii'}}(A_i\beta_i)^a(A_{i'}\beta_{i'})^b \tag{3.26}$$

where $a = \frac{\beta_{i'}}{\beta_i + \beta_{i'}}$ and $b = \frac{\beta_i}{\beta_i + \beta_{i'}}$, and the decay constant, $\beta_{ii'} = \frac{2\beta_i\beta_{i'}}{\beta_i + \beta_{i'}}$. The subscripts *i* stands for the atom of the molecule (namely C or O) and *i'* for the surface ion (i.e. Na^+ or Cl^-).

The dispersion parameter, $\mathbf{C_6^{ai'}}$, of the molecule CO to the ions are estimated using the combining rule from the Casimir-Polder equation,[55] which has the following expression,

$$C_6^{ai'} = \frac{2C_6^aC_6^{i'}\alpha_a\alpha_{i'}}{C_6^a\alpha_{i'}^{\ 2} + C_6^{i'}\alpha_a^{\ 2}} \tag{3.27}$$

where the superscript *a* stands for the CO molecule and *i'* represents the substrate ions (i.e. Na^+ and Cl^-). Again the values for the C_6[46] and the ratio of the 'like-molecule'[46] ($R^{CO\text{-}CO}$) are quoted from the critical study of Mulder *et al.* and the values for the in-crystal ions are from the *ab initio* calculations of Fowler and coworkers.[56]

The ratios $R^{ai'}$ for the molecule-ion interactions (again *a* represents molecule CO and *i'* is the surface ion) are calculated using a simple arithmetic combining rule,

$$R^{ai'} = \frac{C_8^{ai'}}{C_{10}^{ai'}} = \frac{1}{2}\left(R^{aa} + R^{i'i'}\right) \tag{3.28a}$$

and the value for the $C_8^{ai'}$ is calculated according to the following equation,

$$C_8^{ai'} = C_6^{ai'} \cdot R^{ai'} \tag{3.28b}$$

The $C_{10}^{ai'}$ is estimated using the following relation,[57]

$$C_{10}^{ai'} \approx \frac{49}{40}\frac{\left(C_8^{ai'}\right)^2}{C_6^{ai'}} \tag{3.29}$$

The dispersion coefficients between the atoms C and O with the ions Na^+ and Cl^- are partitioned for each 'dislike-pair' (i.e. C-Na^+, C-Cl^-, O-Na^+, O- Cl^-) for each coefficient based on the ratio of the dipolar polarizability as follows,

$$C_{2n}^{ii'} = C_{2n}^{ii'} \cdot \frac{\alpha^{i}}{\alpha_{CO}} \tag{3.30}$$

where i stands for the atoms (C or O) and i' stands for the surface ion (Na^+ or Cl^-), n is an integer with values from 3 to 5 and α_c and α_o are the dipolar polarizabilities of carbon and oxygen, respectively. The values of the 'like-molecule' and the ions as well as the values for the 'dislike-atom' pair are given in the following Table 3.5, Table 3.6, and Table 3.7.

The values of the in-molecule atomic polarizabilities are partitioned using the values of the molecular polarizability of CO and the atomic polarizability of carbon and oxygen. According to the following equation,

$$\alpha^{i} = \frac{\alpha^{CO} \cdot \alpha^{j}}{\alpha^{C} + \alpha^{O}} \tag{3.31}$$

where α stands for the isotropic dipole polarizability and i and j represent the atom in the CO molecule and the free atom, respectively. As mentioned earlier in the induction energy calculation (sec. 3.2.2) the isotropic polarizabilities of the atoms are further partitioned to the anisotropic ones in the parallel and perpendicular directions as follows,

$$\alpha_{\perp}^{i} = \alpha_{\perp}^{CO} \cdot \frac{\alpha^{i}}{\alpha^{C} + \alpha^{O}} \tag{3.32}$$

and

$$\alpha_{//}^{i} = \alpha_{//}^{CO} \cdot \frac{\alpha^{i}}{\alpha^{C} + \alpha^{O}} \tag{3.33}$$

and i stands for the atom in the CO molecule. Their values are listed in Table 3.4

Table 3.4: Calculated atomic polarizabilities and the input parameters of CO molecule. The molecular axis defines the sense of direction for the parallel and perpendicular polarizabilities.

	CO	*C*	*O*
Polarizability α *(a.u.)*	13.07 [a]	9.00 ± 0.5 [a]	4.00 ± 0.5 [a]
α^i *(Å³)*		1.44 [c]	0.66 [c]
α *perpendicular* $\alpha_\perp$ *(Å³)*	1.79 [b]	1.23 [d]	0.56 [d]
α *parallel* $\alpha_{//}$ *(Å³)*	2.32 [b]	1.59 [e]	0.73 [e]

[a]: Ref. [46]

[b]: Ref. [58]

[c], [d], and [e]: calculated α's using Eq. (3.32), (3.33) and (3.34), respectively

Table 3.5: Input parameters for the calculations of repulsion parameters.

	C-C	*O-O*	Na^+- Na^+	Cl^- - Cl^-
β *(Å^{-1})*	3.27 [a]	3.795 [a]	5.857 [b]	2.491 [b]
Arep (K.)	3.952×10^7 [c]	3.743×10^7 [c]	2.352×10^8 [b]	9.853×10^6 [b]

[a]: calculated values using Eq. (3.11)

[b]: Ref. [52]

[c]: calculated values using Eq. (3.10)

Table 3.6: Molecular dispersion coefficients for the CO-NaCl interaction potential and the input parameters for the calculations.

	CO-CO	Na^+ - Na^+	Cl^- - Cl^-	*CO* - Na^+	*CO* - Cl^-
Polarizability (α)	13.07 [a]	1.002 [b]	21.153 [b]		
R (a.u.)	30.400 [a]	8.140	33.880	19.27 [c]	32.14 [c]
C_6 *(a.u.)*	88.400 [a]	1.588	180.300	10.213 [d]	125.270 [d]
C_8 *(a.u.)*				196.799 [e]	4026.178 [e]
C_{10} *(a.u.)*				4.744×10^4 [f]	1.986×10^7 [f]

[a]: Ref. [46]

[b]: Ref. [56]

[c], [d]: calculated values using Eq. (3.28a) and (3.27), respectively

[e], [f]: calculated values using Eq. (3.28b) and (3.29), respectively

Table 3.7: Dispersion coefficients and repulsion parameters for the CO-NaCl interaction potential.

	$C\text{-}Na^+$	$C\text{-}Cl^-$	$O\text{-}Na^+$	$O\text{-}Cl^-$
A^a (kCal/mol)	1.983×10^5	0.2441×10^5	2.092×10^5	0.225×10^5
β^a ($Å^{-1}$)	4.196	2.828	4.606	3.008
$C_6{}^b$ ($Å^6$.kCal/mol)	80.937	1,379.513	36.882	628.522
$C_8{}^b$ ($Å^8$.kCal/mol)	532.196	1,1041.620	242.513	5,030.690
$C_{10}{}^b$ ($Å^8$.kCal/mol)	4,286.689	10,8275.800	1,953.375	49,331.690

[a]: calculated values using Eq. (3.26)

[b]: calculated values using Eq. (3.30)

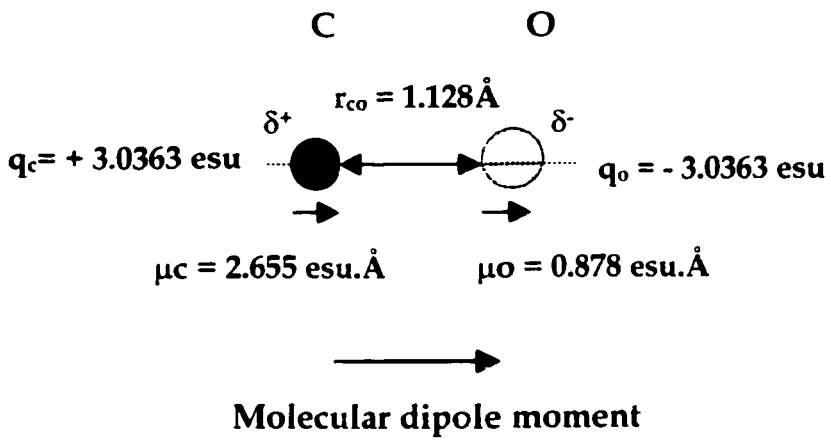

Figure 3.1. The electrostatic model of the CO molecule (1 Debye ≡ 4.805 esu.Å).

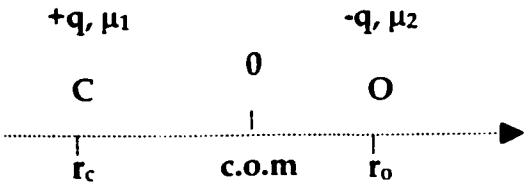

Figure 3.2. "Two-point charge, two-point dipole" model.

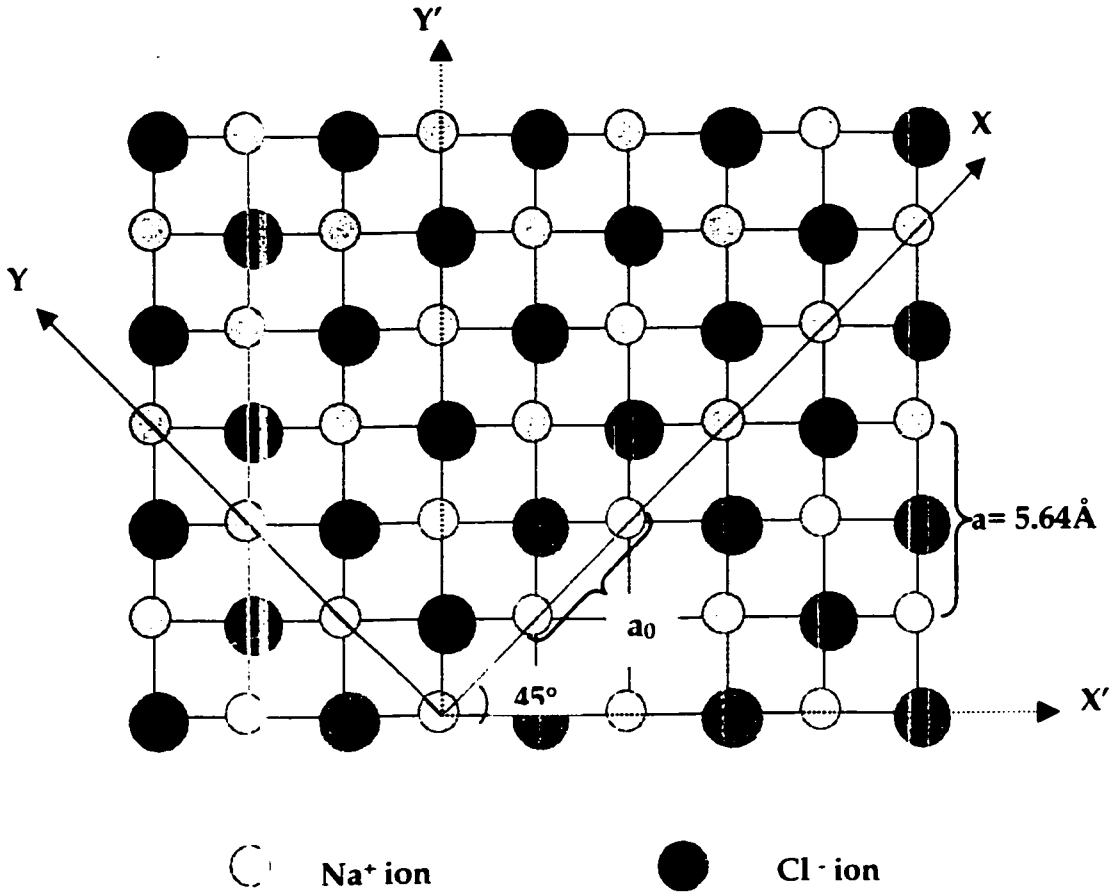

$a_0 = \frac{5.64}{\sqrt{2}}$ Å, and a_0 is the lattice constant of the xy plane of the NaCl(100) surface

Figure 3.3. The schematic diagram of the surface NaCl.

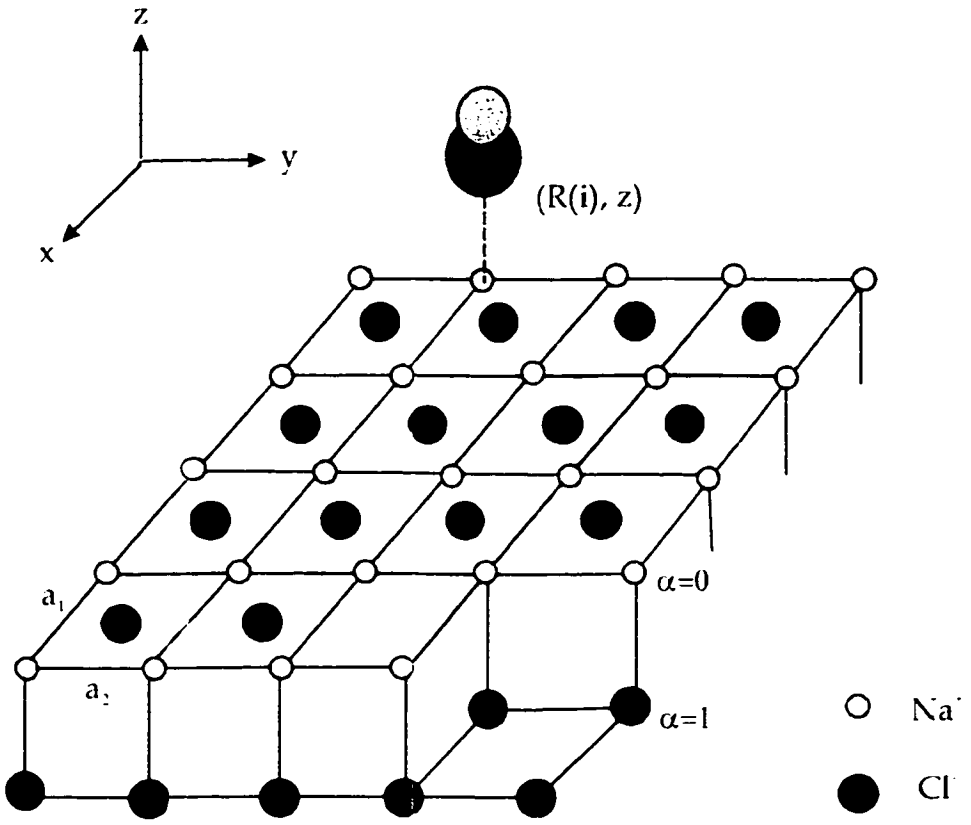

Figure. 3.4. The coordinate axes of the surface NaCl(100) and the adsorbed CO molecule. The length of the unit cell is expressed in Å. Taken from Ref. [37].

CHAPTER 4: RESULTS FOR MONOLAYER CO/NACL(100)

In order to examine the structure of the adsorbed CO layer on the NaCl(100) substrate, we used the Monte Carlo method with a suitable potential function to simulate the interactions between the CO molecules and the surface ions. The ensembles generated in these simulations are of the constant NVT type, *i.e.* the canonical ensemble was used where the number of particles, volume and temperature are kept constant. For a monolayer system (layer with an one-molecule-thickness), we formed a two-dimensional square layer of CO molecules, which has a size of 79.98 Å on each side. The molecules are confined to a region above the solid surface, which is actually a three-dimensional box with the same surface area and a thickness of about 16 Å. The lateral size of the system is made infinite by applying a periodic boundary condition as previously mentioned.

4.1 Adsorption energy

The validity of the potential function relies on the ability of the simulation to reproduce the available experimental results. Besides Monte Carlo simulations we also performed simple energy minimization of an isolated CO molecule adsorbed on NaCl(100) using the Steepest Descent method. The calculated energy was then compared to available experimental values. However, direct comparison is impossible because of the difference between our calculated binding potential energy, which is the lowest energy level of the physisorption

well at zero temperature and zero coverage, and the observed isosteric heat of adsorption, q_{st}, from experiments. The isosteric heat of adsorption is a measurement of an effective binding energy at finite temperature and constant coverage. Using the definition of enthalpy, one can relate both quantities in the following equation,

$$q_{st} = H_g - H_s = \left(\frac{n+2}{n}\right)k_B T - [E_0 + \sum_{\alpha=1}^{n} \frac{\hbar\omega_\alpha}{2} \coth\left(\frac{\hbar\omega_\alpha}{2k_B T}\right)] \qquad (4.1)$$

where q_{st} is the isosteric heat of adsorption, H_g is the enthalpy of the 3-D gas phase, H_s is the enthalpy of the 2-D gas phase adsorbed on the surface, n is the number of degrees of freedom of the molecule (which includes only the vibration and libration of the molecule on the surface and not its internal vibration), ω_α is the frequency of the α^{th} degree of freedom and E_0 is the potential energy minimum at the bottom of the physisorbed energy well. In the high temperature regime, $\frac{\hbar\omega_\alpha}{2k_B T} << 1$ th and $\coth\left(\frac{\hbar\omega_\alpha}{2k_B T}\right) \approx \frac{2k_B T}{\hbar\omega_\alpha}$, hence Eq. (4.1.1) can be rewritten as follows,

$$q_{st} = \left(\frac{n+2}{2}\right)k_B T - E_0 - nk_B T \qquad (4.2a)$$

or

$$q_{st} = -E_0 - \left(\frac{n-2}{2}\right)k_B T \qquad (4.2b)$$

By the use of Eq. (4.2b), along with q_{st} and the temperature of the experiment, one can always calculate the potential minimum, E_0. It is this quantity that we use to compare to our simulated potential at T=0K, and such results can be seen from the following Table 4.1.

Table 4.1 Comparison of heat of adsorption of CO/NaCl(100).

	Method	q_{st} *(kcal/mol)*	E_0 *(kcal/mol)*	T *(Kelvin)*	Θ *(%)*
Ewing[8]	XPS	- 3.346	-3.504	55	~ 0.5
Heidberg[10]	Resonant Infrared Laser Excitation	- 3.890	-4.110	73, 84, 95	0.75
Our result	Energy minimization		-2.971	0	0 (1 CO)
	After adjustment*		-3.9048		

* Adjustment was made to the preexponential factors A_{ij} of the repulsion interactions between the CO atoms and the solid NaCl ions.

According to the result obtained from energy minimization, the resulting surface potential energy is higher than that of the experimental results. This means that our potential function needs to be refined in order to reproduce the experimental heat of adsorption. The adjustments would have to be in the surface-molecule potential section because the combining rule that we used in calculating the atom-ion parameters are simple and therefore are not very precise. Furthermore, we did not include the rumpling effect of the surface into

our calculations for simplicity. In accordance with the result, the molecule is found to bind to the surface less strongly than found experimentally, in another words, the repulsion between the surface ion Cl^- and the molecule is probably too strong. In order to correct this problem, we decided to modify part of the repulsive parameters between the atoms of the molecule and the surface ions. We decreased the strength of the potential of the Cl^- ions and at the same time increased those of the Na^+ ions. By trying a series of values, we came up with one pair of repulsion constants that gave us the closest match to the experimental heat of adsorption (q_{st}). This proposed potential was then used to simulate a monolayer using Monte Carlo simulations to determine its structure. This was then compared to those proposed by the experimentalist,[18] which did not initially match. Further adjustments were made which are shown Table 4.2. The final result was based on the closest match to both the experimental q_{st} as well as the proposed structure. It was obtained when we increased the parameters of the sodium ions by about 27% and decreased those of the chlorine ions by 37% after initially increasing both constants by 10%. Doing this we found that the calculated potential was in agreement with the two experimental values of heat of adsorption[20,22] and leads to the right proposed structure with correct tilt angle at low temperature. Furthermore, at this setting, the potential energy from Monte Carlo (MC) simulations is found to have the lowest value; therefore, it was used as the adjustment parameters for generating the surface potential data file. The discrepancies between the heats of adsorption (q_{st}) can be accounted for by

noticing the differences in percentage of coverage between them. In order to consider this aspect, one has to incorporate the lateral interactions between the molecules. In other words, one has to simulate more than one molecule. This will be done in the Monte Carlo simulations and will be discussed in later sections.

Table 4.2: Results for the determination of the surface potential function using Monte Carlo method for 100 molecules at T=1K

Na^+ + x (%)	Cl^- - y (%)	Energy (kcal/mol)	Polar angle, θ (°)	Azimuthal angle φ, (°)
10	10	-3.8664	16	± 90
15	15	-3.9205	18	± 90
20	20	-3.9788	21	± 90
25	25	-4.0424	23	± 90
25	39	-4.4317	27	± 90
27	27	-4.1016	27	± 90
27	**37**	**-4.3446**	**27**	**± 90**
29	29	-4.0178	24	± 90
31	31	-4.1273	25	± 90

Using the unmodified surface potential as the input for the surface molecule interaction, we used the energy minimization method to determine the binding energy and the position of the one CO molecule adsorbed on the NaCl(100) surface at different adsorption sites. We also studied the possibility of the molecule flipping between a head-tail orientation by comparing the results from the adsorption of the CO molecule with the carbon end pointing down to the surface (we call it normal bound CO) and the inverted molecule (*i.e.* one that has oxygen closer to the surface ion). In those studies, no temperature effect is included, *i.e.* T= 0K. Results of such studies are illustrated in Table 4.3.

Table 4.3: Adsorption energy of a single CO/NaCl(100) at different adsorption sites and head-tail orientations from energy minimization method.

Initial Adsorption Site	*Energy (E_0) (kcal/mol)*		*Final Position and Orientation*	
	Initial	*Final*	*Molecular Head-tail orientation*	*Molecular Position and Orientation*
Na^+	-3.6509	-3.9048	Carbon down	Perpendicular over Na^+
Cl^-	11.7839	-3.9046	Carbon down	Perpendicular over Na^+
Na^+	-1.3465	-1.7237	Oxygen down	Perpendicular over Na^+

The position and the orientation from the energy minimization of an isolated molecule are also in agreement with those reported from others.[18,21] The CO molecule is found to adsorb on the Na^+ site, with the carbon end pointing down towards the surface. When the molecule sits on top of Cl^- ion, there is a very large repulsive energy between the molecule and the surface ion ($E_{initial}$ = 11.7839kcal/mol), which comes from the unfavourable electrostatic interaction between the CO molecule and the Cl^- ion. The molecule ultimately moves over to the sodium ion at the end of the run as shown in the above Table 4.3. The inverted molecule, which also sits on top of Na^+ site, shows that the position of the molecule is less stable than the former one. The difference in energy between those two molecules is ΔE= -2.1811 kcal/mol (~ 1000 K). This implies that it is impossible for the adsorbed molecule to flip in order to have the oxygen end closer to the surface under normal running condition. In all cases, the final molecule is found to bind perpendicularly to the surface ion as predicted by others.[12,18,21,26]

To learn more about the position, orientation and the energy of the CO molecule upon adsorption on the surface, we also performed some simple potential energy calculations based on the modified potential used in the MC simulations. We calculated the energy as a function of position in the z-direction using the same potential energy function. Fig. 4.1 summarizes the potential energy curve and its components. The molecule is adsorbed on top of a Na^+ ion

in a perpendicular fashion with the carbon end down (O-C···Na^+). The result shows that the van der Waals interaction (dispersion plus repulsion) between the molecule and the surface ion goes through a minimum at a height of z= 2.7Å above the surface. Below this height, there exists a strong repulsion between the molecule and the surface ions that prevent the molecule from entering the surface. On the other hand, the electrostatic interaction (dashed curve) between them is always attractive and effectively disappears beyond z= 6Å. Since the electrostatic potential from the surface is strongest at the vicinity of the surface ions, there is a strong attraction force when the molecule is placed close to the Na^+ ion, z~ 2Å. Overall, the total surface potential energy (the sum of the van der Waals and electrostatic) has the same shape as the van der Waals interaction but with a deeper minimum value shifted closer to the surface due to a strong attractive electrostatic force. The value for the total binding energy is found to be -4.7071 kcal/mol using the modified potential. It should be noted that this value is greater than the energy using the unmodified potential from Table 4.3 (where z_c = 2.9764Å) because the modified potential allows molecules to come closer to the surface, resulting in a larger electrostatic interaction. Furthermore, it differs from the monolayer energy, given in Table 4.2, because the CO molecules are tilted in the latter case.

Fig. 4.2 and Table 4.4 demonstrate the interaction potential for three fixed orientations of the molecule: perpendicular, parallel and tilted (θ= 27°). The most

stable orientation for an isolated CO molecule occurs when the molecule is perpendicular to the surface. In this position, the molecule yields the lowest energy minimum. Further testing by moving CO from a Na^+ adsorption site (O-C···Na^+) to a Cl^- site (O-C···Cl^-) shows that the potential energy changes from -4.7071 kcal/mol to -0.3259 kcal/mol. The molecule is found to bind less tightly to the surface at the Cl^- site. Result from Fig. 4.3 strongly demonstrates that the sodium ion is a more favourable adsorption site compared to the chlorine ion. This can be understood by comparing the atomic radius of the two ions. The chlorine ion is almost twice as big as the sodium ion (the ionic radius of Cl^- is 181pm and of Na^+ is 95pm), [13] the molecule will be much closer to the surface if it sits on top of the sodium ion. Thus it will be more influenced by the strong electrostatic field at the surface than if it would be if placed on top of chlorine ion. In addition, the molecular dipole of the molecule interacts more constructively with the direction of the electric field at the sodium site than with that at the chlorine ion. The net effect is that the molecule is found to move away from the surface when CO was placed on top of Cl^- site, so that z_{Cl^-} is equal to 4.51Å. Without the influence of the lateral (molecule-molecule) interaction, the molecule binds perpendicularly to the surface cation because it can maximize the electrostatic interaction with the surface ions. However, a fixed tilt accompanied with a small shift along the direction of the tilt in the molecular axis would help in lessening the unfavourable interaction between the oxygen atom and the chlorine ion. Hence, a tilt in a molecular axis does not change the binding energy

much. On the other hand, when the molecule is placed parallel to the surface the resulting binding energy is significantly lower than the other two results. This is caused by a small electrostatic interaction between the molecule and the surface ion because of the position of the dipole moment of the molecule with respect to the source of the surface electric field.

Table 4.4: Results for the orientation tests of a single CO adsorption.

CO Position	*Perpendicular* $O\text{-}C \perp Na^+$	*Parallel* $O\text{-}C \,//\, Na^+$	*Fixed* $\theta = 27°$ $\angle\, OC\, Na^+$
E_{tot} *(kcal/mol)*	**-4.7071**	-0.7224	-4.0991
z position (Å)	**2.7000**	3.7600	2.7400

What happens to the potential energy when the CO molecule is positioned on the surface with the oxygen end pointing towards the surface ions (inverted molecule), Na^+ (C-O···Na^+) or Cl^- (C-O···Cl^-), instead of those molecules having the carbon ends pointing towards the surface ions? To answer this question, we carried out more calculations with such changes and the results can also be examined in Fig. 4.3. Once more, the potential energies are found to be much smaller than that of the O-C···Na^+ case. The value for the potential energy in the C-O···Na^+ case is about 33% of that of the O-C···Na^+ case. The values of the potential energies can be found in the following Table 4.5.

Table 4.5: Results for the position tests of a single CO adsorption.

CO Position	*O-C···Na⁺*	*O-C···Cl⁻*	*C-O···Na⁺*	*C-O···Cl⁻*
E_{tot} *(kcal/mol)*	**-4.7071**	-0.3260	-1.8640	-0.5145
z position (Å)	**2.7000**	4.5100	4.0400	5.0700

4.2 Results From Monte Carlo Simulations

After being confident about the potential function used, we started to simulate the system using the Metropolis Monte Carlo method. To produce accurate results it is usually required that the system be in equilibrium. The system is equilibrated by running at least 2.5×10^5 cycles, and followed with a production run of anywhere from 5.0×10^5 to 10^6 cycles. Each cycle consists of randomly moving all molecules according to the Monte Carlo principles. The duration of the whole period was not fixed but it rather depended on the simulated temperature. The higher the temperature the longer the time the configuration needs in order to be properly equilibrated. The statistical data used in determining the structures were collected for a period of 5.0×10^4 cycles, whereas data used in the quantitative analysis of the phase transition were gathered over 10^5 - 10^6 cycles. Those results will be presented and discussed in the following sections.

4.2.1 Single Molecule Adsorption

The result of one molecule adsorbed on the NaCl(100) surface is found to support the findings in the energy minimization studies, namely, the molecule is perpendicularly adsorbed on top of a sodium ion, at a distance z= 2.8Å and with the carbon end pointing towards the surface ion. According to the study by Gready *et al.*, it is the octupole moment of the molecule that leads to this orientation.[59] The position and orientation of the single molecule adsorption in this study is found to be in concert with the FTIR analysis as well as other potential calculations.[12,19,26] The total potential energy (Table 4.7) is found to be in accordance with the minimum energy calculated in the above section (Table 4.6).

Table 4.6: Break down of the adsorption energy for a single CO/NaCl(100) for different head-tail orientations calculated by energy minimization method.

T= 1K	*Energy of O-C···Na⁺ (kCal/mol)*	*Energy of C-O···Na⁺ (kCal/mol)*
Distance of carbon from the surface (z_C, Å)	2.8252	3.9612
Dispersion-repulsion	-0.0811	-0.7757
Electrostatic	-2.8895	-0.5922
Total Energy	**-3.5608**	**-1.7451**

Table 4.7: Break down of the adsorption energy for a single CO/NaCl(100) for different head-tail orientations generated by Monte Carlo simulation.

T= 1K	*Energy of O-C···Na⁺ (kCal/mol)*	*Energy of C-O···Na⁺ (kCal/mol)*
Distance of carbon from the surface (z_C, Å)	2.7705	3.8499
Surface Dispersion repulsion	-0.1512	-0.8834
Surface Electrostatic	-3.3602	-0.8050
Surface Induction energy	-0. 4447	-.2356
Total Surface Energy	**-3.9561**	**-1.9240**

The discrepancy between the two methods comes from the fact that the induction energy calculation is excluded in the energy minimization method as well as the difference in the distance of the molecule from the surface. The molecule in the Monte Carlo method can come closer to the surface than that of the energy minimization method, thus its binding energy is greater than that of the latter.

Table 4.7 indicates that the most important contribution to the surface potential energy comes from the electrostatic interaction between the CO molecule and the surface ions. This is no surprise because CO has an appreciable quadrupole moment and NaCl is an ionic substrate with a strong electric field generated at the surface ions. With the carbon atom sitting on top of a Na^+ site, which is very close to the surface where the strongest portion of the electric field is found, the electrostatic force is no doubt a very significant component to the total attractive force between the molecule and the surface. Also in Table 4.7, the molecule with the carbon end pointing towards the surface is energetically more stable compared to the CO with the oxygen end down. The energy difference between the head-to-tail orientation is pronounced as seen in Table 4.7, i.e. ΔE= -2.0321 kcal/mol. In terms of temperature units, $\Delta E=1.023 \times 10^3$ K so that head-tail disorder will not likely happen until the simulated temperature is well above room temperature. This can be explained by knowing that oxygen atom with a larger atomic radius cannot penetrate as close to the surface as the carbon does,

resulting in significantly smaller electrostatic interaction. In addition, the dipole moment of the inverted molecule (*i.e.* molecule with the oxygen end pointing down to the surface ion) and the electric field do not interact favourably with each other. Although the dispersion-repulsion favours the position of the inverted molecule it contributes only a fraction of the total energy (~ 3%), therefore, the electrostatic interaction becomes the key element for calculating the binding energy. In other words, the molecule takes up any position that gives it the largest electrostatic contribution to the binding energy. In this case it would be the position where the carbon atom directly binds to the surface sodium ion. This is in accordance with the observation that the electrostatic interaction between carbon atom and sodium ion is much stronger than that of the oxygen atom and sodium ion, hence random head-tail orientation is not favoured energetically.[18]

Fig. 4.4 shows the angular distribution, as obtained from MC simulations, of one CO on NaCl(100) at T= 1K. The theta distribution (lower panel) of the same system shows a peak at $\theta \sim 0°$. This finding is in agreement with other theoretical studies[12,18,26] where one CO molecule is found to be oriented perpendicular to the surface. Even at very cold temperatures, T= 1K, the phi distribution has no peak. In other words, the molecule does not have a preferred azimuthal orientation, and can spin freely at the adsorption site. Again, the most

favourable site is on top of Na^+ ion, with the carbon end pointing down towards the surface ion.

4.2.2 Monolayer Adsorption

Simulations of monolayer CO/NaCl(100) were also carried out through the use of the Metropolis Monte Carlo method (canonical ensemble) as previously mentioned. A full monolayer was set as an ensemble of 400 molecules placed in the NaCl surface potential. Periodic boundary conditions were imposed as well as a cut off radius of 16.5 Å for the lateral interaction between the CO molecules. The original intention of the study was to define a potential surface that was simple but good enough to reproduce the experimental data in the observed phase transition using the minimum amount of computer time. To simplify the calculations, the internal vibrations of the molecules were ignored, and the surface ions were made static without surface rumpling or defects. Even so the results obtained from simulations are in good agreement with the experimental data as anticipated.

In order to examine the temperature dependence of the structure of the CO/NaCl(100) monolayer, the simulations were performed between 1K and 75K. In the low temperature regime, a p(2x1) structure with two CO molecules per unit cell is formed (as illustrated in Fig. 4.5, left panel). Within the unit cell the

two molecules are adsorbed on identical adsorption sites but are translationally inequivalent and are connected by a glide plane. The molecules have preferred azimuthal orientations and are tilted away from the surface normal in an antiparallel fashion. At high temperatures, T> 35K, the molecules become disordered, resulting in a p(1x1) structure with one molecule per unit cell (Fig. 4.5, right panel). The molecules are found to lose their preferred azimuthal orientation, however they remain tilted at an angle with respect to the surface normal.

4.2.2.1 Energetics

Table 4.8 shows the average values of the total adsorption potential E and its components from a Monte Carlo simulation of 400 CO molecules at T= 1K. Adsorption energy of a CO monolayer on NaCl was calculated as a sum of the lateral interactions between the CO molecules and the surface-molecule energy. According to the results, the largest contribution to the adsorption energy comes from the surface energy (energy between the CO molecules and the surface ions). Its components are both attractive with the electrostatic energy being about 90% of the total potential energy. The dispersion-repulsion portion of the surface energy is found to contribute only an insignificant amount of about 5%. A much smaller amount of the total energy comes from the lateral energy (energy between the adlayer molecules). The dispersion-repulsion energy among

adsorbates is attractive and accounts for about 15% of the total energy. In contrast to its contribution to the surface energy, the electrostatic energy among adsorbates is found to be repulsive with a very small value (about ~ 1% of the total energy). Nonetheless, the lateral energy is required in order for the molecules to have the experimental tilt angle in the simulations.

Table 4.8. Break down of the adsorption energy for a CO/NaCl(100) monolayer generated by Monte Carlo simulation at T= 1K.

T= 1K	*Energy with lateral interaction (kCal/mol)*	*Energy without lateral interaction (kCal/mol)*
Distance of carbon from surface (z_C, Å)	2.7455	2.7690
CO-CO (Dispersion-repulsion)	-0.6104	0.0000
CO-CO (Electrostatic)	0.0409	0.0000
CO-NaCl (Dispersion-repulsion)	-0.1998	-0.1453
CO-NaCl (Electrostatic)	-3.2122	-3.3767
Induction energy (CO-CO+CO-NaCl)	-0.3967	-0.4390
Total Energy	**-4.3782**	**-3.9610**

To test this observation, we also ran a monolayer of CO/NaCl(100) with the lateral interactions (molecule-molecule) being turned off. As expected, the

molecules acted individually and, as in the case of adsorption of one molecule on the surface, the molecules were found to be oriented perpendicular to the surface. The energy profile is also shown in Table 4.8. Similar to the Monte Carlo run of one CO molecule (Table 4.7), the presence of the lateral interaction decreases the surface energy by about 5%. However, the reduced energy is being traded off by an increase in the lateral interaction by about 12% of the total energy. Hence, the net total is an increase of about 9.5% in the total binding energy in the monolayer adsorption. In addition to a more tightly bound monolayer the lateral interaction helps the molecules to tilt to form the p(2x1) structure.

The induction energy, which has contributions from both lateral and surface-molecule energies, is found to reinforce the total energy with about ~10% in value and is attractive. Although having a small value, the induction energy is attractive and helps stabilize the ordered phase, and thus pushing the transition temperature by one degree Kelvin ($\Delta T \sim 1K$) to a slightly higher temperature.

It is of interest to test for other possible structures of the system, since this could indicate whether the p(2x1) is the most stable structure. Two sets of initial monolayer structures, with only one molecule per unit cell, resulting in an ordered p(1x1) structure were simulated with similar running conditions as those of the simulation of the p(2x1) structure. One set had all CO molecular axes

oriented perpendicular to the surface. In the second, the CO molecules were tilted in one direction with a fixed polar angle of 27° (*i.e.* θ~ 27°).

Table 4.9. Break down of the adsorption energy for different structures of the CO/NaCl(100) monolayer generated by Monte Carlo simulation at T= 1K.

T= 1K	*p(2x1)*	*p(1x1) perpendicular*	*p(1x1) θ~ 27° (fixed)*
Distance of carbon from surface (z_c, Å)	2.7455	2.801	2.825
CO-CO energy (Dispersion-repulsion)	-0.6104	-0.6186	-0.6156
CO-CO energy (Electrostatic)	0.0409	0.2941	0.0979
CO-NaCl energy (Dispersion-repulsion)	-0.1998	-0.2141	-0.4783
CO-NaCl energy (Electrostatic)	-3.2122	-3.2806	-2.5602
Induction energy (CO-CO+CO-NaCl)	-0.3967	-0.4497	-0.3537
Total Energy	**-4.3782**	**-4.2689**	**-3.9099**

* Energy per molecule has unit of kcal.mole^{-1}

Table 4.9 compares the energies of the three different structures, p(2x1), p(1x1) perpendicular and p(1x1) tilted. Among the three structures, the energy of the p(2x1) type is truly a minimum although the difference between them is small (about 10%). The lateral electrostatic energy is strongly unfavourable in the perpendicular orientation, which results in a smaller total energy compared to

the p(2x1) structure even though the surface electrostatic energy of the perpendicular structure is the largest value in all three. This is in agreement with the previous observation that the surface electrostatic energy prefers the perpendicular position of the molecule. It is interesting to find that the p(1x1) tilted is the least favoured structure. This might be due to the not-so-very favourable position of the dipoles of the tilted molecules. Another point to be noticed in this structure is that the molecule is adsorbed right on top of the sodium site, with no displacement from the cation site as happens in the other structure. This results in a stronger repulsion from the oxygen atom of the molecule and the surface chlorine ion because the molecule is tilted toward the anion in this case. It is clear that the p(2x1) type is a minimum energy structure in this system. This observation can evidently clarify some uncertainty in other potential calculation works (*e.g.* energy minimization method,[19] and *ab initio* calculations[26]) that stated that the energy difference between these (1x1) and (2x1) structures was small. Hence it was difficult to discriminate between these two structures with confidence. The reason that our potential works better compared to the one used in the energy minimization calculation is the addition of the higher terms in the dispersion series (C_8 parameter between the lateral interactions and both C_8 and C_{10} parameters in the calculations of the molecules-surfaces).

Meredith *et al.* derived the potential energy surface (PES) for the same system using *ab initio* methods,[19] which are based on the perturbation theory of intermolecular forces. The outcome was confusing because of several stationary points have been found in the PES. Again, these structures have very similar energies and in view of the uncertainty arising from their potential calculation, they cannot determine the absolute ordering of the minima. In other words, they are not able to predict the relative energies of the structures. Our potential on the other hand is found to work better probably because its parameters are constructed in a semi-empirical fashion with the use of experimental values (such as calculations of the point dipole and point charge values) in the calculations. We also believe that the use of the point charge and point dipole model to represent the multipole interactions is an important form in producing reliable results because it reproduces both the quadrupole and octupole moments, which are important part in calculating the CO-NaCl interaction. [59]

4.2.2.2 Low-Temperature Structure (T= 1K)

From the simulations, we have been able to reproduce the proposed structure of the monolayer in the low-temperature region. Below T= 35K, an ordered p(2x1) structure had been deduced from the combination of FTIR[18,21] and HAS[24] experiments. The ordered structure was described with two molecules per unit cell, with a tilt angle of ~ 27° with respect to the surface. Also

from the IR work of Heidberg and coworker,[21] it was determined that the CO molecules are adsorbed on identical sites and are connected by a glide plane. However, details on the structure of CO on NaCl(100), such as the position of the CO molecule in the unit cell, the distance z of the molecules from the surface as well as the orientations of the molecules (tilt and azimuthal angles that define the molecular orientation), can not be derived from the infrared measurements alone. Hence a full description of the structure has not yet been given. In contrast, from our Monte Carlo simulations, we can very confidently provide most of the details of the low-temperature structure as follows.

Figure 4.6 shows a snapshot of the configuration of a monolayer at T= 1K. At low temperature, the molecules are found to localize near the Na^+ ions with the carbon atom pointing down towards the surface. This is in agreement with other theoretical studies, which suggested that the interaction of the octupole moment of the molecule with the ionic electric fields favoured carbon toward and oxygen away from the surface.[59,60]

The molecules form alternating rows of ordered molecules whose carbon atoms do not sit directly overtop of the Na^+ ions but instead they are found to displace by approximately ±0.2 Å in the direction of tilt along the x or y-axis. These small displacements are believed to increase their dispersion interaction between the tilted oxygen atoms with the surface chlorine ions by forming a

hexagonal type of structure and at the same time alleviate the repulsions between them to help the molecules having larger tilt angles. Also they help increase the binding energy of the tilted molecules by maximizing their electrostatic interactions with the surface ions.

The molecules are found to tilt away with respect to the surface normal, of $\theta = 27°$ as experimentally reported.[21] The directions of the molecular tilt illustrate that the ordered phase has rows tilted in the same direction with neighbouring rows tilted in the opposite direction, thus forming a p(2x1) structure with two molecules per unit cell, one molecule per row as shown in Fig. 4.6 (dotted rectangle). We are also able to reveal the azimuthal angle (*i.e.* the angle between the projection of the molecular axis and the surface x-y plane), $\varphi \sim \pm 90°$, for the two translationally inequivalent molecules onto the surface, which can be correctly calculated to give the intermolecular angle, $\Delta\varphi = |\varphi_1| + |\varphi_2| = 180°$, between the projections of the molecular axes of the above molecules, in agreement with the infrared experiment.[21] With this intermolecular angle, the molecules are indeed found to orient antiparallel to each other as shown in Fig. 4.5 and 4.6 resulting in a p(2x1) structure as confirmed by HAS diffraction study.[24] A glide plane (a white line cutting the unit cell along the x-axis in Fig. 4.6) is also found to bisect the unit cell along the x-axis. Molecules in one row can be regenerated from molecules in the neighbouring row by two simple operations through the glide plane. First, the molecule from one row is projected

through the glide plane, as a mirror image, and then moved half the unit cell along the glide plane direction.

From our simulated results, we can also determine the average equilibrium distance between the carbon atom of the molecule and the surface Na^+ ion to be z~ 2.75Å (Table 4.8). This information helps giving the adsorbed CO molecule a full description of its position.

We can say with certainty that in the low temperature regime, the molecules of the CO/NaCl(100) monolayer form an ordered p(2x1) and not a p(1x1) type of structure. This is in contrast to Ewing's conclusion that the molecules aligned perpendicularly to the surface at T= 22K.[18] Hence we can resolve some of the discrepancies of the monolayer structure between different groups of experimentalists. Moreover, we are also the first to describe in detail the correct structure of the adsorbed CO/NaCl(100) monolayer, (which cannot be derived just from infrared measurements alone), using Monte Carlo simulation method. This is also in contrast with the finding of Picaud and coworkers.[26] They claimed that the (2x1) structure was not stable and the effort to find it led to a formation of a (1x1) structure using the similar exp-6 potential. Our Tang-Toennies potential is found to give a better result because of the addition of the higher term in the dispersion series.

4.2.2.3 High-Temperature Structure (T> 1K)

After properly reproducing the ordered p(2x1) type of structure at T= 1K, the adsorbed molecules were gradually heated by temperature increments of 5K at a time. The ordered phase is found to persist up to about 25K. Above this temperature, the monolayer structure starts to become disordered as shown in the configuration snapshots at T= 25K (Fig. 4.7). The perfectly ordered structure at T= 1K has been broken into domains of ordered molecules in different directions. The majority of molecules still have a p(2x1) type of structure in the y-direction. However, some molecules change direction, and form an equivalent p(2x1) structure along the x-axis. One striking observation from Fig. 4.7 is the formation of another type of structure: vortices (circle) or antivortices (cross). Most of the vortices and antivortices structures are found to be near each other, forming vortex-antivortex pairs, which are scattered over the entire surface.

At T= 35K (Fig. 4.8) the ordered 2x1 phase is mostly replaced by a disordered structure with molecules having no preferred azimuthal orientation. Yet some existing domains formed in the T= 25K configuration are getting larger but more disordered. The number of vortex-antivortex pairs has not only multiplied in this configuration but they are also found to bind to each other. They form regions of ordered structure of a different type. The long-range order between the molecules within the monolayer has been destroyed, resulting in the

disappearance of the p(2x1) structure; yet some short-range order is still present, through the formation of the vortex-antivortex structure as in Fig. 4.8.

The structure became further disordered as the temperature was raised. The disappearance of the domain boundaries signals the formation of the disordered (1x1) phase where there is one molecule per unit cell with no azimuthal correlation with the others. Fig. 4.9 shows an example of the configuration at T= 75K. At this temperature the configuration is found to contain some molecules that are vertically oriented but overall the molecules remain tilted. The vortex-antivortex pairs are still present even at this high temperature regime. However, they are found to unbind and are scattered throughout the surface.

In conclusion, the ordered p(2x1) structure with two molecules per unit cell of the NaCl substrate has become a disordered p(1x1) structure with one CO molecule per unit cell when the temperature was raised from T= 1K to T= 75K by loosing their preferred azimuthal orientations. Residual short-range order persists through vortex-antivortex pairs. But the frequency of occurrence of these structures has diminished. The molecules are also found to displace further from the sodium site yet remain titled with respect to the surface. This is in contrast with Ewing's interpretations that at high temperature the CO molecules bind perpendicularly to the surface ions.[18] The lack of s-polarized IR signals can be

interpreted as either the molecules being adsorbed perpendicular to the surface, or that the molecular axis spin freely around the surface normal resulting in the disappearance of the s-signal which was due to an averaging of the parallel components of the molecular dipole moments. This latter interpretation is consistent with our observation that the molecules remain tilted at high temperature. This can rule out the assumption of a transition from a tilted to a perpendicular orientation as deduced by the FTIR analysis.[18]

4.2.3 Phase Transition

4.2.3.1 Qualitative Analysis

One method used in studying the phase transition is to look at the variation of the polar angle, θ, (angle between the molecular axis and the surface normal) as a function of temperature. The result of such a study is shown in Fig. 4.10. At temperatures up to T= 10K, the curve of the polar angle is found to be sharp, resulting in one narrow peak at $\theta \sim 27°$. The peak is also found to broaden when the temperature is raised as seen in Fig. 4.10. However, even at T= 75K the molecules remain tilted as shown by a distinct peak at the same theta value as before ($\theta \sim 27°$) in spite of their increased thermal disorder. Consequently the peak in the polar distribution is still present throughout the simulations and thus the azimuthal angle φ remains a valid measure of the degree of order. This

suggests that the phase transition belongs to an order-disorder type rather than a structural phase transition.

One can inspect the development of the phase transition by monitoring the orientational (azimuthal) distribution of the CO molecules as a function of temperature. Azimuthal (φ) distributions for a monolayer of CO/NaCl(100) at different temperatures are shown in Fig. 4.11. At T=10K, the distribution function exhibits two sharp and symmetric peaks centered on $\varphi \sim \pm 90°$. The peaks demonstrate that the ordered phase has a preferred azimuthal orientation where the molecules from two neighbouring rows are found to tilt in opposite direction, resulting in a (2x1) type of structure. This is consistent with the configuration of the monolayer at low temperature (Fig. 4.5). Between the temperatures of T= 30K and T= 35K, even though the observed peaks are still centered on $\varphi \sim \pm 90°$, the height of the peaks are found to be drastically suppressed and broadened. The broadening of the peak is consistent with the fact that at high temperature with larger thermal motion, the molecules have larger librations, resulting in a loss of azimuthal ordering. At the same time, peaks at $\varphi \sim 0°, 180°$ are found to emerge as seen in Fig. 4.11. This is in agreement with the observation that the ordered monolayer has broken up into multiple domains with different azimuthal directions. Nevertheless, the curves at these temperatures show that the structure of the monolayer is still mainly ordered. At very high temperature, T= 75K, the azimuthal ordering found in the low temperature regime is lost, signalling the

existence of a completely disordered phase. Interestingly enough, the phi distribution does not wash out as expected, but converts to a ripple curve with four small bumps at $\varphi \sim \pm 45°$ and $\pm 135°$. This is probably due to the previously observed vortex-antivortex type structures in the configurations at high temperatures.

4.2.3.2 Quantitative Analysis

We are able to confirm the occurrence of the phase transition at around T~ 35K as deduced from the FTIR spectra[21] with just the examination of the angular distributions (θ and φ distributions). However, to determine the type as well as the exact temperature of the transition and estimate the critical exponents we have further calculated two other quantities to monitor the phase transition: the system energy and order parameter as functions of temperature. In addition, their fluctuations, the heat capacity and susceptibility, are also studied. As noted earlier, data used in the quantitative analysis were collected for a million cycles. Then an average was calculated and plotted as a function of time. Results of this analysis are presented in Fig. 4.12 to 4.15.

Fig. 4.12 shows a plot of the potential energy of the system as a function of time. As one can see, the curve shows a linear increase of energy as the temperature is increased. At around T= 25K, the energy curve gradually changes

its slope. Above T= 35K, the curve is again found to linearly increase with temperature. The shape of the curve clearly suggests that the transition is of a continuous type and the temperature range of the transition will be above 30K as observed from the phi distribution curves, Fig. 4.10. Preliminary results of the analysis demonstrate that there is no gap found in the binding energy curve. Hence, the phase transition is believed to be of the continuous type.

Fig. 4.13 shows a plot of the heat capacity as a function of temperature of the same system. The heat capacity was derived as a fluctuation of the above potential energy. The values are found to gradually increase with increasing temperature. However, the heat capacity plot is not very conclusive because of large fluctuations around the transition regime (Fig. 4.13), hence, no definitive peak can be made out to determine the exact transition temperature as well as the transition type as hoped. Still there exists a peak at T~ 32K. This is evidence that a transition has taken place around that temperature. However, the curve that does not drop off as fast as expected, it rather shows large fluctuations after the transition temperature even when the temperature is raised above T= 38K. Large fluctuations prevent a better estimation of the exact transition temperature, but the peak does appear to be positive if small at around T= 32K. At this temperature, the long-range order has been broken up but the local orders are found to dominate, forming an intermediate type of structure, which has only

short-range order. Such structure has been observed as vortex-antivortex pairs in the snapshot of the system at temperature above 25K (Fig. 4.6 to 4.9).

In addition, the CO molecules have permanent dipoles and the long-range interactions between their dipole moments make the system become much more susceptible to fluctuations at the phase transition regime compared to other similar systems. It has been found that the N_2/NaCl(100)[61] system shows a very similar result to the CO/NaCl(100) system such that the monolayer also forms an ordered structure at low temperature; and the layer also undergoes an order-disorder phase transition at high temperature. However, because N_2 molecule has no dipole moment the quantitative analysis shows no fluctuations and the heat capacity displays a characteristic λ divergence with a peak at the transition temperature; hence the determination of the transition type as well as temperature have become easier with the same usage of the potential function and simulation method. One way to modify the problem of long-range interactions is using direct summations (or Ewald sum) in the calculations of the electrostatic interactions. However, the molecules are constantly moving in a Monte Carlo simulation, it is impossible to use the Ewald sum to calculate the electrostatic interactions between the constituents. Nevertheless it is believed that with a large enough cut-off radius one can minimize the effect of the long-range interactions upon fluctuations.[62] In our simulations the cut-off radius is set to be 16.5Å, which was believed large enough[62] to reduce the effect of fluctuations on

the calculations of the desired quantities. However, this is not the case, as we could not damp out the fluctuations as wanted. Further attempts to decrease the effect of fluctuations by increasing the system size (in order for it to be large enough to be a good approximation of an infinite system, *i.e.* close to the thermodynamic limit) also failed due to the large amount of computer time needed for the simulations. Nonetheless, the heat capacity curve does show a continuous increase leading edge before the transition temperature; which can be interpreted as a lambda (λ) transition. Therefore, the heat capacity curve does support the observation that the transition is of a continuous type, yet the exact temperature cannot be determined using this feature as hoped because of large fluctuations present at the transition regime.

Similar conclusions can be seen in the study of the order parameter and the susceptibility, which is calculated using the fluctuations of the order parameter. The order parameter was constructed from the molecular orientation (azimuthal angle φ). An order parameter value of 1 means that the system is perfectly ordered, and on the other hand, an order parameter value of 0 means the system is totally disordered. Fig. 4.14 shows the order parameter of the same system of 400 CO adsorbed on NaCl(100). A linear decrease of the order parameter in the 1-25 K region is found. The curve drops more quickly and continuously as the temperature is increased, and a rapid drop has been found above T~ 30K. As seen in Fig. 4.14, again fluctuations are found to dominate at

the transition temperature and make it impossible to determine the exact temperature of the phase transition. It seems that there exists two types of structures, one upper order structure and a lower ordered type. Nevertheless, the order parameter does eventually drop below 0.25 at high temperature. Although the drop in the order parameter is not as fast as expected, it confirms the existence of a phase transition at around T~ 32K. Wide fluctuations at the transition temperature might be accounted for by the fact that we did not include the vortex-antivortex structure in the order parameter calculations. At that time, these types of structure did not stand out as a local ordered structure at high temperature in the smaller size system (100 CO).

Fig. 4.15 shows the plot of susceptibility as a function of temperature. The data points of the susceptibility in the low temperature region gradually increase to a higher value at around T~ 32K. This is indicative of a phase transition although large fluctuations in this region (T= 30K to T= 35K) inhibit a determination of the exact transition temperature. It is important to note that the estimations of the transition temperatures using the heat capacity and susceptibility plots are consistent with each other (both graphs, Fig. 4.13 and 4.15, show peaks in the region of T~ 32K). Therefore, it can be concluded from both graphs that there exists an ordered-disordered phase transition between low-temperature and high-temperature structures at around T~ 35K. This is in agreement with a conclusion made by Heidberg *et al.* that a reversible phase

transition was observed in the system CO/NaCl(100).[21] Unfortunately, our quantitative analysis cannot to determine the exact transition temperature. Such a determination would rely on a finite size scaling analysis that we are unable to do because of time as well as computer power constraints. Nonetheless, the transition temperature can be approximated somewhere between T~ 32K to T~ 35K; and careful analysis of the above quantitative studies shows evidence of a continuous transition that can best be described as of the order-disorder type.

With the ability to incorporate the finite temperatures into the Monte Carlo simulations, we are not only able to confirm the existence of the phase transition but also to approximate a correct transition temperature, which is around T~ 32K to T~ 35K. In contrast to our firm conclusion about the phase transition, other theoretical works[9,26] presumed that the phase transition was possible because of a small energy difference between the p(2x1) and p(1x1) structures.

4.3 Potential Energy Tests

In order to have a better understanding of the effects of the potential energy function on the monolayer structure and its stability, tests where the potential was modified were done. Monte Carlo simulations were running on the system of 100 CO/NaCl(100) at T= 1K for a total of $10x10^5$ cycles. The potential

function used is the same as that used before except that one part of the potential function is turned off for each study.

The total energy is a sum of the molecule-molecule and molecule-surface interactions where each portion is in turn a sum of the dispersion-repulsion and electrostatics contributions. According to Table 4.8, we concluded that the electrostatic energy between the molecule-surface interactions is the most important contribution to the total energy. The dispersion-repulsion contribution is very small compared to its counterpart and therefore is much less important. On the other hand, from the molecule-molecule interactions, these two constituents are almost equal in value. For this reason, more tests needed to be done to understand their importance in calculating the potential function. Hence, the molecule-molecule interactions were modified and the surface-molecule interactions were kept intact. The resulting energy and structural data were examined to determine the interactions necessary for the formation of the p(2x1) structure.

MC simulations of the CO monolayer without lateral interactions showed that the molecule-molecule interactions (which had contributions from electrostatic and dispersion energies) were needed in order for the CO layer to form the order p(2x1) structure. To understand more clearly the importance of

each contribution, one contribution at a time was systematically turned off. These results were compared with simulations where all interactions were present.

Fig. 4.16 shows the theta (polar) distributions of the above cases. The importance of the electrostatic interaction is highlighted as shown by the 'Disp.' curve in the figure. The polar angle (θ) is peaked on 0 in this case. This explains the flat line in the phi distribution curve in Fig. 4.17 because the molecules are, on average, perpendicular to the surface, and hence the p(2x1) structure with the molecules tilted to the surface normal is not observed. The electrostatic interaction is needed in order for the molecules to tilt in the monolayer. In the absence of the dispersion contribution (the dash curve, 'Elec.'), the molecules are found to untilt only by a few degrees. Consequently, the dispersion energy has a minimal effect on the total outcome of the structure of the monolayer CO/NaCl(100). Still to get the maximum tilt we have to include all contributions in the potential calculation as shown by the solid curve in Fig. 4.16

The phi (azimuthal) distributions were plotted in Fig. 4.17 again for all three cases studied. The solid curve represents a simulation where both contributions are present. The curve shows two distinct peaks at $\pm 90°$. The peaks are symmetric and they are in agreement with the observation of a formation of p(2x1) structure. The dashed curve ('Elec.') corresponds to the case where the dispersion interaction is set to be zero. In other words, the lateral interactions in

this case contain only the electrostatic potentials. Two sharp and symmetric peaks are also found at $\varphi = \pm 90°$. The heights of the peaks are even more pronounced than the case where all interactions are present. The higher peaks show that the dispersion energy destabilizes the structure. Nevertheless, we have to include the dispersion energy to prevent the molecules from coming too close together. The almost flat line ('Disp.') in the figure represents the distribution when the electrostatic energy is turned off. No peaks are found which is in accord with no p(2x1) structure formation. Again, this is consistent with the above observation that the electrostatic interaction between molecules is the most important factor that helps the monolayer to adopt the p(2x1) structure. Knowing that the electrostatic interaction is the most important contribution for the forming of the (2x1) structure, suggests that in future work one can try to simplify the other interactions and concentrate on building a well-defined model to represent the electrostatic interactions between the molecules.

4.4 Summary

We have presented results of Metropolis Monte Carlo simulations of CO monolayer adsorbed on NaCl(100) surface, at temperatures ranging from 1 to 75K. We have shown that Monte Carlo simulations at finite temperatures can be used to reproduce the experimental proposed structure.[18,21,24] The CO molecules are found to form a well-ordered monolayer on the NaCl(100) surface at low

temperature. The CO molecules form an ordered p(2x1) structure with a surface unit cell consisting of two molecules adsorbed on identical sites and connected by a glide plane. The molecules then are found to lose their ordered structure and become a disordered p(1x1) phase with one molecule per unit cell in the regime of higher simulated temperatures (above 35K). However, the molecules are azimuthally uncorrelated yet remain tilted with respect to the surface. This is in contrast with proposals that the molecules bound perpendicularly to the surface at high temperature.[18,21] And so, we are able to clarify the discussion of the molecular orientation at the high temperature p(1x1) phase.

Evidence from the qualitative analysis confirms the existence of a phase transition between these two structures at around T~ 32 to 35K as deduced from the FTIR[21] spectra and HAS[24] study. Further quantitative analysis as well as the presence of the tilted molecules in the whole range of simulations demonstrate that the monolayer undergoes a continuous type of transition from an ordered low-temperature p(2x1) structure to a disordered high-temperature p(1x1) structure.

Based on those results, we are confident that our potential is a reliable one. Furthermore, we have shown from our studies that the molecule-surface electrostatic interaction is the most important contribution for the total binding energy. In addition, the electrostatic energy also plays a much more important

role than the dispersion interaction in defining the structure of the monolayer. Although, the repulsion energy is much less significant than the electrostatic energy, it is still needed to prevent the molecules coming too close together. The presence of the dispersion energy helps the molecule to tilt more and consequently helps the system to attain a higher transition temperature. Hence, knowing the importance of each contribution we can try to modify the potential in a way that will maximize the most important factor while minimizing the less significant one. As a result, we can modify a potential model that requires the least computer effort yet gives the most reliable results. In other words we know the key factors in modifying the potentials and how to find them should additional work and adjustments be needed in the future.

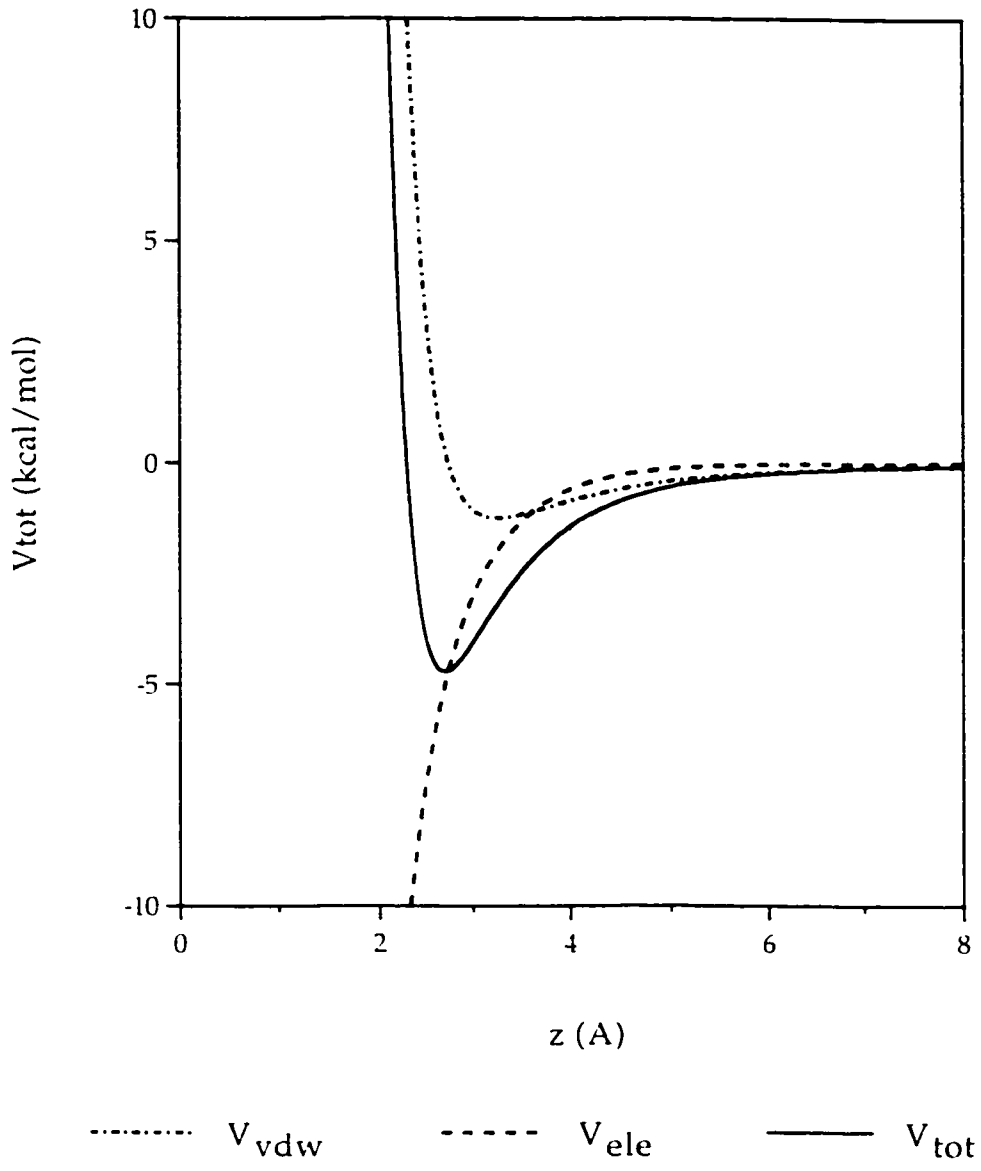

Figure 4.1. Plot of energies of a single molecule adsorption on NaCl(100) at the sodium site in a perpendicular orientation.

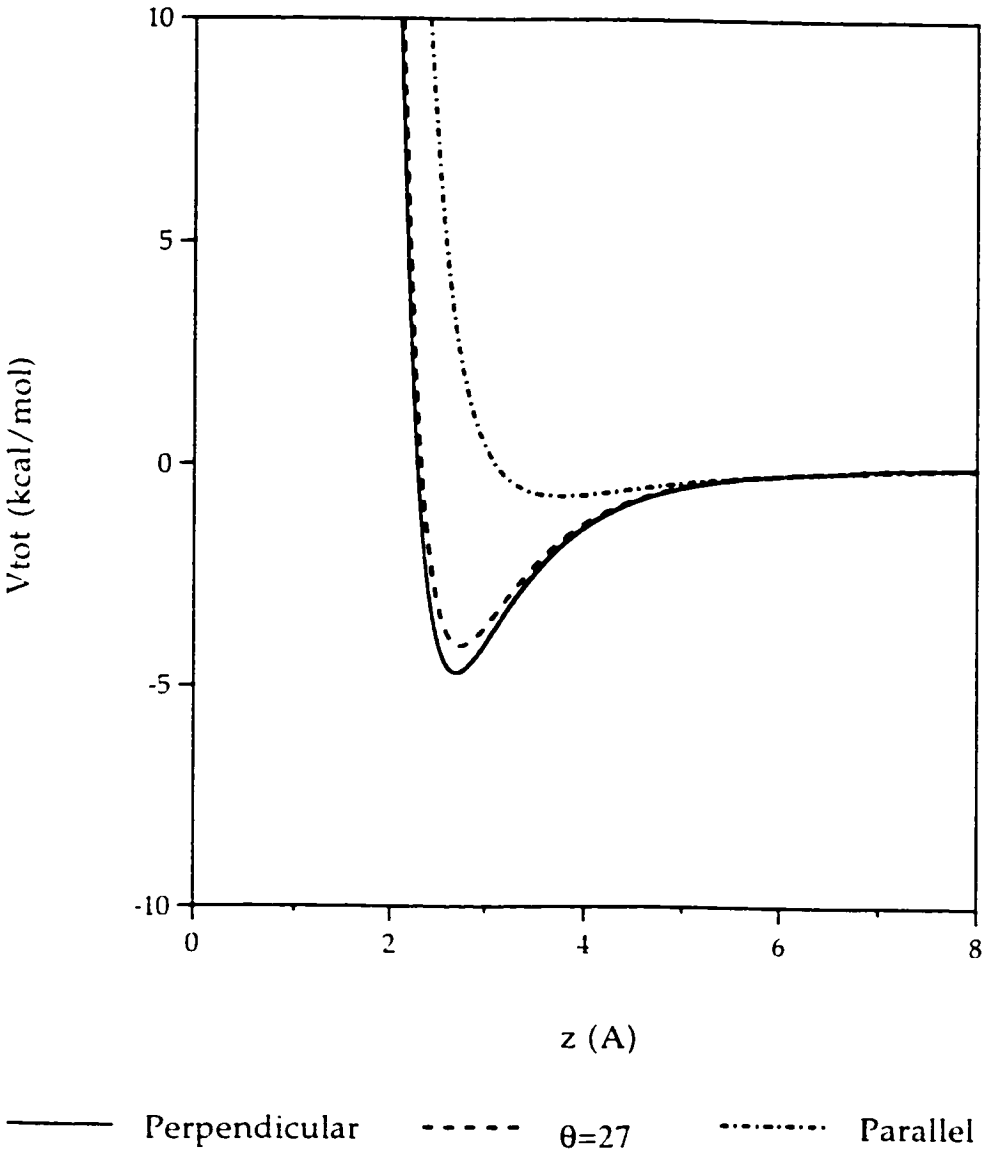

Figure 4.2. Plot of energies of a single molecule adsorption on NaCl(100) at different orientations.

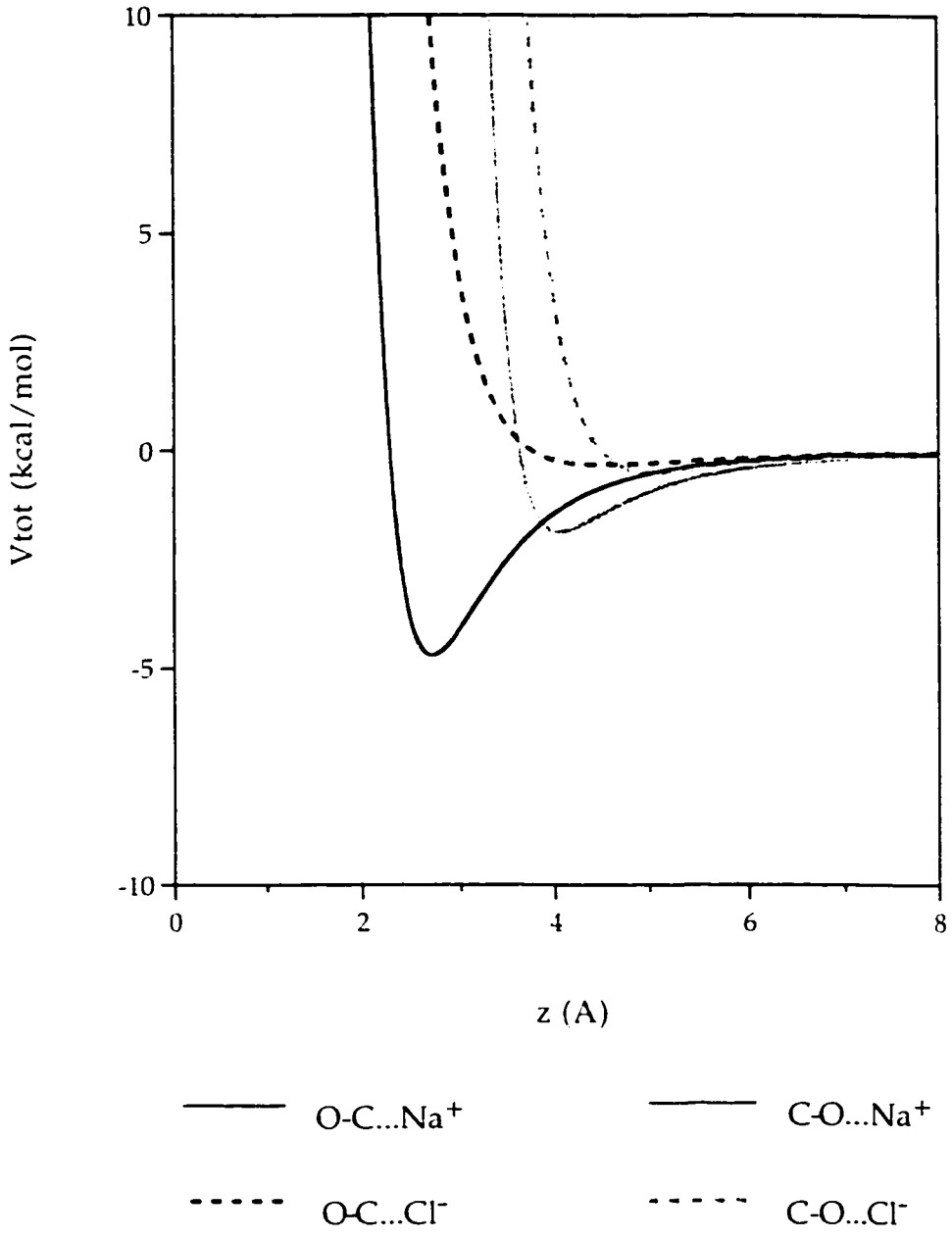

Figure 4.3. Plot of energies of a single molecule adsorption on NaCl(100) with different head-tail orientations.

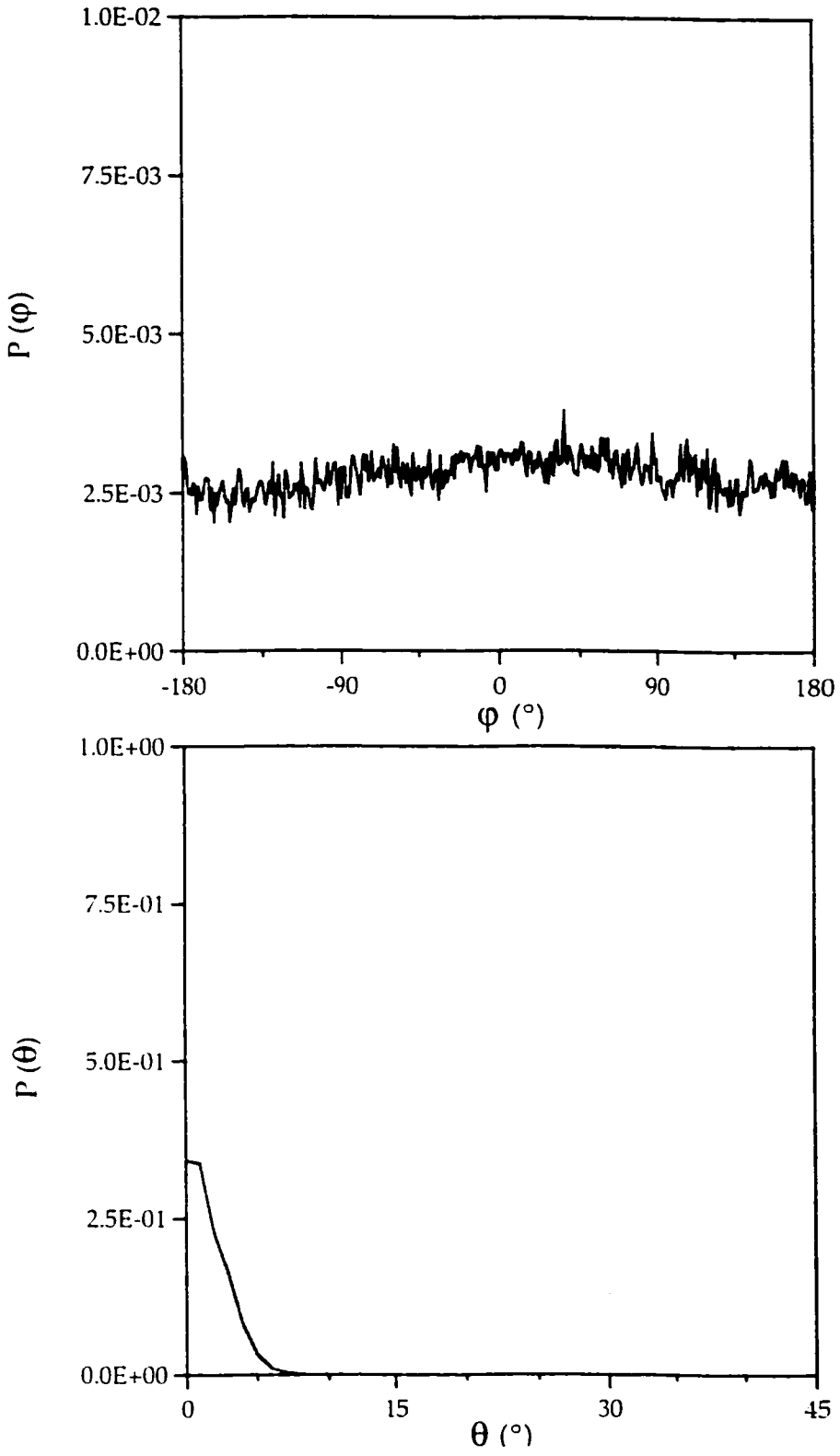

Figure 4.4. Monte Carlo results for the angular distributions for a single molecule adsorption on NaCl(100) at T= 1K. Polar, θ, (lower panel) and azimuthal, φ, (upper panel) distributions.

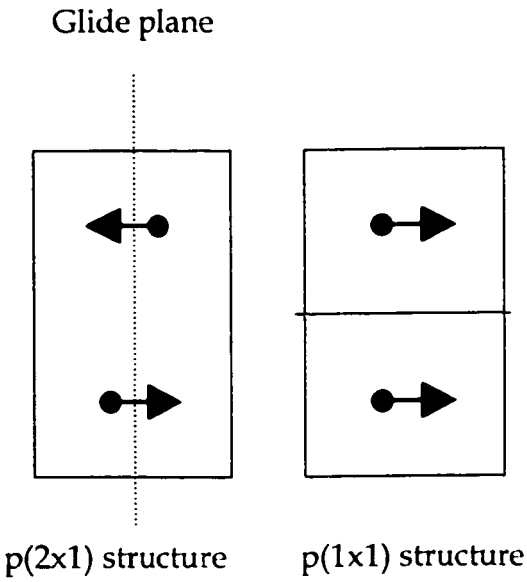

Figure 4.5. Illustration of the p(2x1) and the p(1x1) structures.

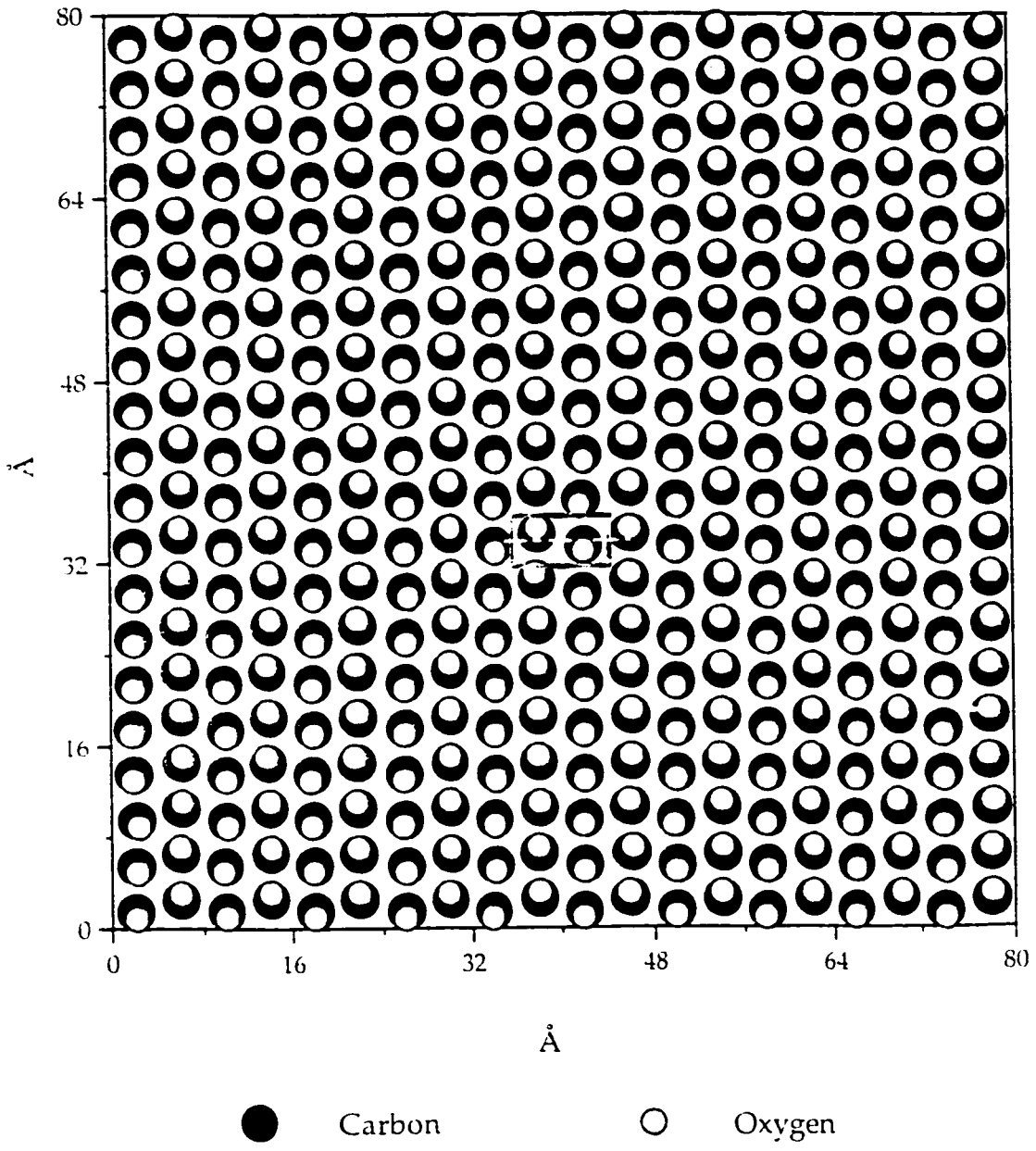

Figure 4.6. Configuration of a 20x20 lattice monolayer CO/NaCl(100) generated by Monte Carlo simulation at T 1K. The unit cell (grey line) contains two molecules and a glide plane (white dash line).

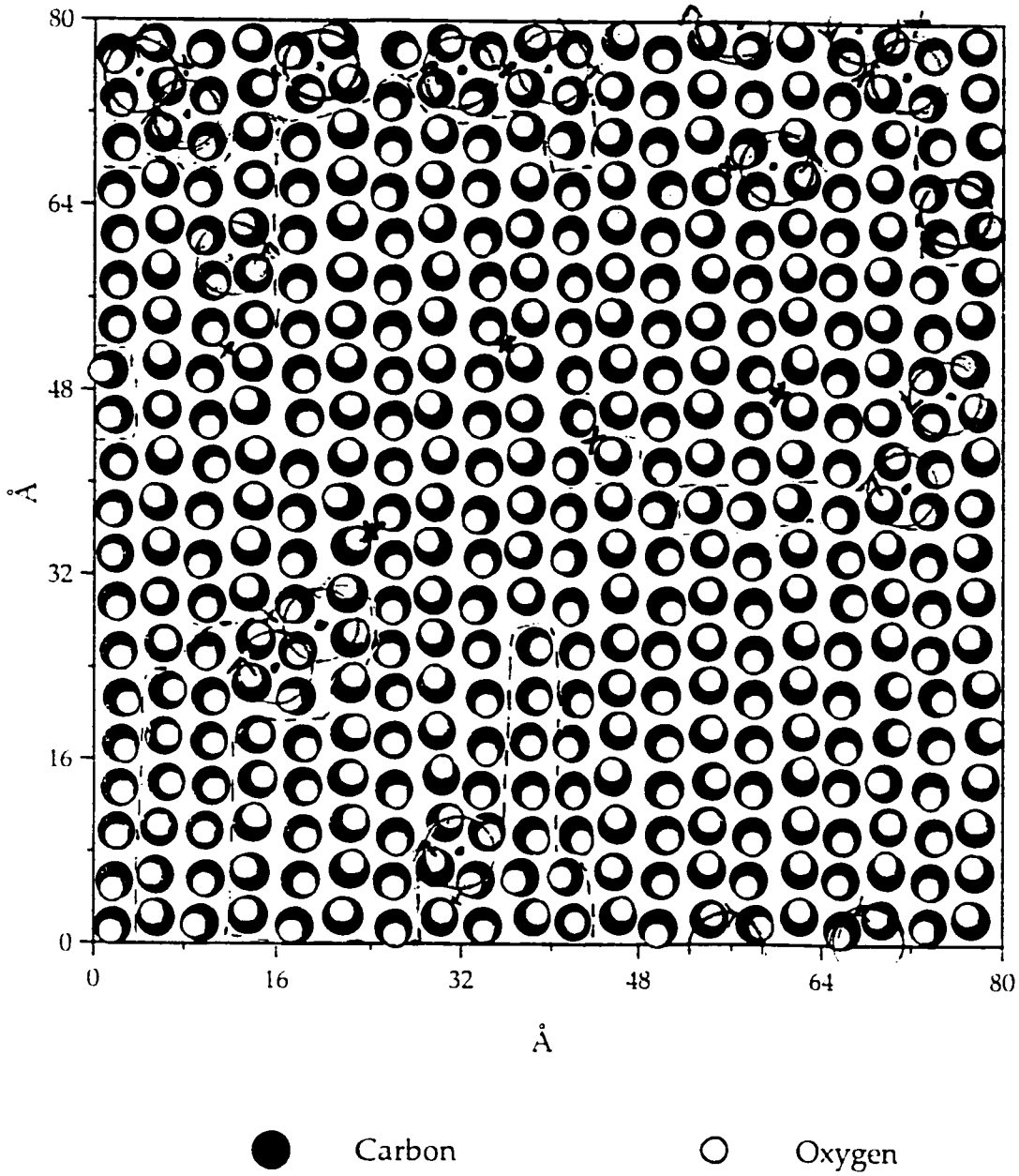

Figure 4.7. Configuration of a 20x20 lattice monolayer CO/NaCl(100) generated by Monte Carlo simulation at T 25K . The circle (vortex) and the cross (antivortex) represent the vortex-antivortex pair. The dashed regions represent domains of p(1x1) structure.

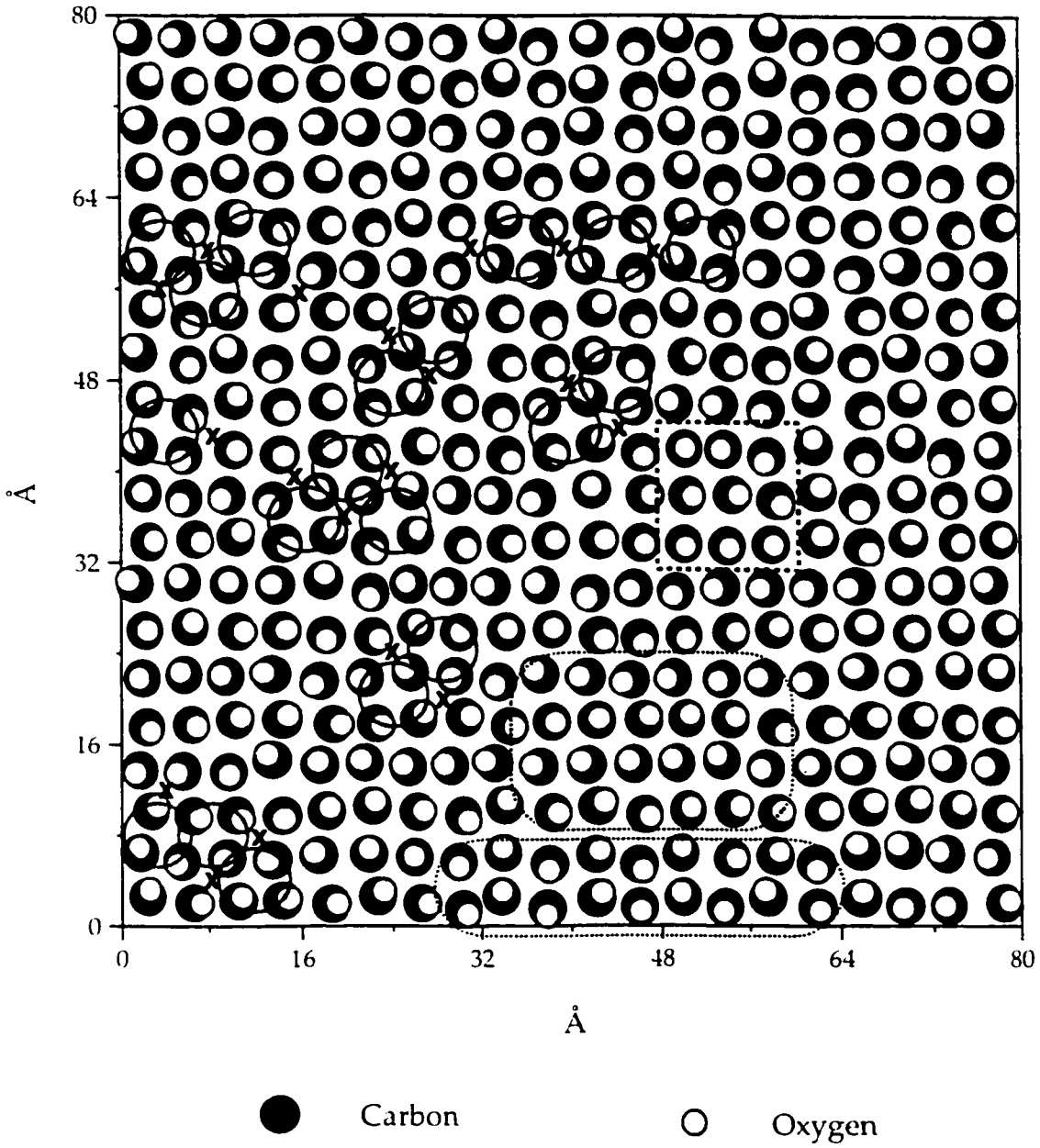

Figure 4.8. Configuration of a 20x20 lattice monolayer CO/NaCl(100) generated by Monte Carlo simulation at T 35K . The circle (vortex) and the cross (antivortex) represent the vortex-antivortex pair. The dotted and dashed rectangles represent domains of p(2x1) and p(1x1) structures, respectively.

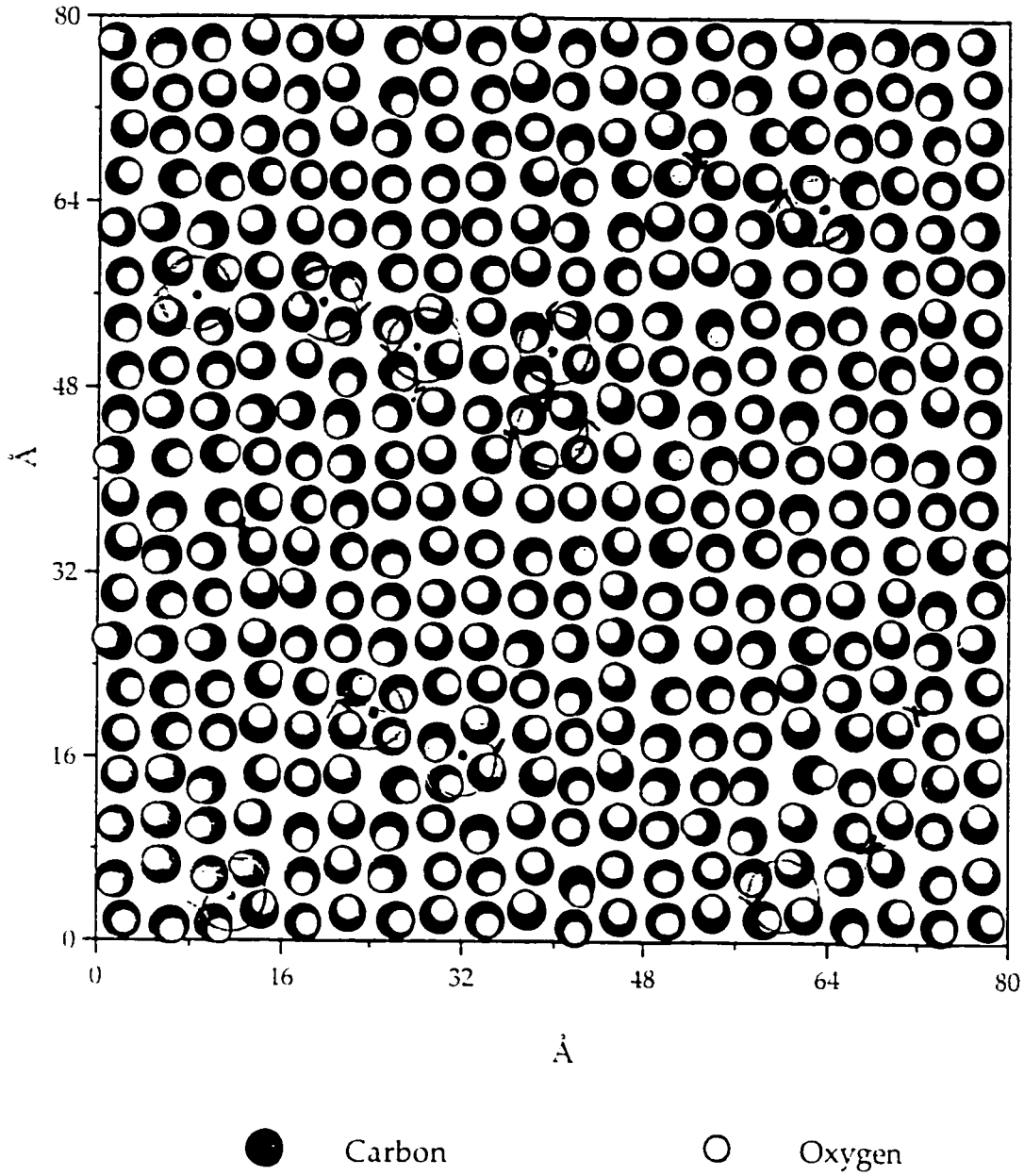

Figure 4.9. Configuration of a 20x20 lattice monolayer CO/NaCl(100) generated by Monte Carlo simulation at T 75K. The circle (vortex) and the cross (antivortex) represent the vortex-antivortex pair.

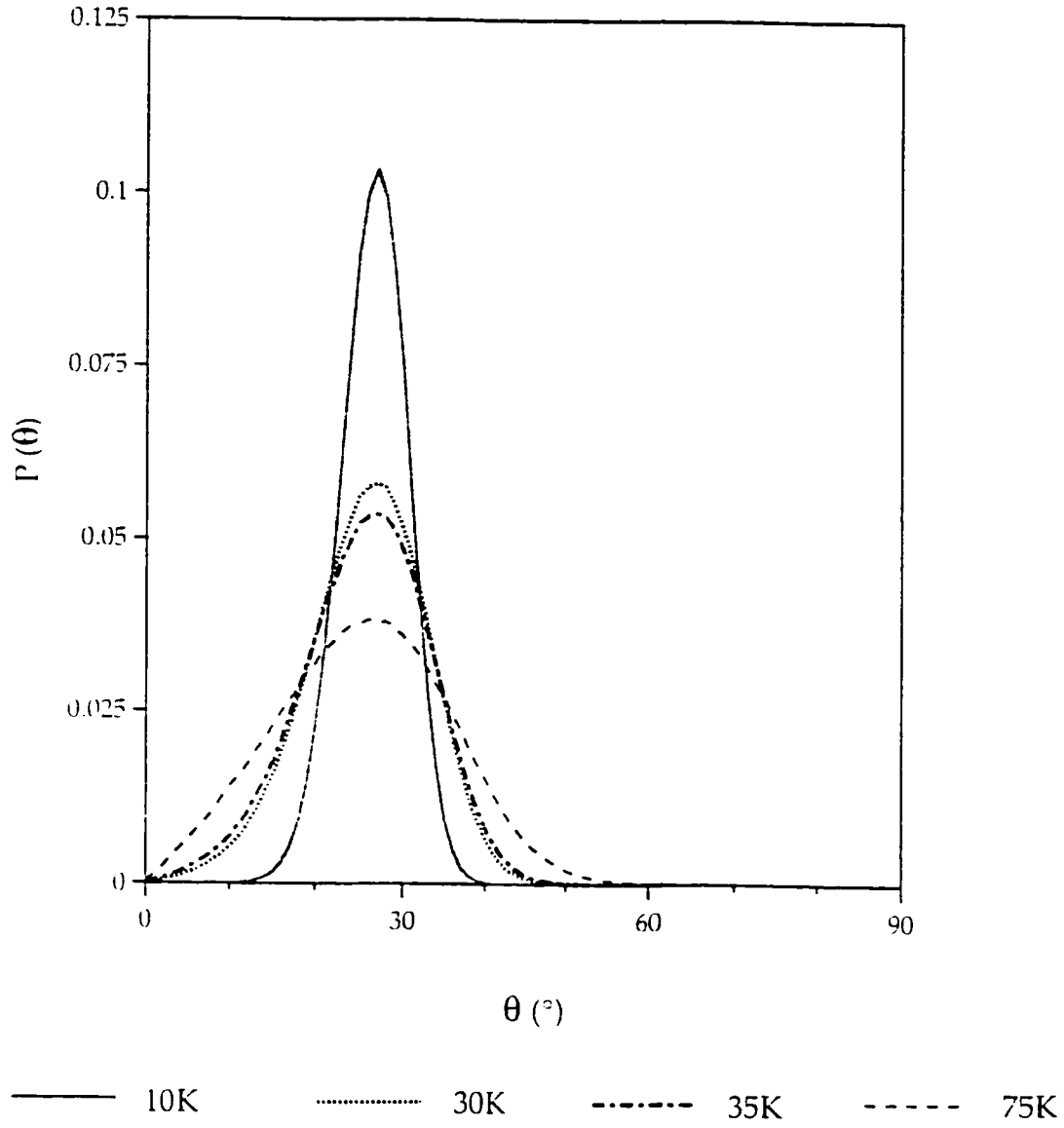

Figure 4.10. The polar (θ) distribution for a 20x20 lattice monolayer CO/NaCl(100) generated by Monte Carlo simulation.

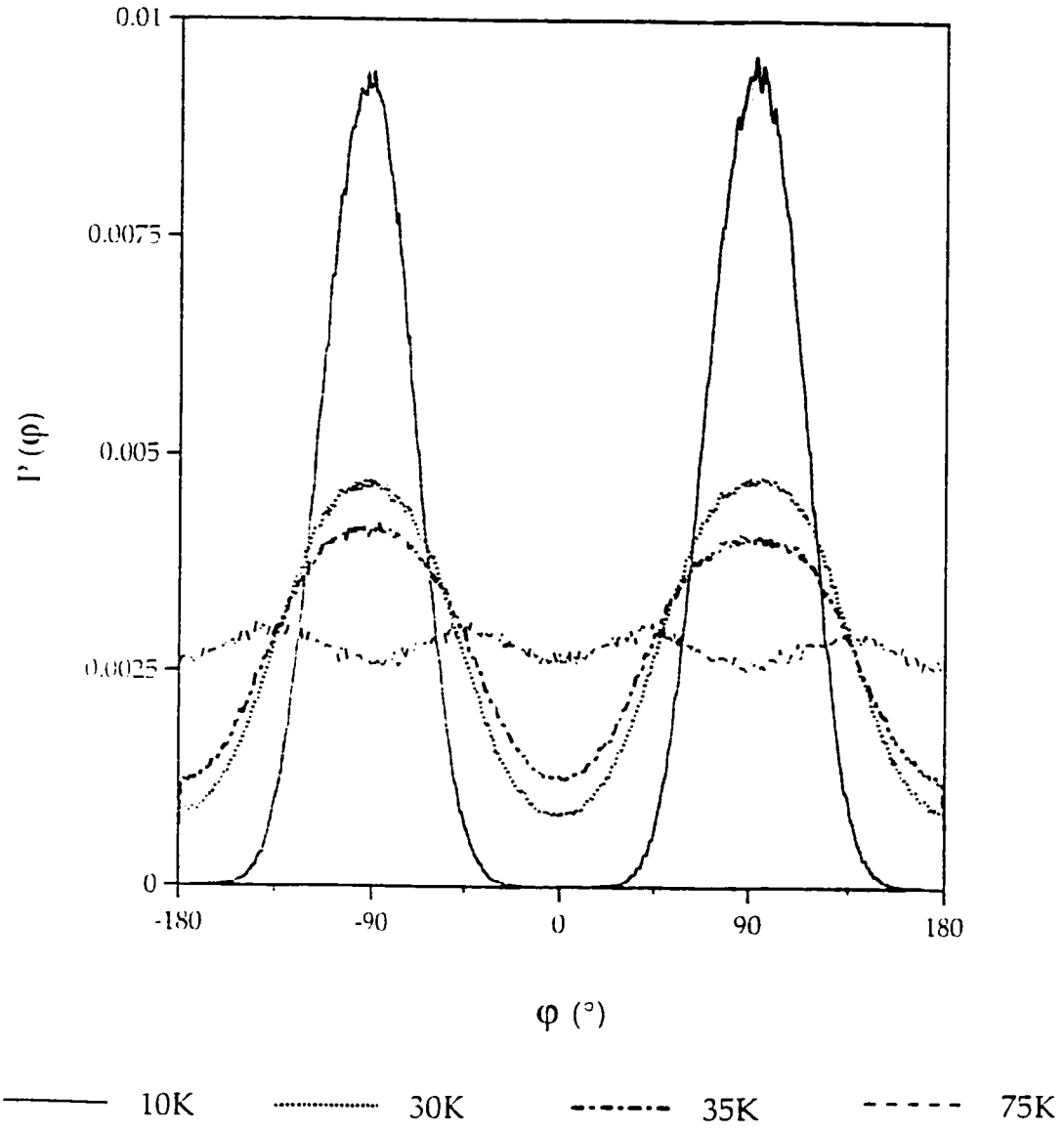

Figure 4.11. The azimuthal (φ) distribution for a 20x20 lattice monolayer CO/NaCl(100) generated by Monte Carlo simulation.

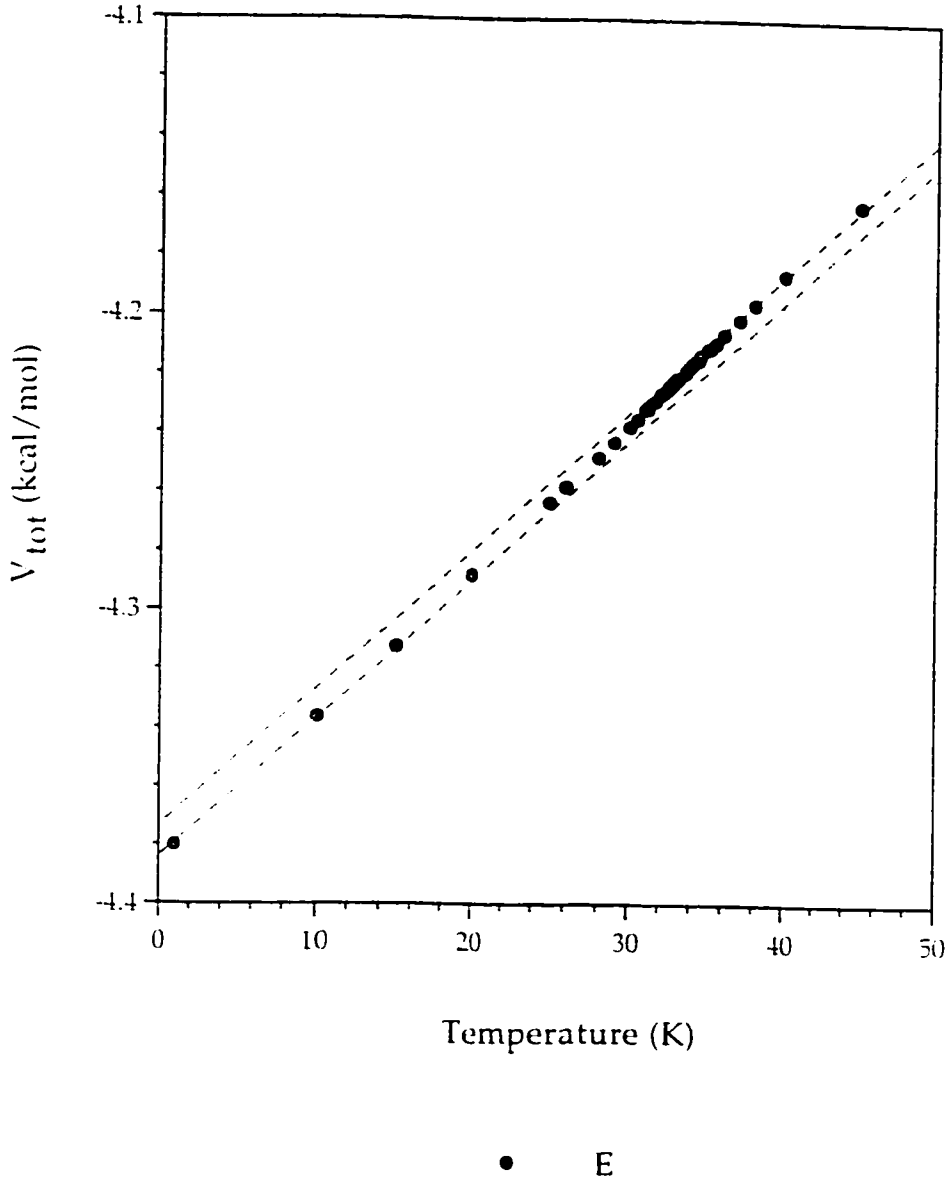

Figure 4.12. Monte Carlo results for the energy, E, as a function of temperature for a 20x20 lattice monolayer CO/NaCl(100).

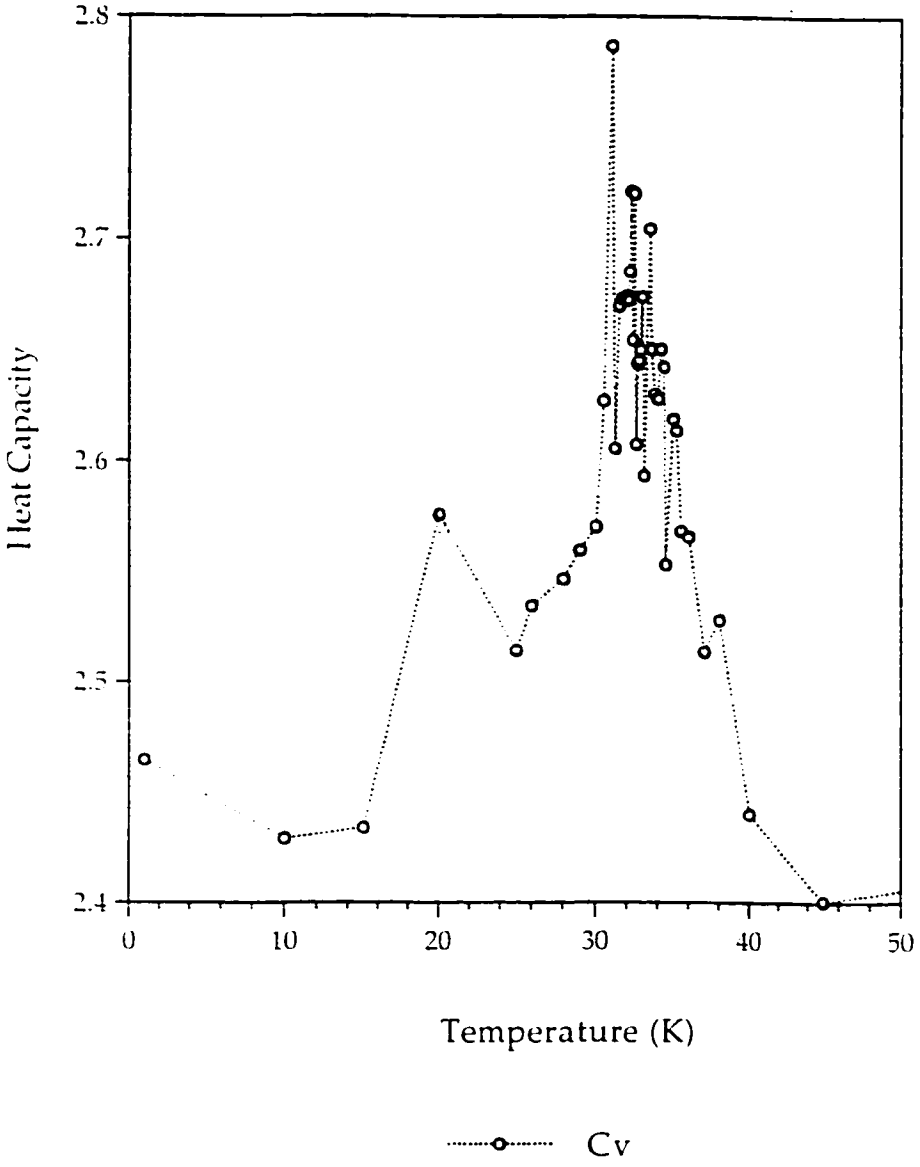

Figure 4.13. Monte Carlo results for the heat capacity, C_v, as a function of temperature for a 20x20 lattice monolayer CO/NaCl(100).

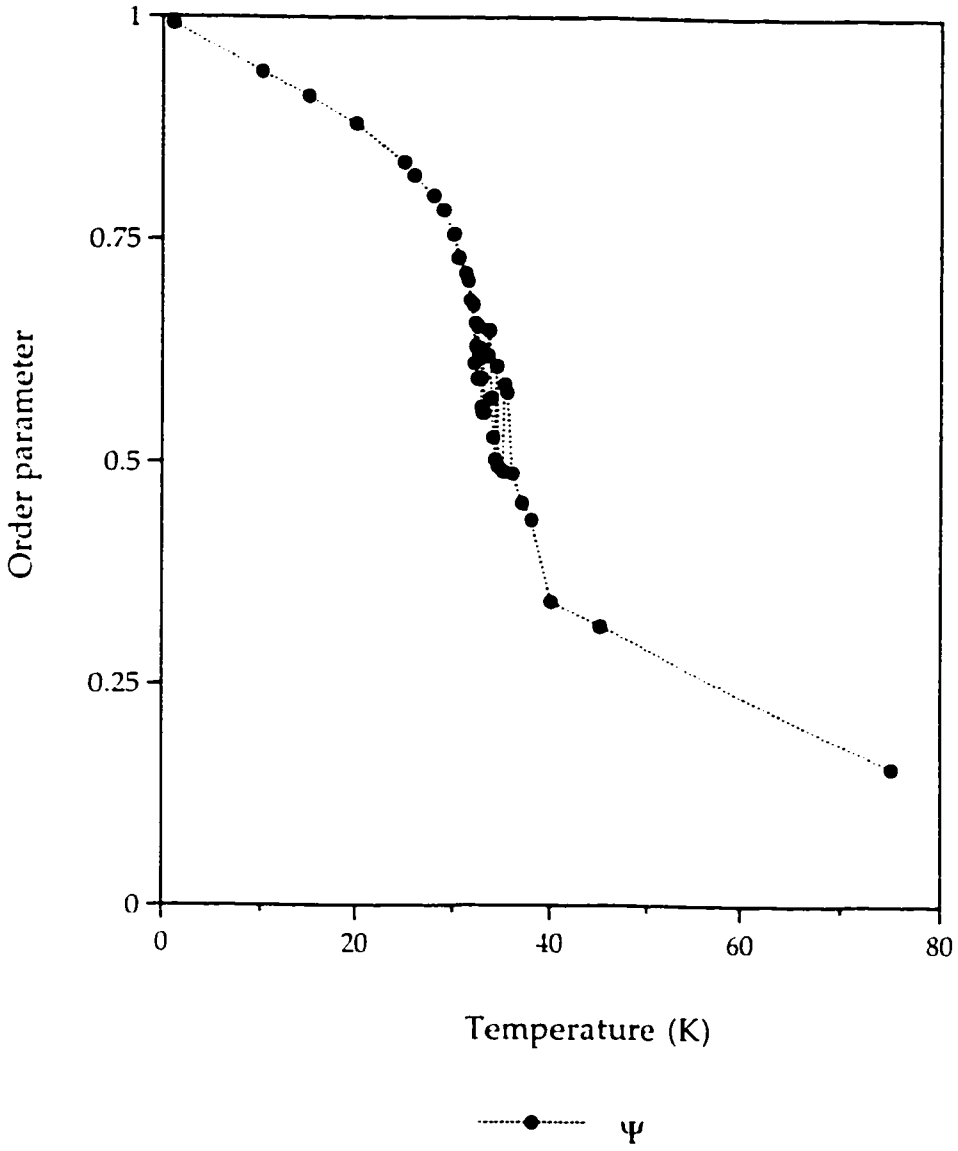

Figure 4.14. Monte Carlo results for the order parameter, ψ, as a function of temperature for a 20x20 lattice monolayer CO/NaCl(100).

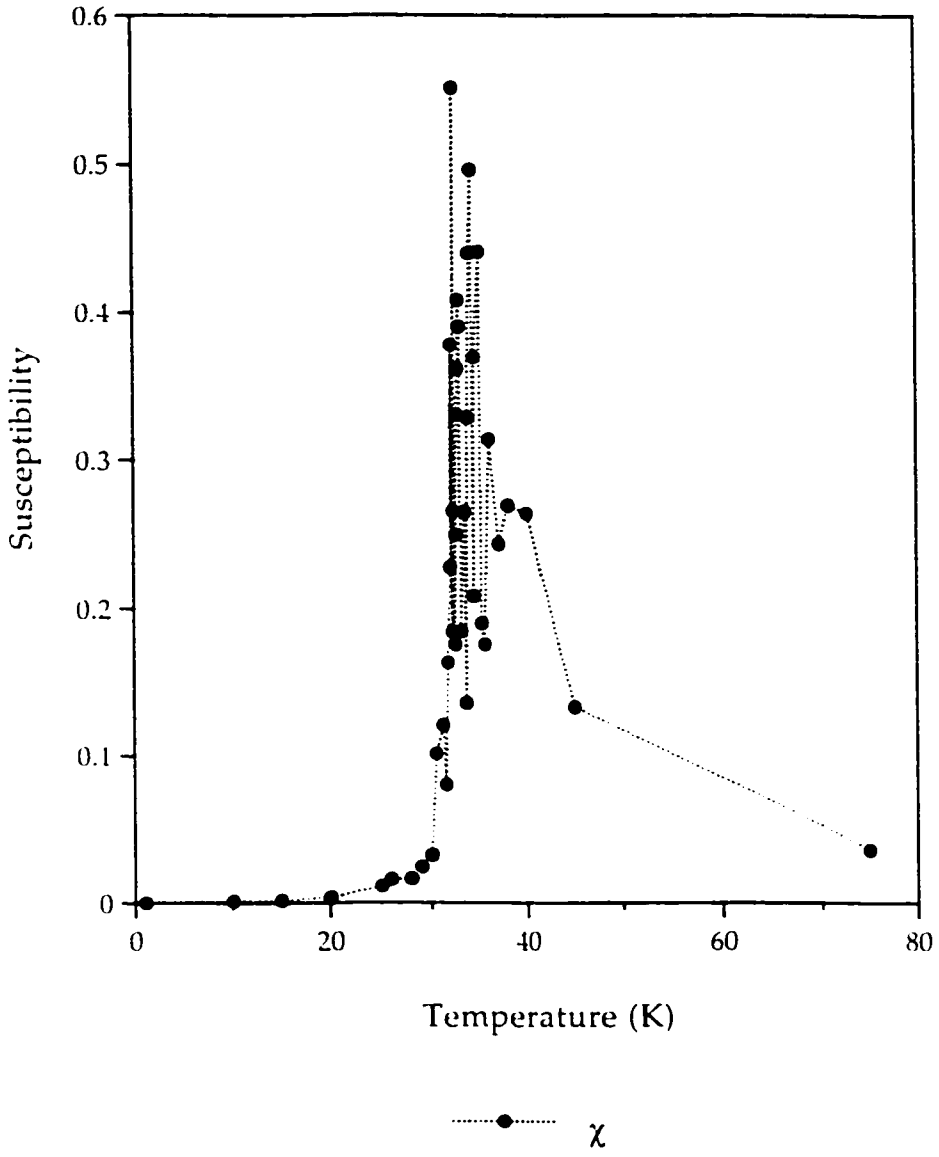

Figure 4.15. Monte Carlo results for the susceptibility, χ, as a function of temperature for a 20x20 lattice monolayer CO/NaCl(100).

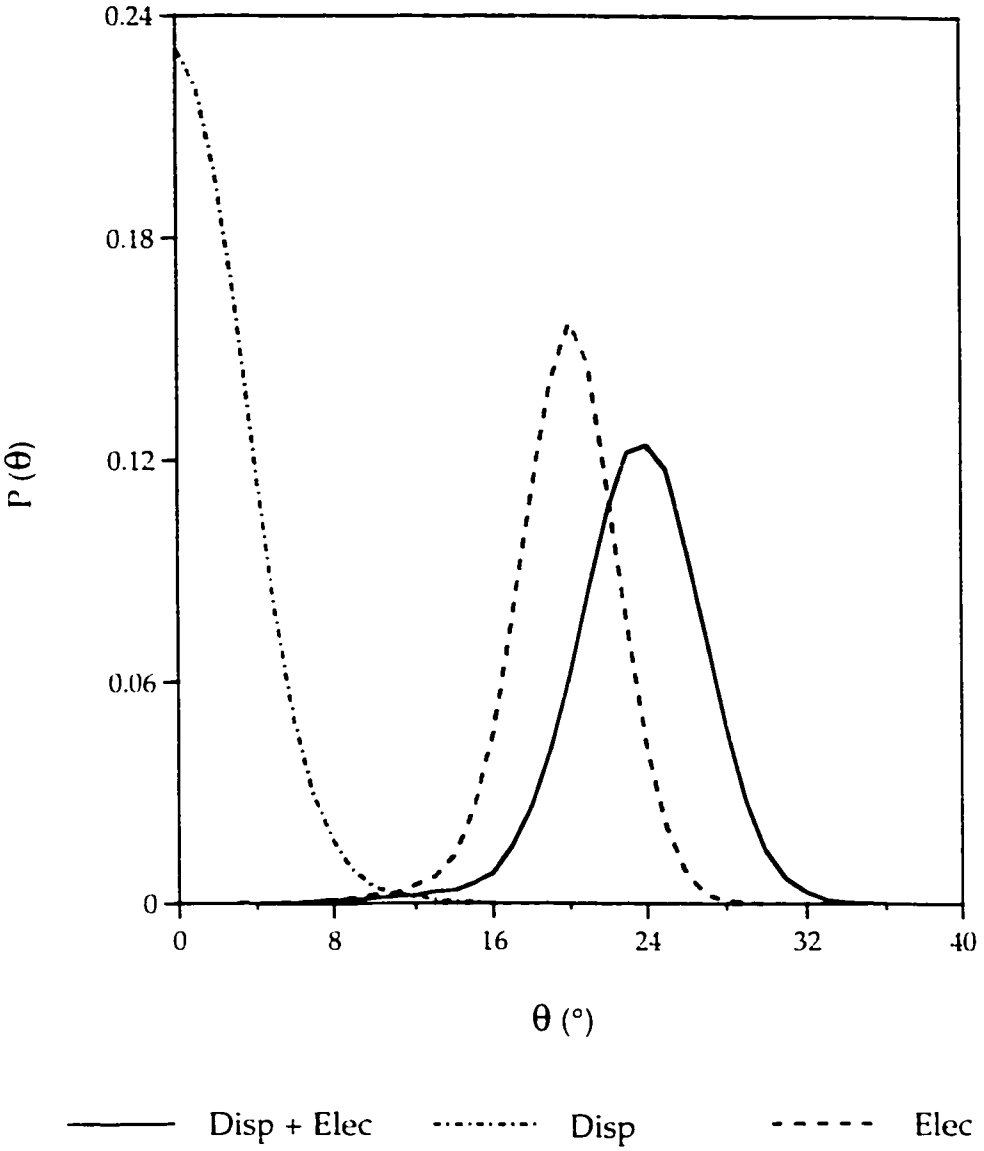

Figure 4.16. The polar (θ) distribution for a 10x10 lattice monolayer CO/NaCl(100) generated by Monte Carlo simulation for different potential energy tests.

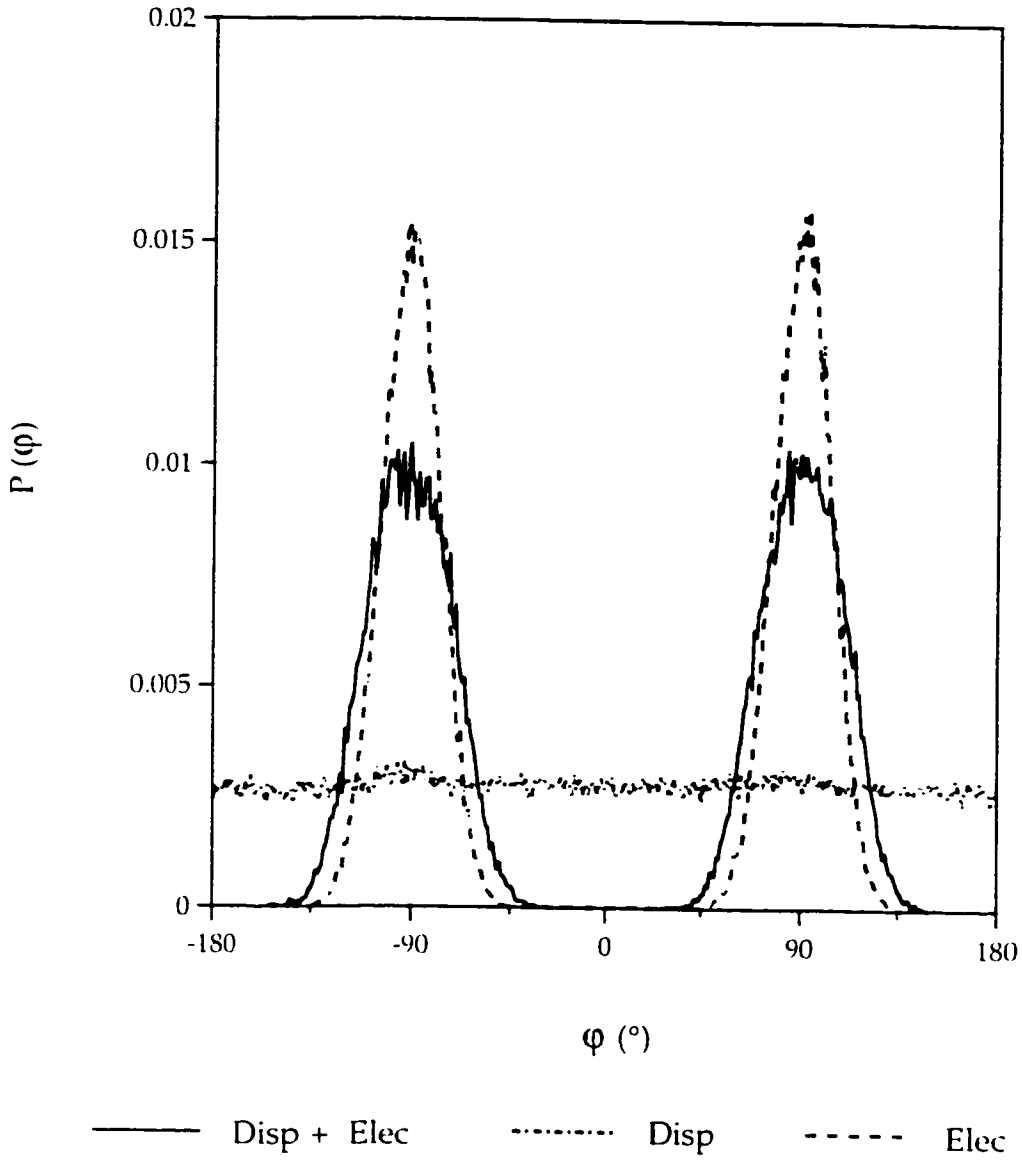

Figure 4.17. The azimuthal (φ) distribution for a 10x10 lattice monolayer CO/NaCl(100) generated by Monte Carlo simulation for different potential energy tests.

CHAPTER 5: RESULTS FOR SUBMONOLAYER CO/NaCl(100)

Apart from the study of the monolayer system, investigations into the structure of submonolayer systems (any CO adsorbed coverage that is less then 100%) were also conducted to find out if the full monolayer system was needed to see the p(2x1) structure. We studied the structure of several submonolayer systems using Monte Carlo simulations, with conditions similar to that of the study of the full monolayer system.

5.1. Adsorption of Two CO Molecules on NaCl(100)

At first, two CO molecules were placed next to each other in a nearest and next nearest neighbour, positions on a full surface as illustrated in Fig. 5.1 (*e.g.* 1-2 and 1-4, respectively). The molecules are found to have a minimal tilt angle, θ of about 1°, so on average the molecules are almost perpendicular to the surface, as in the case of a single molecule adsorption. The plot of phi distributions for molecules in the nearest-neighbour and next-nearest-neighbour positions show some preferences in the azimuthal orientation as illustrated in Fig. 5.2, although they do not fully form a p(2x1) pair as in the full monolayer. At these positions the two molecules are found to librate around $\varphi \sim \pm 90°$ as nearest neighbours (lower panel) and $\varphi \sim +45°, -135°$ as next nearest neighbours (upper panel) but their azimuthal orientations do not fully lock into those angles. Thus, the molecules show instantaneous preferences even though on average their orientation with respect to the surface normal is very small as shown by the

small tilt angle ($\theta \sim 1°$) as previously observed. On the other hand, if two CO molecules are placed farther than a next nearest neighbour positions (for example positions 1 and 5 in Fig. 5.1) then they do not have any effects on each other and the azimuthal distribution is flat.

5.2. Adsorption of Three CO Molecules on NaCl(100)

The adsorption of three CO molecules was also examined. They were placed in a row aligned on positions 1, 3, and 5 in the unit cell as illustrated in Fig. 5.1. The molecules are found to tilt at a much larger angle, $\theta \sim 16°$ at T= 1K (Fig. 5.3, lower panel). This is quite a significant increase compared to the adsorption of two molecules because the lateral interaction (interaction between CO molecules) is greater in this case. As in the previous test (in section 4.3) the dispersion interaction is found to be responsible for the molecules tilting away from the surface normal. Furthermore, the dispersion energy is also known to increase with increasing number of interactions in the system. Therefore, with more molecules adsorbed in the structure, an increase of tilt angle is expected. Nonetheless the molecules are rapidly untilted ($\theta \sim 5°$) when the temperature is raised to around T~ 5K. The phi distribution shows a very sharp peak at 0° (see Fig. 5.3, upper panel) at T= 1K, demonstrating that the molecules have a preferred azimuthal orientation. However, the pointed peak is significantly smaller at T= 5K and a second peak at $\varphi \sim 180°$ appears. With only three

molecules adsorbed on a row, we did see the similar azimuthal orientations compared to the molecules within a row of a full monolayer, yet this azimuthal orientation quickly disappears with an increase of temperature. It is worth noting that with the addition of only 1 molecule, we observed a substantial increase in the polar tilt angle from $\theta\sim 1°$ (two-molecules adsorption) to $\theta\sim 16°$ (three-molecules adsorption).

5.3. Adsorption of Four CO Molecules on NaCl(100)

A close look at the structure of the adsorption of four molecules on NaCl(100) reveals an anti-vortex structure (Fig. 5.4, lower panel). If this structure is replicated to form several more structures that are placed close to each other, then the vortex-antivortex pairs can be created as illustrated in Fig. 5.5. This type of structure was previously observed at the level of the full monolayer of CO/NaCl(100) in the region of the phase transition (Fig. 4.8). This finding emphasizes the presence of the vortex-antivortex structures that are formed by the close range interactions between the CO molecules within the layer. An increase in tilt angle ($\theta\sim 20°$) is found as expected according to an increase in dispersion energy as previously mentioned. Four distinct peaks (two sharp peaks at $\varphi\sim 45, -135°$ and two broader double peaks at $\varphi\sim \pm 45°$) are observed in the phi distribution plot of the four-molecule adsorption as shown in Fig. 5.4, upper panel. This demonstrates that the molecules have strong preferences in the

azimuthal orientation, and couples with the rather large polar angle the molecules lock into this structure at low temperature. However, the stability of this structure quickly disappears at around T= 5K, as shown in the same Fig. 5.4, upper panel.

5.4. Adsorption of CO/NaCl(100) at Submonolayer Regimes: Sixteen, Thirty-six and Sixty-four Percent Coverage

The p(2x1) structure does not occur with 4 molecules or less so studies of larger islands were also conducted to examine the dependence of the p(2x1) structure on the size of the adsorbed layer. In particular, studies of square islands of 16, 36 and 64 CO molecules were conducted. The systems were equilibrated at low temperature (T= 1K) and then were gradually heated up to T= 50K. Snapshots at T= 10K of the different island sizes were taken to examine the structures and are shown in Fig. 5.6. The molecules located in the inside of the islands are found to form a structure that is close to the p(2x1) as highlighted by the dashed line in all three panels. The closeness to the p(2x1) structure of the monolayer results is found to increase with the growing size of the island as expected since the larger the size of the island, the greater the lateral interactions between the molecules become. Still the molecules at the edges of the islands do not form the p(2x1) structure because of the boundary effects of the islands. With weaker molecule-molecule interactions, these molecules show a tendency

to be perpendicular because of greater influence by the molecule-surface interactions. However, the imperfections at the boundary also show an improvement with the increasing size of the islands. This is understandable because the boundary effect gets smaller when the size gets larger and eventually goes to zero 100% coverage.

The "not-so-perfect-order" structures in the middle of the islands also show an increasing degree of disorder as the temperature is raised during the simulations. This transition can be studied by examining the angular distributions of the different island sizes, which are shown in Fig. 5.7, 5.9, and 5.11. From the theta distributions plots (lower panels) one can see that substantial numbers of molecules in the island structures in all three sizes untilt at high temperature. According to those preliminary results, the phase transitions in these cases are best characterized as structural phase transitions, not order-disorder phase transition as in the full monolayer case because the tilt angles have significantly broadened and shifted towards $\theta \sim 0°$ as the temperature is raised. These remarks can also be confirmed by looking at the snapshots of the islands at T=50K in Fig. 5.8, 5.10, and 5.12 (upper panels). At this temperature, the majority of the molecules are found to orient perpendicular to the surface, regardless of the size of the islands. However, there is still evidence of some tilted molecules in the layer, evidence of an order-disorder type of transition. The peaks observed at low temperature in the phi distributions are also found to

broaden and eventually to go flat as shown in Fig. 5.7, 5.9 and 5.11, (upper panels). This is in part due to the shifts in polar angles towards $\theta \sim 0°$. At this angle, the molecules are adsorbed perpendicularly to the surface, and hence, the molecules do not show any preferences in the azimuthal orientations. These observations suggest that the CO islands also undergo a phase transition as in the study of the full monolayer system although at a much lower temperature. More studies needed to be done in order to determine the transition type although preliminary observations might suggest that the layers also undergo an order-disorder type of phase transition.

5.5. Adsorption of CO/NaCl(100) at Submonolayer Regime: Twenty Thirty and Fifty Percent Coverage at Random Adsorption Sites

Besides the studies of the islands structures, we also conducted another sub-monolayer systems where 25 (25%) and 50 CO molecules (50%) were randomly placed on the surface. To make the adlayer more mobile, the molecules were allowed to jump from site to site within the Monte Carlo program. The top panel of Fig. 5.13 shows that at T= 10K the molecules aggregate to form two small islands. Strips of molecules in the middle of the big island are found to adopt the "not-so-perfect" p(2x1) structure. As the temperature is increased to T=30K (Fig. 5.14, lower panel), two small islands are found to form a rather bigger one with the molecules (even those in the middle of the island) losing

their preferred azimuthal orientations and becoming disordered as expected. At T= 50K (upper panel of Fig. 5.14) the molecules are dispersed to three small islands and they are found to coexist with seven CO gas molecules, which scatter throughout the surface. The molecules remaining in the island are found to adopt the p(1x1) structure in an disordered fashion.

As previously mentioned, simulations of 50 CO molecules were also performed. Behaviours similar to the 25% coverage study were obtained. Namely, the molecules aggregate to form an elongated island as shown in the lower panel of Fig. 5.15. Again, molecules in the middle of island are observed to form the p(2x1) structure at T=10K. When the temperature is raised to T= 50K, the molecules form a single large island where the majority of the molecules adopt the p(1x1) structure. The number of gas molecules, which have broken free of the island and constitute a "2-d gas" in this system is less pronounced than those in the 25% system because the molecules need a larger amount of energy to break free from the island due to a greater number of molecule-molecule interactions. Nonetheless, it is evident that the coexistence of the island and "2-d gas" is present as seen in the upper panel of Fig. 5.15.

5.6. Summary

It is apparent from our results that in order to see the ordered p(2x1) structure it is necessary to have a full monolayer system. As previously discussed, none of the sub-monolayer systems studied produce a perfect p(2x1) structure. Nevertheless, the above studies reveal that the degree of formation and "perfection" of a p(2x1) structure is size dependent. The larger the size of the island the better the p(2x1) structure observed in the interior of the island because the CO-CO interactions are enhanced with the increase in numbers of molecules in the system. The molecules at the borders on the other hand, which are not surrounded by other CO molecules, do not form a p(2x1) structure because they do not have the same number of interactions between the molecules as the other ones. As a consequence, they are subject to an asymmetric boundary effect.

The ability of the random gas molecules to aggregate to form islands at low temperature does not agree with the FTIR analysis of Ewing *et al.*[17] They claimed that the gas molecules at low percentage of coverage were likely to adsorb randomly upon hitting the surface. There exists a weak net interaction within the adsorbed layer favouring a random arrangement of submonolayer CO/NaCl(100). This could happen if the energy barrier of the adsorbed molecules is large compared to the mobile molecule. In other words, when a

molecule sticks to the surface, it takes a considerable amount of energy to make it mobile again in order for it to move around and to form an island. In our simulations, we ignored that possibility and made the molecules as mobile as possible. As a result, the molecules aggregate to form islands in the study.

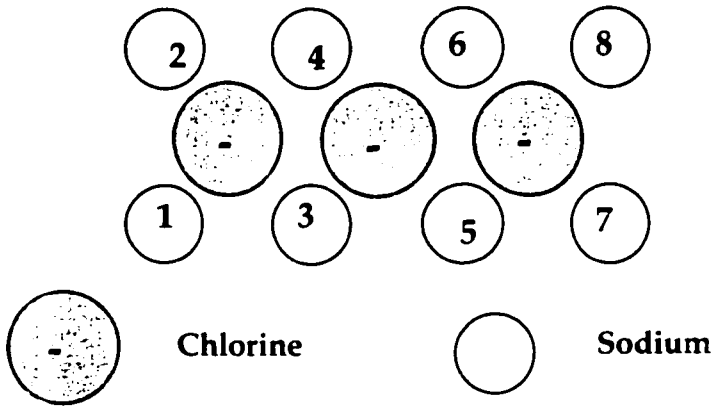

Figure 5.1. Positions of adsorbed CO with respect to the unit mesh of the NaCl surface. The numbers are the adsorbed positions discussed in the text.

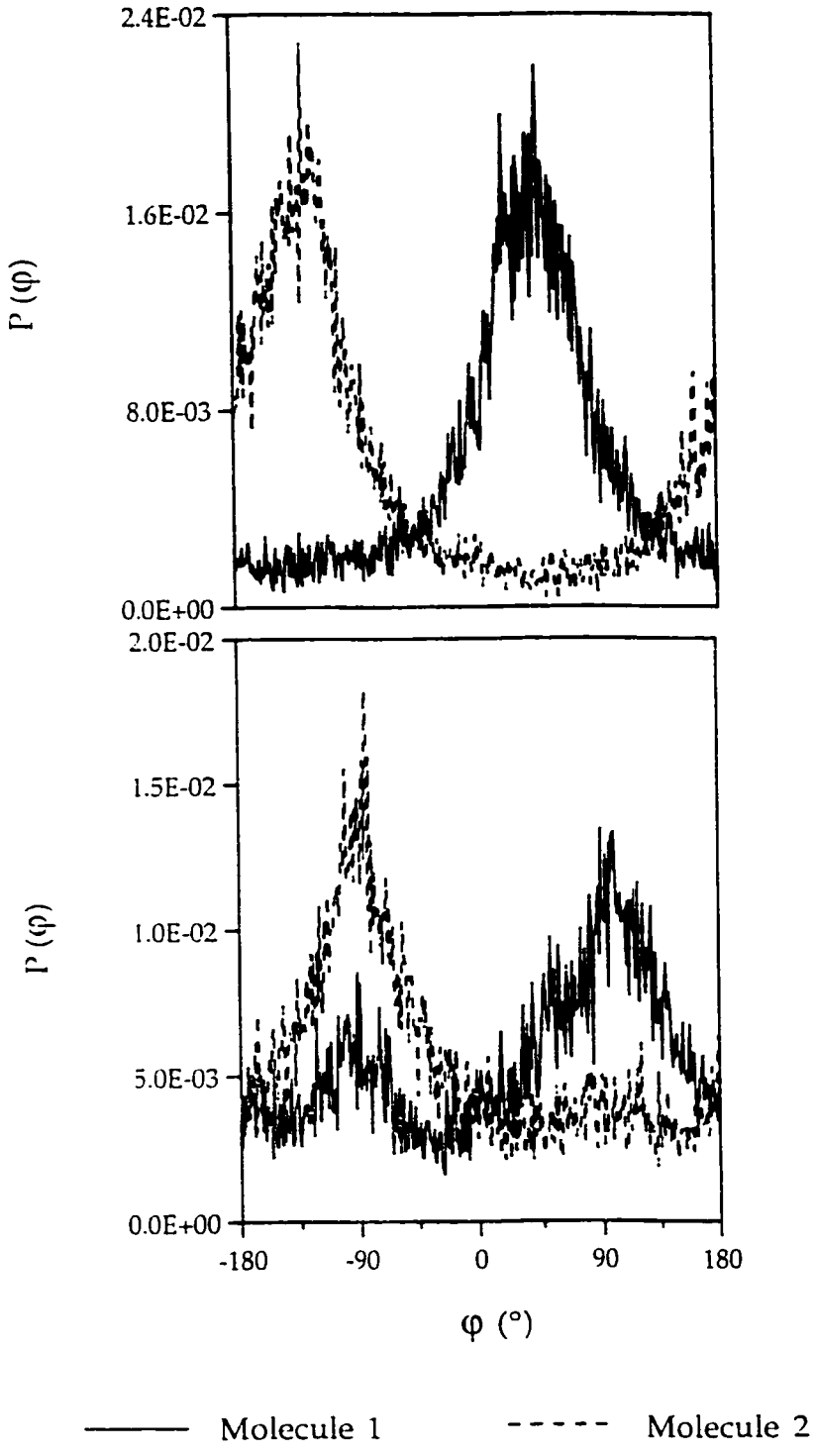

Figure 5.2. The azimuthal (φ) distributions of two CO/NaCl(100) at positions 1-2 (lower panel) and 1-4 (upper panel).

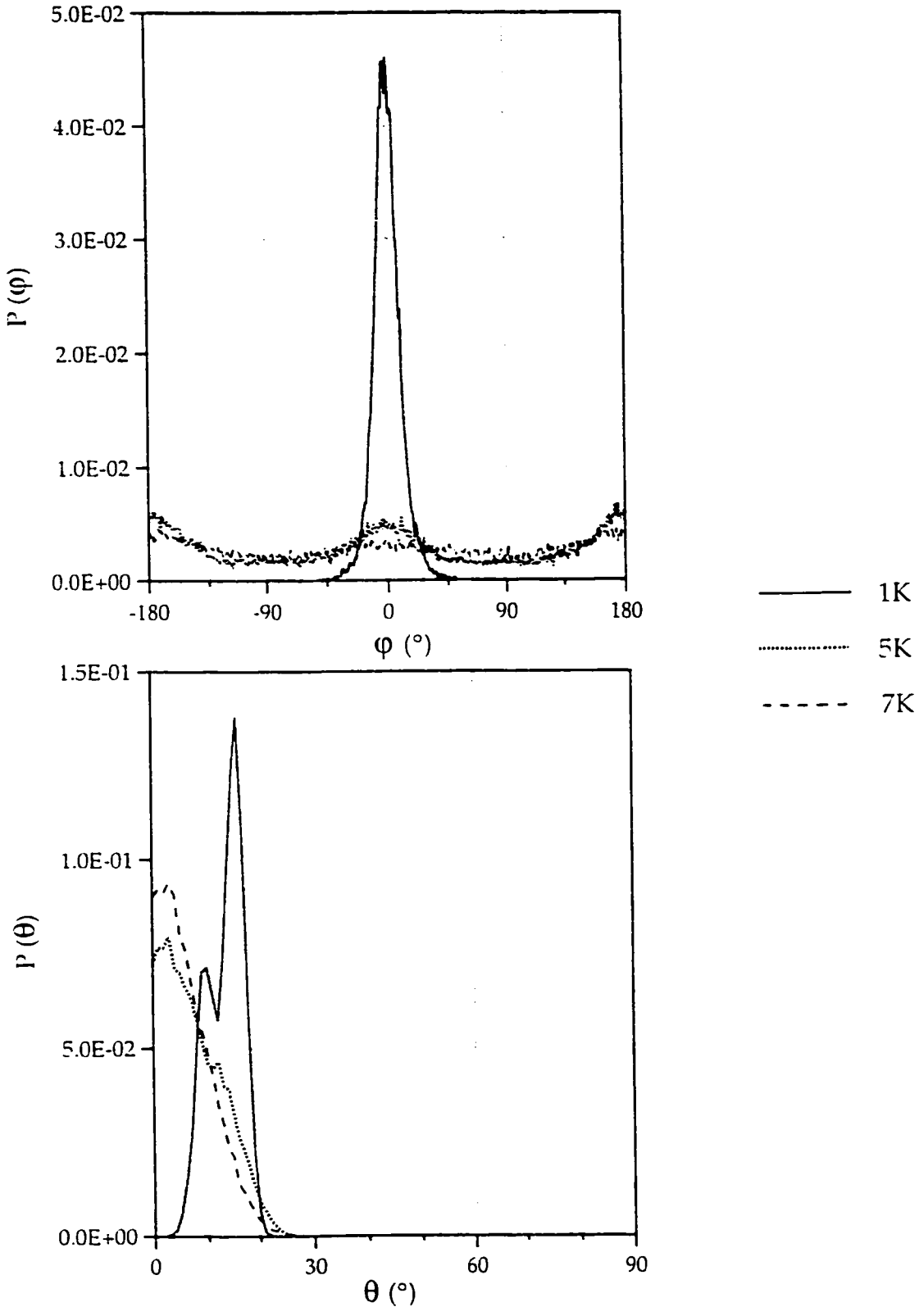

Figure 5.3. The angular distributions of three CO/NaCl(100): polar, θ (lower panel) and azimuthal, φ, (upper panel) distributions.

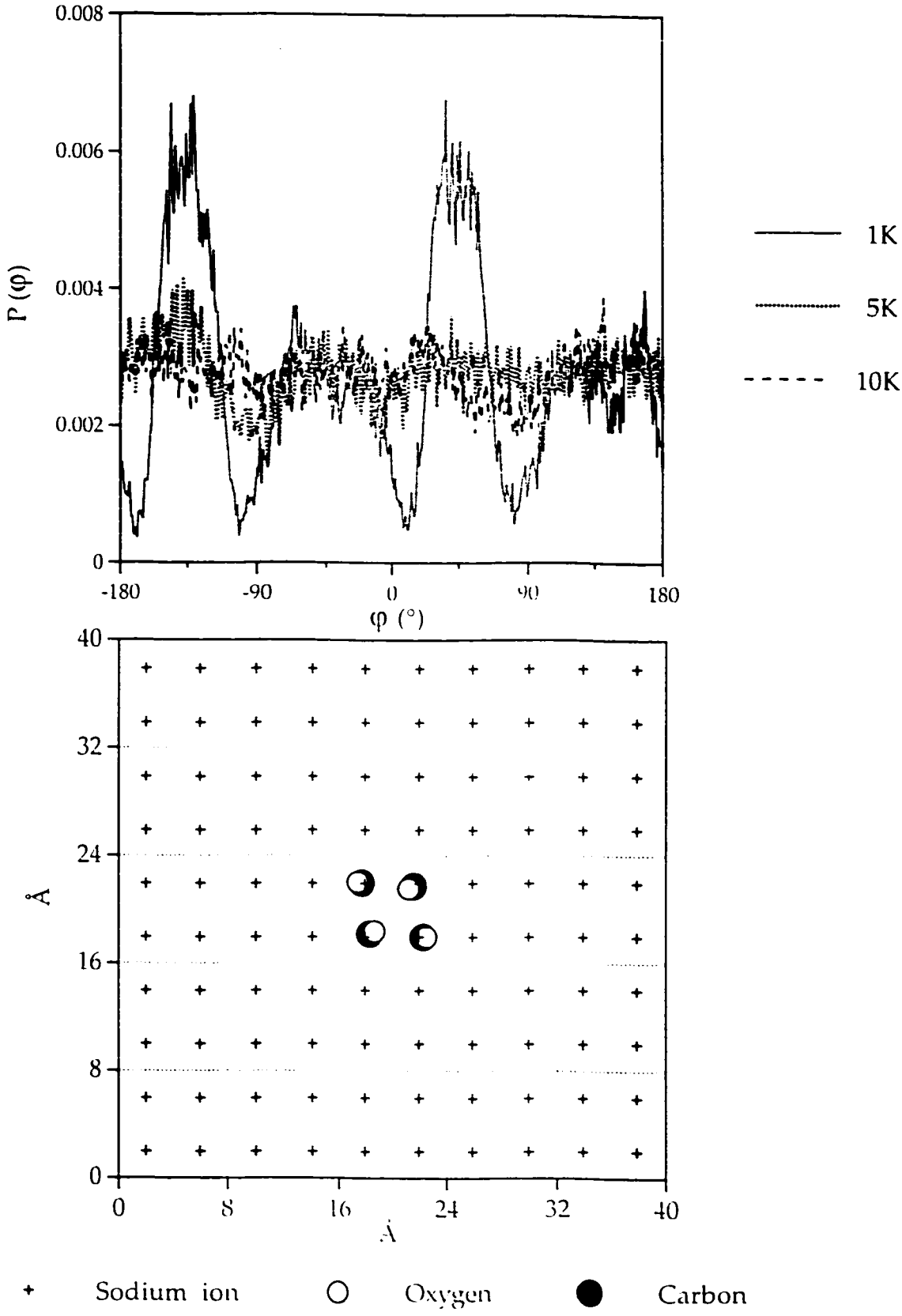

Figure 5.4. Four CO/NaCl(100) configuration (lower panel) generated by Monte Carlo simulation at T=1K and azimuthal, φ, distribution (upper panel) for four CO/NaCl(100).

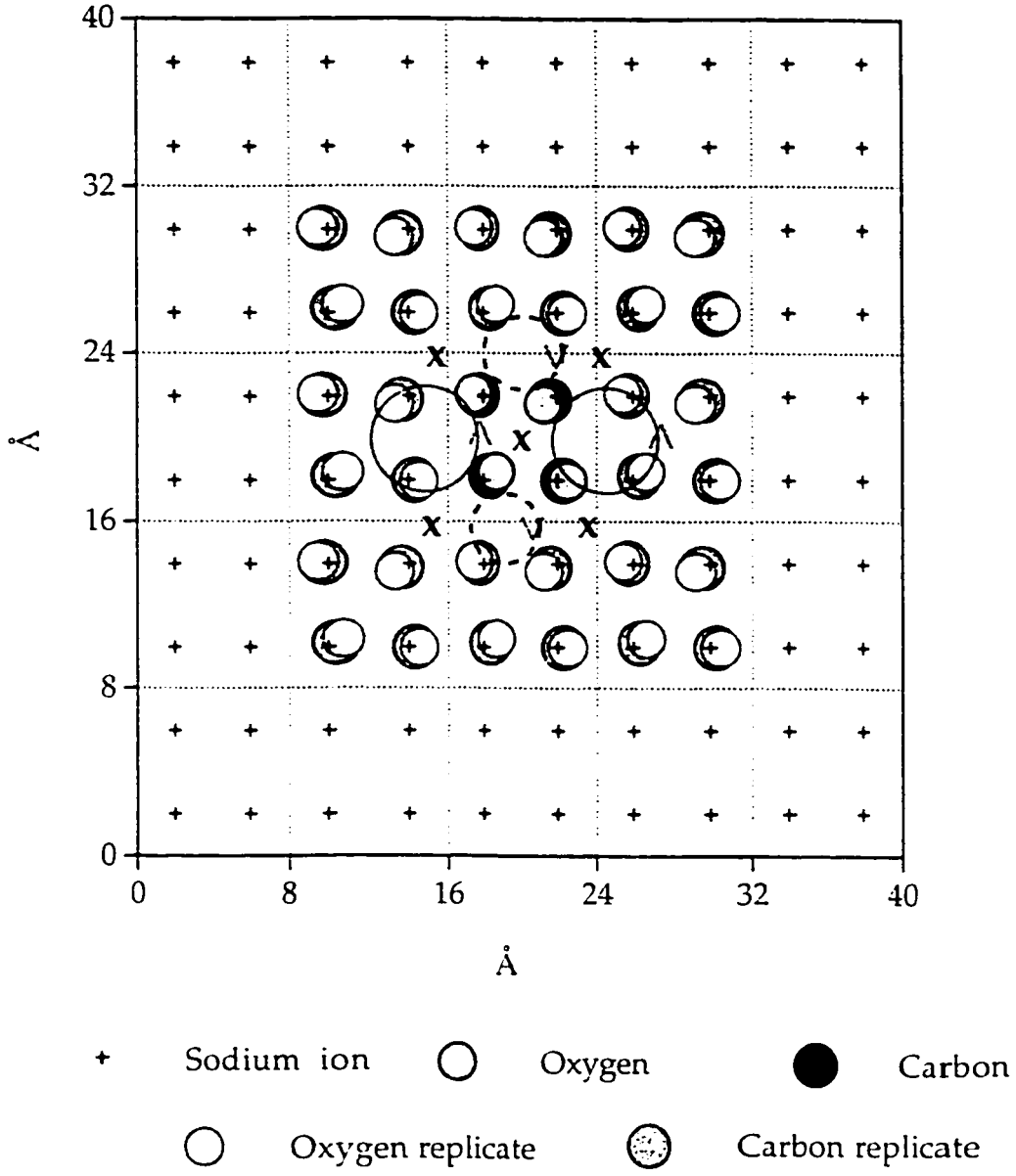

Figure 5.5. Four CO/NaCl(100) configuration in dark colour and their replications in light colour. The x, the solid circle and the dash circle represent the antivortex, the counter clockwise vortex and the clockwise vortex, respectively.

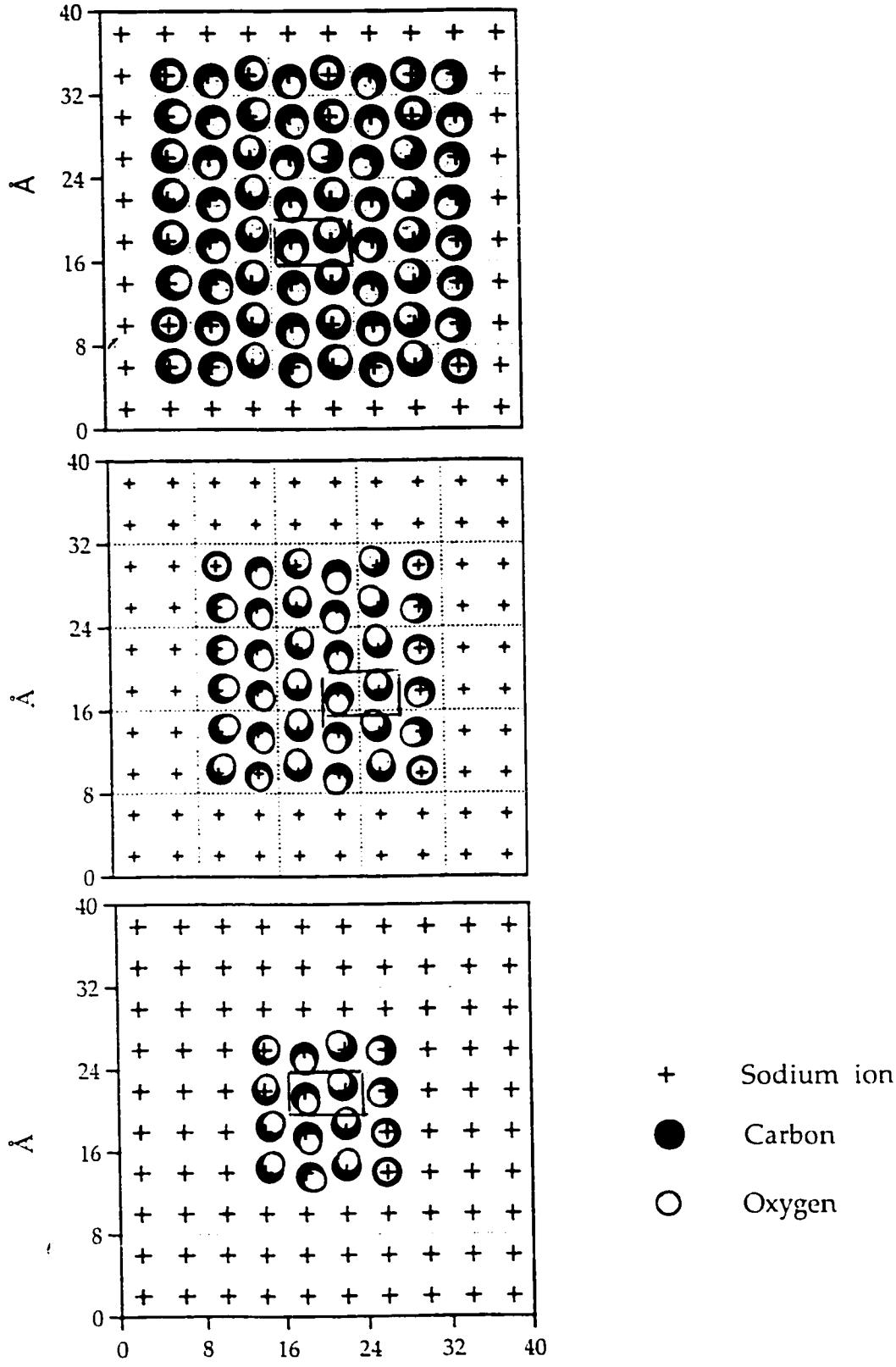

Figure 5.6. Configurations for different percent coverages for submonolayer CO/NaCl(100) systems generated by Monte Carlo simulation.: sixteen (lower panel), thirty-six (middle panel) and sixty-four (upper panel) percent coverage.

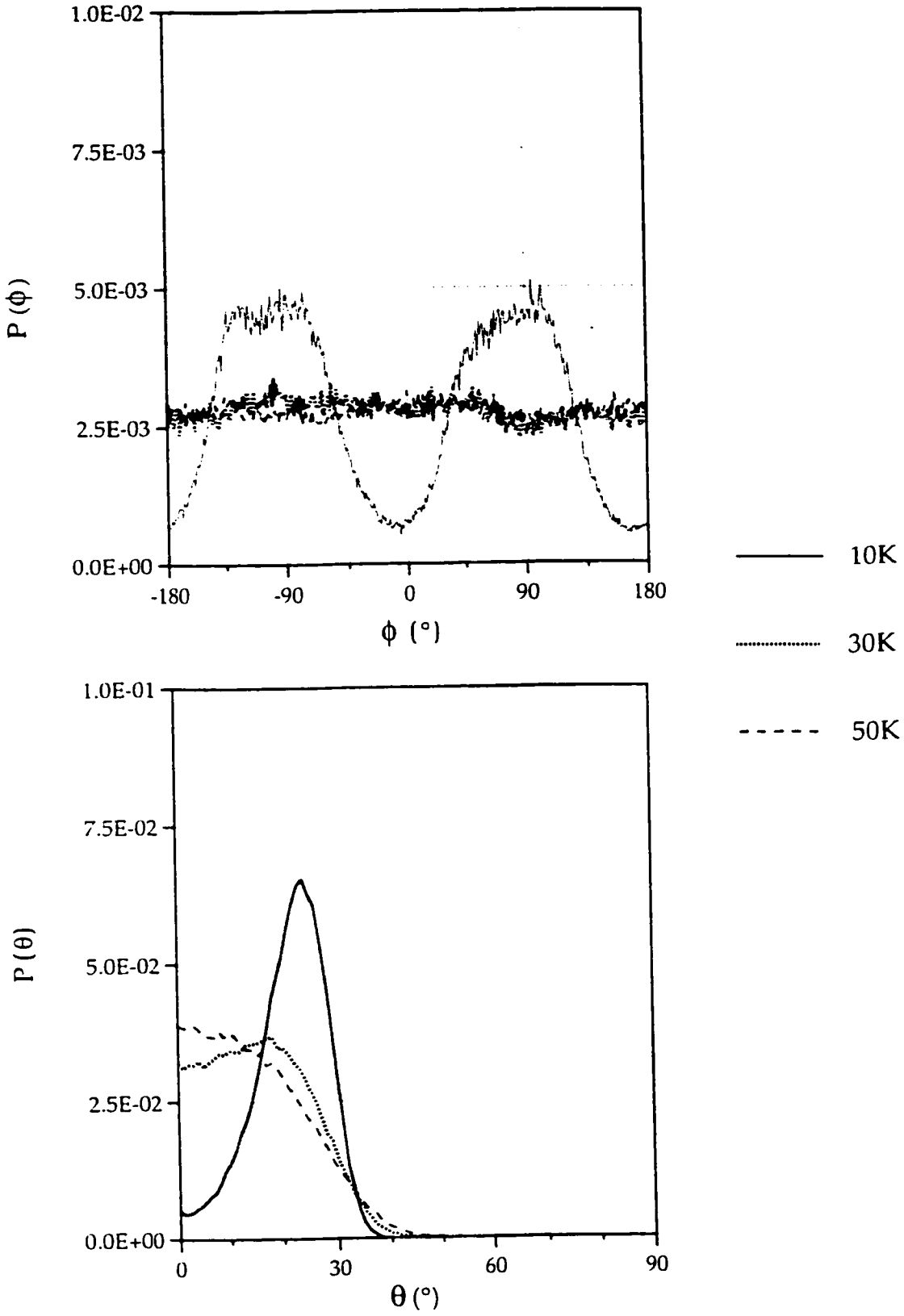

Figure 5.7. Angular distributions for sixteen percent CO/NaCl(100) system: polar, θ, (lower panel) and azimuthal, φ, (upper panel) distributions.

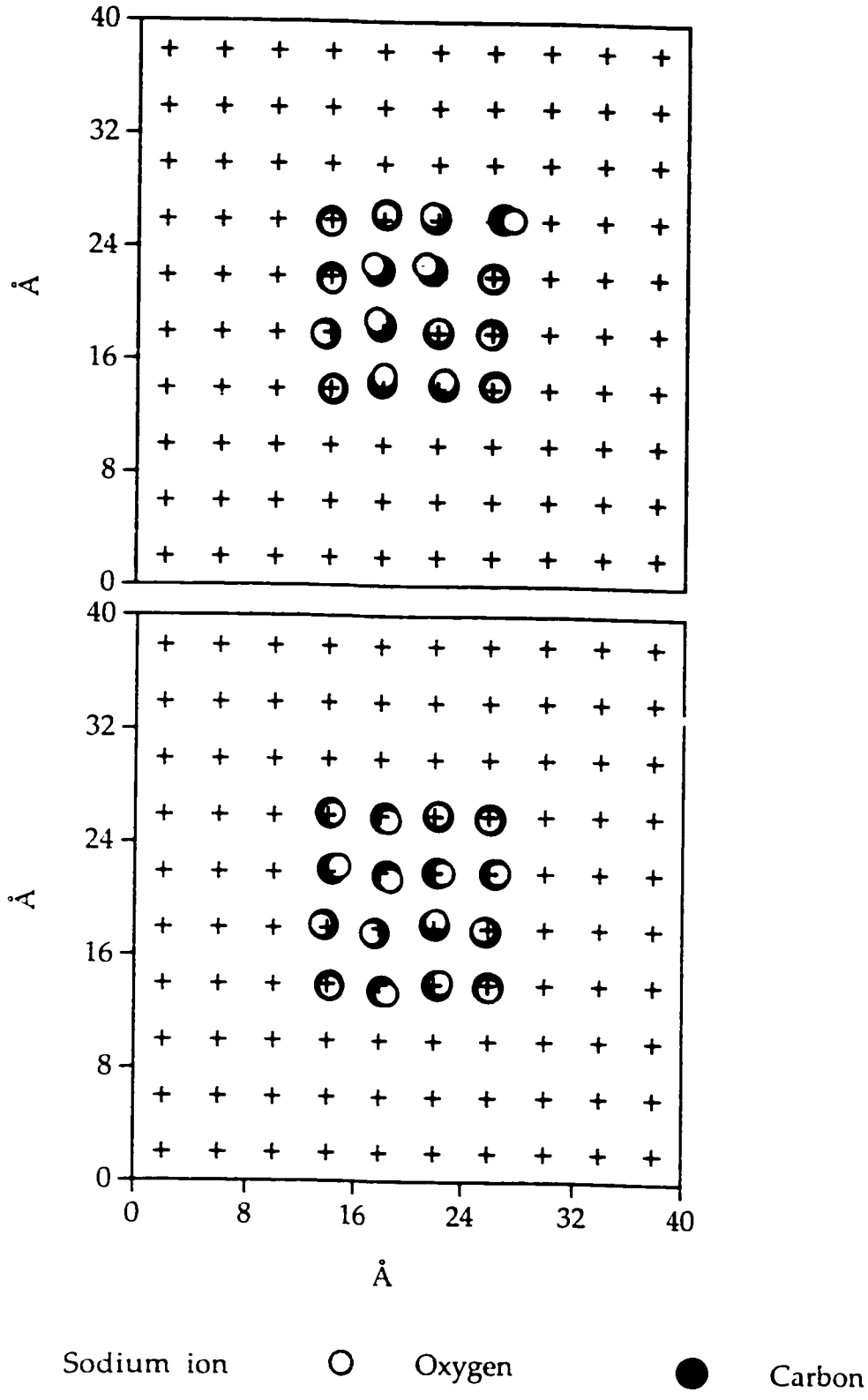

Figure 5.8. Configuration for sixteen percent CO/NaCl(100) generated by Monte Carlo simulation at T= 30K (lower panel) and at T= 5K (upper panel).

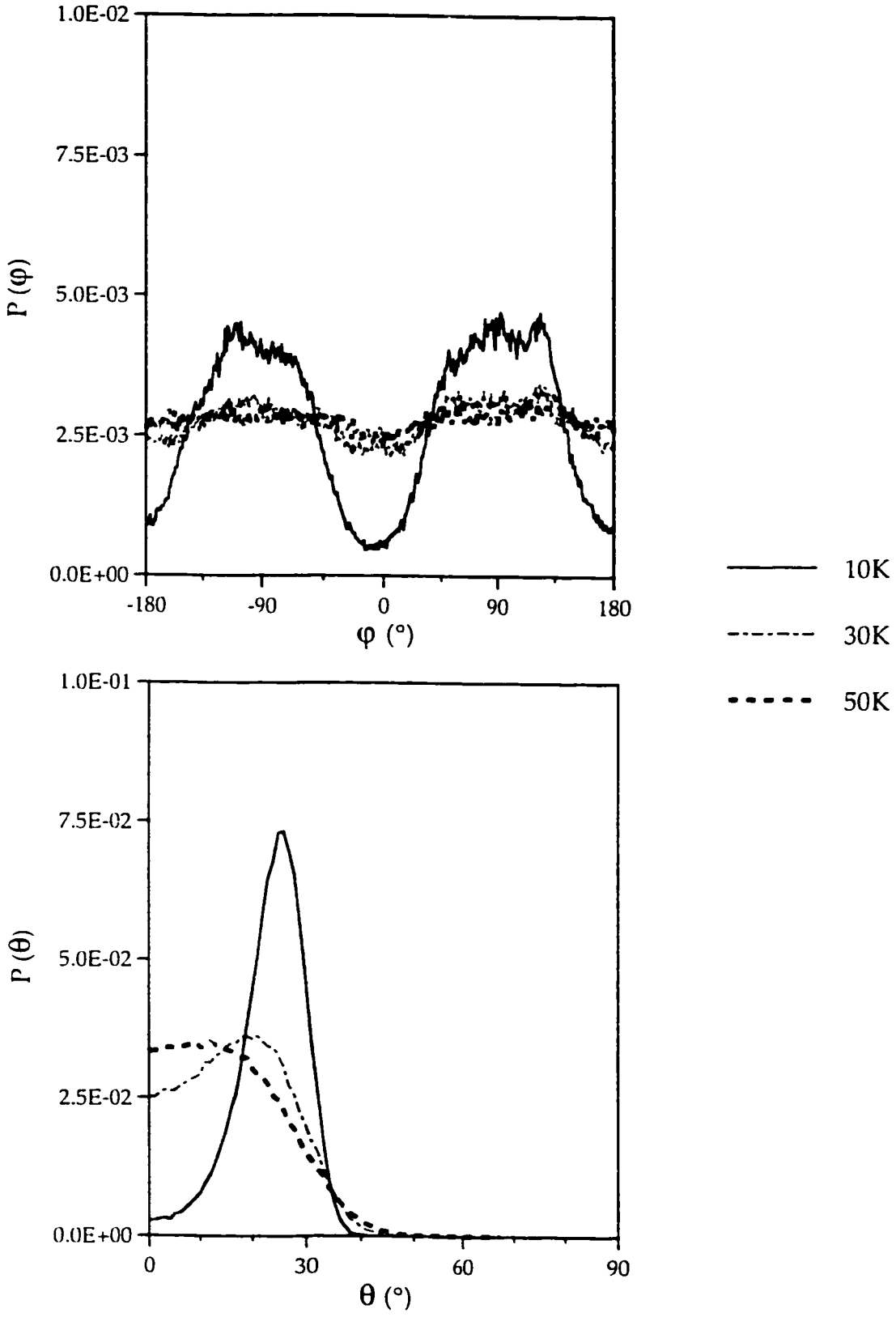

Figure 5.9. Angular distributions for thirty-six percent CO/NaCl(100) system,: polar, θ, (lower panel) and azimuthal, φ, (upper panel) distributions.

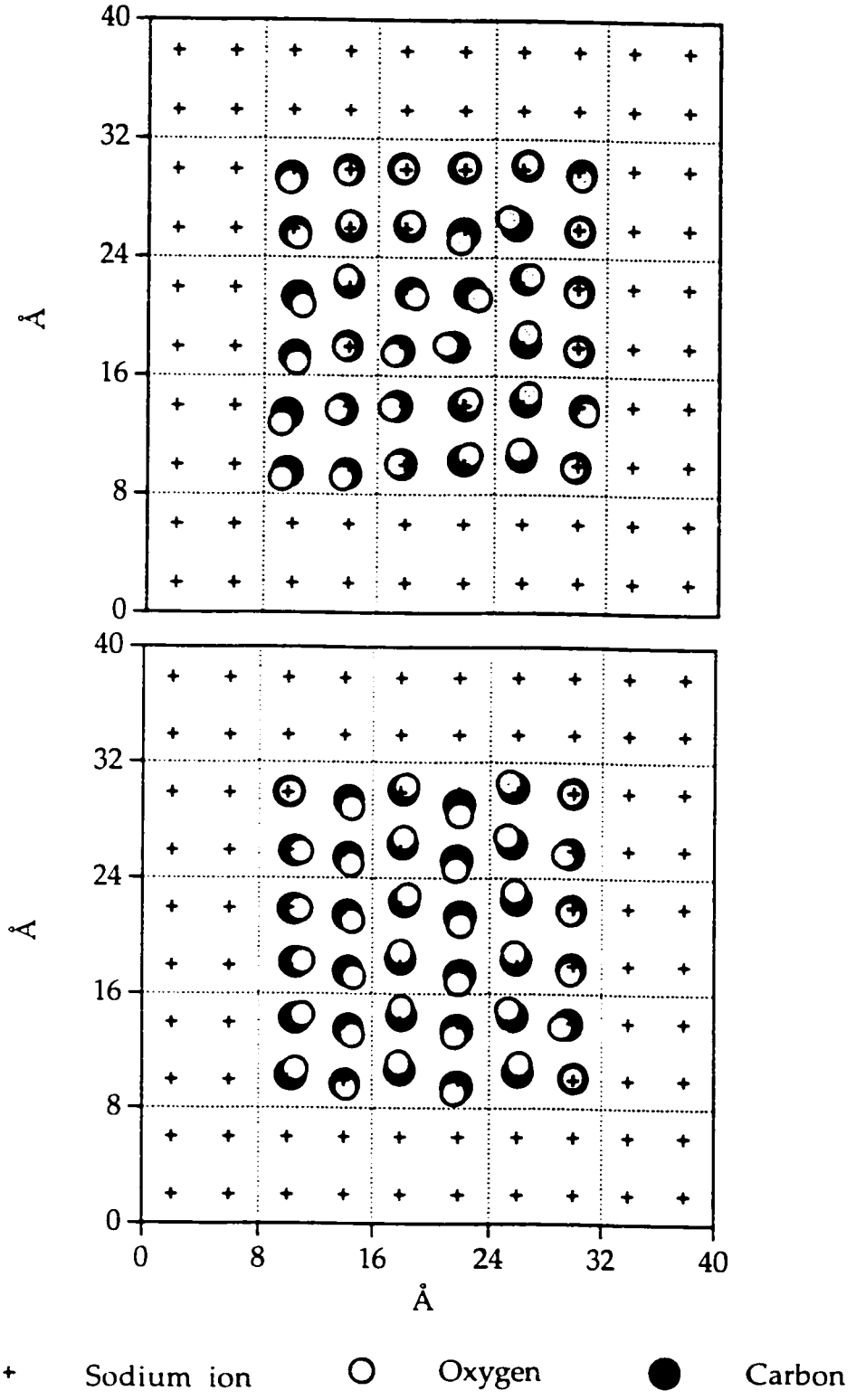

Figure 5.10. Configuration for thirty-six percent CO/NaCl(100) generated by Monte Carlo simulation at T= 30K (lower panel) and at T= 50K (upper panel).

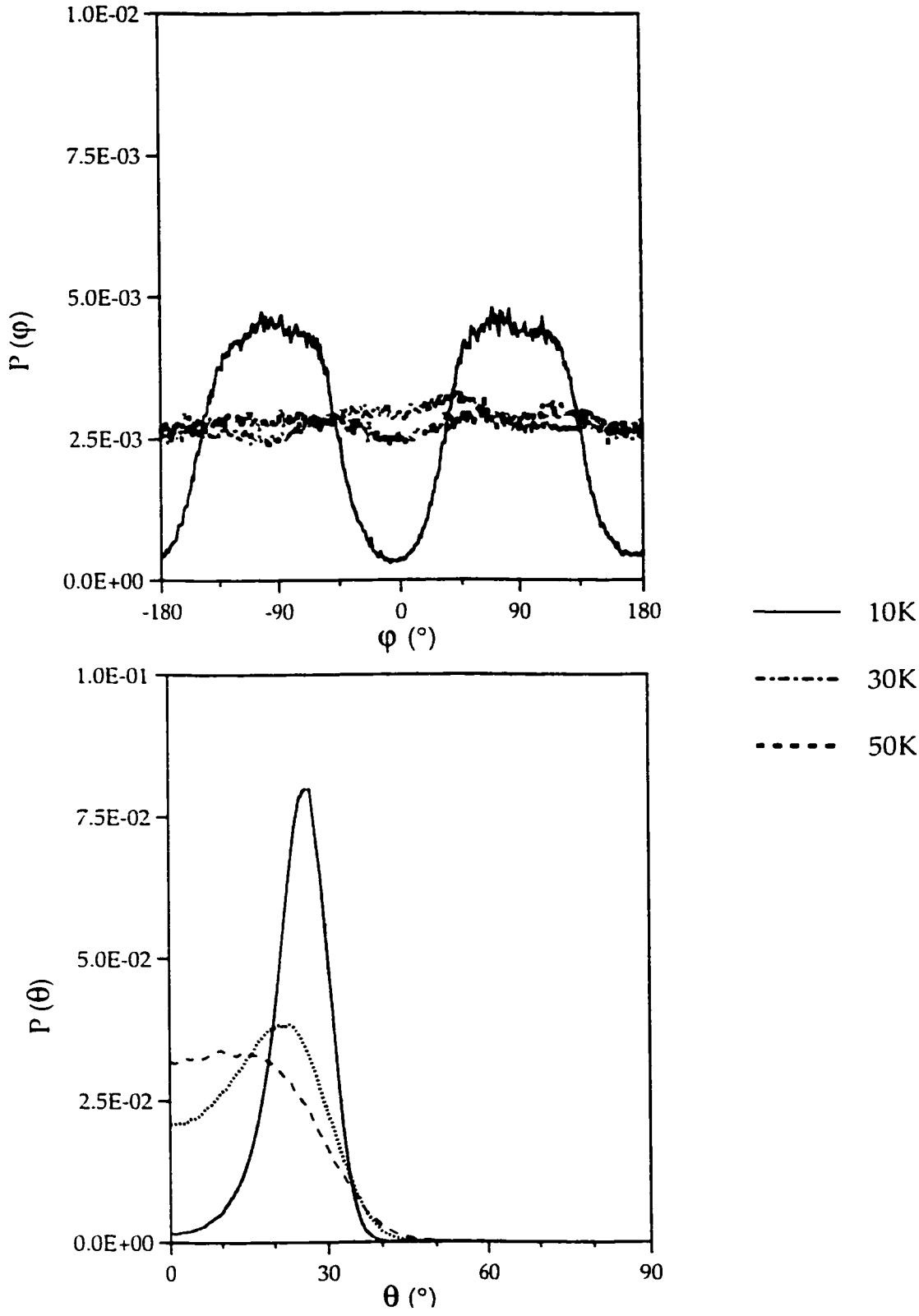

Figure 5.11. Angular distributions for sixty-four percent CO/NaCl(100) system: polar, θ, (lower panel) and azimuthal, φ, (upper panel) distributions.

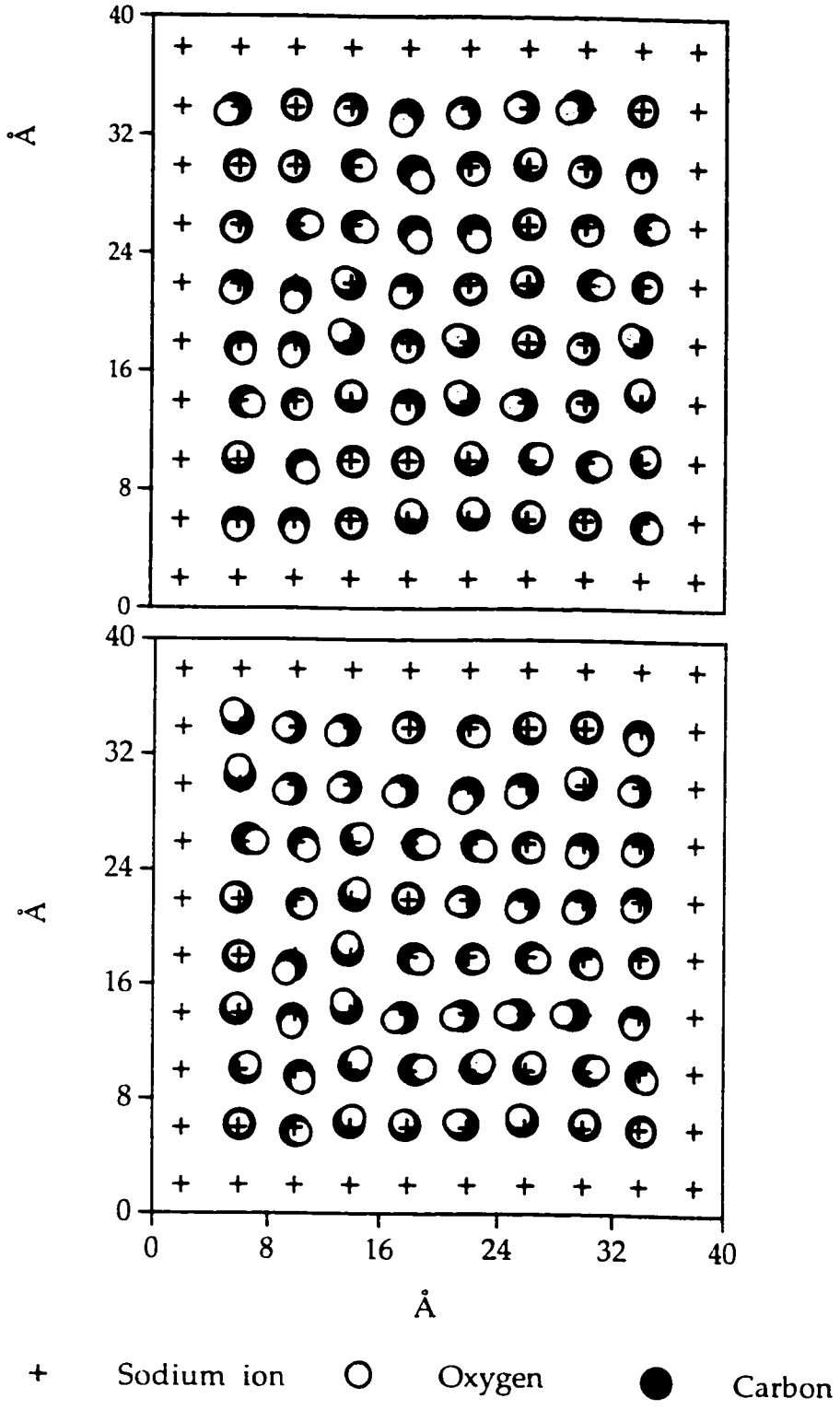

Figure 5.12. Configuration for sixty-four percent CO/NaCl(100) generated by Monte Carlo simulation at T= 30K (lower panel) and T= 50K (upper panel).

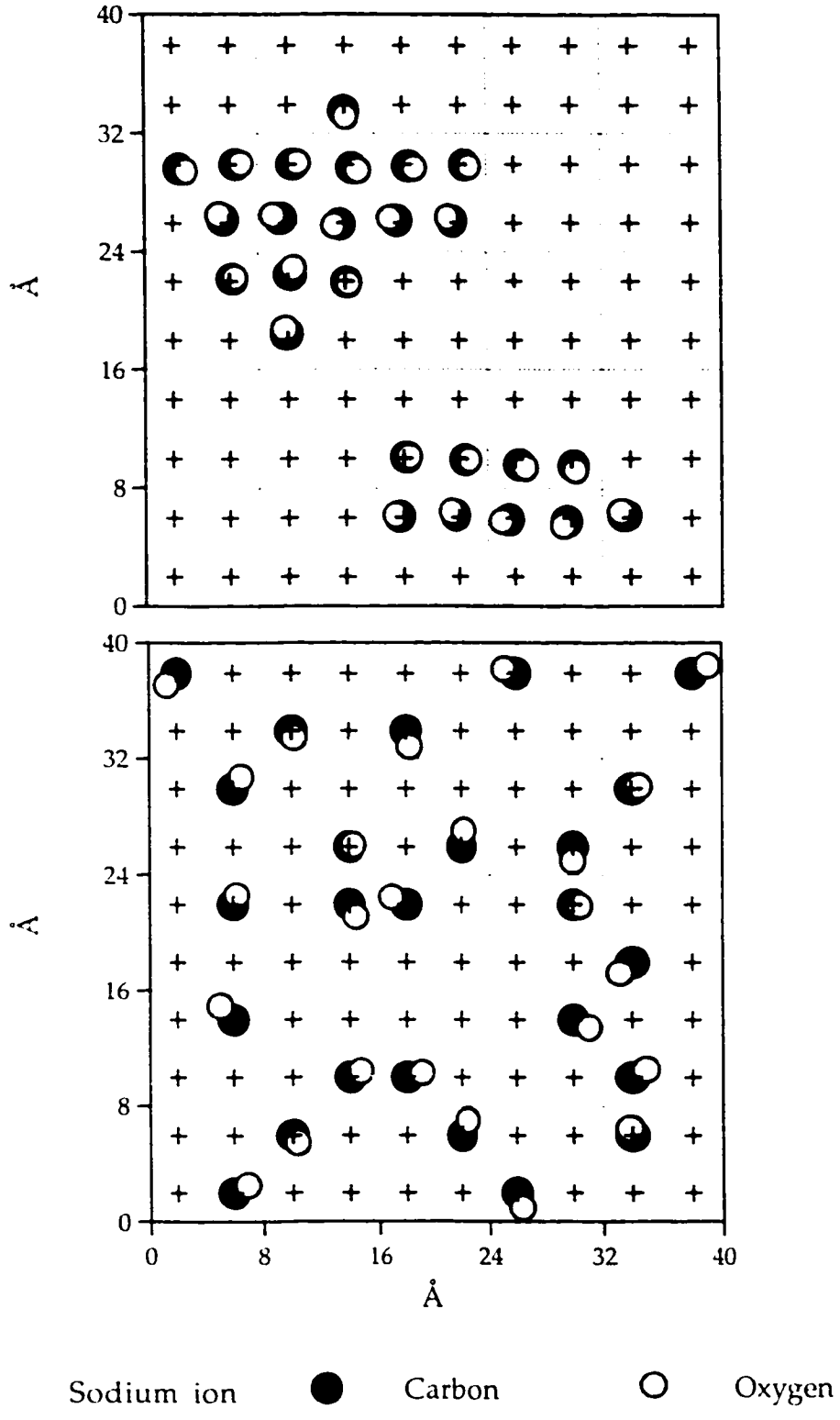

Figure 5.13. Configuration for twenty-five percent CO/NaCl(100) generated by Monte Carlo simulation at initial setting (lower panel) and at T= 10K (upper panel).

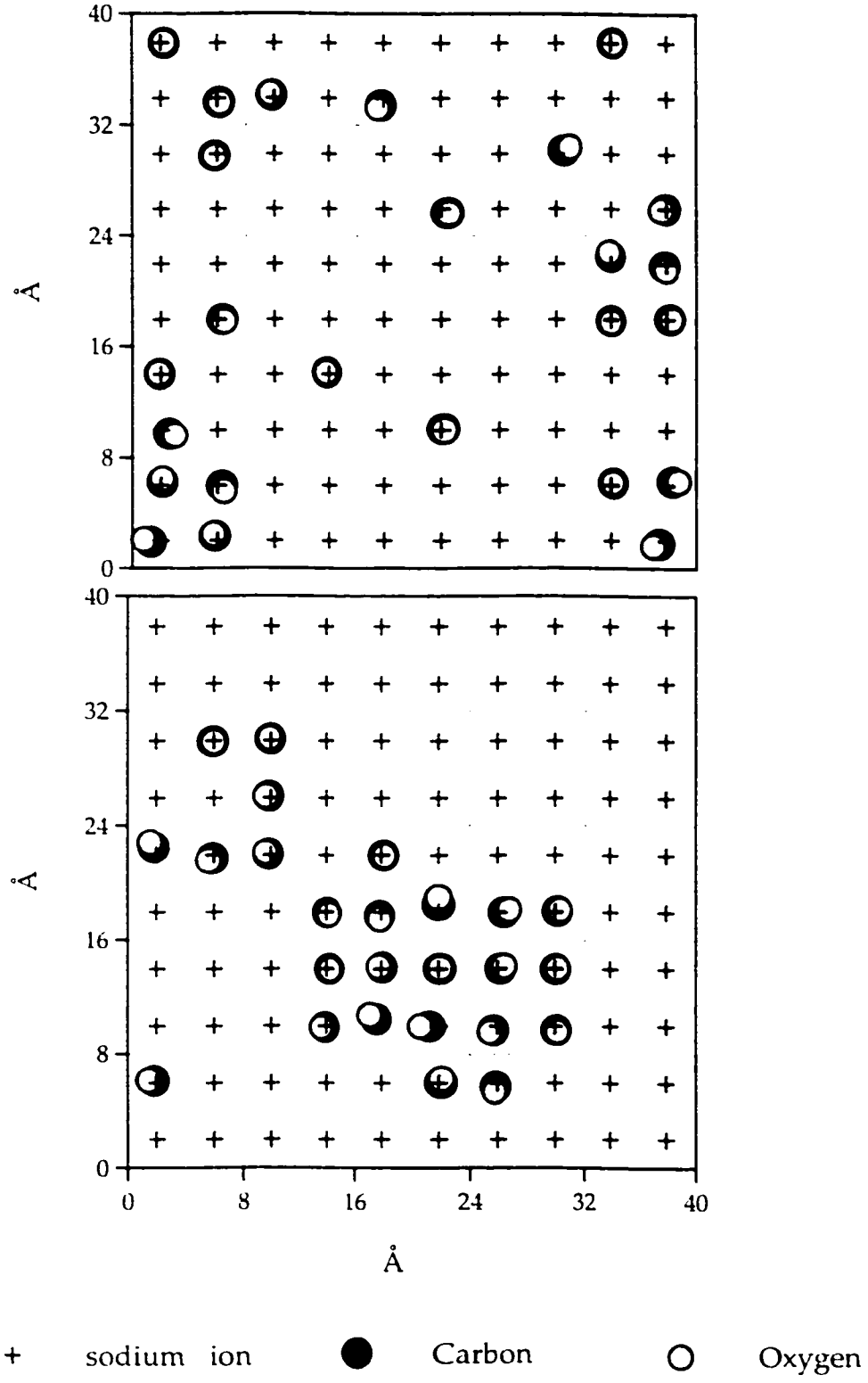

Figure. 5.14. Configuration for twenty-five percent CO/NaCl(100) generated by Monte Carlo simulation at T= 30K (lower panel) and at T= 50K (upper panel) .

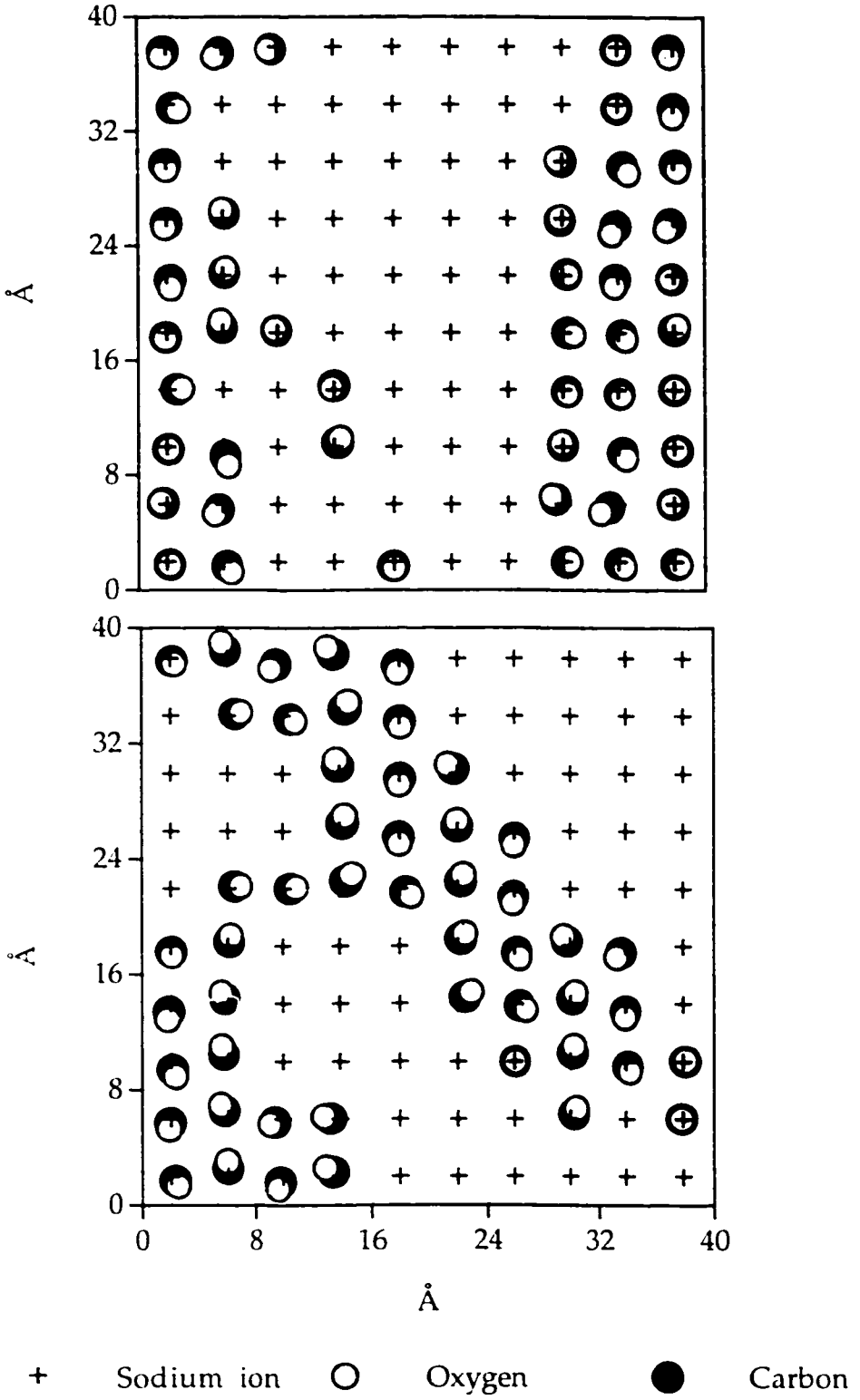

Figure 5.15. Configuration for fifty percent CO/NaCl(100) generated by Monte Carlo simulation at T= 10K (lower panel) and at T= 50K (upper panel) .

CHAPTER 6: RESULTS FOR MULTILAYER CO/NaCl(100)

Multilayer adsorption is one of the characteristic properties of physical adsorption.[14] Once the surface atoms/ions are covered with the adsorbed species at a unimolecular level, this monolayer becomes a newly formed surface that can accept added adsorbed species, forming a so-called multilayer system. The points of interest for the CO/NaCl system are the stability of the bottom layer (will the p(2x1) structure persist?) as well as the ability of the overlayers to form the bulk structure of solid α-CO. The term "bulk-like structure" in the following sections refers to this structure. If it is feasible for the CO molecules to obtain the bulk structure then what is the appropriate thickness of the overlayers in order to for the system to obtain the bulk solid structure? At low temperature ($T \leq 61.5K$) and under its own vapour pressure, solid carbon monoxide crystallizes in the ordered α-phase: a face-centered cubic crystal with the molecules aligned along the <111> body diagonals. The unit cell of α-CO has four molecules per unit cell (Fig. 6.1) and the lattice constant at 8K is 5.646Å.[63,64] The ordered molecules presumably adopt the antiferroelectric structure in this phase. However, it is evident from residual entropy detected in calorimetric measurement[65] that there exists a random head-tail disorder of the CO molecules even at temperature is as low as 5K.[66] Hence the fully-ordered theoretical antiferroelectric structure can never be observed. Yet there still exists some short-range head-tail disorder in the structure.[63] Other questions of interest to us are, does the structure of the multilayers system also undergo a phase transition if the temperature of the

system is raised? If the answer is yes then will the phase transition be similar to the phase transition of the monolayer of the same system CO/NaCl(100)?

To answer these questions, a series of simulations of multilayer systems of CO adsorbed on the NaCl(100) surface have been performed. Three different sets of simulations were conducted to study the structure of the bilayer (two-layer), trilayer (three-layer), and tetralayer (four-layer) systems. We examined their structures at low temperatures and their changes in the high temperature region. All systems have similar initial configurations, and simulation protocols, *e.g.* all simulations have been run for at least $6x10^4$ cycles, with the first $3x10^4$ cycles discarded. After ensuring that the structure were properly equilibrated, the configurations were then used to simulate the final structures in the temperature range of T= 5K to T= 45K. The cut off radius of the CO-CO interaction was 18.5Å to ensure the inclusion the same number of molecule interactions within the cut off radius in each layer, and hence we could increase better yields in the head-tail ordering. Data was collected for a running time of at least $3x10^4$ cycles. The results will be presented and discussed in the followed section.

6.1. Bilayer System of CO/NaCl(100)

In order to study the structure of the multilayer system, Monte Carlo simulations have been done on a bilayer system that has an initial structure

constructed as follows. The bottom layer was given an ordered p(2x1) structure as shown in the lower panel of Fig. 6.2. To speed up the process of equilibration, the top layer was constructed to have a bulk-like structure but with all molecules having the C ends pointing toward the surfaces. A sample of such a structure is shown in the upper panel of Fig. 6.2.

At T= 5K, the initial p(2x1) ordered structure of the bottom layer is found to be unstable. It immediately transforms to an ordered p(1x1) structure as may be seen in the lower panel of Fig. 6.3. The molecules are found to tilt in the same direction (φ~ -135°), with one molecule per unit cell, instead of being tilted away from each other as in the case of an ordered p(2x1) structure of a monolayer system. A small change in the polar angle of the bottom layer is observed in comparison to the monolayer structure (from θ_{mono}~ 27° to θ_{bot}~ 28°). Thus the structure of the bottom layer is believed to undergo a change in structure where it is originally an ordered p(2x1) to a final ordered p(1x1) structure with a small increase in the polar tilt. Thus the presence of the second layer of CO is found to destabilize the p(2x1) structure of the ordered monolayer structure when it becomes the bottom layer of the multilayer system.

As the temperature is increased to T= 25K, the ordered p(1x1) structure also becomes disordered as shown in the upper panel of Fig. 6.3. The molecules start to lose their preferred azimuthal orientations yet remain tilted. In Fig. 6.4, in

the higher temperature region, where T= 35K (lower panel) and T= 40K (upper panel), the molecules show more disorder as expected as the orientational ordering of the p(1x1) is destroyed. However, the molecules on average remain tilted throughout the simulations despite some of the molecules orienting perpendicular to the surface as seen in Fig. 6.4. A phase transition is then predicted to be of order-disorder type according to this observation.

A change in structure can also be studied by examining the angular distributions of the bottom layer in Fig. 6.5. Theta (polar angle) distribution (lower panel) shows a sharp peak, $\theta \sim 28°$, at T= 5K. The peak is found to widen as the temperature is raised as expected. The peak is gradually shifted from $\theta \sim 28°$ at T= 5K to $\theta \sim 23°$ at T= 40K. On average the molecules are found to remain tilted in the high temperature region although the molecules are found to untilt by about 5°. At T= 5K, the phi (azimuthal orientation) distribution peaks sharply at $\varphi \sim -135°$. This agrees well with the observation that the molecules are tilted in the same direction, resulting in one molecule per unit cell. As the temperature is raised the observed peak decreases in height and broadens in width because the molecules can librate more freely due to the increase in kinetics energy with high temperature. Again the molecules are found to lose the ordered azimuthal orientations of the low-temperature structure. At T= 40K the phi distribution peak turns very broad with the addition of another broad peak at $\varphi \sim 135°$, thus presumably signalling the existence of another domain of locally ordered

molecules. Through this qualitative aspect, one can say that the layer undergoes a transition from an ordered to a disordered phase at around T~ 40 K. However, a prediction of the exact transition temperature and the determination of the phase transition cannot be given without performing more study.

An overview of a snapshot of the top layer shown in Fig. 6.6 (lower panel) shows that it does not adopt the bulk-like structure even at temperature as low as 5K. The original set-up that has the orientational order of the bulk-like structure is not stable, instead it becomes another ordered p(1x1) structure. The molecules are also found to be titled in the same direction with φ~ 45°, thus resulting in one molecule per unit cell. A larger tilt angle, however, is observed in comparison to the polar angle of the bottom layer, viz. θ_{top}~ 45° whereas θ_{bottom}~ 28°. As the temperature is raised, the molecules become more disordered as typically seen at the high temperature region of all simulations. Another striking feature of the top layer that emerges is the appearance of some inverted molecules. The inverted molecules, which have the oxygen ends pointing towards the surface, form a ratio of 73:183 carbon ends up versus carbon ends down as shown in the configuration of the layer at T= 25K (Fig. 6.6, upper panel). However, there exist no specific or ordered pattern of the head-tail orientation; they tend to form small clusters that scatter throughout the layer.

As the temperature is raised to T= 35K, (Fig. 6.7, lower panel), due to thermal effects at high temperature more molecules tend to lose their preferred orientations. At the same time, the number of the inverted molecule (with carbon ends pointing up) also increases to 110 carbons up versus 146 carbons down (110:146). Again the inversion is random and does not form any special structure although the clusters of inverted molecules tend to form longer lines that almost run across the entire layer, hence forming large clusters as seen in the same figure. The configuration of the layer at T= 40K shows that the molecules are totally in an azimuthally disordered state, yet the number of the inverted molecules stays more or less the same (the ratio of carbons up versus carbons down is 119:137). The molecules are even displaced farther from the adsorption sites resulting in distorted row of molecules as seen in Fig. 6.7 (upper panel).

Figure 6.8 (lower panel) shows the dependence of the theta distribution with the temperature of the top layer. At low temperature, T= 5K, a sharp peak is observed at $\theta \sim 45°$, which is in accordance with the observation that the molecules are tilted away from the surface normal. As expect, the peak is found to broaden as the temperature increases. At T= 25K, a second peak, which is smaller in height, is observed at $\theta \sim 125°$. This peak represents the molecules that have inverted as previously described. At high temperature, both peaks are found to widen. In addition, the height of the first peak decreases at the expense

of the increase in height of the second one, until they are both the same in the region of T= 35K and onwards as seen in the figure.

The upper panel of the same figure (Fig. 6.8) shows the phi distribution of the top layer of a bilayer system. At low temperature, T= 5K, a well-defined and symmetric peak at $\varphi \sim 45°$ is observed. The peak broadens dramatically when the temperature is raised up to T= 25K. An additional and much smaller peak is also seen in the same figure. This peak at $\varphi \sim -135°$ is due to the inverted molecules as previously described. The second peak is found to increase at the expense of the first peak as the system is heated. This is in agreement with the increase in number of the inverted molecules. The distribution is almost equal in proportion between the two peaks at T= 35K. When the temperature is raised up to T= 40K, the distribution turns very broad (almost flat) as shown in the upper panel of Fig. 6.8. This is a signal of a transition from an ordered p(1x1) structure at low temperature to a disordered p(1x1) structure at high temperature. The fact that the phi distribution does not turn completely flat is probably due to the fact that the molecules remain tilted at high temperature even after they lose their low-temperatures ordered azimuthal orientations.

In short, from this study we conclude that the adsorption of the second layer on top of the p(2x1) structure would destabilize the p(2x1) structure. The p(2x1) changes to a p(1x1) even at very cold temperature and it becomes

disordered at high temperature. Being influenced in turn by the bottom layer that has a p(1x1) structure, the top layer in this study does not adopt the bulk structure. In contrast, the orientational ordering of the bulk structure, which was initially set up to speed up the process of equilibration, also disappears. Similar to the bottom layer, the top layer also forms a p(1x1) structure at low temperature and becomes orientationally disordered at high temperature. This is most likely due to the strong effect of the structure of the bottom layer. Although some of the molecules flip at high temperatures the structure of these inverted ones do not contribute to a formation of a bulk-like structure as hoped. The head-tail orientation observed in this case can be viewed more as the thermal excitations of the molecules at high temperature. Moreover, since this is the top layer of a bilayer system, one can best consider it as the surface of solid α-CO rather than bulk α-CO. Therefore, a reconstruction of the surface structure is expected. More experimental studies have to be done to confirm this observation.

6.2. Trilayer System of CO/NaCl(100)

Being unable to form a bulk structure of solid α-CO with a bilayer system, we decided to increase the number of layers of the system to three in the next set of simulations. Again the bottom layer is an ordered p(2x1) structure as in the previous system. The over layers are also constructed with the right orientational ordering as in the solid α-CO bulk structure with alternating rows of molecules

tilted in the 0 and +90° azimuthal directions. However the correct head-to-tail orientations has been left out so that all molecules have carbon ends pointing down towards the surface as shown in Fig. 6.9. The molecules in the middle layer are shifted diagonally by x=y= ¼ of the lattice constant so that they sit above the chlorine ions. The molecules in the top layer are moved back so that they sit above the sodium ions. Hence the two layers are offset by 1.999Å as shown in the same Fig. 6.9.

Figure 6.10 shows configurations of the bottom layer of a trilayer system at T= 5K (lower panel) and at T= 25K (upper panel). Similar to the bilayer system, the bottom layer is not stable, the ordered p(2x1) structure transforms immediately to apparently a p(1x1) structure upon adsorption of the over layers even at very cold temperature, T=5K. However, a close look reveals that the structure is not a perfect (1x1) structure. The molecules between the adjacent columns have small different in the azimuthal orientations on the y direction. Still, the layer represents an ordered structure that is very different than that of the initial p(2x1) structure. Again the structure shows an increase in degrees of disorder as the temperature is raised to T=25K. The molecules can freely rotate in the x-y plane due to thermal effects at high temperature. As expected, the molecules lose more ordering in the azimuthal orientations as the temperature is continuously increased up to T= 40K as shown in the panels of Fig. 6.11.

However, at this high temperature region the structure is still quite azimuthally ordered and the molecules also remain tilted away from the surface normal.

The progress of the change in the polar angle of the bottom layer with temperature can also be studied by examining the theta distribution in the lower panel of Fig. 6.12. At low temperature, T=5K, one sharp peak at $\theta \sim 30°$ has been observed. As the temperature is increased the peak becomes very broad and shifts to $\theta \sim 27°$ at the same time. The peak continues to broaden as the temperature is raised. Nonetheless, the molecules stay tilted in this high temperature region. Hence, no phase transition can be predicted at this temperature (T= 44K). Unfortunately the study had to be stopped at this point because of high mobility of some molecules causing the simulation to stop. If wished to cover this complex movement then Monte Carlo method using the grand canonical ensemble is required to run the simulations.

Phi distribution of the same layer (upper panel of Fig. 6.12) can also be used to examine the transformation from an ordered to a disordered structure, if any occurs, when the system is heated up. One point to notice here is that at T= 5K, the distribution at $\varphi \sim 135°$ is found to be asymmetric at the top of the peak. This probably is due to the shorter time of running the simulation. At T= 25K, the distribution broadens to a much wider range of angle and the peak is found to split into two peaks on both side of the central peak ($\varphi \sim 180°$). The molecules are

caught up in two possible domains of the structure at that time resulting in two separated peaks. Therefore, they disappeared at higher temperatures and the central peak is shifted back to around $\varphi \sim -135°$ where it remains up to T= 44K. According to the phi distribution the molecules are still highly ordered, therefore, no phase transition is predicted in this region. Since the study had to be stopped because of the high mobility of the molecules in the over layers as previously mentioned no definite conclusion on this matter can be made.

Figure 6.13 shows the configurations of the middle layer of the trilayer system at T= 5K (lower panel) and T=25K (upper panel). In contrast to the outcome of the second layer of the bilayer system, the bulk-like structure in the second layer is stable, although the molecules cannot adopt the correct head-to-tail orientation as present in the bulk solid α-CO. Nonetheless, 204 molecules are found to invert so that the oxygen ends are pointing towards the bottom layer as seen in Fig. 6.13 (lower panel). This resulted in a ratio of 204 carbons up versus 52 carbons down. However, this is expected because of the presence of the head-tail disordered of the CO molecules even at low temperature (T=5K) as explained by Klein.[63] As the temperature is raised (T= 25K), more molecules are found to invert. The ratio in this case is 213 carbons up versus 43 carbons down. The inverted molecules are scattered throughout the whole layer and again they do not show any pattern of adopting the correct head-to-tail orientation of the bulk solid α-CO. In terms of ordering orientations, on average the molecules still

preserve the preferred azimuthal orientations of the bulk-like structure. As the temperature is elevated the number of the molecules that inverted back also decreases so that the ratio of carbons up versus carbons down at T= 35K (Fig, 6.14, lower panel) is 173:83 and at T= 40K (Fig.6.13, upper panel) is 160:96, respectively. Most of the molecules now have the oxygen end pointing toward the bottom layer. Again, no specific pattern related to the head-to-tail ordering of the bulk-structure can be found in these structures. Yet, the inverted molecules tend to aggregate in elongated clusters as shown in the snapshots of Fig. 6.14. At T= 40K, some of the molecules start to lose their preferred orientations, but on average they remain locked in the orientations found at low temperature. Thus a phase transition might occur at a higher temperature than this one. More study has to be done to verify the above prediction.

An examination of the angular distributions confirms that no phase transition has occurred up to T= 44K. Figure 6.15 shows the theta distribution (lower panel) and phi distribution (upper panel) of the middle layer of the trilayer system. A look at the theta distributions reveals the progress of the polar angle as predicted. The distribution at T= 5K shows a sharp peak at $\theta \sim 118°$ and a much smaller peak at $\theta \sim 41°$. This second peak represents the number of inverted molecules. These two peaks are found to decrease in height and broaden in width when the temperature is raised as shown in Fig. 6.15 (lower panel). As the system is heated, the second peak increases in area, at the expense of the first

one, until at T= 44K the two peaks are approximately equal. This is in agreement with the observation from the configuration that almost half of the molecules are inverted at T≥ 40K. Another point to notice here is that the molecules remain tilted at high temperature. The phase transition can be qualitatively observed by examining the change in the phi distributions of the molecules at different temperature (Fig. 6.15, upper panel). At low temperature, T= 5K, two sharp peaks at φ~ -90° and φ~ -180° with two smaller peaks at φ~ 18° and φ~ 72° are observed. These four peaks are found to significantly broaden when the temperature is elevated to T= 25K with the two smaller peaks being shifted to φ~ 102° and φ~ 180°. In addition, a much smaller and broad peak appears at φ~ 0°. The peaks are also found to widen with elevated temperatures. At T= 44K, the peaks shown are very broad but still localized at φ~ 45° and -135°. This means that the molecules have not lost all their preferred orientations, and therefore they have not yet undergone an order-disorder type phase transition at T= 44K.

Similar to the middle layer, the top layer at T= 5K also preserves the correct azimuthal orientations of the bulk structure of solid α-CO as seen in the lower panel of Fig. 6.16. Again clusters of inverted molecules are found to be present in the structure with a ratio of 56 carbons up and 200 carbons down. At T= 25K (Fig. 6.16, upper panel) more molecules invert so that they have carbon end pointing up with the ratio of 59:197 where 59 carbons up versus 197 carbons down. The number of inverted molecules increases with the elevated

temperature as well. At T=35K (lower panel of Fig. 6.17) the ratio of carbons up versus carbons down is 91:165. However, at T= 40K (Fig. 6.17, upper panel), a small drop in the number of carbon up has been observed (84 carbon up: 172 carbon down). The decrease instead of an increase in the number of carbon up with temperature might suggest that above 35K the change in this ratio is merely a fluctuation between the CO molecules and the inverted ones. No more change would likely to be observed above this temperature. This in turn indicates that we would not be able to obtain the correct head-tail ordering of the bulk solid structure as expected. Again no definite pattern that can be related to the formation of the head-to-tail ordering, which is present in the bulk structure of the solid α-CO, has been noticed. The inverted molecules are instead spread throughout the layer in small clusters. This is dissimilar to the elongated clusters of the inverted molecules found in the middle layer. Concerning the ordering orientation, the molecules within the top layer are also found to gradually disorder as the system is heated up. In spite of that, at T= 40K (the upper panel of Fig. 6.17) the molecules still have preferred orientations on average; no transition to a completely disordered state has been observed.

A quick examination of the angular distributions of the top layer also reveals very similar behaviour to those of the middle layer previously described. Namely, the theta distribution at low temperature, when T= 5K (Fig. 6.18, lower panel) shows one not so well defined peak at θ~ 65° as well as a smaller peak at θ~ 130°which represents the inverted molecules. The two peaks are both found

to broaden with elevated temperatures. At T=44K, they are very broad and almost equal in height. This is in accordance with observation that almost 45% of the molecules are inverted at high temperature. The process of the molecules losing their preferred orientations in the top layer is very alike to the one of the middle layer if one look at the phi distributions (Fig. 6.18, upper panel). Specifically, at T= 5K two small peaks at $\varphi\sim$ -90° and $\varphi\sim$ -180° are found in addition to the presence of two sharp peaks at $\varphi\sim$ 0° and $\varphi\sim$ 90°. These four peaks become wider at T=25K. The only difference that can be made out in comparison to the one of the middle layer is that at T= 44K, the phi distribution of the top layer is much broader. This means that the molecules are in a more disordered state where more molecules are observed to lose their preferred orientations. Based on this observation we predicted that the top layer is entering the phase transition at T= 44K. Unfortunately, no more studies can be done at this time to confirm this prediction because of computer time constraints as well as the mobility of the molecules in the overlayers.

In conclusion, the results of the trilayer system also show that the initial p(2x1) structure of the bottom layer is not stable. Even at T= 5K, the structure changes to another p(2x1) structure with a very small difference in the azimuthal orientations of alternating columns of molecules. The structure also becomes more and more disordered at elevated temperature; however, the molecules remain tilted as seen in the polar distribution. On the other hand, the overlayers

show more stability in preserving the ordering orientations in the low temperature region. As the temperature increases, the molecules also lose their preferred orientations but on average the azimuthal distributions of the molecules are still locked in two directions rather than being totally washed out. This is because the molecules are found to stay tilted at high temperatures, therefore allowing for a meaningful φ but not fixing it in position. Based on the result discussed earlier, we predicted that the trilayer system also undergoes a phase transition at temperatures higher than T= 44K. In order to predict the exact temperature more studies need to be done on the system. Some molecules are found to invert so that the oxygen ends point towards the surface. Nonetheless, the inverted molecules do not contribute to the correct head-to-tail orientations seen in the structure of the bulk solid α-CO. One more feature to be noticed is that the number of inverted molecules in the system increases with elevated temperature. Nonetheless, no specific pattern can be assigned to these structures. In short, the overlayers of the trilayer system are found to adopt the correct orientational ordering of the bulk-like structure but without the right head-to-tail ordering. The tetralayer system is studied next to determine the condition needed for the overlayers to adopt the right head-to-tail orientation.

6.3. The Tetralayer System of CO/NaCl(100)

The initial configuration for the tetralayer system is constructed in the same manner as those of the trilayer system. Namely, the bottom layer has an ordered p(2x1) structure and the over layers all have the p($\sqrt{2}$x$\sqrt{2}$) structure found in the bulk solid α-CO, where all molecules have the carbon ends point towards the surface. The system was run at T= 5K and then the temperature increased to T= 25K to study the structure of the over layers. No thermal stability has been examined for this tetralayer system because of short computer time.

Similar to other systems, the adsorption of the overlayers destabilizes the p(2x1) structure of the bottom layer even at cold temperature, T= 5K (Fig. 6.19, lower panel). The molecules are found to change from a p(2x1) structure to a slightly imperfect p(1x1) with a small splitting at the azimuthal orientation. The polar angle is found to have a maximum at θ~ 24° as shown in Fig. 6.20. At T= 25K, the molecules alter their preferred azimuthal orientations as indicated by the single peak.

In the second layer, the molecules are found to preserve the initial orientation as seen in Fig. 6.21 (lower panel). However, all molecules have carbon ends pointing up, away from the surface. As the system is heated, some molecules scattered throughout the layer are found to invert back so that they

have the carbon ends pointing down towards the surface as shown in the upper panel of Fig. 6.21. Again no pattern can be linked to the head-to-tail ordering in the structure of the bulk solid α-CO. The polar angle of the molecules at this layer is θ~ 129° (Fig. 6.22, lower panel). At T= 25K, the peak broadens and at the same time, another small peak appears at θ~ 49° which represents the number of inverted molecules. Phi distribution (upper panel of Fig. 6.22) also shows the well-defined herringbone structure of the layer at low temperature. The sharp peaks are found to decrease in height at higher temperature with the addition of the smaller peaks, which represent the inverted molecules observed in the layer.

In the third layer, the inverted molecules are present even at T= 5K (Fig. 6.23, lower panel). The inverted molecules are found to aggregate to form one large cluster and several small ones. The ratio of the inverted molecules versus the regular one is 46:210 (carbons up versus carbons down), the number is far from suggesting that the layer would likely to form a bulk structure which has a 50% of inverted molecules. However, when the temperature is elevated to T= 25K, more inverted molecules are found (Fig. 6.23, upper panel). The ratio of the two types of molecules at this temperature is 123:133, a tripling in value compared to the value at 5K. The number of carbons up versus carbon down is almost equal as in the bulk phase. Nevertheless, the positions of the inverted molecules do not fall into the right spots for the layer to adopt the correct head-to-tail ordering found in the bulk solid α-CO. Although the results are

suggestive, the conclusion is not straight forward: the running time might be not long enough for the system to evolve into the right structure of the bulk solid α-CO or more over layers have to be added before the middle layers can adopt the expected and correct head-to-tail ordering. Or simply one cannot adopt the bulk solid structure because even in reality no perfect head-tail ordering has been observed in the structure of solid α-CO.[63] More study has to be done to prove these hypotheses.

As demonstrated in the angular distributions, theta (θ, lower panel) and phi (φ, upper panel), the inverted molecules are found to increase in number when the temperature is raised from T= 5K to T= 25K. At T= 5K, two well-defined peaks with different areas can be seen from the lower panel of Fig. 6.24. The large one at θ ~ 55° represents the majority of the molecules with the carbon atom pointing towards the surface, and the much smaller one at θ ~ 120° corresponds to a small number of inverted molecules. As the temperature is increased to T=25K, the two peaks are found to become equal in height. This is found to match with the observation that the ratio of the normal and the inverted molecules at T=25 K is around 1. The phi distributions (Fig. 6.24, upper panel) show that most of the molecules retain the initial orientations with peaks at φ~ -90°, -180°, at T=5K with some inverted molecules at φ~ 0°, 90°. At higher temperature (T= 25K) the areas under the curves of the peaks are found to be

practically equal. This is in agreement with the previous observation that about 50% of the molecules within the layer were inverted.

Again similar to other system, at low temperature (T= 5K) the orientational ordering of the top layer is found to be stable, with all molecules having carbon ends pointing down towards the surface (Fig. 6.25, lower panel). As the system is heated up to T= 25K (upper panel of Fig. 6.25) the inverted molecules appear and scatter throughout the surface without any specific pattern. At T= 25K, the molecules are found to be able to librate and rotate more freely around their equilibrium positions, but still their orientational ordering is localized at the preferred low temperature configuration. This is seen in Fig. 6.26 (upper panel) where the azimuthal distributions at low temperature, T=5K, broaden at T= 25K but their peaks have the same maxima at $\varphi\sim 13°$ and $\varphi\sim 75°$. The two smaller peaks again represent the inverted molecule in the layer. The molecules are found to tilt away from the surface normal at an angle of about $\theta\sim 55°$ as seen in Fig. 6.26, lower panel. There exists only one well defined peak at T= 5K. This is accordance with all the molecules having carbon ends pointing down towards the surface as shown in Fig. 6.25, lower panel. At T= 25K a number of the inverted molecules have appeared. This is demonstrated by the appearance of the second peak at $\theta\sim 120°$. Again the first peak is found to broaden at elevated temperature yet remains localized at the same position as seen at low temperature.

The results of the tetralayer system are found to be very similar to those of the trilayer system. With one exception that there exist some inverted molecules in the third layer even at T=5K. This can be understood by looking at the system in a slightly different angle. Since all CO molecules in the second layer are found with carbons end pointing down, in contrast to the top layer where all molecules have carbons end pointing up. Hence, if one looks sideways at the tetralayer system one would see a sandwich of a layer of carbons down (from the second layer), then a layer of mixed carbons (from the third layer) and finally a layer of carbons down (from the top layer). Being influenced by the different ordering of the second and the top layer, some of the molecules in the third layer want to invert to balance out the interactions between the layers. In spite of this early inversion at cold temperature, the number and the positions of the inverted molecules do not fall into the correct head-to-tail ordering found in the bulk solid α-CO as expected. As the temperature is raised, the number of the inverted molecules also increases up to 50% at T= 25K for the third layer. This ratio of the head-tail ordering makes the structure of the middle layer in this system the closest to the bulk solid α-CO compared with the other multilayer systems. Nonetheless, the positions of the inverted molecules are mostly incorrect compared to those in the bulk solid α-CO. At first glance, we conclude that one needs to built at least three layers up from the surface in order to see the beginning of the formation of the bulk solid α-CO. However, more study needs

to be done before a conclusive result can be made on how many layers one needs to have in order for the overlayers to adopt the correct bulk solid structure.

6.4. Quantitative Analysis

Preliminary data from the quantitative analysis of the bilayer system does not show any promising results on the phase transition of the system. The energy curve does show a change in its slope, however, above T= 35K, the energy plot is found to change slope two more times before coming back to the same slope as before. This is probably due to the fact that the energy is expressed as a total energy of the whole system rather than energy of each layer. And from the examinations of the qualitative aspect, each layer demonstrates a different way of changing depending on the number of layers that are adsorbed upon the first one. This can change the total interaction between the molecules. In addition the energies at the top and bottom of the layers are expected to be different than those in the middle. Therefore, separate energies between layers should be used in the quantitative analysis to get more conclusive results. Although the heat capacity plot converges at T~ 36K, the leading and the trailing edges also show several more smaller peaks (Fig. 6.27). Fluctuations or the onset of the inverted molecules or a combination of both might be accounted for those peaks. For that reason, this study cannot be considered conclusive for the determination of the phase transition without performing more tests. The quantitative study could not

be done on the tri- and tetralayer systems because of high mobility of some molecules that cause the program to stop in the high temperature regime, therefore, no significant results could be drawn regarding this subject at the moment.

6.5 Summary

In summary for this section, we have investigated the stability of the ordered p(2x1) structure of the bottom layer and the ability for the overlayers to adopt the correct bulk structures. We gather the following conclusions from analyzing the simulated data.

The adsorption of the over layers destabilizes the ordered p(2x1) structure of the bottom layer and induces a new p(1x1) structure. This is in agreement with one explanation given by Heidberg and coworkers in interpreting the changes in the FTIR spectra.[23] Another explanation was based on an altered dipolar coupling in or to the first layer. They concluded that more experiments needed to be done to determine for certain which explanation better corresponds to the spectral changes. The newly formed p(1x1) structure is qualitatively observed to undergo a phase transition from an ordered state at low temperature to a disordered state at high temperature. The exact temperature of the transition is found to depend on the number of the over layers. It seems that the more layers

one has on the system, the higher the phase transition temperature. However, a more quantitative study has to be performed to determine the exact temperature as well as the nature of the transition.

The over layers are found to preserve the orientational ordering of the bulk solid α-CO at low temperature only when two or more overlayers are present. However, the head-tail ordering of the molecules are found not to be in agreement with the bulk solid α-CO. As the temperature of the system is elevated, the ratio of the carbons up (inverted molecules in the structure) versus carbons down comes close to the ratio of the bulk solid α-CO without having the right positions of the inverted molecules in the bulk. Because of close match of the lattice constants between the solid α-CO and NaCl(100) surface (mismatch ~ 0.5%)[6], epitaxial growth of single crystal α-CO on NaCl(100) is possible. Since the monolayer forms an epitaxial relationship with the surface cell, all layers beyond the monolayer are thought to form solid α-CO according to a study of Ewing *et al.*[18] However, the results in our simulations indicate that the structure of the overlayers depends on the number of the overlayers presented in the system. It was found that the greater the number of the overlayers the closer the structure of the system is to the bulk. In spite of this, we cannot say for certain that our multilayer systems will adopt both the correct orientation and head-to-tail orderings of the solid α-CO without performing more simulations on all three systems.

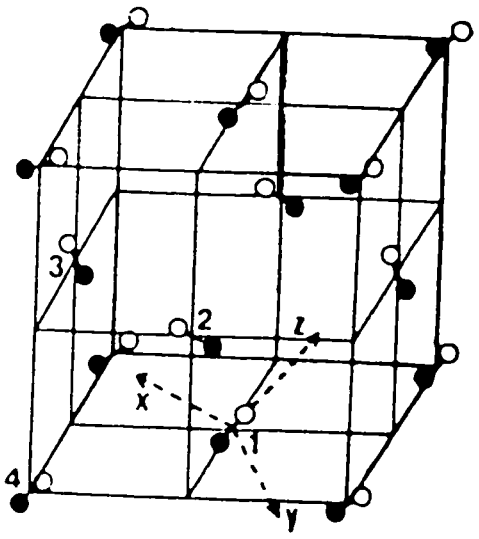

Figure 6.1. The crystal structure of solid alpha-form carbon monoxide. Taken from Ref [63].

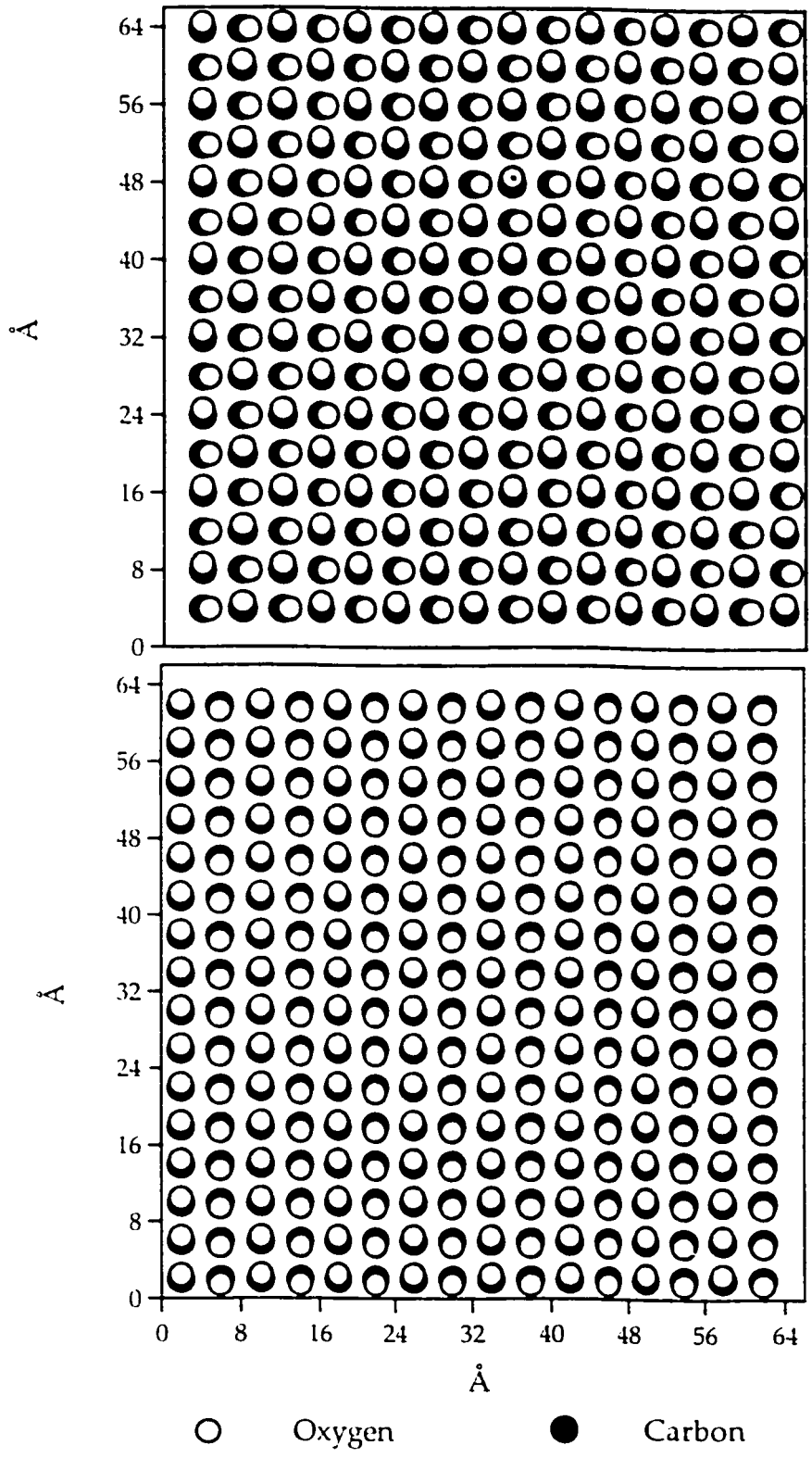

Figure 6.2. The initial configuration of a two-layer system CO/NaCl(100): the bottom layer (lower panel) and the top layer (upper panel).

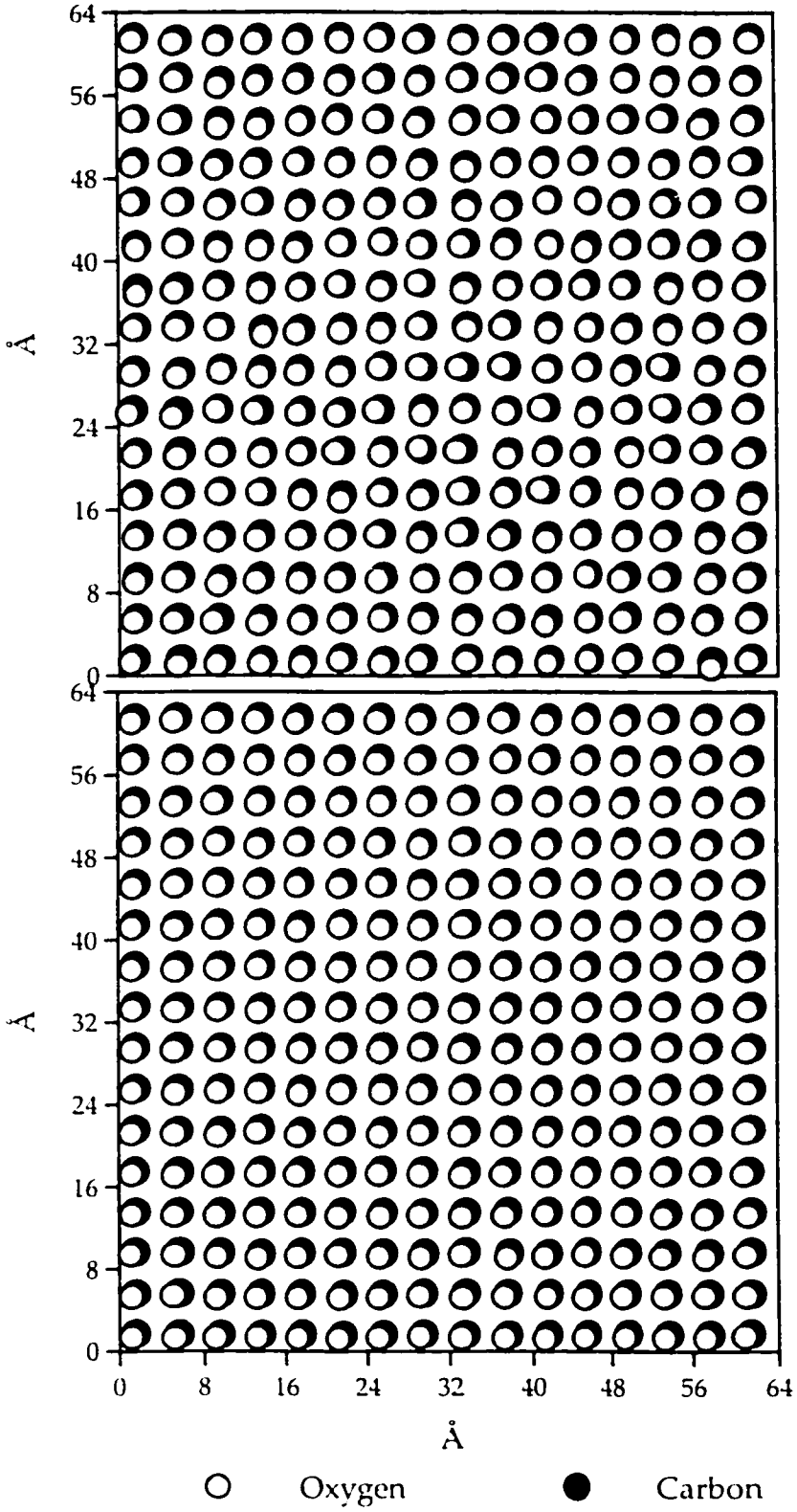

Figure 6.3. The bottom layer of a two-layer system CO/NaCl(100) configuration generated by Monte Carlo simulation at T= 5K (lower panel) and at T= 25K (upper panel).

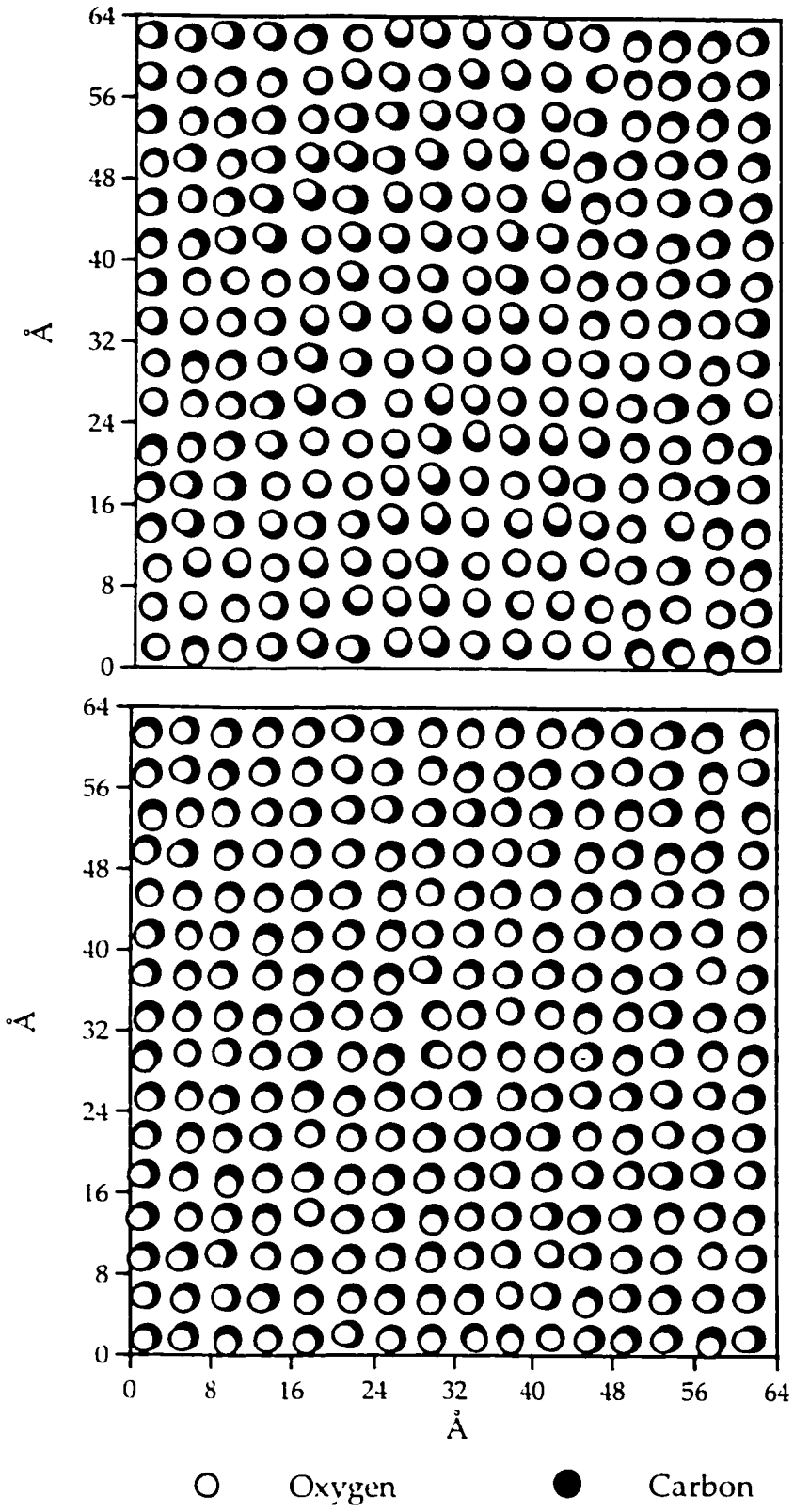

Figure 6.4. The bottom layer of a two-layer system CO/NaCl(100) configuration generated by Monte Carlo simulation at T= 35K (lower panel) and at T= 40K (upper panel).

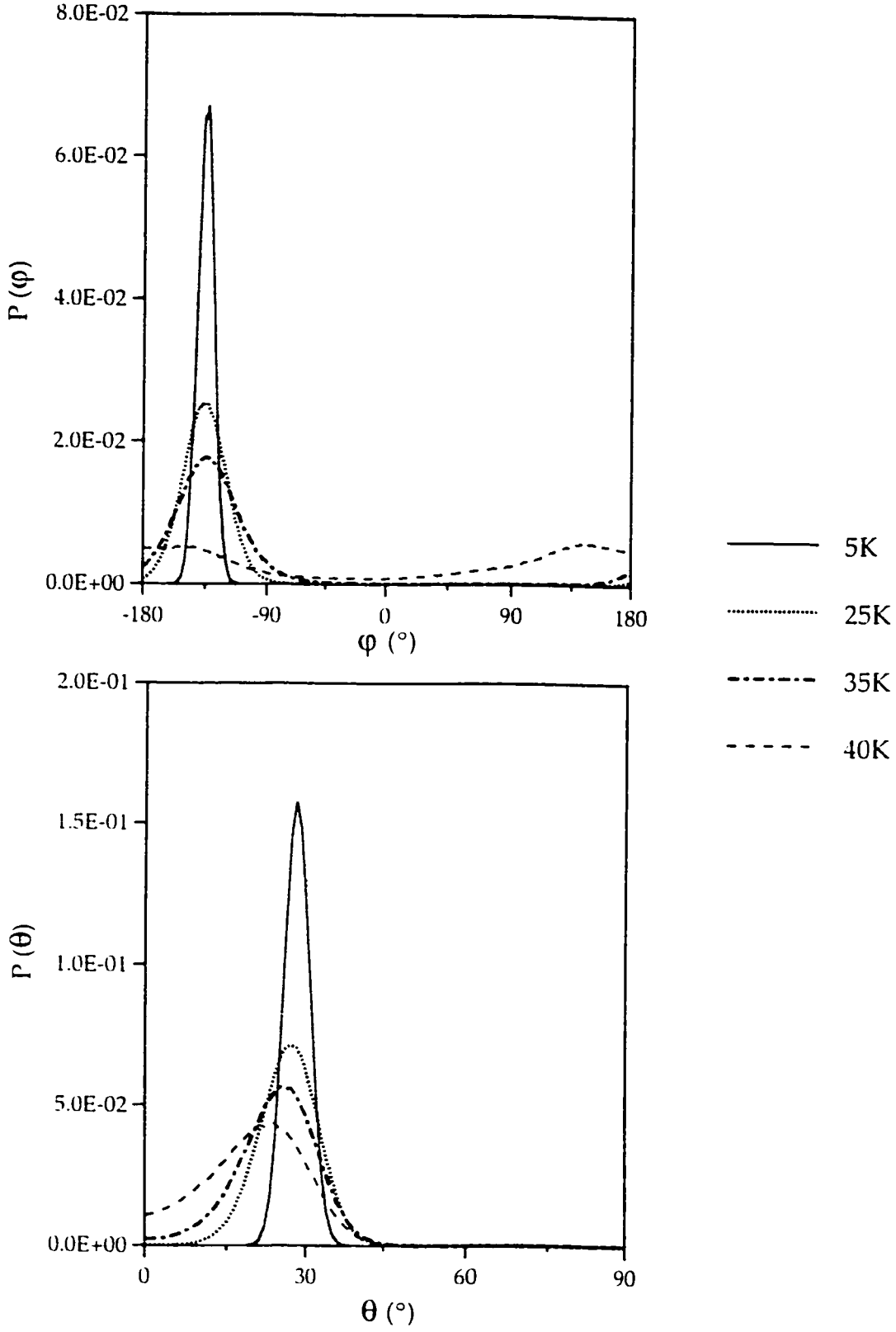

Figure 6.5. Monte Carlo results for the angular distribution for the bottom layer of a two-layer system CO/NaCl(100): polar, θ, (lower panel) and azimuthal, φ, (upper panel) distributions.

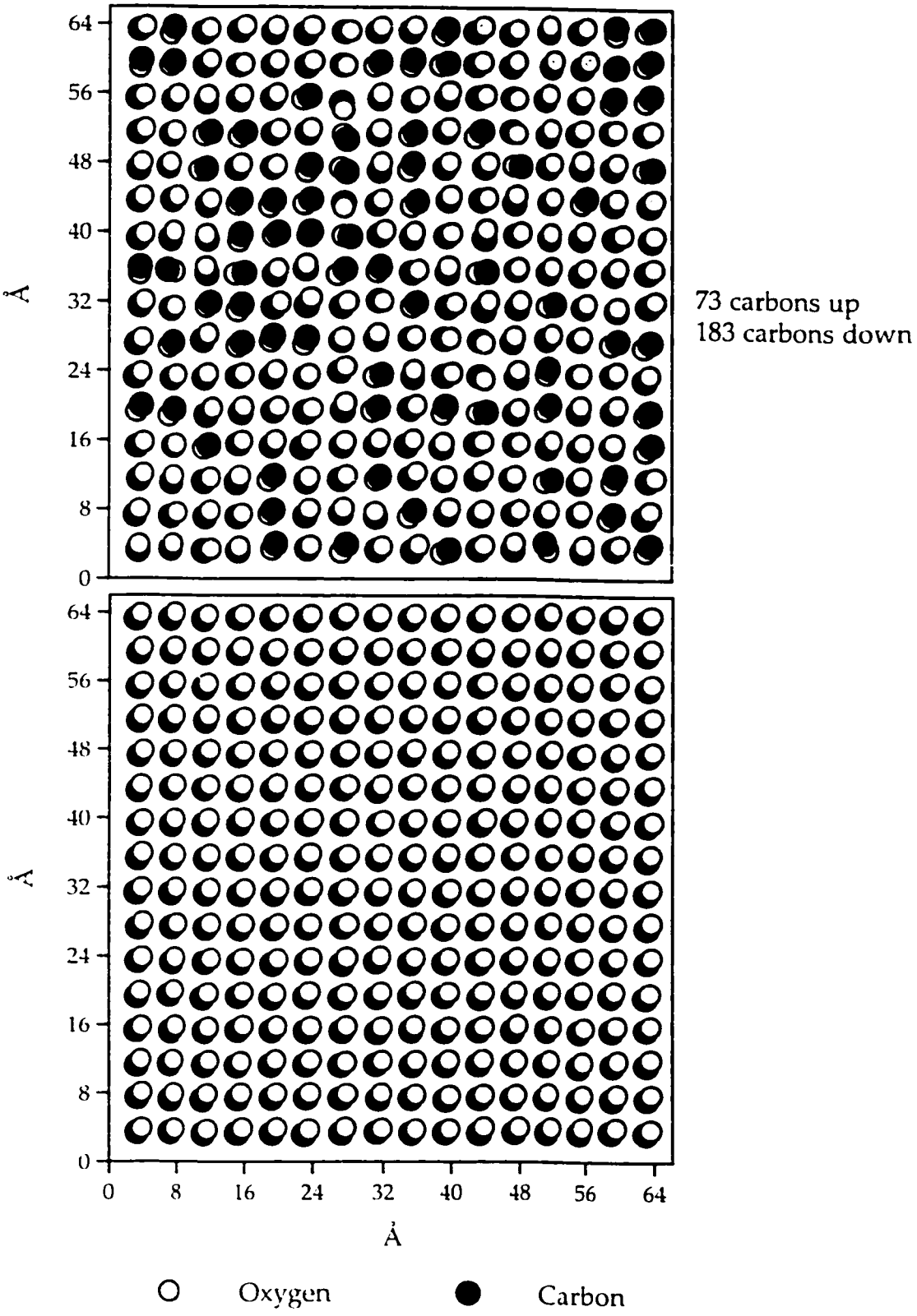

Figure 6.6. The top layer of a two-layer system CO/NaCl(100) configuration generated by Monte Carlo simulation at T= 5K (lower panel) and at T= 25K (upper panel).

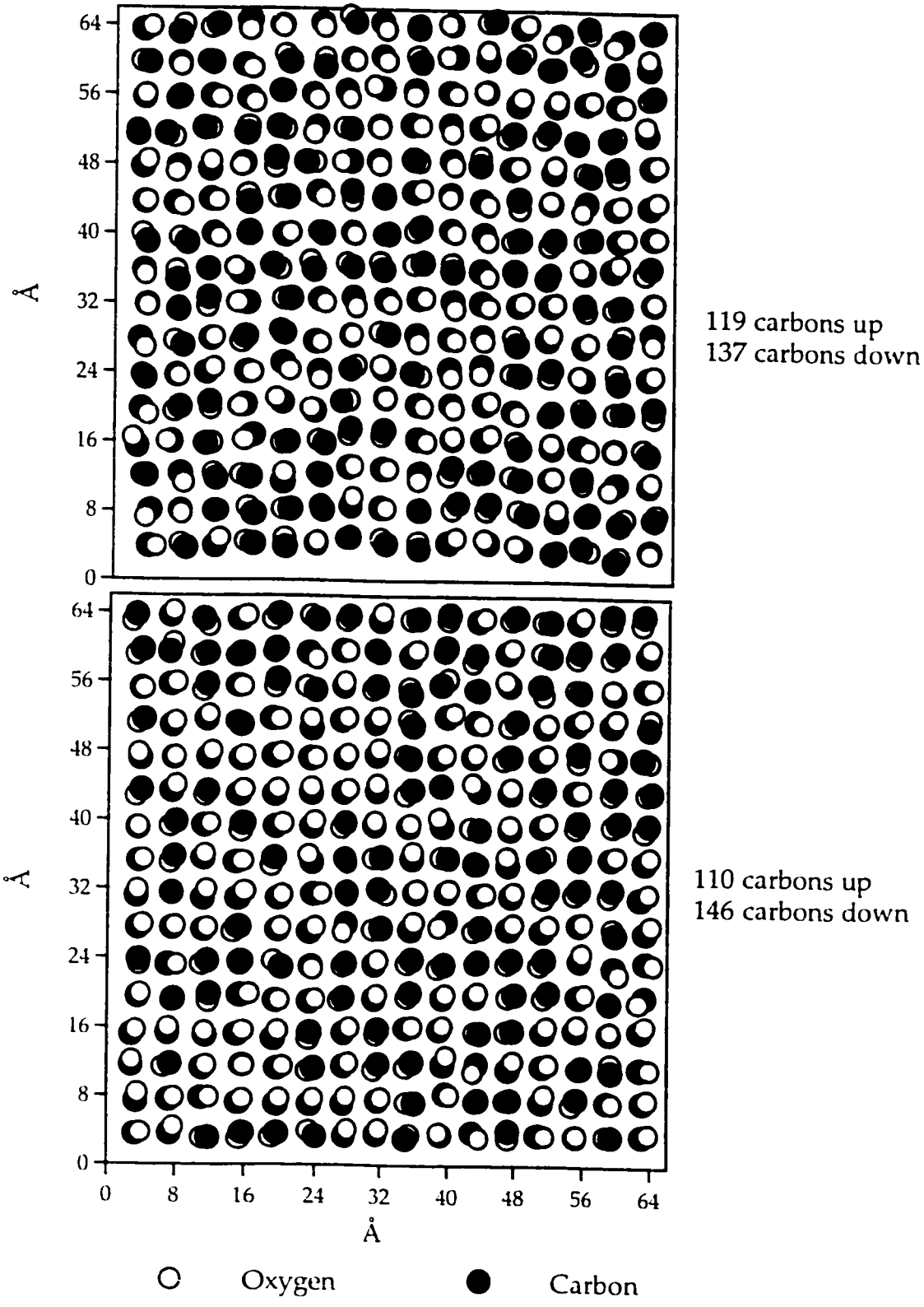

Figure 6.7. The top layer of a two-layer system CO/NaCl(100) configuration generated by Monte Carlo simulation at T= 35K (lower panel) and at T= 40K (upper panel).

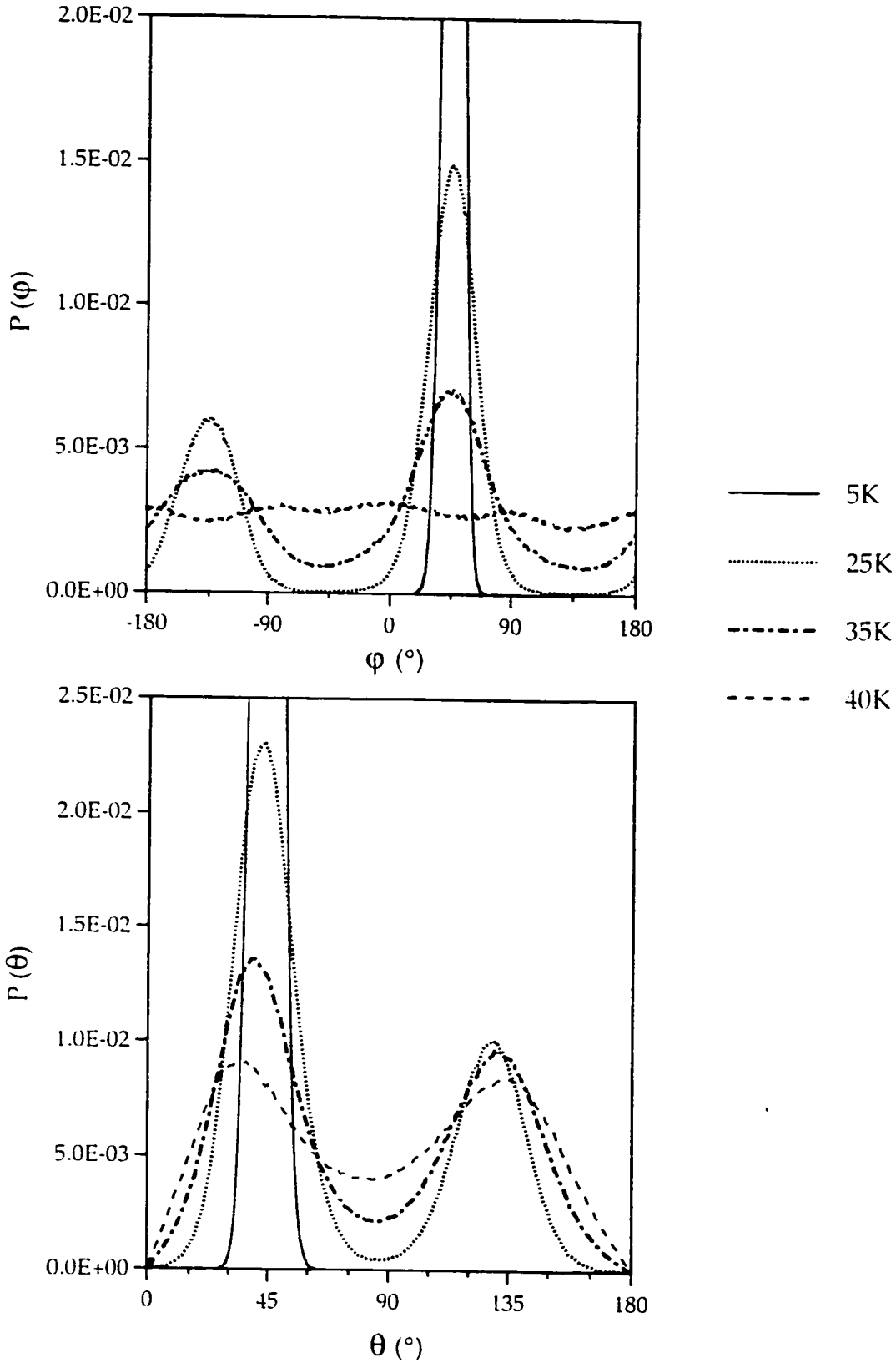

Figure 6.8. Monte Carlo results for the angular distribution for the top layer of a two-layer system CO/NaCl(100): polar, θ, (lower panel) and azimuthal, φ, (upper panel) distributions.

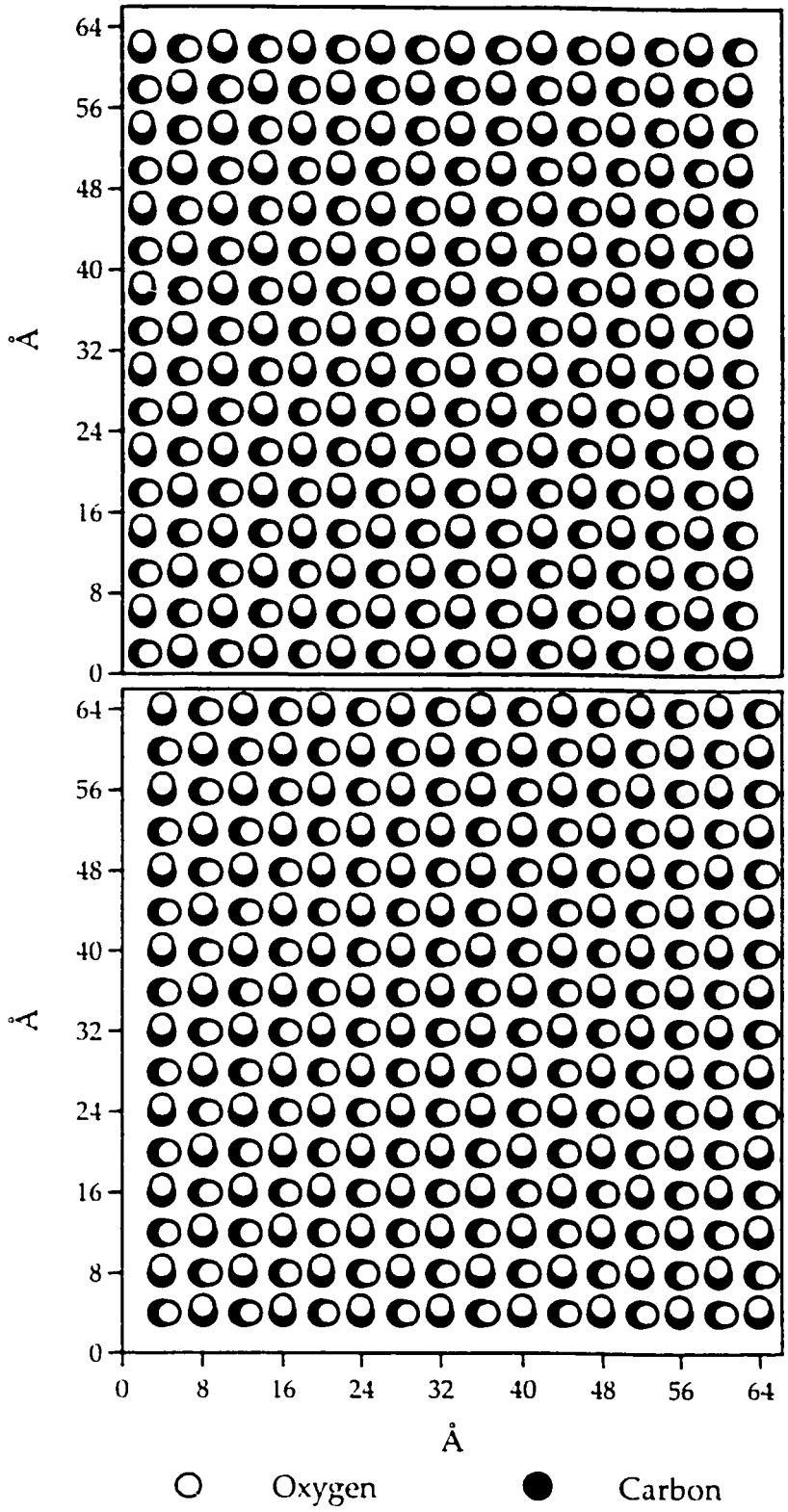

Figure 6.9. The initial configuration of a three-layer system CO/NaCl(100): the middle layer (lower panel) and the top layer (upper panel).

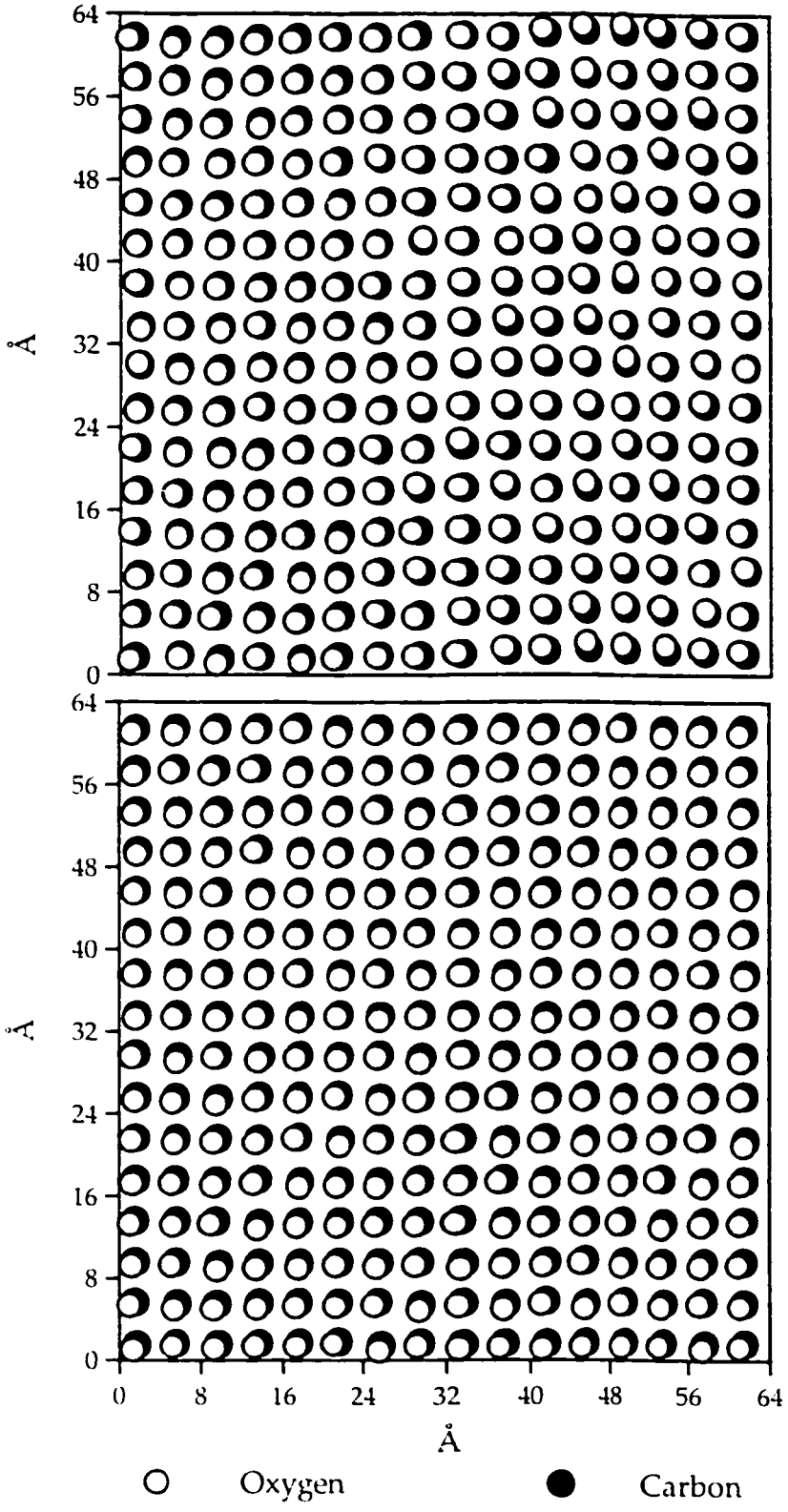

Figure 6.10. The bottom layer of a three-layer system CO/NaCl(100) configuration generated by Monte Carlo simulation at T= 5K (lower panel) and at T= 25K (upper panel) .

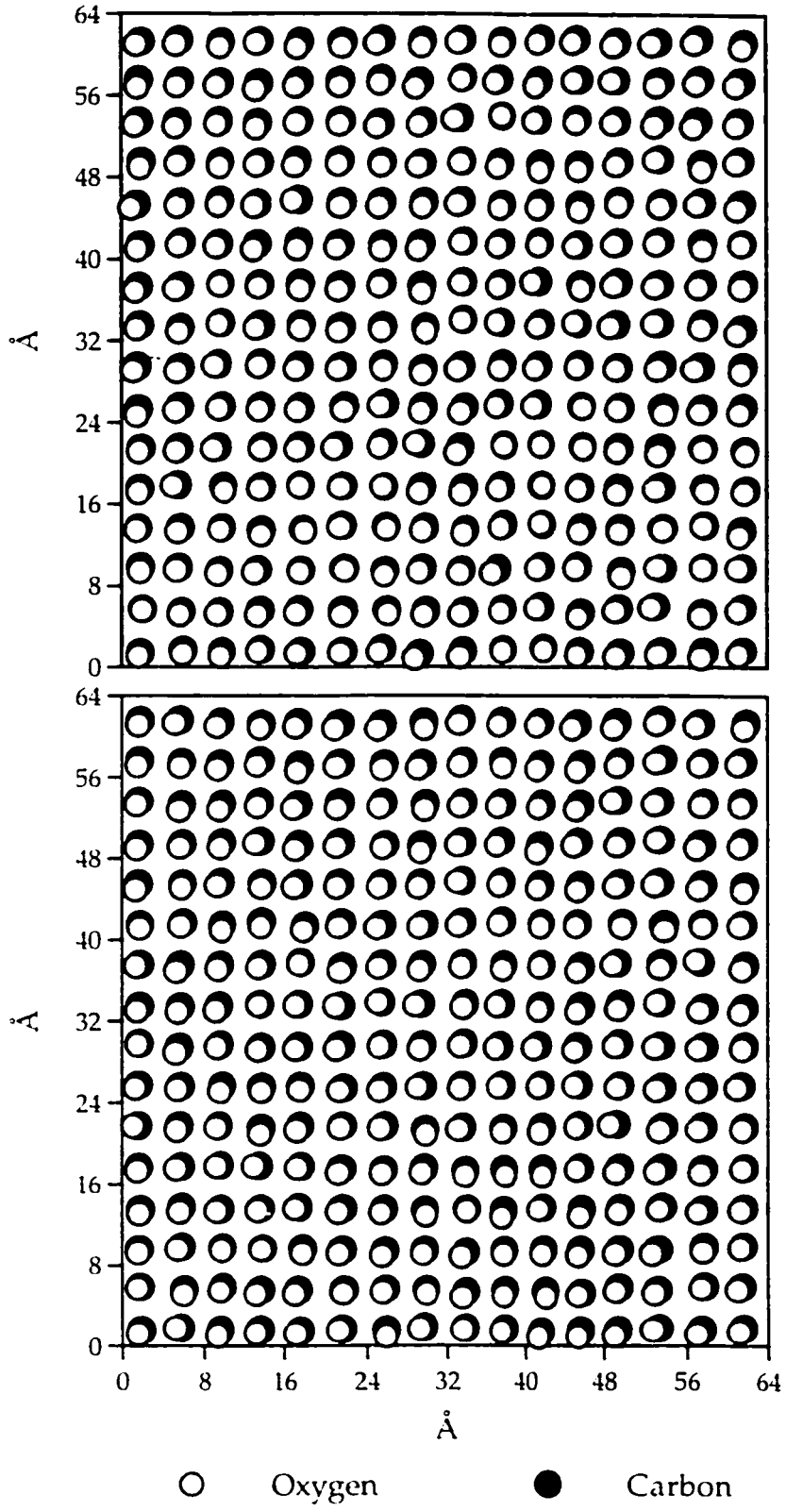

Figure 6.11. The bottom layer of a three-layer system CO/NaCl(100) configuration generated by Monte Carlo simulation at T= 35K (lower panel) and at T= 40K (upper panel).

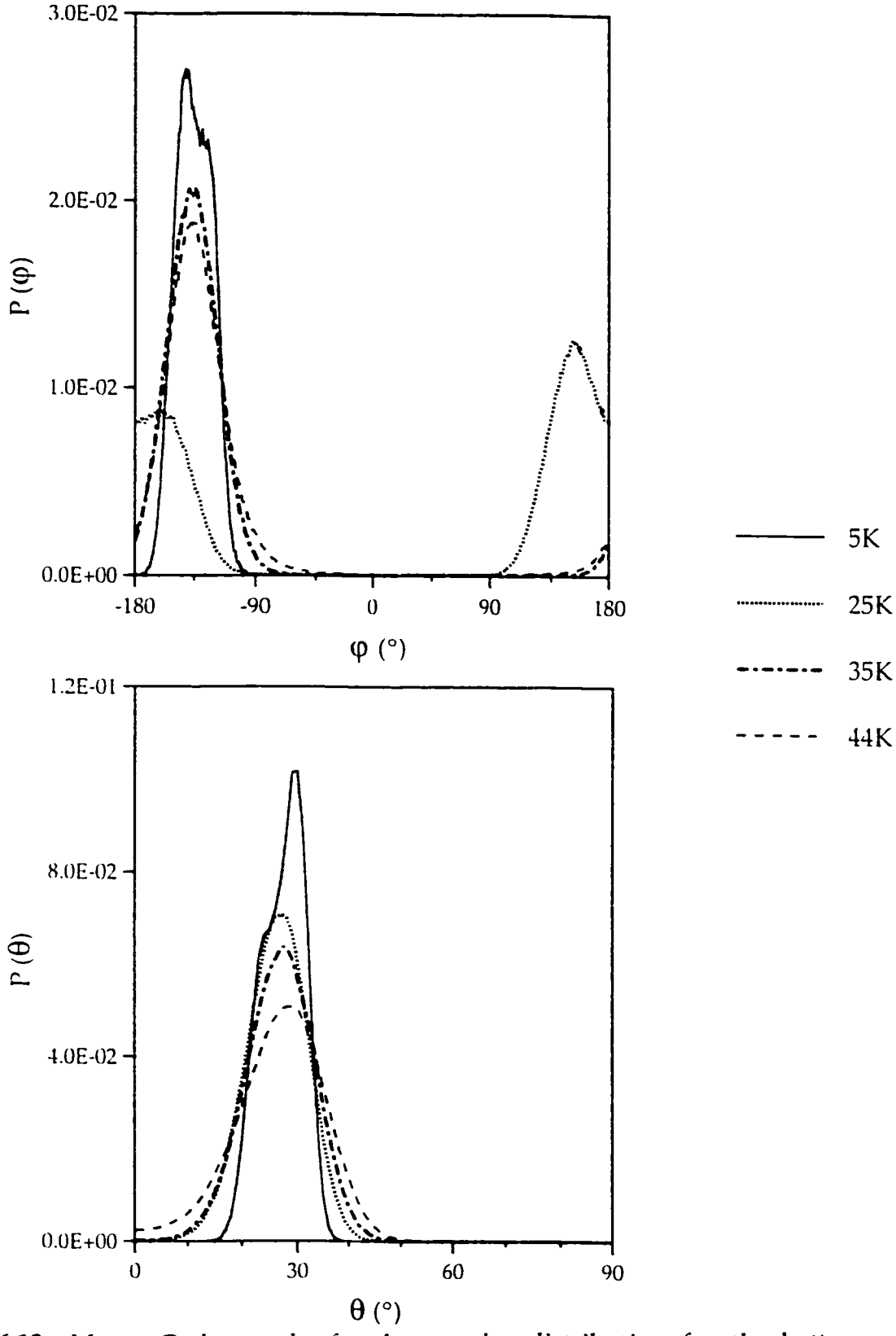

Figure 6.12. Monte Carlo results for the angular distribution for the bottom layer of a three-layer system CO/NaCl(100): polar, θ, (lower panel) and azimuthal, φ, (upper panel) distributions.

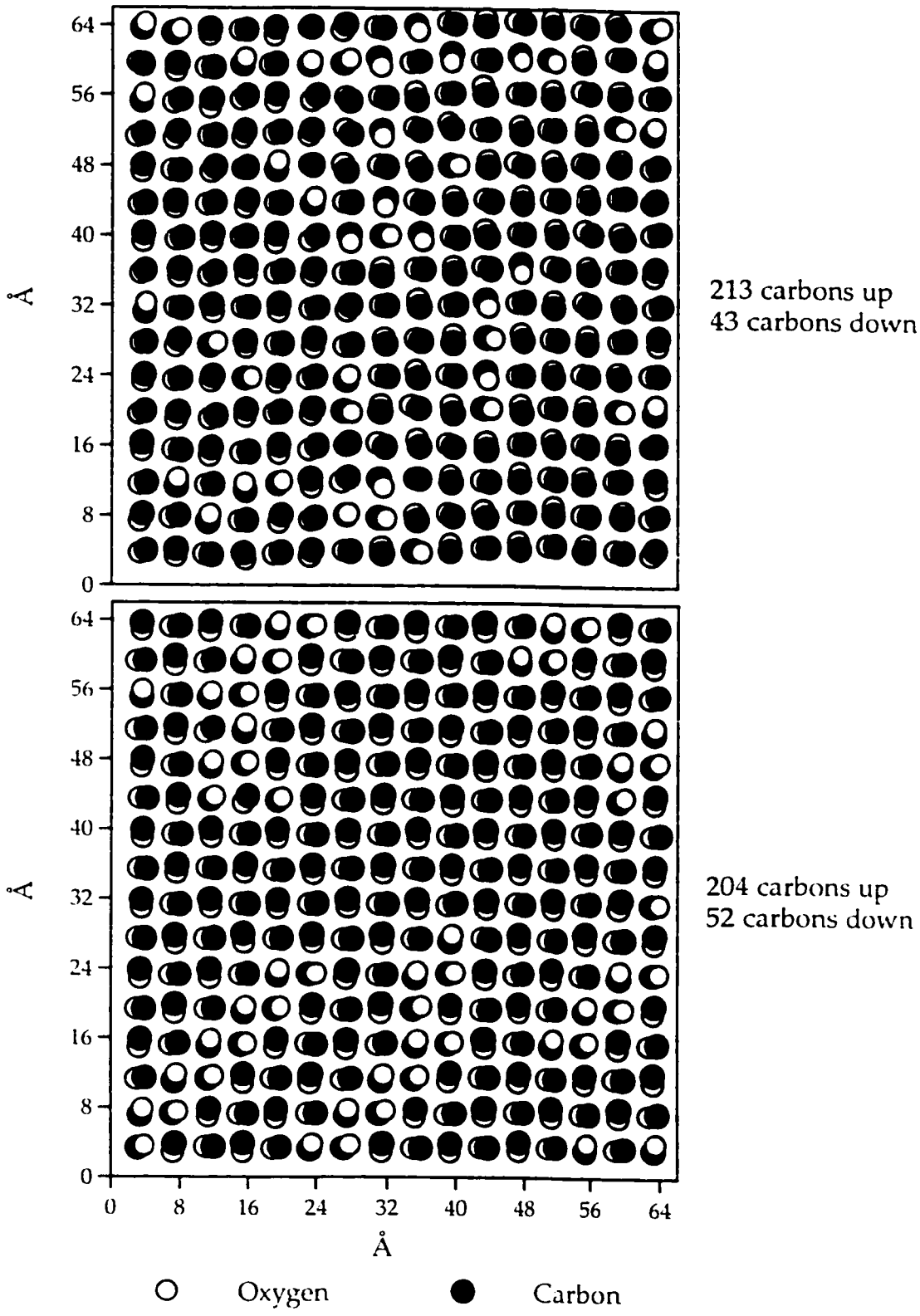

Figure 6.13 The middle layer of a three-layer system CO/NaCl(100) configuration generated by Monte Carlo simulation at T= 5K (lower panel) and at T= 25K (upper panel).

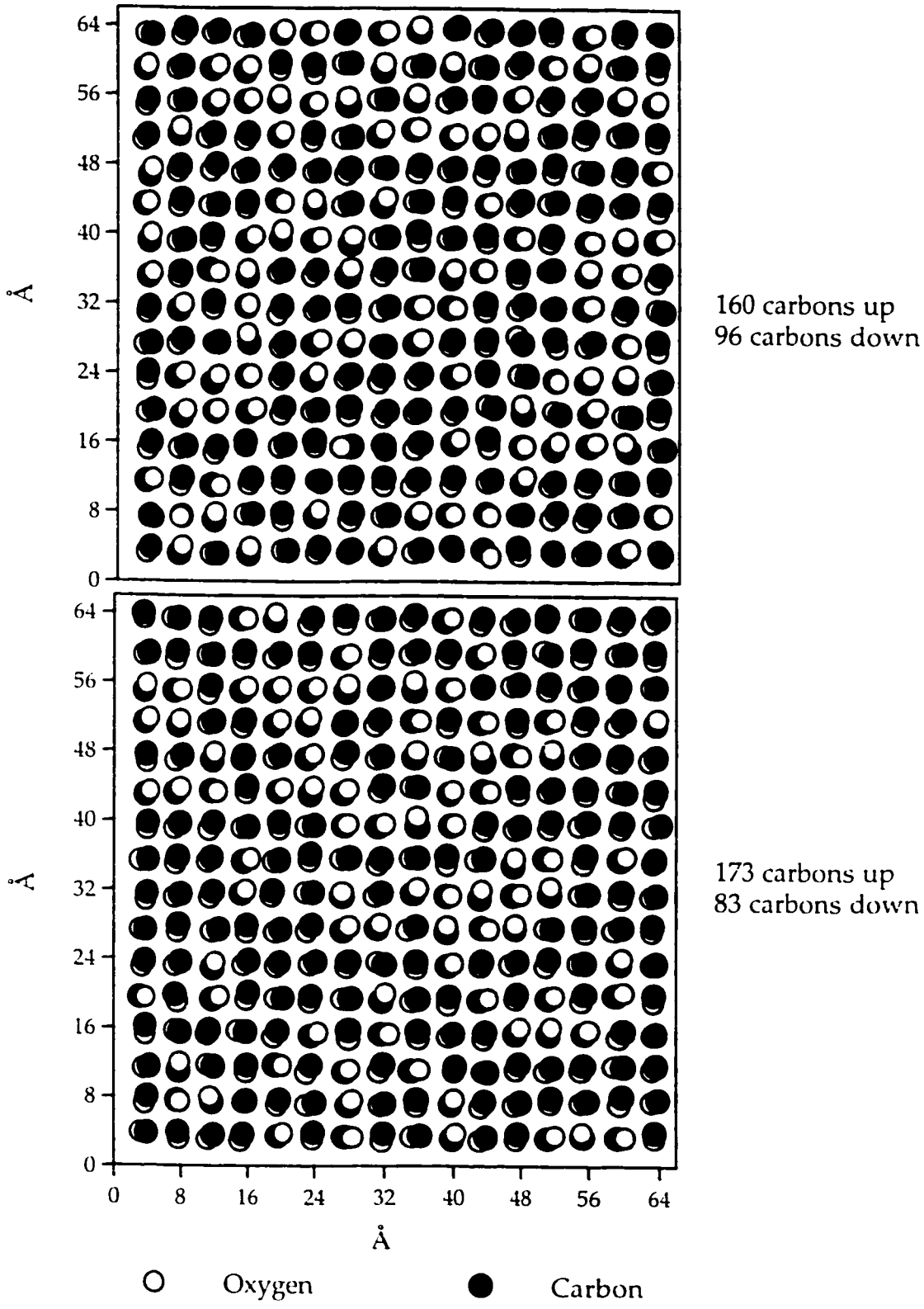

Figure 6.14. The middle layer of a three-layer system CO/NaCl(100) configuration generated by Monte Carlo simulation at T= 35K (lower panel) and at T= 40K (upper panel).

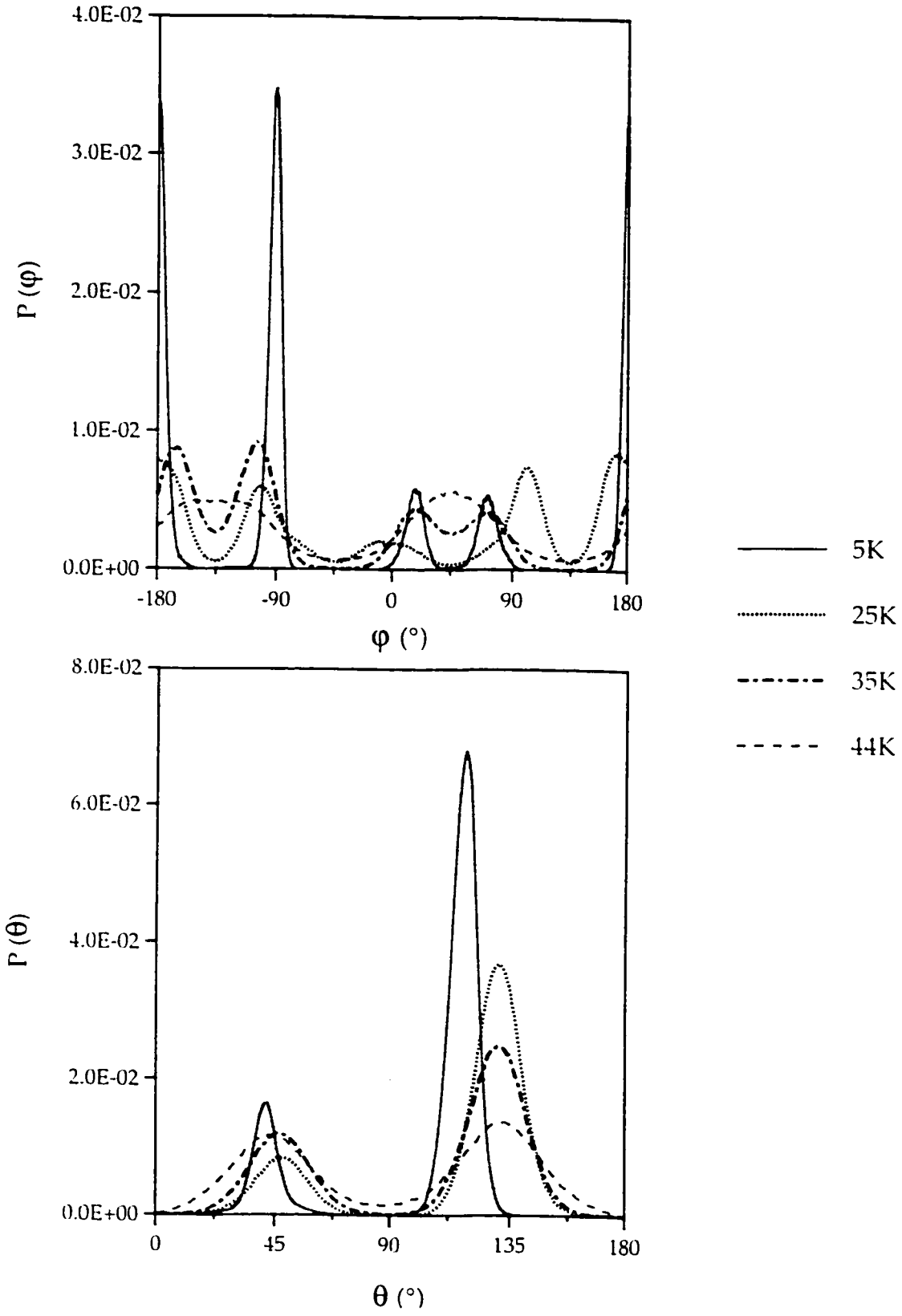

Figure 6.15. Monte Carlo results for the angular distribution for the middle layer of a three-layer system CO/NaCl(100): polar, θ, (lower panel) and azimuthal, φ, (upper panel) distributions.

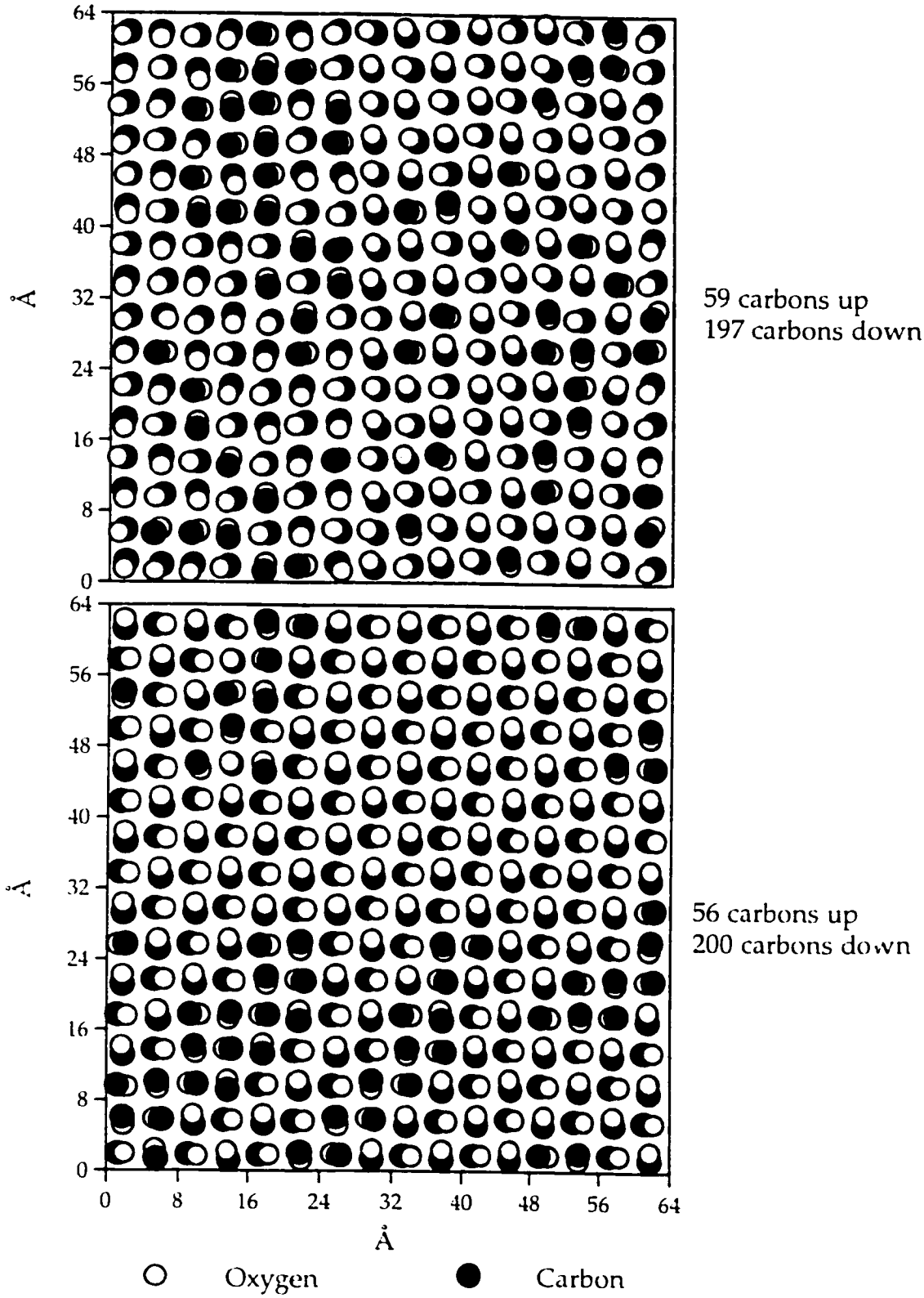

Figure 6.16. The top layer of a three-layer system CO/NaCl(100) configuration generated by Monte Carlo simulation at T= 5K (lower panel) and at T= 25K (upper panel).

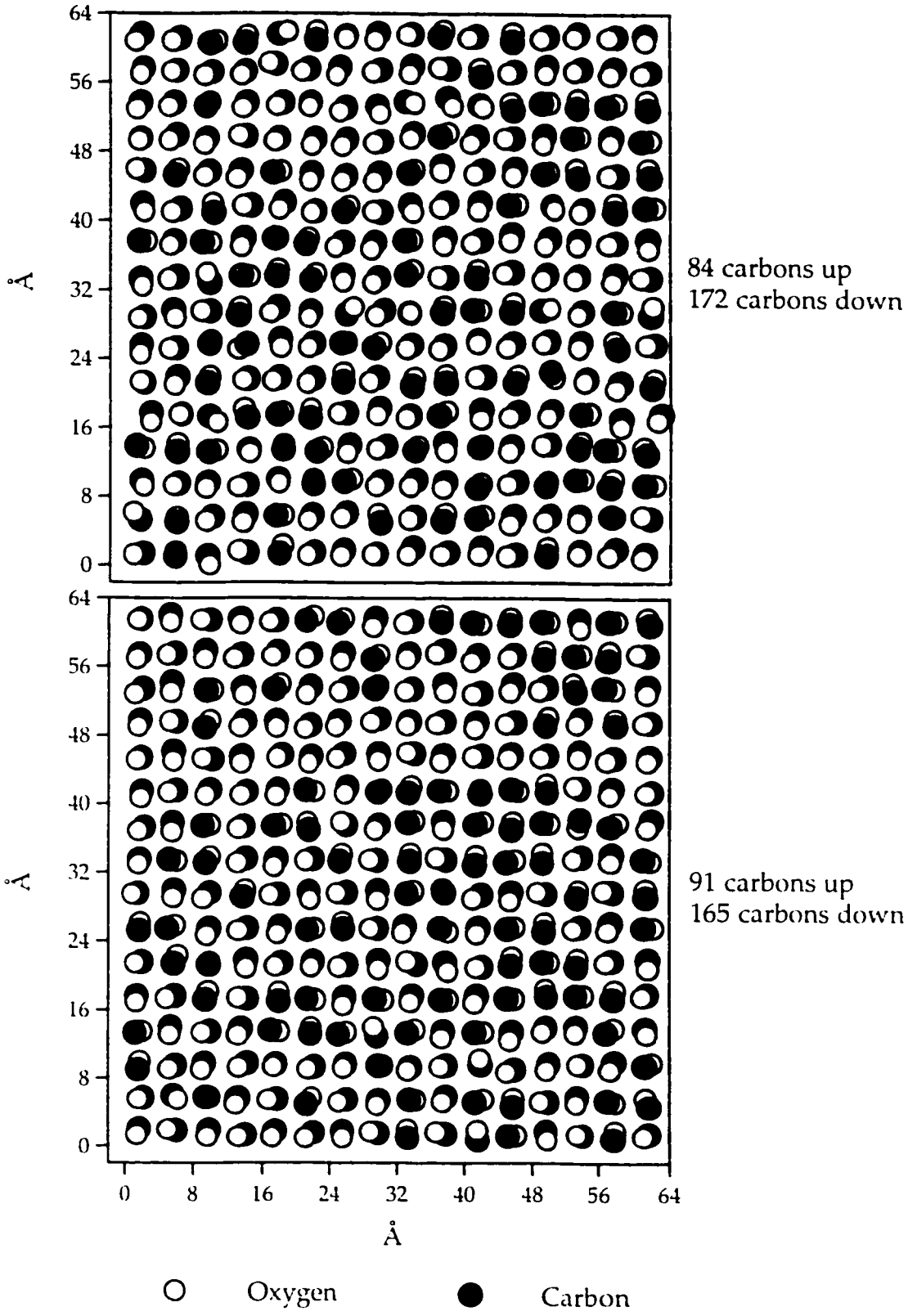

Figure 6.17. The top layer of a three-layer system CO/NaCl(100) configuration generated by Monte Carlo simulation at T= 35K (lower panel) and at T= 40K (upper panel).

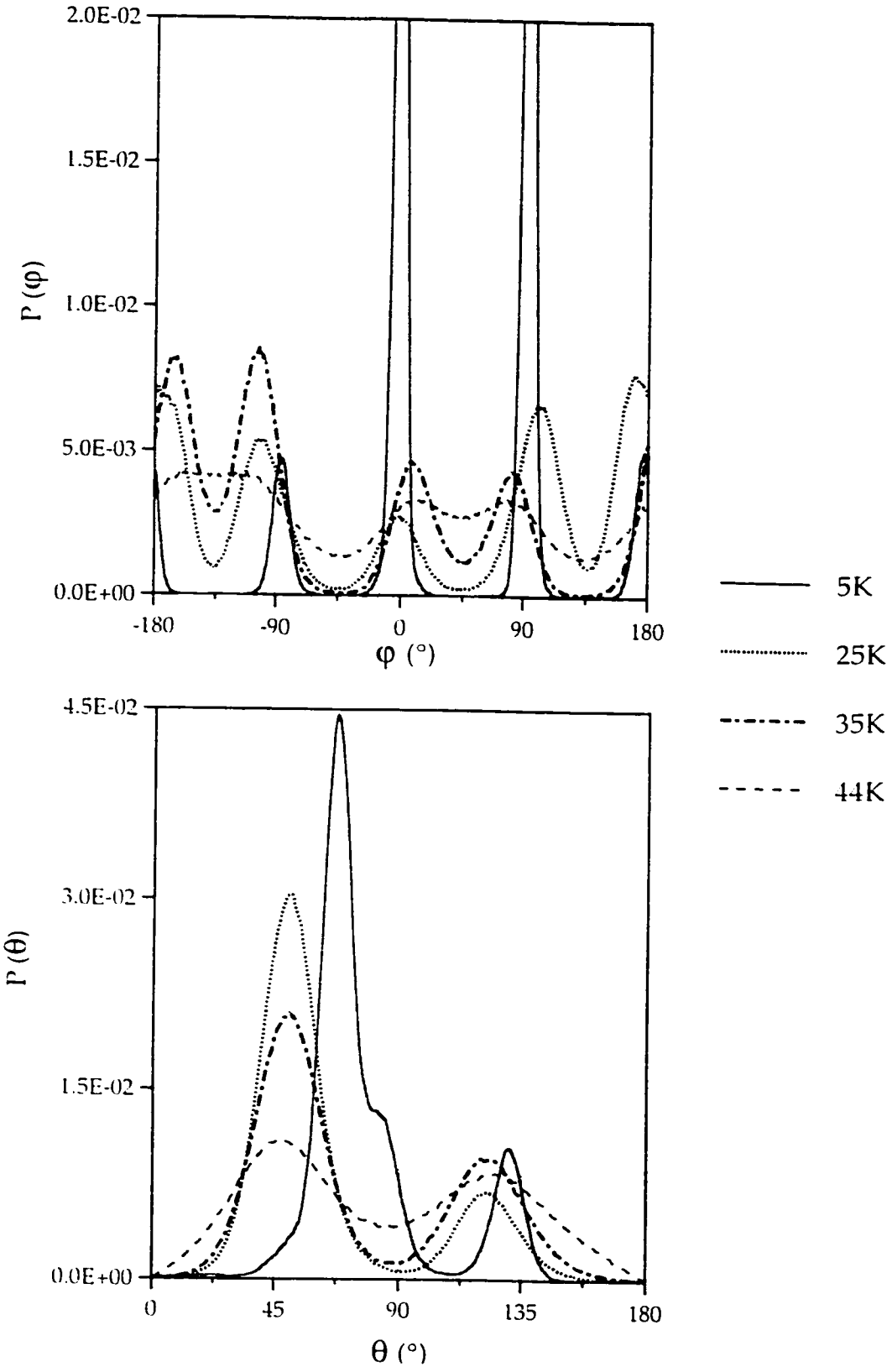

Figure 6.18. Monte Carlo results for the angular distribution for the top layer of a three-layer system CO/NaCl(100): polar, θ, (lower panel) and azimuthal, φ, (upper panel) distributions.

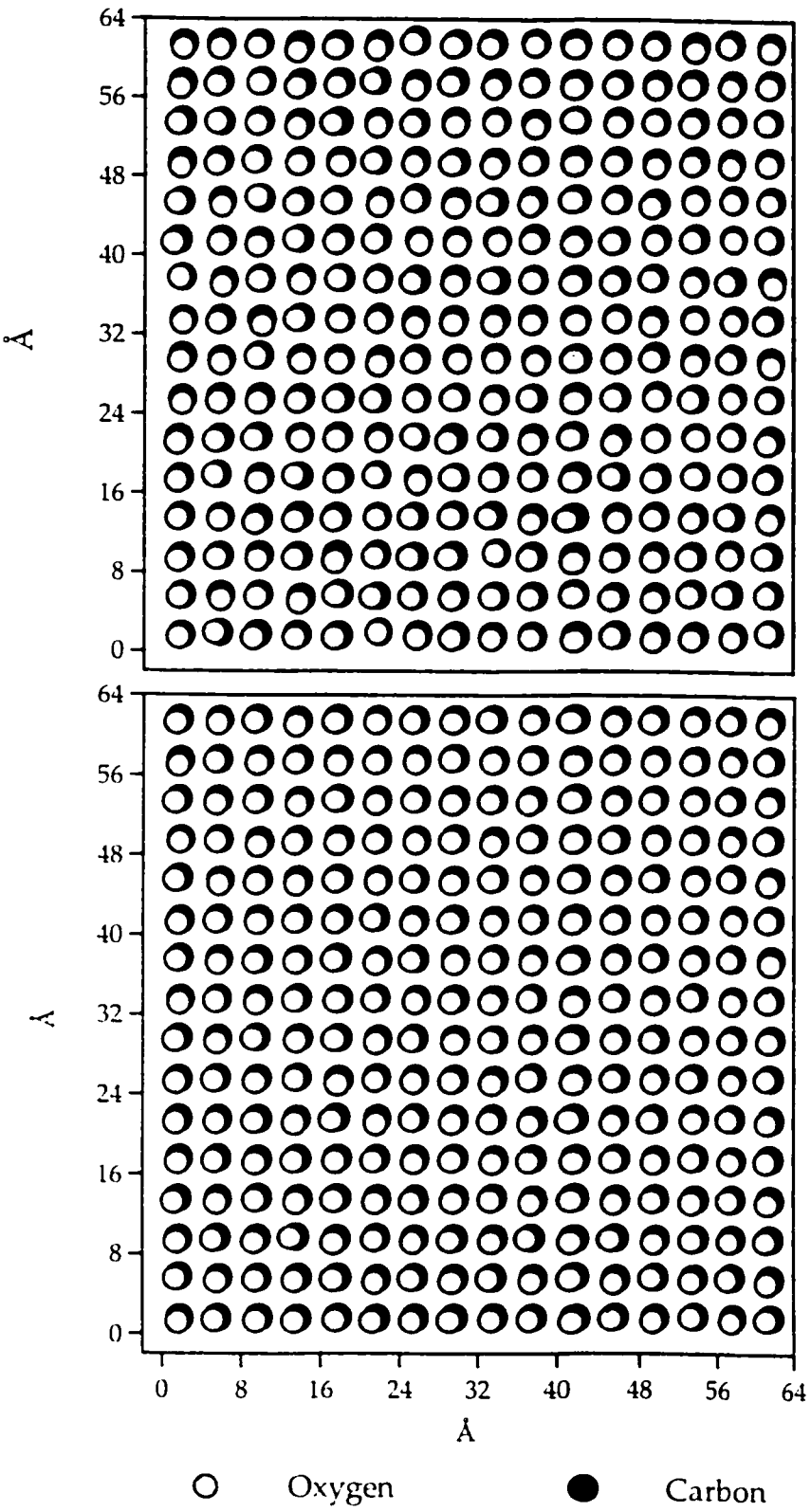

Figure 6.19. The bottom layer of a four-layer system CO/NaCl(100) configuration generated by Monte Carlo simulation at T= 5K (lower panel) and at T= 25K (upper panel).

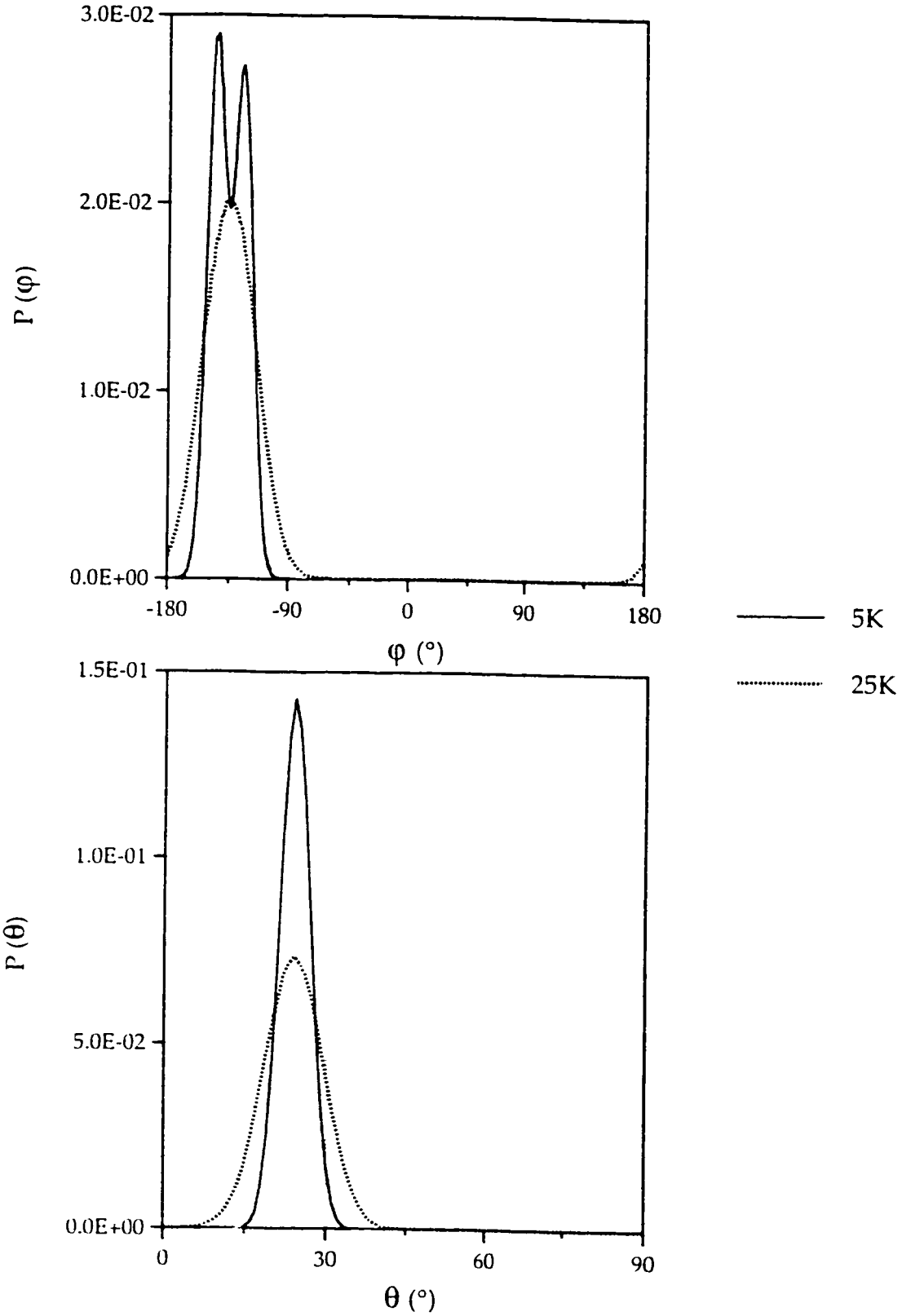

Figure. 6.20. Monte Carlo results for the angular distribution for the bottom layer of a four-layer system CO/NaCl(100): polar, θ, (lower panel) and azimuthal, φ, (upper panel) distributions.

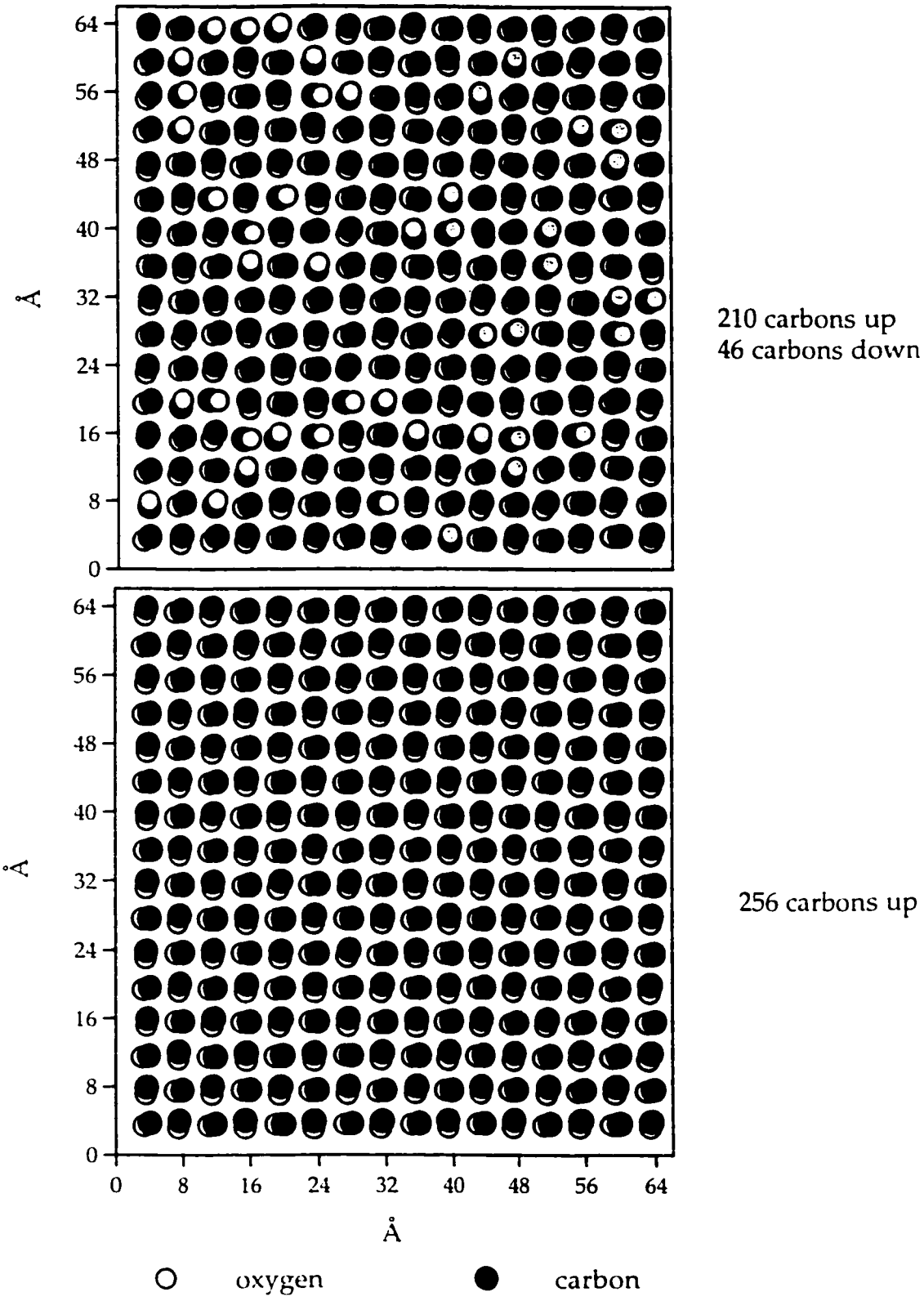

Figure 6.21. The first middle layer of a four-layer system CO/NaCl(100) configuration generated by Monte Carlo simulation at T= 5K (lower panel) and at T= 25K (upper panel).

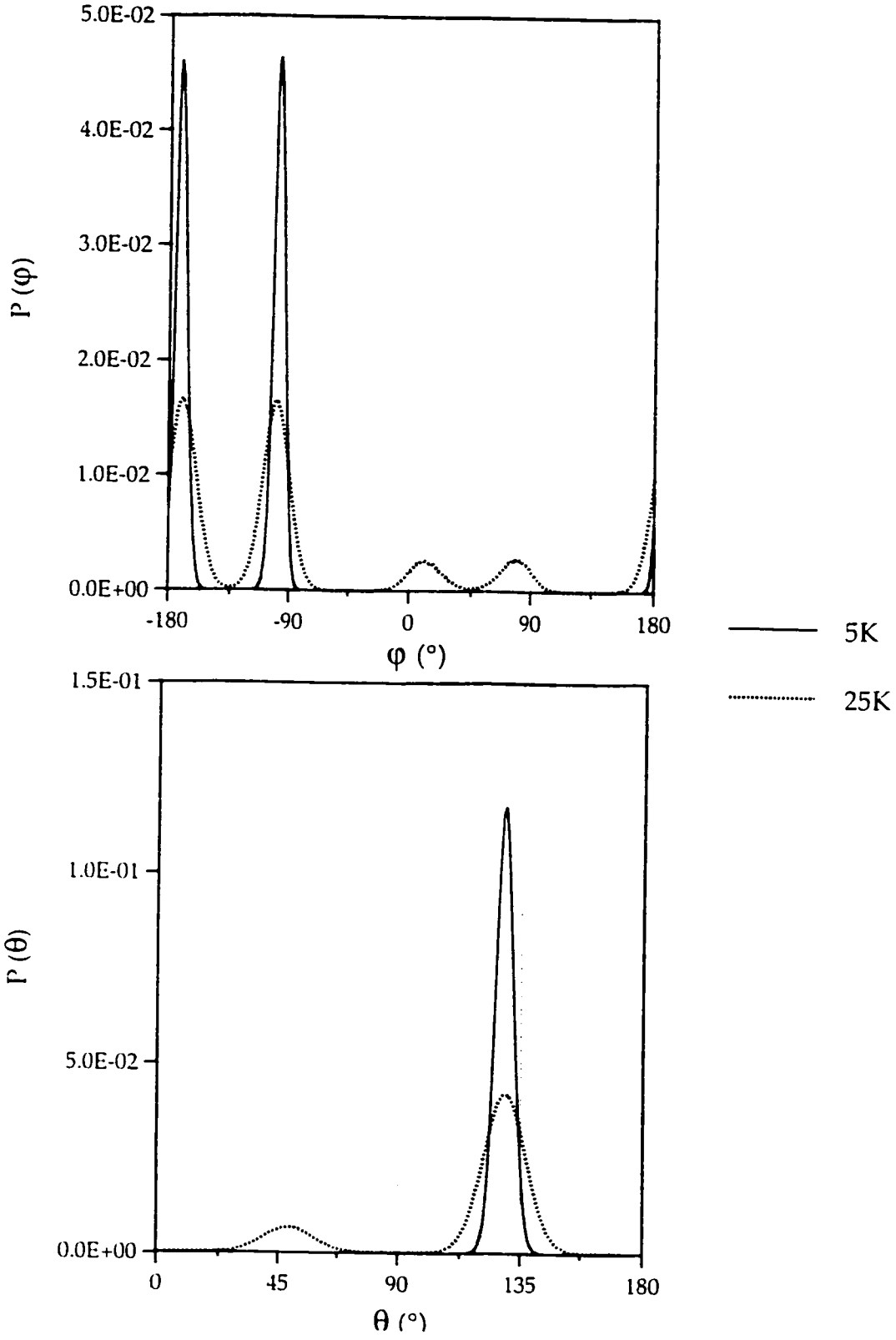

Figure. 6.22. Monte Carlo results for the angular distribution for the first middle layer of a four-layer system CO/NaCl(100): polar, θ, (lower panel) and azimuthal, φ, (upper panel) distributions.

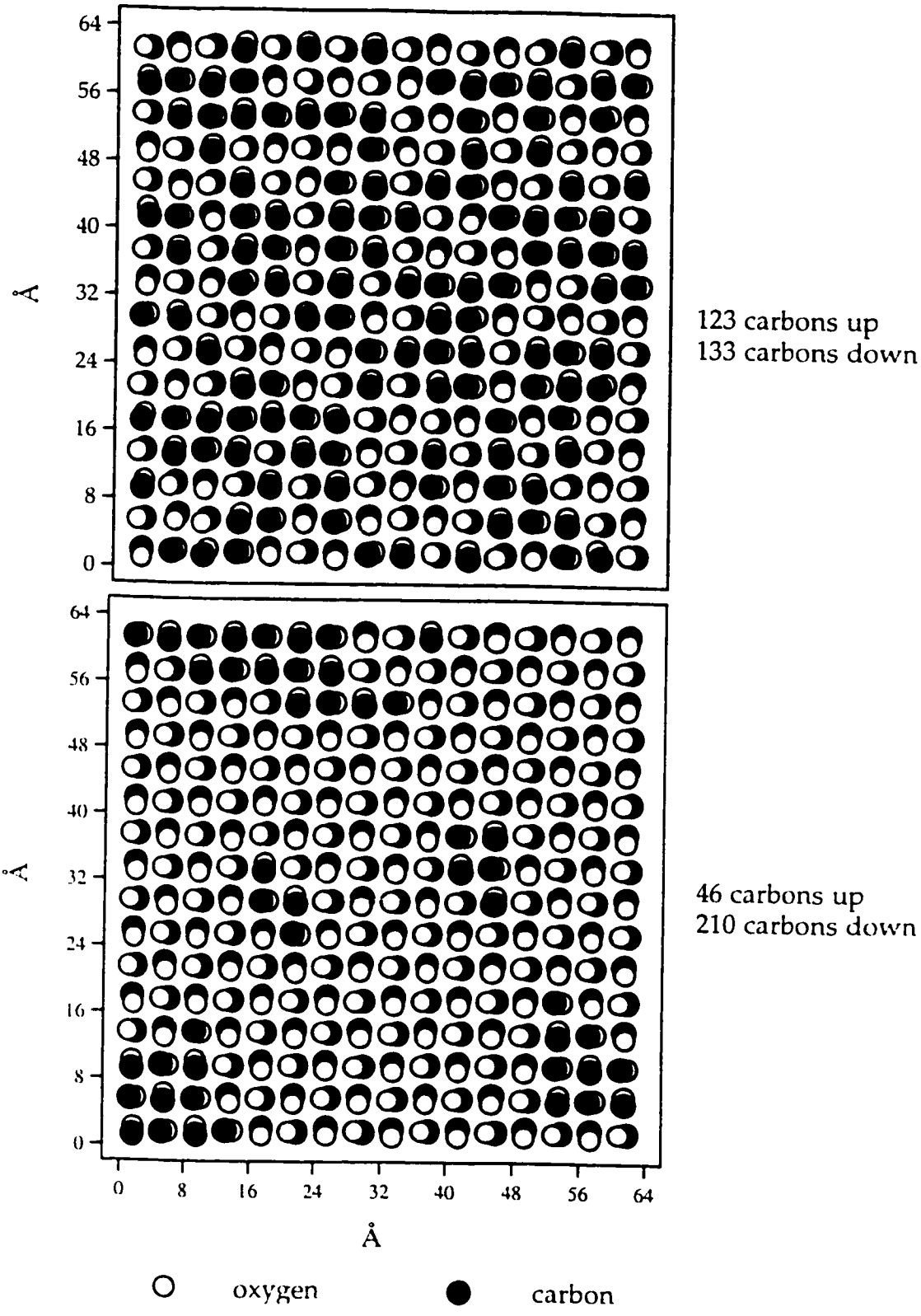

Figure 6.23. The second middle layer of a four-layer system CO/NaCl(100) configuration generated by Monte Carlo simulation at T= 5K (lower panel) and at T= 25K (upper panel) .

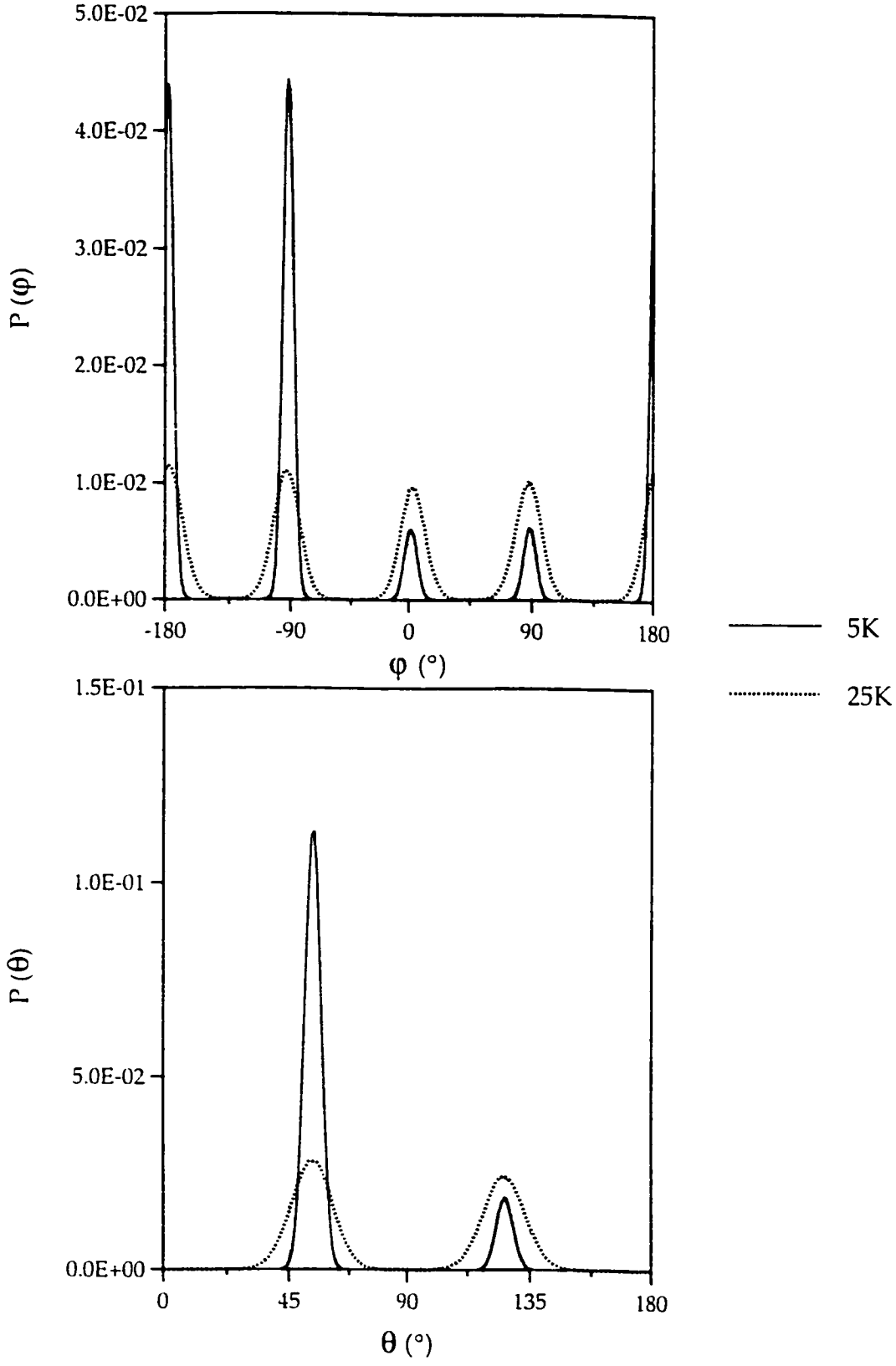

Figure. 6.24. Monte Carlo results for the angular distribution for the second middle layer of a four-layer system CO/NaCl(100): polar, θ, (lower panel) and azimuthal, φ, (upper panel) distributions.

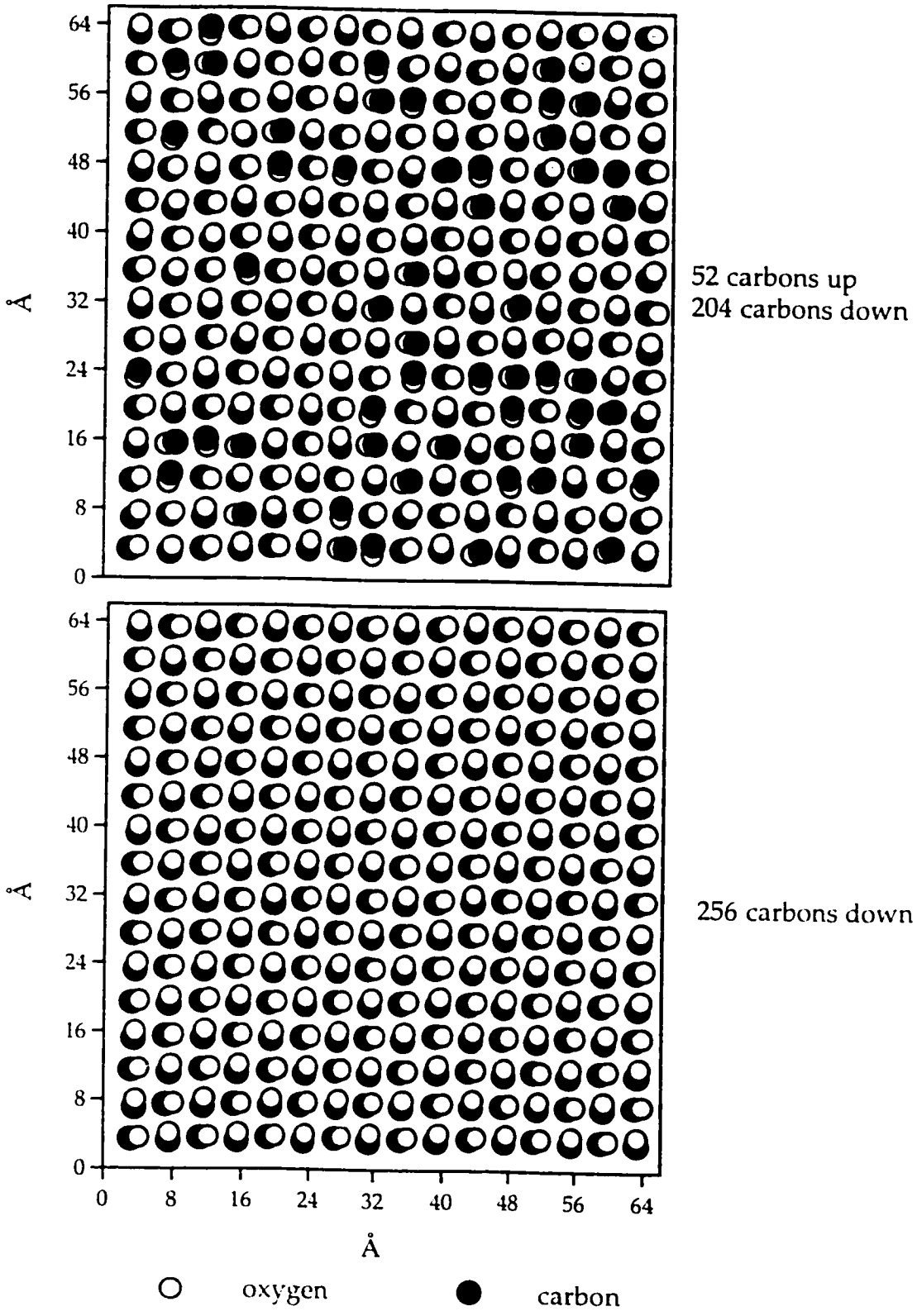

Figure 6.25. The top layer of a four-layer system CO/NaCl(100) configuration generated by Monte Carlo simulation at T= 5K (lower panel) and at T= 25K (upper panel).

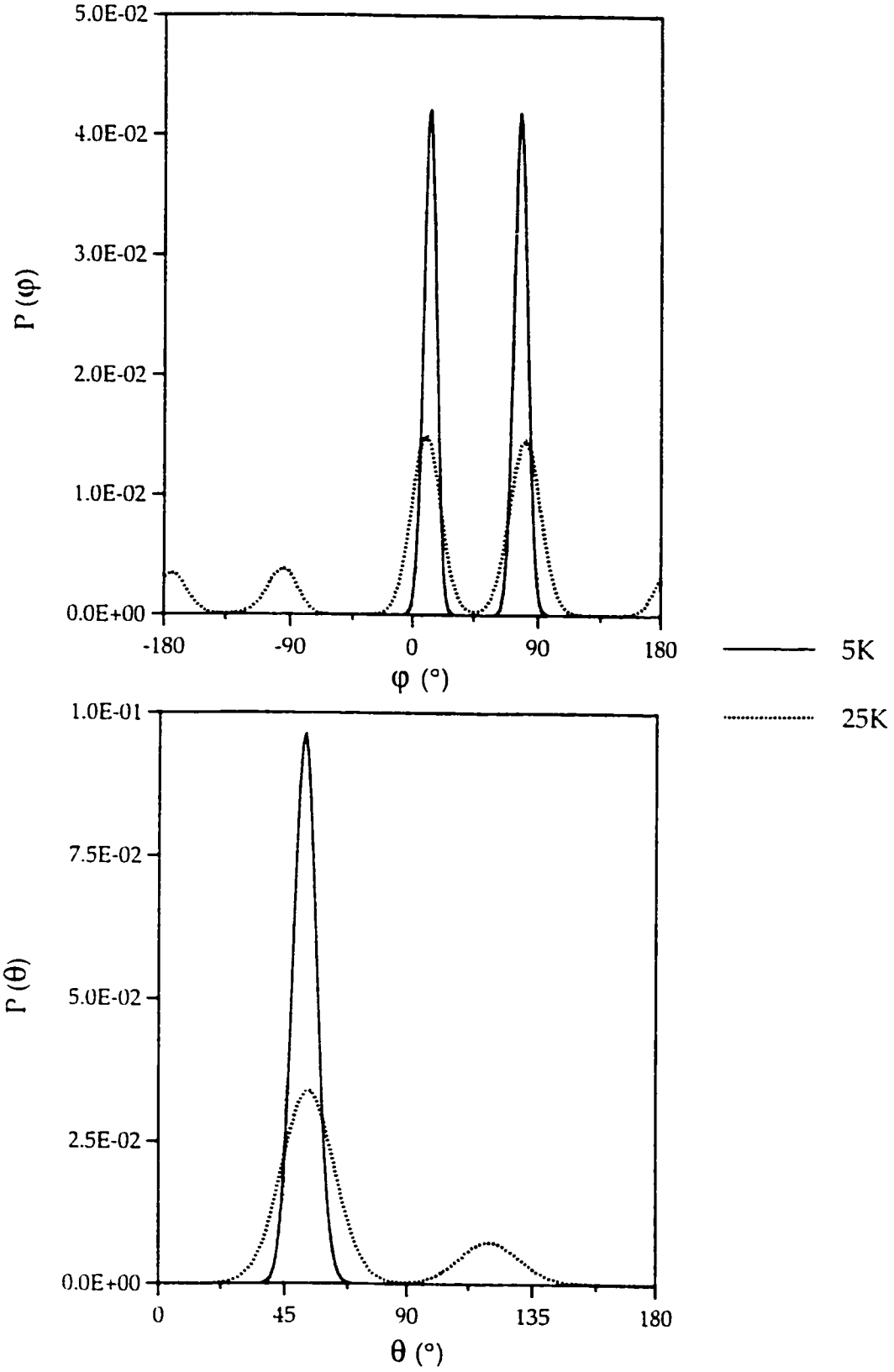

Figure. 6.26. Monte Carlo results for the angular distribution for the top layer of a four-layer system CO/NaCl(100): polar, θ, (lower panel) and azimuthal, φ, (upper panel) distributions.

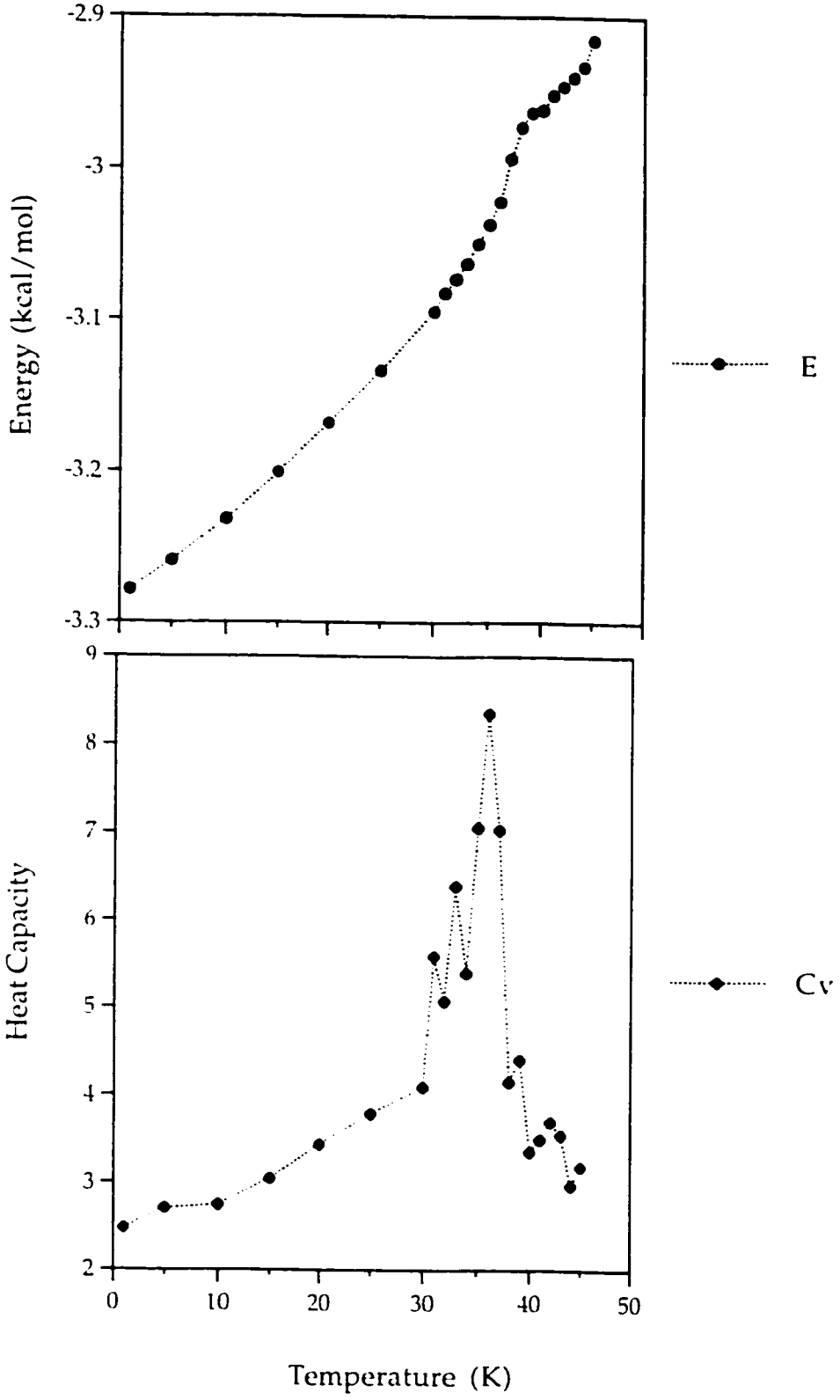

Figure 6.27. Monte Carlo results for the heat capacity, C_v, (lower panel) and energy, E, (upper panel) as functions of temperature for a two-layer system CO/NaCl(100).

CHAPTER 7: RESULTS FOR MONOLAYER CO/LIF(100)

After successfully simulating the CO/NaCl(100) system, we decided to use the same potential model to search for other systems that might exhibit similar behaviour. The CO/LiF(100) system was chosen to be examined because of the similarities of the LiF and NaCl surfaces. Both surfaces are cubic with univalent charges and their lattice constants allow for an epitaxial relationship with CO adlayers, even though LiF has a smaller lattice constant compared to the one of NaCl (the unit cell of the former is 4.03Å in value while one of the later is 5.64Å). CO molecules adsorb at every second site of the Li^+ cations instead of at every Na^+ site as in the case of the NaCl substrate. In addition, the input parameters[67] for the calculations of the potential energy parameters are available in the literature.

The potentials and methods used in this simulation were the same as those used to simulate the CO/NaCl(100) system. Empirical atom-atom and atom-ion potentials, within the two-body approximation, were employed to describe the repulsion and dispersion interactions and distributed multipoles (point charges and point dipoles) were used to represent the electrostatic interactions. The difference occurs in the parameters used to characterize the CO-surface interactions. In order to construct the CO/LiF(100) surface potential we again used the Tang-Toennies form to describe the non-electrostatic interactions between individual atom-ion pairs. The details of the intermolecular calculations and the values of the parameters, which characterize the CO-CO potentials as

well as surface potential, can be viewed from Chapter II (Potential Calculations). The values of the CO-LiF coefficients for the various atom-ion pairs are given in Table 7.1.

Table 7.1. The values for the parameter of the molecule-surface (CO-LiF) interaction potential.

	C atom		*O atom*	
	Li^+	F^-	Li^+	F^-
A (kcal/mol)	72.6×10^3	27.2×10^3	72.3×10^3	24.8×10^3
β ($Å^{-1}$)	4.40	3.22	4.48	3.46
C_6 ($Å^6$ kcal/mol)	19.6	425	9.0	195
C_8 ($Å^8$ kcal/mol)	92.4	2910	42.4	1330
C_{10} ($Å^{10}$ kcal/mol)	533	245	24 300	11 200

The origin was also located on a F^- anion in the plane of the surface. The position and the orientation of the molecule is constructed similar to those of the CO/NaCl(100) system and can be viewed in chapter III (Potential Calculations, section 3.2)

7.1 Results of a Single CO Adsorption on LiF(100) Surface

An energy minimization (steepest descend method) was performed on a single CO molecule on a LiF(100) surface. The result revealed that the single CO molecule sits perpendicular to the LiF(100) surface above a Li^+ ion with the carbon atom end down. The distance between the C atom and the Li^+ ion is found to be 2.8967Å. The tilt angle is determined to be zero with the carbon end pointing down towards the surface ion Li^+ just as in the case of CO on NaCl(100). However, the surface binding energy is calculated to be -1.5217 kcal/mol, which is much less than the surface binding energy of the CO/NaCl(100), (the latter is -3.5608 kcal/mol). On the other hand the obtained value for CO/LiF is close to the value (-1.84 kcal/mol) calculated using *ab initio* methods.[68] Like the CO/NaCl(100) system, the main contribution to the surface binding energy is the electrostatic interaction (-0.9050 kcal/mol) between the molecule and the surface. When the molecule is inverted (i.e. the oxygen end is closer to the surface ion Li^+) then the binding energy is calculated to be -1.2594 kcal/mol, resulting in a small difference in energy between the head-tail orientation of ΔE= -0.2623 kcal/mol. The details of the potential from the energy minimization method can be seen from the following Table 7.2.

Table 7.2. Break down of the adsorption energy for a single CO/LiF(100) calculated by energy minimization method.

T= 1K	*O-C...Li⁺ orientation*	*C-O...Li⁺ orientation*
Distance of carbon from the surface (z_C, Å)	2.8967	3.5559
Dispersion-repulsion Energy (kcal/mol)	-0.6168	-0.8945
Electrostatic Energy (kcal/mol)	-0.9050	-0.3649
Total Energy (kcal/mol)	**-1.5218**	**-1.2594**

7.2 Results for CO/LiF(100) Monolayer

To simulate a full monolayer of CO an ensemble of 288 CO molecules was placed in the LiF surface potential. Periodic boundary conditions in the lateral direction were imposed as well as a cutoff radius of 18.5Å for the CO-CO interactions. MC simulations were run for $5x10^4$ cycles at various temperatures over the range 1 - 55K. Statistical data for the variables of interest were collected for the last $3x10^4$ cycles of each run after throwing away the first $2x10^4$ cycles. The results will be discussed in the following paragraphs.

7.2.1 Low-temperature Structure (T= 10K)

At temperatures T= 10K the monolayer adopts an azimuthally ordered $p(2\sqrt{2}x\sqrt{2})R45°$ phase with a herringbone structure, which can be regarded as a p(2x1) structure rotated by 45°. The structure can be viewed in Fig. 7.1, a snapshot of the monolayer at T= 10K. The unit cell is marked by a grey dotted rectangle and contains two molecules: one from each of the diagonals. The CO molecules are shifted off of the Li^+ ion by about 0.2Å towards the neighbouring cation in a <1,1,0> type direction and are tilted away from the surface normal by an angle $\theta \sim 45°$. As in the CO/NaCl(100) system, the CO/LiF(100) system forms an ordered phase at low temperature where the molecules have the same azimuthal orientation along diagonals, with diagonals alternating their orientation. At T= 10K the total binding energy of the herringbone structure is determined to be -2.3419 kcal/mol (Table 7.3) with the most important contribution comes from the surface electrostatic energy (-0.9694 kcal/mol) as in the case of CO/NaCl(100).

Table 7.3. Break down of the adsorption energy for a CO/LiF(100) monolayer generated by Monte Carlo simulation at T= 10K.

T= 10K	*Energy (kcal/mol.molecule)*
CO-CO (Dispersion-repulsion)	-0.58729
CO-CO (Electrostatic)	-0.13304
CO-LiF (Dispersion-repulsion)	-0.63032
CO-LiF (Electrostatic)	-0.96944
Induction energy (CO-CO+CO-LiF)	-0.02182
Total Energy	**-2.34191**

7.2.2 High-temperature Structure (T> 10K)

At T= 25K (Fig. 7.2), the CO structure is found to remain highly ordered with the appearances of some small defects. On average the molecules still have preferred orientations and remain tilted at $\theta \sim 45°$. In addition, inversion defects occurred whereby some to the molecules flip over with the oxygen atom closer to the surface than the carbon atom. The oxygen atom is localized near the Li^+ site but is slightly offset towards one of the four neighbouring Li^+ sites. This characteristic has never been observed in the case of CO/NaCl(100), and is due

to the smaller energy barrier to inversion for the LiF substrate which is suggested by the smaller binding energy of CO/LiF(100), -2.3419 kcal/mol per molecule compared to -4.3782 kcal/mol per molecule for CO/NaCl(100). This results in a smaller energy difference in the head-tail ordering between the two positions (i.e. carbon end down and oxygen end down) as previously mentioned (ΔE= -0.2623 kcal/mol). In either case, the inverted molecules would not be considered as disordered because the head-tail orientation was not considered in those studies as one form of disorder. Moreover, the orientation of the inverted molecule is basically the same in the structure compared to the other molecules. Hence the structure is still considered as an ordered structure despites the presence of the inverted molecules at T= 25K.

It is not before T= 35K that the herringbone structure starts to break up into disordered regions with some molecules losing their preferred orientations (dash circles in Fig. 7.3). As the temperature was further increased, the number of inversions is found to increase as well, although most of them still contribute to an ordered phase, as shown in the snapshot of Fig. 7.3. At this high temperature, only traces of the herringbone structure remain. However, rows of molecules in the diagonal remain highly ordered in the CO layer at T= 35K.

The degree of disorder amongst the CO molecules continues to increase as the temperature rises to T= 40K. Yet on average the molecules stay titled at a

same angle from the surface normal as in the low temperature ordered phase. Similar to the case of CO/NaCl(100) the CO molecules are found to lose their preferred azimuthal orientations even those inverted molecules (as shown the snapshot of CO/LiF at T= 45K in Fig. 7.5) although they remain tilted at high temperatures. The number of inversion molecules in this case is found to increase with the raising of the temperature as shown in the configuration of the CO layer at T= 40K (Fig. 7.4) and T= 45K (Fig. 7.5). It is worth noticing that the molecules have high mobility at high temperature because the CO molecules do not occupy every adsorption site in this system. This can be best demonstrated by the molecules in circle in the snapshot of CO/LiF(100) at T= 45K (Fig. 7.5). These molecules are found to move from one adsorption site to another. In addition to that, because of small binding energy, the molecules are found to desorb at around T~ 50K. Hence, the order-disorder transition temperature in this system is predicted to be above T> 44K. However, a more conclusive prediction cannot be completed because of the early desorption of the molecules in this system.

The appearance and progression of the inverted molecules can be followed in the polar angle (θ) distributions at different temperatures as shown in Fig. 7.6. At T= 10K, the distribution shows a well-defined thermal distribution as expected at θ~ 45°. At T= 25K a new peak appears at θ~ 115° due to the inversion of the CO molecules. As the temperature is increased to 40K this peak continues to grow at the expense of the original peak. This is again in accord

with the increase in number of the inverted molecules as seen in the snapshots of the CO molecules at high temperatures. The slight untilting of the CO molecules can be observed by the shift of the original peak from $\theta \sim 45°$ to 30° in Fig. 7.6. This means that the molecules remain tilted even in the disordered phase. Hence the system of CO/LiF(100) can also be predicted to undergo an order-disorder phase transition similar to the CO/NaCl(100) system, with the transition temperature above T > 40K.

Fig. 7.7 demonstrates the monitoring of the phase transition of monolayer CO/LiF(100) using the phi (azimuthal orientation) distributions. At low temperature, T= 10K, two sharp peaks are observed at φ = 0° and 90°. This is in agreement with diagonal rows of molecules oriented in one of these two directions as can be seen in Fig. 7.1. As the temperature is raised, the peaks broaden as expected due to thermal fluctuations around an equilibrium orientation. The positions of the peaks remain the same indicating that the herringbone structure persists to at least 40K. In addition, one very small bump at -90° is also observed in the distribution at T = 40K. This represents orientations of the inverted molecules in the structure. Its width continues to grow and broaden as the temperature rose to 45K, concurring to the increase in number of inverted molecules in the snapshots of the monolayer of CO/LiF(100) at high temperature region. At T= 45K the four peaks (which come from two sharply peak at low temperature regime and two additional bumps at $\varphi \sim$ -90° and -180°)

become equal and never fully washed out indicating that the molecules still have a preferential orientation with respect to the substrate.

7.2.3 Quantitative Analysis for the Phase Transition

The transition temperature can also be confirmed by monitoring the temperature dependence of the internal energy and heat capacity, C_v. Other quantitative analysis is helpful in this matter. In particular the examination of the order parameter and its fluctuations, i.e. the susceptibility, as functions of temperature, can also help to identify the transition type and better predict the transition temperature. The methods of calculation of these quantities are similar to those of the CO/NaCl system. The internal energy for every cycle from the MC simulation was stored and its average was calculated for each temperature. To ensure good statistical data, the average was calculated over a large number of cycles (usually 30,000 cycles). And the heat capacity was calculated using the fluctuation of the internal energy. The order parameter, ψ, is only a measurement of the degree of order from the azimuthal orientation. As previously discussed, an order parameter of one means that the structure is in perfect order, always in terms of the azimuthal orientation.

The energy curve (Fig. 7.8, upper panel) displays a continuous change throughout the phase transition. No evidence of a sudden jump in energy at the

transition is found. This is in agreement with the observation from the qualitative analysis that there is a phase transition occurring at high temperature (T > 40K). However, there exist two changes in the energy curve, one is found at around T~ 25° and another one is much higher temperature, T~ 40°. The first change is likely to represent the onset of the inversion of CO molecules. However, we do not believe that those inverted molecules indicate a head-tail phase transition. The inverted molecules are found to scatter throughout the layer with no definitive structure determined; therefore it cannot be considered as a transition to another type of structure. The inverted molecules are believed to be an excitation process activated by greater thermal motion at high temperature (T ~ 25K) couple with a small activation energy of inversion, ΔE= -0.2623 kcal/mol. Furthermore, if the molecules are flipped back so that the carbon end is pointing towards the surface, then their azimuthal orientations show no change. On the other hand, the change at T~ 45° is comparable to the predicted transition temperature (T~ 45°) of an orientational transition observed in the qualitative analysis of the angle distributions. The heat capacity, shown in Fig. 7.8 (lower panel) in contrast is inconclusive because so many small peaks are found and the base line cannot be well established. However, the curve does show a highest peak at T= 45°, again suggesting that there exist a phase transition as predicted. Moreover, the study had to be stopped at T= 50° because of desorption was taken place at this temperature, and the Monte Carlo simulation that we used in the study does not handle a change in the number of molecules. To handle this

problem, Monte Carlo method with a grand canonical (variant number of molecules) ensemble must be used instead of a canonical ensemble (fixed number of molecules) as the one we used in these studies and are beyond the scope of this study.

The plot of the order parameter as a function of time in Fig. 7.9 (upper panel) shows a linear drop at low temperature up to around T~ 26°. The drop then increases its rate and has the largest drop at T~ 44° to T~ 45°. It seems to have a large gap between those temperatures, however more study has be done in order to determine the exact nature of the drop in this case, consequently to determine its transition type. Nevertheless, the curve suggests that there truly is a phase transition, which occurs at T~ 45° as previously expect. Again the susceptibility curve, shown in Fig. 7.9 (lower panel), is calculated from the order parameter fluctuations and also displays one dominant peak at around T= 45K, which suggests that a phase transition occurs at this temperature although the base line of the curve cannot be completed since the simulations had to be stopped at T= 50K due to desorption of the CO molecules.

7.3 Summary

It is apparent from our results that our potential model is reliable enough to predict structures of the new system CO/LiF(100). Analysis from the

qualitative characteristic (e.g. angle distributions and snapshots of configurations) shows that at low temperature an ordered phase is observed and the structure is found to be $p(2\sqrt{2}x\sqrt{2})R45°$. The molecules have preferred azimuthal orientations with a polar angle of $\theta \sim 44°$. The ordered structure is found to persist up to $T \sim 40°$ before the structure becomes disordered. A phase transition is predicted to occur near $T \sim 44K$. At $T \sim 25°$, some of the molecules are inverted so that the oxygen end is pointing towards the surface. The number of inverted molecules is found to increase with temperature as expected because of greater thermal excitation at higher temperatures. The quantitative analysis (e.g. energy and order parameter study) does show evidence of a phase transition, yet it is not conclusive enough to either determine the exact transition temperature or to estimate the critical exponents. This uncertainty can be explained by the existence of the long-range interactions between the dipoles of the CO molecules, which in two-dimensional systems are very susceptible to fluctuations in the transition region.

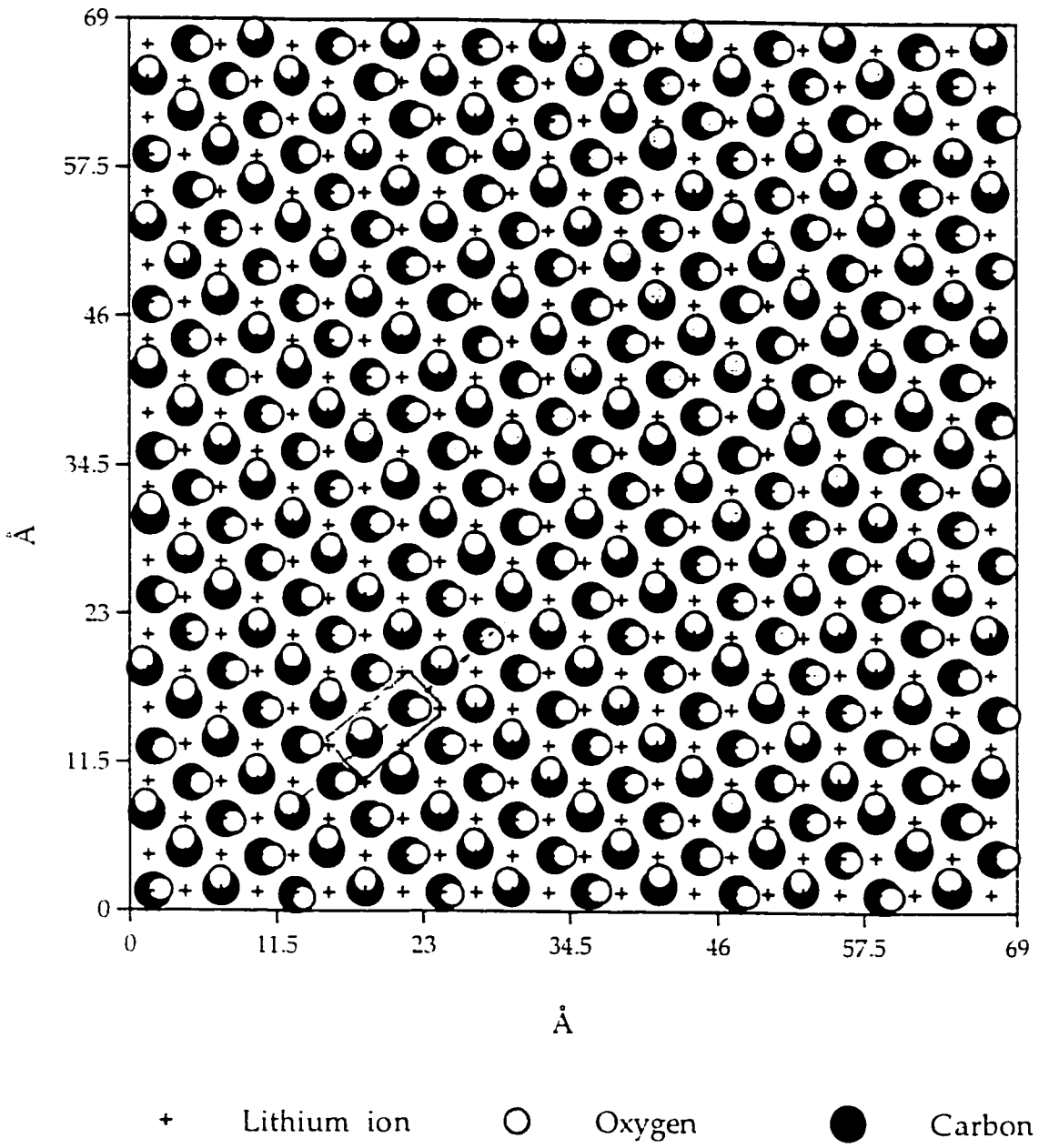

Figure 7.1. Configuration of a 24x24 lattice CO/LiF(100) monolayer generated by Monte Carlo simulation at T= 10K. The unit cell (solid rectangle) contains two molecules with a glide plane (dash line) runs through it.

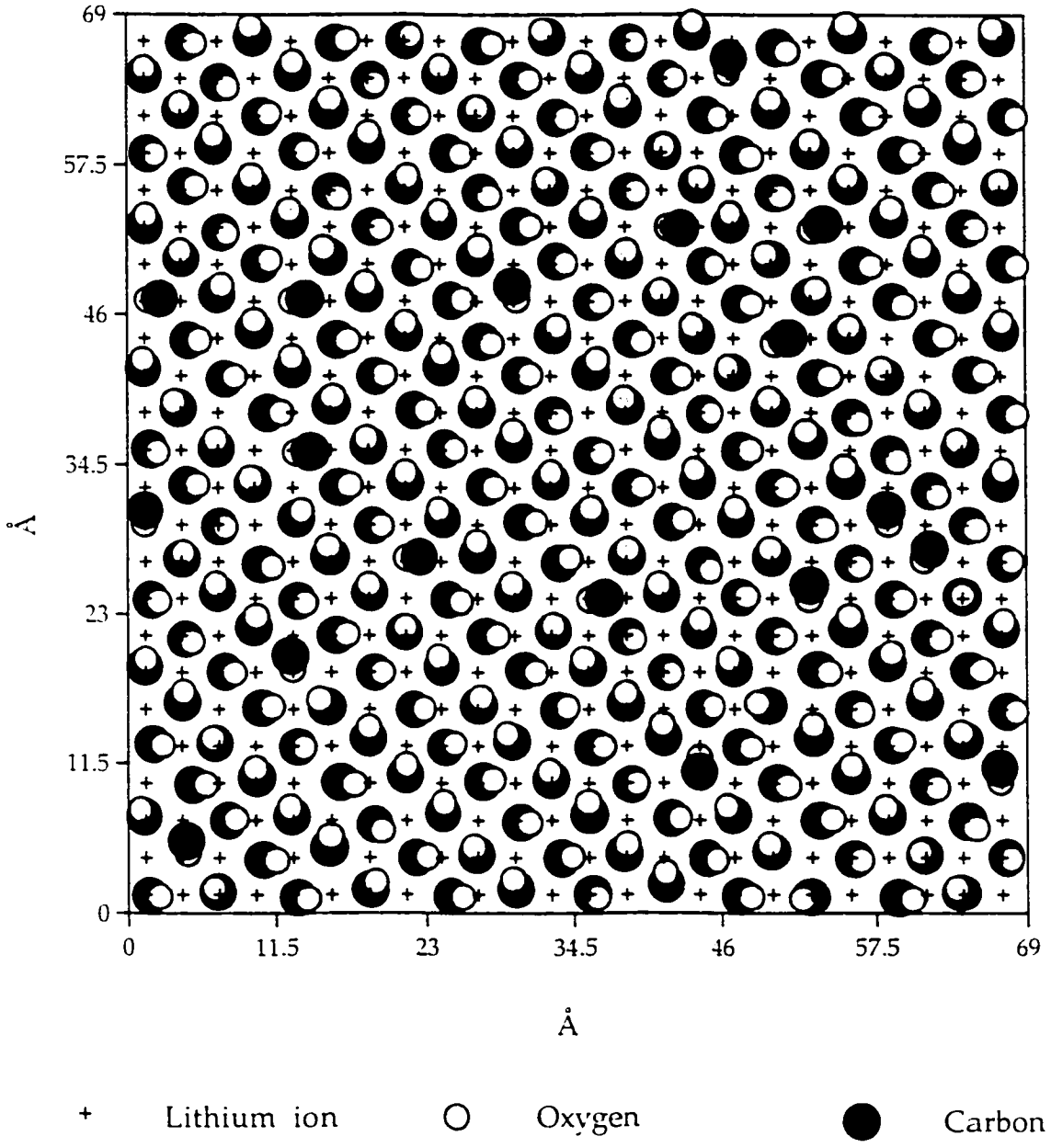

Figure 7.2. Configuration of a 24x24 lattice CO/LiF(100) monolayer generated by Monte Carlo simulation at T= 25K.

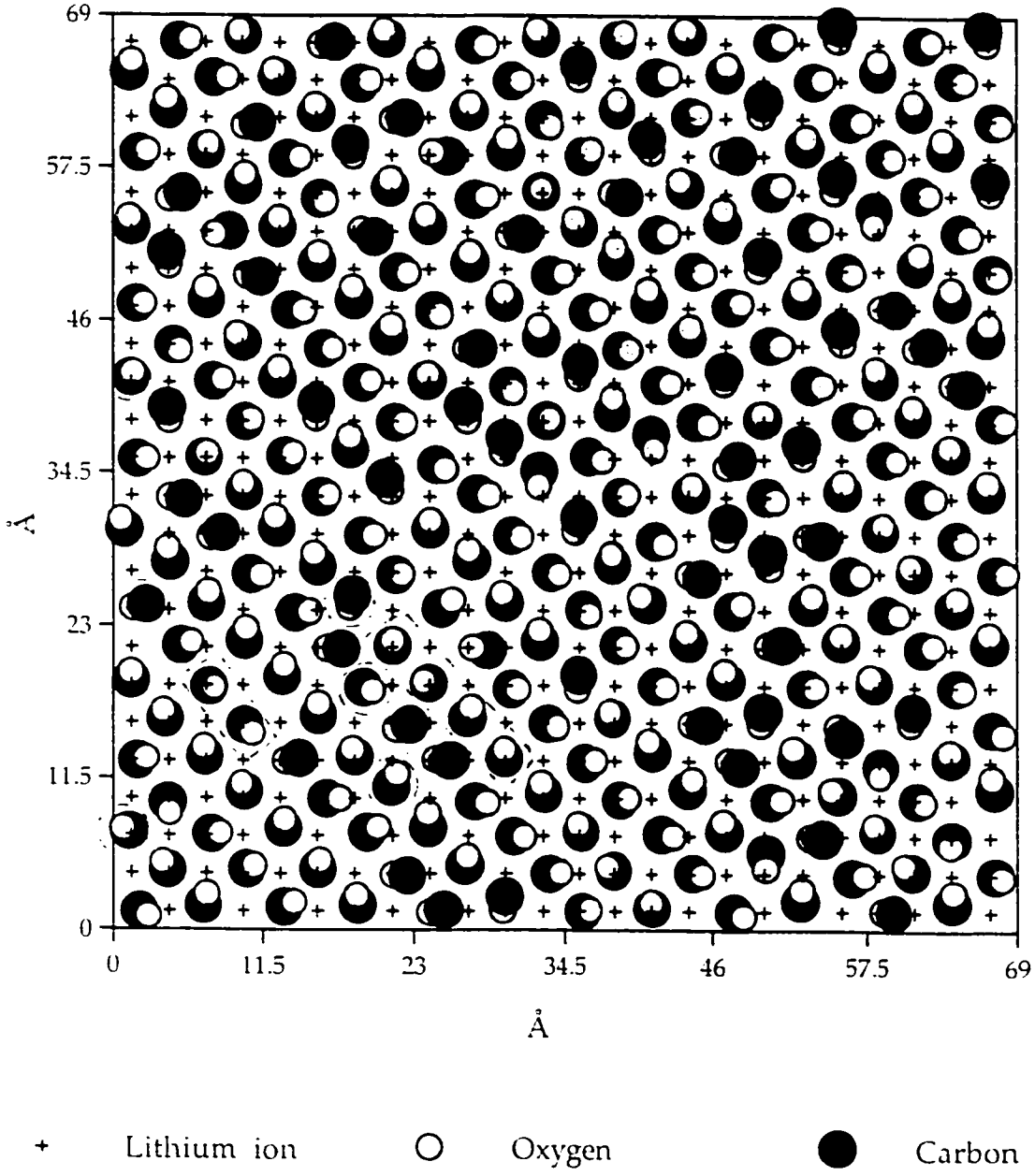

Figure 7.3. Configuration of a 24x24 lattice CO/LiF(100) monolayer generated by Monte Carlo simulation at T= 35K.

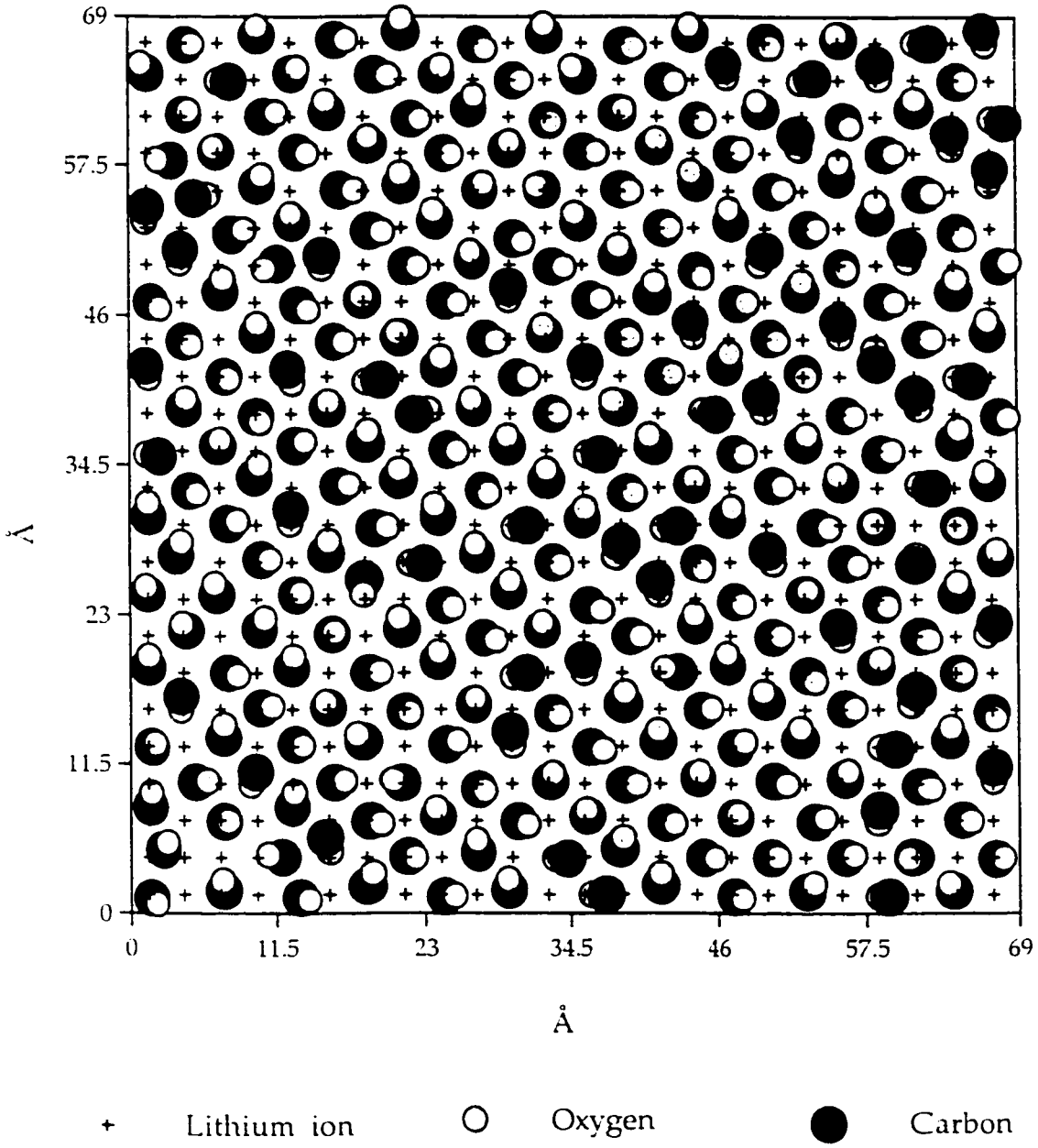

Figure 7.4. Configuration of a 24x24 lattice CO/LiF(100) monolayer generated by Monte Carlo simulation at T= 40K.

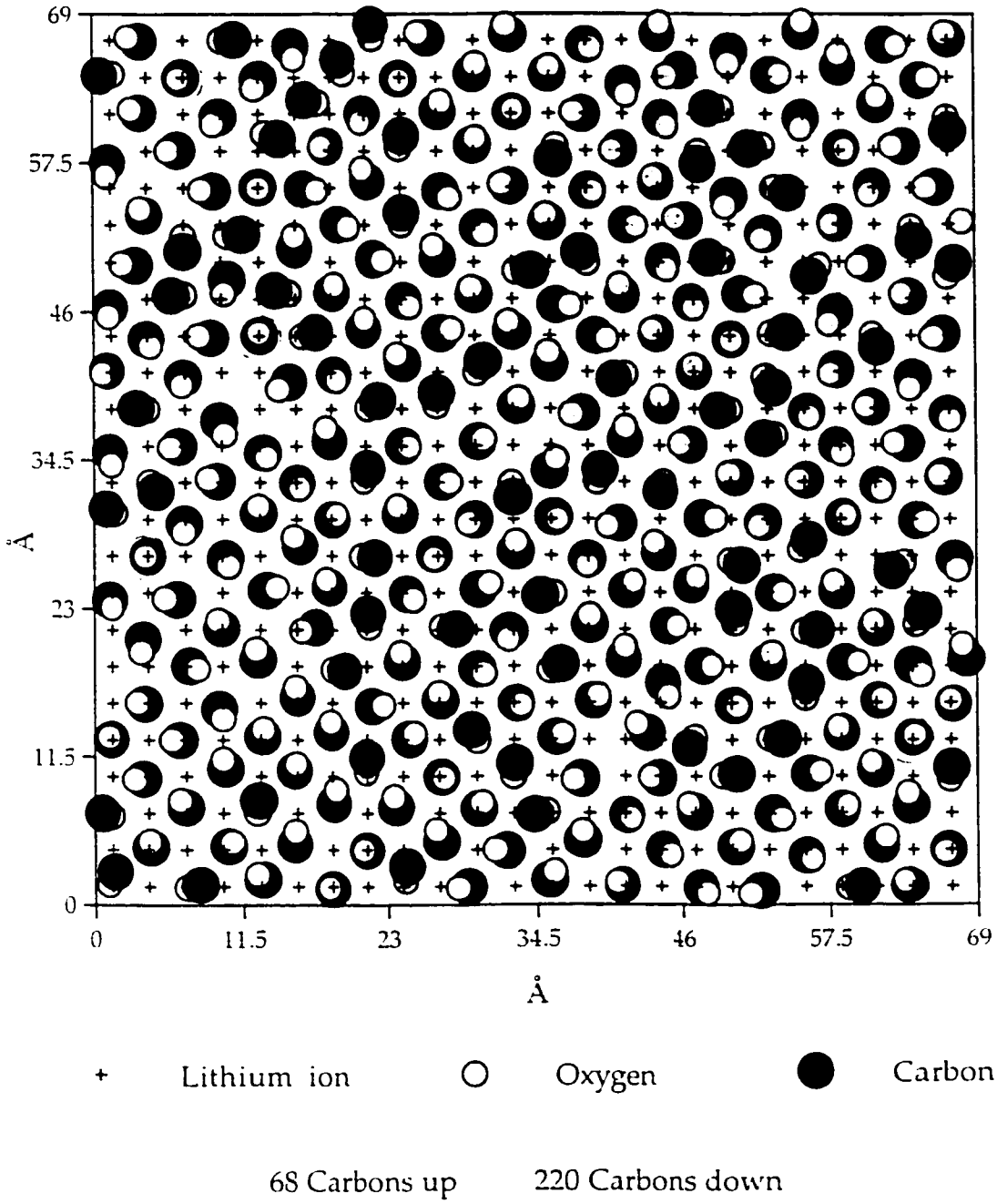

Figure 7.5. Configuration of a 24x24 lattice CO/LiF(100) monolayer generated by Monte Carlo simulation at T= 45K.

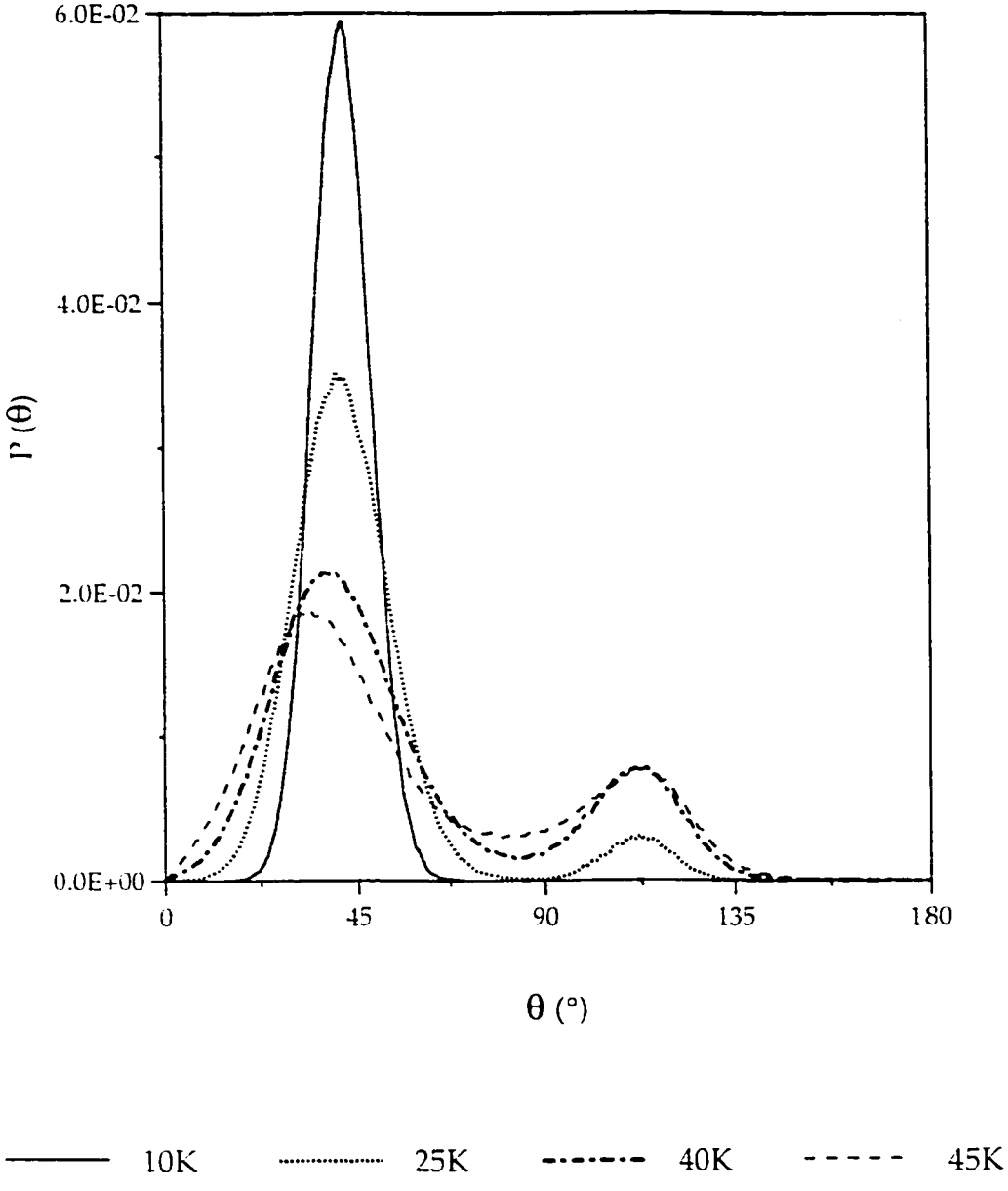

Figure 7.6. The polar (θ) distribution for a 24x24 lattice CO/LiF(100) monolayer generated by Monte Carlo simulation.

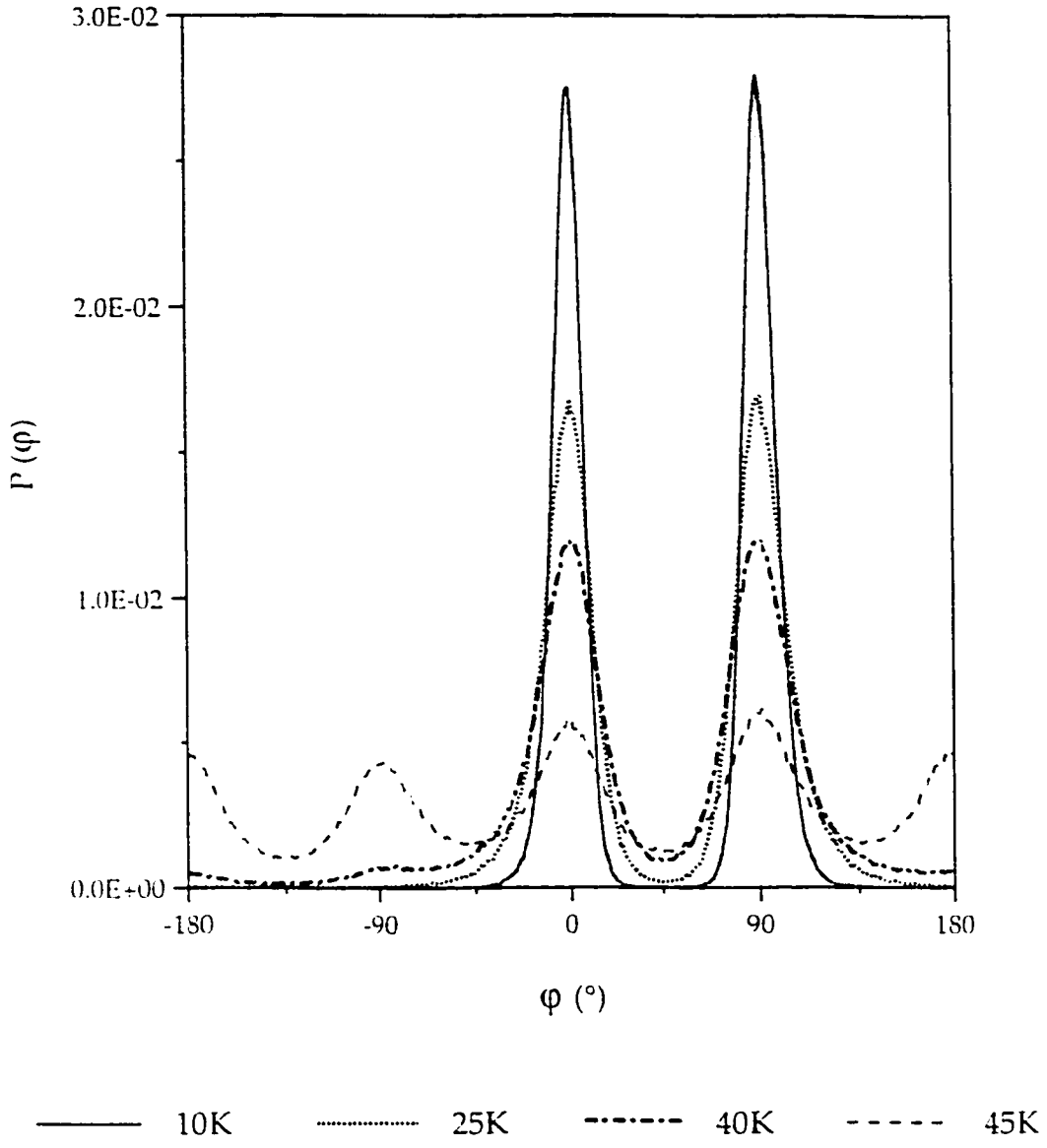

Figure 7.7. The azimuthal (φ) distribution for a 24x24 lattice CO/LiF(100) monolayer generated by Monte Carlo simulation.

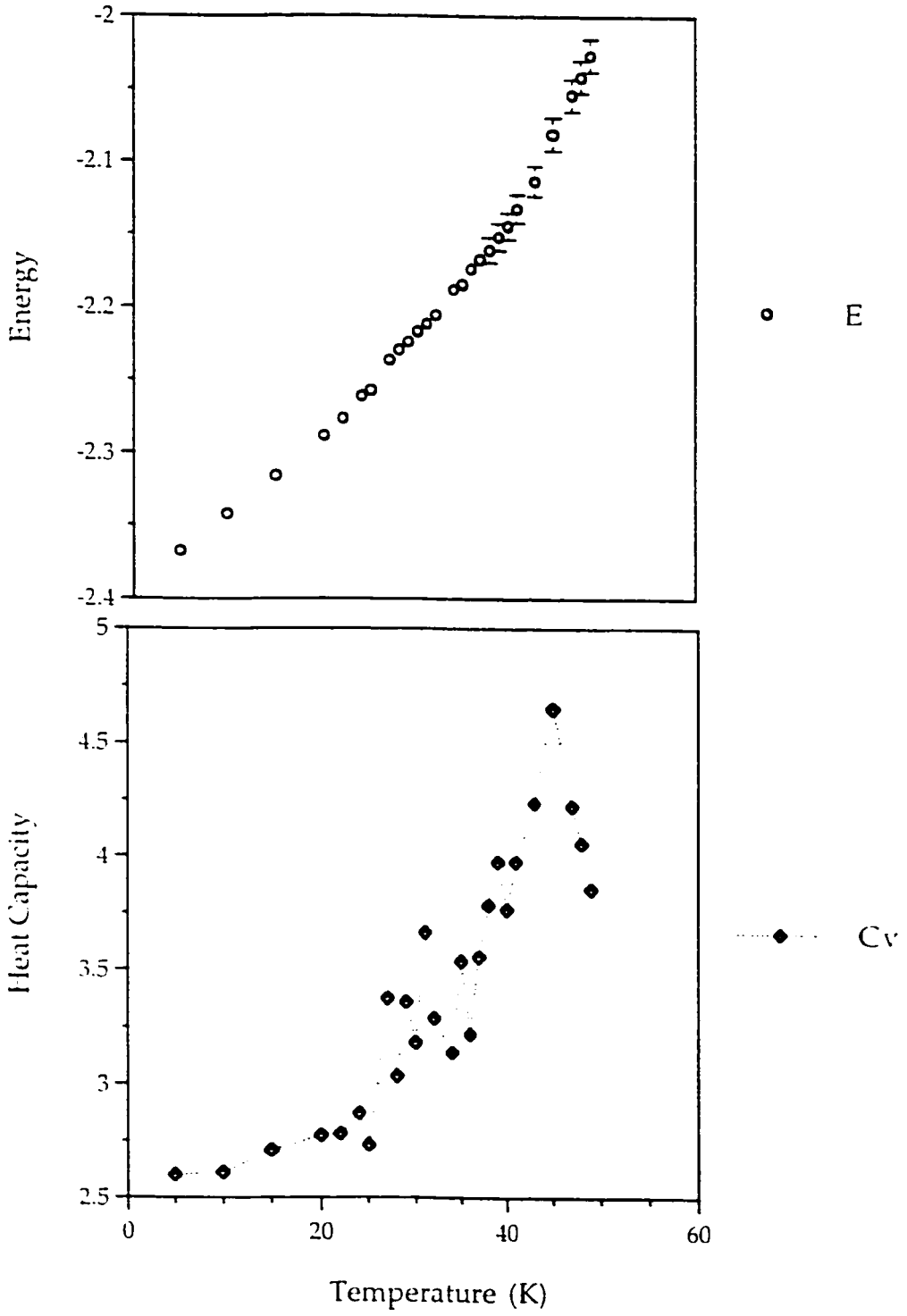

Figure 7.8. Monte Carlo results for the heat capacity, C_v, (lower panel) and energy, E, (upper panel) as functions of temperature for a 24x24 lattice CO/LiF(100) monolayer.

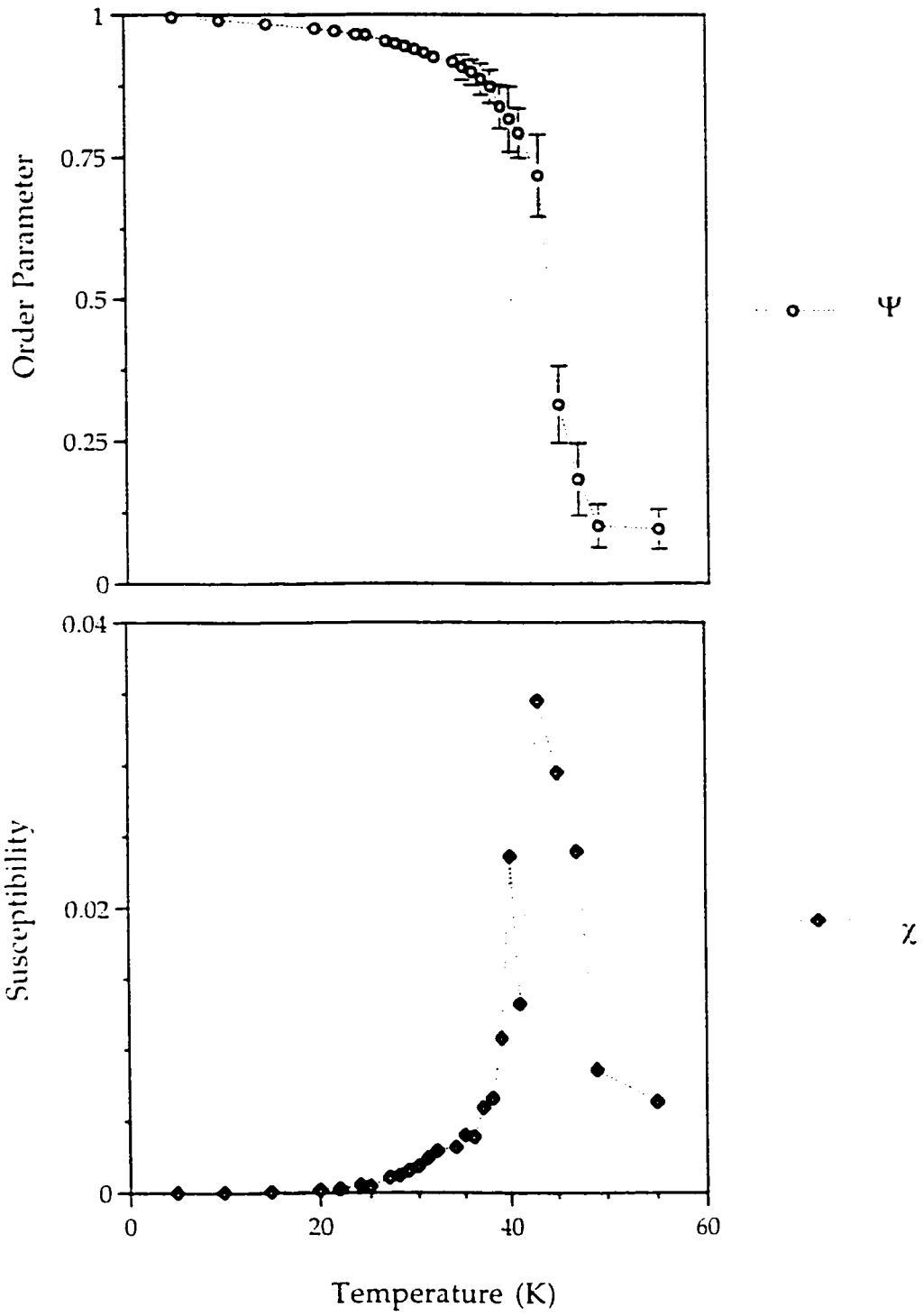

Figure 7.9. Monte Carlo results for the susceptibility, χ, (lower panel) and order parameter, Ψ, (upper panel) as functions of temperature for a 24x24 lattice CO/LiF(100) monolayer.

CHAPTER 8: CONCLUSION

We have presented the results of our study on the structure and phase transition of the adlayers CO molecules adsorbed on NaCl(100) and LiF(100) surfaces. Simulations were done using the Metropolis Monte Carlo method (canonical ensemble) and most of simulations were done in the temperature range of T= 1K to T= 75K.

It is known that the CO molecules are held to the underlying ionic surface by physisorption bonds with contributions from electrostatic, dispersion, induction, and repulsion terms. From our simulated results, we believe that the electrostatic interactions are particularly important and it is indeed the largest contribution to the total potential, both between molecule-molecule and molecule-surface interactions. Also the electrostatic interaction is found to be the most important contribution to the formation as well as the stability of the p(2x1) structure of the monolayer CO/NaCl(100).

Also in this work, we successfully report the simulation of the p(2x1)→p(1x1) phase transition for the above systems for the first time using Metropolis Monte Carlo simulations. It is found that CO molecules form a well-ordered monolayer on both surfaces at low temperature. The ordered low-temperature phase changes to a disordered structure in the regime of higher simulated temperatures. The results of the phase transition study, although primitive, shows evidence of an order-disorder type of transition.

It is confirmed that the CO molecules adopt an azimuthally ordered p(2x1) with two molecules per unit cell in an antiferroelectric fashion and have a glide plane that runs along the x axis on the NaCl(100) surface (T≤ 25K) in the monolayer regime. The two molecules are found to adsorb on inequivalent identical sites, with the molecular axis at an angle of 27Å with respect to the surface normal, in accord with experiment. The azimuthal orientation is coordinated with the direction of displacement of the C atom ($\delta y = \pm 0.2$Å) and results in the formation of rows tilted in the same direction with neighbouring rows tilt in the opposite direction ($\varphi \sim \pm 90$Å). As a result, the unit cell of this structure contains a pair of molecules tilted antiparallel to each other: one molecule from each row resulting in a low temperature p(2x1) structure. In addition, the CO molecules are found to bind to the NaCl(100) surface at the sodium ions with the carbon end closer to the surface. The average equilibrium distance between the carbon atom of the molecule and the surface ion has been calculated to be $z \sim 2.75$Å from the simulations at T= 1K. At higher temperatures (T> 25K), the low temperature (2x1) phase becomes orientationally disordered and transforms to the high temperature (1x1) phase. The correlation between the two molecules within the (2x1) unit cell is gradually destroyed as the temperature is raised resulting in a disordered p(1x1) structure with one CO molecule per unit cell. Yet on average the molecules remain tilted with respect to the surface normal despise of thermal broadening in the polar distribution. Although long range azimuthal order has been lost resulting in the formation of

the p(1x1) structure, some degree of short range order remains in the form of small ordered domains with the p(2x1) structure and the newly formed vortex-antivortex pairs. These vortices appear both below and above the transition temperature. The role and their effect of these vortices on the transition temperature as well as transition type are yet to be determined. In short, we are able to predict that the monolayer undergoes a continuous order-disorder transition from an azimuthally ordered phase into a disordered one at high temperature. However, the estimated range of transition temperature (T= 32 - 35K) reflected the difficulty in determining the exact temperature using the quantitative analysis because of the presence of a weak permanent dipole moment on the CO molecules. This leads to the formation of a dipolar interaction that can further lead to long relaxation times for energy and order parameter equilibration; thus making the system very susceptible to fluctuations at the transition regime. Consequently, clean results from the analysis cannot be obtained.

Besides adsorption on NaCl(100), we also report on a set of simulations of CO molecules adsorbed on LiF(100) surface. These simulations predict that at low temperatures the CO molecules form an ordered p($2\sqrt{2}$x$2\sqrt{2}$)R45 herringbone structure with two molecules per unit cell. In this structure the CO molecules are also localized near Li^+ sites with the carbon atoms down and are tilted by ~ 44° from the surface normal. Similarly, this ordered low temperature structure also

becomes disordered when the temperature exceeds 30K. It is interesting to note that at high temperature regime the long-range order in the molecular azimuthal orientations has been destroyed although the molecules in the disordered phase still show local correlations. Also in our simulation, the tilt angle of the molecules with respect to the surface normal does not significantly vary when temperature increases. Such a behaviour, which couples with the appearance of a growing orientational disorder in the monolayer, is responsible for an order-disorder phase transition. One striking difference to the NaCl(100) system is that at the transition temperature some of the molecules invert, so that the oxygen atom is down. The number of molecules, which adopt this new orientation, increases as the temperature rises past the transition temperature. It is of no surprise to find out that preliminary quantitative analysis of this system also suggests that the monolayer undergoes a continuous order-disorder type of phase transition at around T~ 40°.

Although being confident that the potential used in the simulations is good enough to get reliable results on studying the structure of the adsorbed layers, we believe that more efforts in modifying the electrostatic interactions has to be considered in order to minimize large fluctuations around the transition regime due to the long range dipolar interactions between the CO molecules. In addition, the occurrence of the vortex-antivortex pairs in the case of adsorption of CO/NaCl(100) as well as the molecular inversions and the displacement of the

molecules off of the Li^+ sites suggest it might be necessary to reconsider more complex models for the calculations of the order parameters in order to obtain better results in determining the transition type as well as transition temperature.

In the submonolayer regime, the CO molecules are found to aggregate into small islands with the ordered p(2x1) structure present in the middle of the island when adsorbed on NaCl(100) surface. Hence, it is apparent that in order to see an ordered (2x1) phase we need to look at the monolayer regime. The molecules in the middle of the island also show evidence of going through a phase transition to a more disordered state at higher simulated temperature. Also at high temperature, gas-solid coexistence in two dimensions is also present.

Multilayer systems of CO/NaCl(100) show that the ordered p(2x1) structure is not a stable configuration for the bottom layer. It transforms into an ordered p(1x1) structure even at very cold simulated temperature, *e.g.* T=1K. This is true for all simulated multilayer systems. The formation of the bulk structure of solid α-CO of the upper layers depends on the number of layers present in the system. It seems that the more layers the system has, the upper layers increasingly adopt the correct orientation of the bulk structure. We have not been able to get the molecules in the upper layers to adopt the correct head-to-tail orientations of the bulk solid α-CO. The ordered structures within the layer also

become more disordered when the simulated temperature has been increased. However in the present case, no conclusive information on this subject can be given without performing more thermal stabilities studies of the systems.

In the long run, larger systems will be applied trying to extract better quantitative values for the energy, order parameter, and their fluctuations. Finally note that a different type of simulation such as a Molecular Dynamics method could be performed using the same potential function. This would allow us to study dynamical aspects of the monolayer adsorption.

REFERENCES

1. *'Physical Chemistry'*, K. J. Laidler and J. H. Meiser, (The Benjamin/Cummings Publishing Company, Inc., 1982) 770
2. R. Imbihl, R. J. Behm, K. Christmann, G. Ertl and T. Matsushima, *Surf. Sci.* **117** 257 (1982)
3. G. Lange, D. Schmicker, J. P. Toennies, R. Vollmer, and H. Weiss, *J. Chem. Phys.* **103**, 2308 (1995)
4. O. Berg, R. Kisselkamp, and G. E. Ewing, *Surf. Sci.* **277**, 8 (1992)
5. J. Schimmelpfenig, S. Fölsh, and M. Henzler, *Surf. Sci.* **250**, 198 (1992)
6. A. Zecchina, S. Coluccia, G. Spoto and D. Scarano, *J. Chem. Soc. Faraday Trans.* **86**, 703 (1990)
7. L. Marchese, S. Coluccia, G. Martra and A. Zecchina, *Surf. Sci.* **269/270** 135 (1992)
8. S. Fölsh and M. Henzler, *Surf. Sci.* **247**, 269 (1991)
9. L. W. Bruch, A. Giebov, J. P. Toennies, and H. Weiss, *J. Chem. Phys.* **130** (12), 5109 (1995)
10. D. J. Dai, S. J. Peters, and G. E. Ewing, *J. Phys. Chem.* **99**, 10299 (1995)
11. D. J. Dai, *J. Chem. Phys.* **104**, 2461 (1996)
12. R. Gevirzman, Y. Kozirovski and M. Folman, *Trans. Faraday Soc.* **65**, (1969) 2206

13. G. E. Ewing, *International Reviews in Physical Chemistry*, **10** (4), 391 (1991)

14. *'Physical Adsorption of Gases'*, D. M. Young and A. D. Crowell, (London Butterworths, 1962) 1

15. G. P. M. Poppe, C. M. J. Wijers and A. van Silfhout, *Surf. Sci.* **251/252**, 321 (1991)

16. C. Noda, H. H. Richardson, and G. E. Ewing, *J. Chem. Phys.* **92** (3) (1990) 2099

17. C.Noda and G. E. Ewing, *Surf. Sci.* **240**, 181 (1990)

18. H.-C. Chang, H. H. Richardson, and G. E. Ewing, *J. Chem. Phys.* **89**, 7561 (1988)

19. A. W. Meredith and A. J. Stone, *J. Chem. Phys.* **104** (8), 3058 (1996)

20. J. P. Hardy, G. E. Ewing, R. Stables and C. J. S. M. Simpson, *Surf. Sci.* **159**, 1474 (1985)

21. J. Heidberg, E. Kampshoff, and M. Suhren, *J. Chem. Phys.* **95** (12), 9408 (1991)

22. J. Heidberg, H. Stein, and H. Weiss, *Surf. Sci.* **184**, 1431 (1987)

23. J. Heidberg, M. Suhren and H. Weiss, *Journal of Electron Spectroscopy and Related Phenomena* **64/65**, 227 (1993)

24. D. Schicker, J. P. Toennies, R. Vollmer, and H. Weiss, *J. Chem. Phys.* **95** (12), 9412 (1991)

25. *'Computational Chemistry'*, G. H. Grant and W. Graham Richards, (Oxford Science Publications, 1995) 33

26. S. Picaud, P. N. M. Hoang, C. Girardet, A. Meredith and A. J. Stone, *Surf. Sci.* **294**, 149 (1993)

27. P. N. M. Hoang, S. Picaud, and C. Girardet, and A.W. Meredith, *J. Chem. Phys.* **105** (18), 8453 (1996)

28. N.-T. Vu, A. Jakalian, and D. B. Jack, *J. Chem. Phys.* **106** (6), 2551 (1997)

29. N.-T. Vu and D. B. Jack, *Surface Review and Letters*, **6** (5), 683 (1999)

30. N.-T. Vu and D. B. Jack, *J. Chem. Phys.* **108** (14), 5653 (1998)

31. *'A Monte Carlo Simulation Study of Adsorption of $NaNO_3$ and H_2O on NaCl Surfaces'*. N.-T.Vu, A Research Proposal (1997)

32. S. J. Peters and G. E. Ewing, *J. Chem. Phys.* **100**, 14093 (1996)

33. *'Molecular Modeling Principles and Applications'*, A. R. Leach, (Longman, 1996)

34. *'Computer Simulation of Liquids'*, M. P. Allen and D. J. Tildesley, (Oxford Science Publications, 1986) 110

35. *'Computational Chemistry A Practical Guide for Applying Techniques to Real World Problems'*, D. Young, (A John Wiley & Sons, Inc., Publication, 2001) 62

36. *'Statistical Mechanics of Phase Transition'*, J. M. Yeomans, (Clarendon Press. Oxford Science Publications, 1992) 21

37. J. P. Polanyi, R. J. Williams, and S. F. O'Shea, *J. Chem. Phys.* **94**, 978 (1991)

38. V. J. Barclay, D. B. Jack, J. C. Polanyi and Y. Zeiri, *J. Chem. Phys.* **97**, 9458 (1992)

39. *'Chemistry of the Element'*, N. N. Greenwood and A. Earnshaw, (Butterworth Heinemann Publications, 2nd Edition, 1997) 291, 929

40. *'The Forces Between Molecules'*, M. Rigby, E. Brian Smith, W. A. Wakeham, and G. C. Maitland, (Oxford Science Publications, 1986) 1

41. C. A. Burrus, *J. Chem. Phys.* **28**, 427 (1958)

42. R. K. Nesbet, *J. Chem. Phys.* **40**, 3619 (1964)

43. F. P. Billingsley and M. Krauss, *J. Chem. Phys.* **60**, 2767 (1974)

44. R. D. Nelson, D. R. Lide and A. A. Maryott, *Natl. Std. Ref. Data Ser.*, No 10 (Natl. Bur. St. Washington, 1967)

45. P. F. Fracassi, R. Righini, R. G. Della Valle, and M. Klein, *Chem. Phys.* **96**, 361 (1985)

46. F. Mulder, G. F. Thomas and W. J. Meath, *Mol. Phys.* **41**, 249, (1980)

47. *'WMIN: A Computer Program to Model Molecules and Crystals in terms of Potential Energy Functions'*, W. R. Busing, ORNL-5747 (available through QCPE)

48. *'Atoms and Molecules'*, M. Karplus and R. N. Porter, (Benjamin/Cummings, Menlo Park, 1970)

49. J. E. Lennard-Jones and B. M. Dent, *Trans. Farad. Soc.* **24**, 92 (1928)

50. K. T. Tang and P. J. Toennies, *J. Chem. Phys.* **80**, 3725 (1984)

51. W. A. Steel, *Chem. Rev.* **93**, 2355, (1993)

52. P. W. Fowler and N. C. Pyper, *Mol. Phys.* **59** (2), 317 (1986)

53. T. L. Gilbert, *J. Chem. Phys.* **49**, 2640 (1968)

54. F. T. Smith, *Phys. Rev. A* **5**, 1708 (1972)

55. K. T. Tang and J. P. Toennies, *Z. Phys. D* **1**, 91 (1986)

56. P. W. Fowler P. J. Knowles and N. C. Pyper, *Mol. Phys.* **56**, 83 (1985)

57. C. Douketis, G. Scoles, S. Marchetti, M. Zen, and A. Thakkar, *J. Chem. Phys.* **76**, 3057 (1982)

58. N. J. Bridge and A. D. Buckingham, *Proc. R. Soc.* **295** A, 334 (1996)

59. J. E. Gready, G. B. Backsay, and N. S. Hush, *Chem. Phys.* **31**, 375 (1978)

60. S. Mahmud and E. Davidson, *Surf. Sci.* **322**, 342 (1995)

61. E. Spohr, *J. Chem. Phys.* **107** (16), 6342 (1997)

62. A. K. Sallabi and D. B. Jack, *Phys. Rev.* B **62** (8) 4841 (2000)

63. P. F. Fracassi, R. Righini, R. G. Della Valle, and M. L. Klein, *Chem. Phys.* **96**, 361 (1985)

64. W. B. J. M. Janssen, J. Michiels, and A. van der Avoird, *J. Chem. Phys.* **94** (12), 8402 (1991)

65. J. O. Clayton and W. F. Giauque, *J. Am. Chem. Soc.* **54**, 2610 (1932)

66. M. W. Melhuish and R. L. Scott, *J. Phys. Chem.* **68**, 2301 (1964)

67. P. W. Fowler and P. A. Madden, *Phys. Rev. B* 29, 1035 (1984)

68. M. Causà, R. Dovesi and F. Ricca, *Surf. Sci.* **280**, 1 (1993)